# SNAREs, 14-3-3 proteins and cholesterol dependent membrane domains

**Carolyn Brechin**

Thesis submitted for the degree of Doctor of Philosophy

The University of Edinburgh

2006

## Abstract

Lipid rafts are suggested to be sphingolipid and cholesterol rich domains that segregate out from the bulk plasma membrane by forming a more ordered lipid phase. Lipid raft-like domains have been described as cell signalling platforms and have been implicated in the regulation of an array of signal transduction events. This study investigates the association of two classes of protein, 14-3-3 proteins and plasma membrane SNAREs, with lipid raft-like domains. The 14-3-3 family of proteins are important regulators of numerous cell signalling pathways and are essential for cell survival; recently there has been some interest in the roles of these soluble proteins at the membrane, though this area remains poorly characterised. 14-3-3 has also been linked to CJD progression, which is directed by the lipid raft associated prion protein. SNAREs are essential mediators of exocytosis, a process that is also reported to depend on cholesterol, implying lipid raft involvement. SNAREs have also been isolated in detergent resistant membranes (DRMs) that are believed to represent clustered lipid rafts.

To examine the association of 14-3-3 and SNAREs with lipid raft-like domains in N2a and PC12 cells two approaches were taken. Initially, detergent resistant membranes were isolated and analysed for protein association. The second approach involved quantitative analysis of the colocalisation of 14-3-3 and SNAREs with membrane domains in intact cells by confocal microscopy, using the lipid raft marker cholera toxin B subunit (CTXB). Discrepancies between results from these two methods add to evidence implying that DRMs do not necessarily represent pre-existing membrane domains. Cholesterol depletion, which affects the integrity of lipid raft-like domains, caused a rearrangement CTXB labelled clusters in N2a and PC12 cells. The colocalisation of 14-3-3 with CTXB was unaffected by cholesterol depletion, a result which does not support the localisation of 14-3-3 to lipid raft-like domains. Interestingly however, the membrane distribution of the lipid raft marker Thy-1, a GPI-anchored protein, was also unaltered when cholesterol was depleted. In contrast to previous reports, disruption of SNAP-25 or syntaxin1a (SNARE) clusters

was not observed following cholesterol depletion. However, in N2a cells, the colocalisation of SNAP-25 with CTXB was reduced, though this was not the case in PC12 cells. Taken together these results suggest that cholesterol depletion may affect various raft-associated proteins and cell types in different ways. The findings from N2a cells indicate a role for lipid raft-like domains in controlling the spatial distribution of SNAP-25 on the plasma membrane. The membrane distribution of syntaxin1a appears to be differently regulated from that of SNAP-25, which may have implications for the regulation of exocytosis.

## Declaration

This thesis is composed entirely of my own work. The contribution of others in facilitating this work has been clearly acknowledged within the text or the Acknowledgements section. The work contained in this thesis has not been submitted for any other degree or professional qualification.

Carolyn Brechin

## Acknowledgements

I would like to thank my supervisor Alastair Aitken for giving me the opportunity to undertake this project. I very much appreciate the help and support I received from past members of his group, Sam Clokie, Shaun Mackie, Alex Peden and Helen Baxter.

I will be forever indebted to Rory Duncan for his guidance and encouragement and for providing me with the opportunity to carry out the imaging experiments included in this thesis. I would like to thank members of Rory Duncan's group and other members of the MBG for their help and friendship during my time in the department. I am especially grateful to Colin Rickman for his invaluable advice and patience, and to Mike Cousin for all his support.

I would like to acknowledge the work of David Moulton and Florian Scharinger, who were involved in automating batch processing procedures for aspects of the image analysis presented here. In addition, I would like to thank Linda Wilson and Rolly Wiegand for their instruction in confocal microscopy.

Finally, I would like to say a big thank you to my family and friends for their endless encouragement and support throughout my studies.

# Contents

## List of Figures

## List of Tables

## Abbreviations

| | |
|---|---|
| CFP | cyan fluorescent protein |
| CJD | Creuzfeldt-Jakob disease |
| CLSM | confocal laser scanning microscopy |
| CSF | cerebrospinal fluid |
| CTXB | cholera toxin subunit B |
| DDT | dithiothreitol |
| DMEM | Dulbecco's modified Eagles medium |
| DOPC | dioleoyl-phosphatidylcholine |
| DOPE | dioleoyl-phosphatidylethanolamine |
| DRM | detergent resistant membrane |
| DPPC | dipalmitoyl-phosphatidylcholine |
| DSC | differential scanning calorimetry |
| EDTA | ethylenediaminetetraacetic acid |
| ESR | electron spin resonance |
| FBS | foetal bovine serum |
| FITC | fluorescein-5-isothiocyanate |
| FRAP | fluorescence recovery after photobleaching |
| FRET | Förster resonance energy transfer |
| GFP | green fluorescent protein |
| GM1 | a ganglioside (type of glycosphingolipid) |
| GPI | glycosylphosphatidylinositol |
| GPI-AP | glycosylphosphatidylinositol-anchored protein |
| GSL | glycosphingolipid |
| GST | glutathione-S-transferase |
| IPTG | isopropyl-β-D-thiogalactopyranoside |
| $L_\alpha$ | liquid crystalline phase |
| $L_\beta$ | gel phase |
| $L_d$ | liquid disordered phase |
| $L_o$ | liquid ordered phase |
| LAT | linker for activation of T cells |
| MβCD | methyl-β-cyclodextrin |
| mol % | molar fraction as a percentage |
| N2a | Neuro-2-a cells |
| NMR | nuclear magnetic resonance |
| NSF | N-ethyl-maleimide-sensitive fusion protein |
| PBS | phosphate buffered saline |
| PC | phosphatidylcholine |
| PE | phosphophatidylethanolamine |
| PFA | paraformaldehyde |
| PMSF | phenylmethylsulfonylfluoride |
| PMT | photomultiplier tube |
| PrP | Prion protein |
| PS | phosphophatidylserine |
| PSF | point spread function |

| | |
|---|---|
| R | Pearson's coefficient |
| RPMI | Roswell Park Memorial Institute (medium) |
| SDS | sodium dodecyl sulphate |
| SDS-PAGE | sodium dodecyl sulphate polyacrylamide gel electrophoresis |
| SEM | standard error of the mean |
| SM | sphingomyelin |
| SNAP-23 | SNAP-25 homologue of 23 kDa |
| SNAP-25 | synaptosomal-associated protein of 25 kDa |
| SNARE | soluble NSF attachment receptor |
| SPM | synaptic plasma membrane |
| SPT | single particle tracking |
| TCA | trichloroacetic acid |
| TCR | T cell receptor |
| TCZ | transient confinement zone |
| TfR | transferrin receptor |
| Thy-1 | GPI-AP involved in T cell activation and non-immune processes, also known as CD90 |
| $T_m$ | melting temperature |
| Tris | trishydroxymethylaminomethane |
| TX-100 | Triton-X-100 |
| VAMP | vesicle associated membrane protein |
| YFP | yellow fluorescent protein |

# Chapter 1: Introduction

# 1. INTRODUCTION

## 1.1. LIPID RAFTS

The plasma membrane bilayer is composed of many different species of lipid; the lipid raft hypothesis suggests that part of the functional significance of this lies in the creation of lateral heterogeneities with specific properties. This model is particularly attractive because it allows for compartmentalisation of particular lipids, membrane-anchored proteins and complexes with affinity for these lipid rafts, producing a potential mechanism for regulating cell signalling. This introduction aims to give an overview of the development of the lipid raft hypothesis and the biochemical and microscopy based investigations that have attempted to verify the hypothesis. Since its emergence in the late 1980s the lipid raft model has evolved and current theories concerning raft size and stability are addressed. Finally some of the suggested biological functions of lipid rafts are discussed.

### 1.1.1. The origin of the lipid raft hypothesis

#### 1.1.1.1. Phase separation in model membranes

In 1972 Singer and Nicolson described their fluid mosaic model of cell membranes (Singer and Nicolson, 1972), this model has entered into the text books and shaped the study of biomembranes. In Singer and Nicolson's model membrane proteins are suspended in a fluid lipid bilayer and both proteins and lipids are free to diffuse laterally without constraints. The lipid raft hypothesis seeks to modify this model by inducing small, mobile domains in which particular lipids and proteins are trapped preventing their free intermixing with all the other components of the membrane. The formation of these domains is suggested to be driven by interactions between specific classes of lipid and cholesterol that cause them to separate out from the bulk

fluid phase of the cell membrane. The origin of this idea can be found in the study of phase separation in model membranes, beginning in the 1970s.

Phase separation in model membranes has been studied using a number of spectroscopic techniques including nuclear magnetic resonance (NMR), electron spin resonance (ESR) and differential scanning calorimetry (DSC). NMR and ESR provide information about the physical environment of a labelled molecule or probe by exciting the spin of nuclei (NMR) or unpaired electrons (ESR) in a magnetic field. DSC monitors the amount of heat required to increase the temperature of a sample compared to a reference substance. When the sample undergoes a physical transformation, such as a phase transition, more heat will be needed to increase its temperature. Förster resonance energy transfer (FRET) and conventional light microscopy have also been employed to investigate the partitioning of fluorescently labelled lipid probes between phases. FRET involves excitation of an acceptor fluorophore by emission from an excited donor fluorophore. Fluorophores must be $< 10$ nm apart for detectable FRET to occur so this technique can provide information about nanometre scale interactions. These methods provide the basis for the studies described in the following discussion.

Temperature determines the state or phase of a phospholipid bilayer. A bilayer composed of a single lipid species can exist in one of two physical states; at low temperatures the bilayer will be in a solid state (also called the gel or $L_\beta$ phase) and at higher temperatures the bilayer will be in a fluid state (also called the liquid crystalline ($L_\alpha$) or liquid disordered ($L_d$) phase), as illustrated in figure 1.1 (Binder et al., 2003; Hancock, 2006; London and Brown, 2000). In the gel phase the hydrocarbon chains of the phospholipids are fully extended, the lipids are tightly packed together and molecular motion is severely restricted. In the $L_\alpha$ phase the lipids are more disordered, the hydrocarbon chains have greater conformational freedom and lateral mobility is increased. For a particular lipid species the phase transition temperature or melting temperature ($T_m$) is the temperature at which the gel phase converts to the $L_\alpha$ phase and depends on the chemical structure of the lipid.

The polar headgroup structure, acyl chain length and degree of saturation have all been shown to affect $T_m$ (Barenholz et al., 1976; Barton and Gunstone, 1975).

Mammalian cell membranes are mixtures of glycerophospholipids, sphingolipids and cholesterol. A large proportion of the glycerophospholipids have unsaturated hydrocarbon chains and a much lower $T_m$ (0°C and below) than sphingolipids ($T_m > 37$°C) (Barenholz et al., 1976; Koynova and Caffrey, 1995). The presence of two lipids of very different $T_m$ in biological membranes led to the study of the possible coexistence of gel and $L_\alpha$ phases in binary mixtures of phospholipids. McConnell and co-workers detected the coexistence of solid (gel) and fluid phases in binary mixtures of two phophatidylcholine (PC) molecules differing in acyl chain structure (Hong-wei and McConnell, 1975; Shimshick and McConnell, 1973a), using a spin probe (for ESR) that was excluded from the solid phase. When binary mixtures of a phosphatidylcholine (PC) and cholesterol were studied these authors detected the possible presence of two immiscible fluid phases (Shimshick and McConnell, 1973b).

Further investigations into the effect of cholesterol on phospholipid bilayers led to the concept of a second, more ordered liquid phase in coexistence with the $L_\alpha$ phase. Ipsen and co-workers collated previous experimental studies describing the effect of increasing cholesterol concentration on the phase behaviour of dipalmitoyl-phosphatidylcholine (DPPC) bilayers (Ipsen et al., 1987; Ipsen et al., 1989). These DSC studies demonstrated that cholesterol broadens the usually sharp phase transition from the gel to $L_\alpha$ phase for DPPC. The authors suggested that cholesterol has a disordering effect on solid DPPC and an ordering effect on DPPC in the $L_\alpha$ phase. Ipsen *et al* postulated a separate cholesterol induced phase intermediate between the gel and $L_\alpha$ phases, which they termed the liquid ordered ($L_o$) phase (see figure 1.1). Importantly, over certain temperature ranges and cholesterol concentrations their model predicts the coexistence of the $L_o$ phase with a liquid crystalline disordered ($L_\alpha$ or $L_d$) phase. An important property of the $L_o$ phase

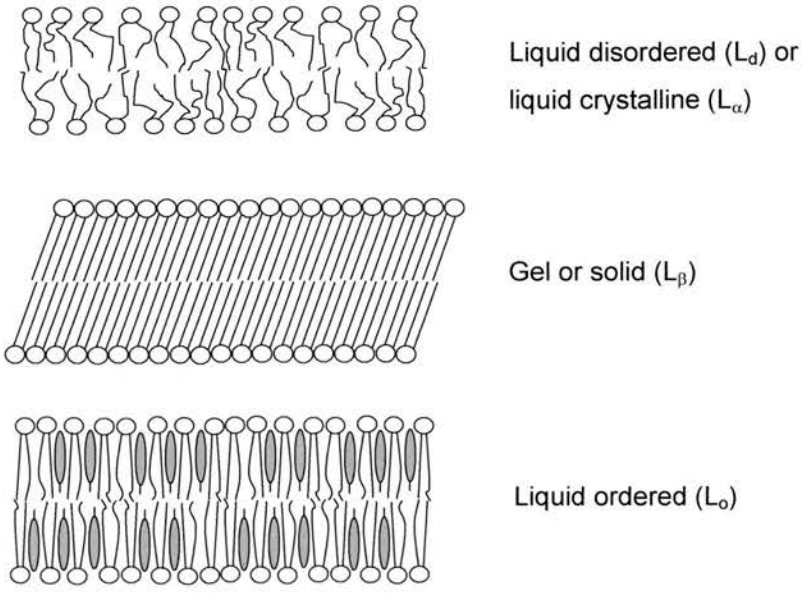


**Figure 1.1. Lipid bilayer phases**

Bilayers composed of a single lipid species exist in the liquid disordered phase ($L_d$, top) above the $T_m$ and in the gel phase (middle) below the $T_m$. The $L_d$ phase is characterised by conformational freedom of acyl chains and high lateral mobility. In the gel phase lipids are tightly packed and their mobility is severely restricted. The liquid ordered ($L_o$, bottom) is thought to be formed by the addition of a particular mol % cholesterol to a bilayer composed of mainly saturated lipids. The $L_o$ phase has properties intermediate between the $L_d$ and gel phases. See text for further details.

is that whilst the lipid hydrocarbon chains are more ordered than in the $L_d$ phase (i.e. the configurational freedom of the chains is decreased) the lateral mobility of the lipids is similar to the $L_d$ phase (Edidin, 2003; Silvius, 2003a; Vist and Davis, 1990). The $L_o$ phase is therefore an intermediate phase in which the high degree of acyl chain ordering resembles the gel phase but the rapid lateral diffusion observed in the $L_d$ phase is retained.

Experimental support for the coexistence of a liquid ordered phase with the disordered liquid crystalline phase was produced by a number of studies in the early 1990s. Vist and Davis used NMR to monitor the degree of orientational averaging of $^2$H-labelled hydrocarbon chains in a DPPC bilayer. Addition of cholesterol increased the average orientational order of DPPC acyl chains, confirming the ordering effect of cholesterol on the $L_d$ phase (Vist and Davis, 1990). This study went on to use NMR and DSC to detect the coexistence of $L_o$ and $L_d$ phases at 10 – 22 mol % cholesterol, at temperatures above the $T_m$ of DPPC. ESR studies came to similar conclusions concerning the coexistence of $L_o$ and $L_d$ phases in binary mixtures of cholesterol and PC or sphingomyelin (SM) (Sankaram and Thompson, 1990a; Sankaram and Thompson, 1991), as did the DSC studies of McMullen and co-workers (McMullen et al., 1993; McMullen and McElhaney, 1995).

Ternary mixtures of a high $T_m$ phospholipid (usually DPPC or SM), a low $T_m$ phospholipid (such as dioleoyl-phosphatidylcholine, DOPC) and cholesterol later replaced binary mixtures of cholesterol and PC, with the aim of producing a better model for the mammalian plasma membrane. Recent studies have used a combination of DSC, NMR and fluorescence microscopy to confirm the coexistence of $L_o$ and $L_d$ phases in vesicles composed of these ternary mixtures (de Almeida et al., 2003; de Almeida et al., 2005; Dietrich et al., 2001a; Feigenson and Buboltz, 2001; Silvius et al., 1996; Veatch and Keller, 2003; Veatch and Keller, 2005; Veatch et al., 2004). De Almeida and co-workers detected fluid-fluid phase separation at 10 – 35 mol % cholesterol, similar to the studies in binary mixtures (de Almeida et al., 2005). In ternary mixtures the $L_d$ phase was rich in the lower $T_m$ lipid, whilst the higher $T_m$ lipid and cholesterol were concentrated in the $L_o$ phase (Feigenson and

Buboltz, 2001; Veatch and Keller, 2003; Wang et al., 2000a). Some of these studies considered the size of $L_o$ phase domains; de Almeida and co-workers detected domains in the range of < 20 nm up to 100 nm, depending on the mol % cholesterol (de Almeida et al., 2005). One study using fluorescent lipid probes detected large (~ 200 nm) $L_o$ domains that could be observed by light microscopy but these domains were only present at < 16 mol % cholesterol (Feigenson and Buboltz, 2001). However, nanometre scale domains were detected at 16 – 25 mol % cholesterol by a loss of FRET between $L_o$ and $L_d$ phase probes. This agrees with a recent FRET study in which $L_o$ domains of tens of nanometres in size were detected at 37°C in model membranes of similar composition to the plasma membrane (Silvius, 2003b).

#### 1.1.1.2. The liquid ordered phase and cholesterol

The interaction of cholesterol with phospholipids is central to the formation of the $L_o$ phase. The studies described in the previous section determined that, in ternary systems, cholesterol partitions with the higher $T_m$ lipid into $L_o$ domains and the lower $T_m$ lipid forms the $L_d$ phase. There is experimental evidence for the preferential interaction of cholesterol with particular lipid species (discussed in detail in Silvius's recent review (Silvius, 2003a)) but the mechanism that drives formation of $L_o$ phase domains remains controversial; a number of different models have been presented to explain this phenomenon.

Studies of the area condensing effect of cholesterol and cholesterol partitioning into lipid vesicles both demonstrated that cholesterol interacts preferentially with fully saturated acyl chains (Demel and De Kruyff, 1976; Silvius, 2003a). In binary mixtures of cholesterol and PC or SM the average molecular area occupied by the lipid is smaller than would be predicted, indicating that cholesterol constrains the conformation of the lipids. Smaby and co-workers studied the reduction in molecular area induced by cholesterol and found that increasing acyl chain unsaturation reduced the condensing effect of cholesterol (Ali et al., 1994; Smaby et al., 1994; Smaby et al., 1997), suggesting that cholesterol interacts less strongly with unsaturated phospholipids. Cholesterol preferentially partitioned into vesicles

composed of SM or PC with saturated acyl chains rather than vesicles containing unsaturated PC species (Lange et al., 1979; Leventis and Silvius, 2001; Nakagawa et al., 1979; Niu and Litman, 2002). The headgroup and backbone structure of the lipid also affects the interaction with cholesterol. Cholesterol prefers SM over glycerophospholipids and negatively charged headgroups promote interaction with cholesterol (Demel et al., 1977; Leventis and Silvius, 2001; Sankaram and Thompson, 1990a; van Dijck, 1979; Van Dijck et al., 1976; Wattenberg and Silbert, 1983).

The reason for the preferential interaction with SM and other saturated acyl chain phospholipids is suggested by consideration of the molecular structure of cholesterol. Cholesterol contains a rigid aromatic ring system, as shown in figure 1.2 C and D. Monounsaturated PC constitutes the major glycerophospholipid species in the mammalian plasma membrane. The fatty acyl chains usually have a 16 – 20 carbon atom backbone and the cis double bond in the unsaturated acyl chain is often at the ninth carbon (see figure 1.2 A and E). Sphingomyelin is composed of a sphingosine base which contributes one of the hydrocarbon backbones and contains a trans unsaturation; the second hydrocarbon chain is an amide linked fatty acid, containing up to 24 carbons, which is usually fully saturated, as shown in figure 1.2 B and F (McMullen et al., 2004; Simons and Vaz, 2004). Cholesterol inhibits the formation of rotational conformers in saturated DPPC acyl chains at carbon positions 4 and 6, presumably due to the insertion of the rigid sterol ring system parallel to the DPPC (Davies et al., 1990; Engelman and Rothman, 1972; Rothman and Engelman, 1972). Thus it is suggested that cholesterol can impose conformational ordering on saturated acyl chains, constraining them to the extended trans conformation and allowing strong hydrophobic interactions to form. However, the presence of a rigid cis double bond before the fifteenth carbon in the lipid acyl chain prevents this ordering and therefore unsaturated species interact more weakly with cholesterol (Silvius, 2003a; Simons and Vaz, 2004).

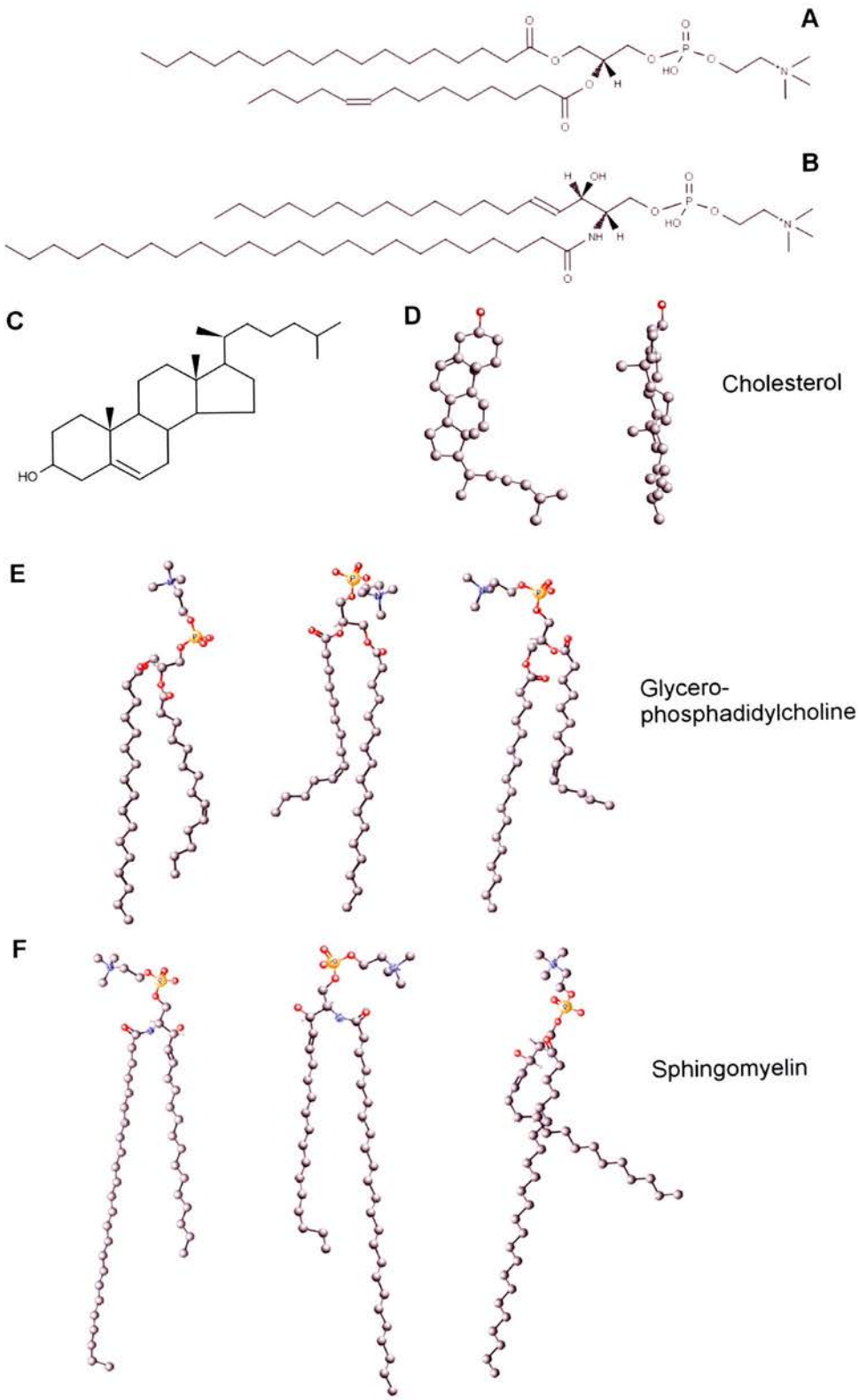


**Figure 1.2. Structures of the major lipid classes of the mammalian plasma membrane**

Sankaram and co-workers extended this reasoning by suggesting that the immiscibility of the $L_d$ and $L_o$ phases results from hydrophobic length mismatch (Almeida et al., 2005; Sankaram and Thompson, 1990b). The long sphingolipid chains interacting with cholesterol are in an extended conformation, whilst the generally shorter acyl chains in the $L_d$ phase are less constrained; therefore it is favourable to minimize the mismatch in bilayer thickness by segregating the different lipid species into domains. McConnell and co-workers present an alternative model in which cholesterol forms reversible complexes of defined stoichiometry with particular phospholipids, based on their observations of the condensing effect of cholesterol (McConnell and Radhakrishnan, 2003). In fact the SM headgroup has been suggested to hydrogen bond with cholesterol, using a functional group not present in glycerophospholipids (Simons and Vaz, 2004). However, recent NMR and fluorescence spectroscopy studies found no evidence for this hydrogen bonding (Guo et al., 2002; Holopainen et al., 2004). Huang and Feigenson present another possible explanation for $L_d/L_o$ phase separation. They suggest that tight packing of phospholipid headgroups with cholesterol is needed to shield cholesterol from unfavourable interactions with water (the 'umbrella model'), thus lipid species that can interact more closely with cholesterol are preferred (Almeida et al., 2005; Hancock, 2006; Huang and Feigenson, 1999).

Mammalian plasma membranes are composed of glycerophospholipids, which make up the greatest proportion of the membrane at 40 – 60 mol % , sphingolipids at 10 - 20 mol % and cholesterol at 30 – 40 mol % (McMullen et al., 2004; van Meer, 1989). The specific concentrations of cholesterol that promote phase separation and the preferential interactions of cholesterol with saturated sphingolipids support the concept of domain segregation in biological membranes as described by the lipid raft hypothesis (Brown and London, 1997; Brown and London, 1998; Brown and London, 2000; Hancock, 2006; Silvius, 2003a; Simons and Vaz, 2004). However, some authors maintain that the high concentration of cholesterol in the plasma membrane would mean that the bulk membrane phase would be liquid ordered, with dispersed domains of $L_d$ phase (Almeida et al., 2005; McMullen et al., 2004). In any

case, the detection of lateral heterogeneities in living cell membranes has proved challenging, as discussed in subsequent sections.

#### 1.1.1.3. Lipid sorting studies

The detection of the $L_d/L_o$ phase separation in artificial membranes provided the chemical basis for the lipid raft hypothesis. However, lipid sorting studies in epithelial cells during the late 1980s provided the first indication that lateral domain segregation might actually occur in biological membrane systems. In epithelial cells the apical and basolateral membranes have different lipid and protein compositions, maintained by tight junctions that prevent lateral diffusion (Simons and van Meer, 1988; van Meer and Simons, 1982; van Meer and Simons, 1986). The apical membrane is enriched in glycosphingolipids (GSL) compared to the basolateral membrane, which more closely resembles the plasma membrane of non-polarised cells. Particular membrane proteins, including glycosyl-phosphatidylinositol (GPI) anchored proteins, also target preferentially to the apical membrane (Brown and Rose, 1992; Lisanti et al., 1988; Wandinger-Ness et al., 1990). Investigations into the mechanism of polarised sorting were carried out in Madin-Darby canine kidney (MDCK) cells. Using a fluorescently labelled precursor of GSLs van Meer and co-workers determined that GSLs are produced in the Golgi apparatus and from there preferentially transported to the apical plasma membrane (van Meer et al., 1987). They postulated that GSLs form microdomains in the Golgi apparatus due to inter-lipid hydrogen bonding and apical proteins associate specifically with these microdomains, which are then somehow targeted to the apical membrane (van Meer and Simons, 1988).

The seminal investigations of Brown and Rose into the sorting of GPI-anchored protein placental alkaline phosphatase (PLAP) in stably transfected MDCK cells provided support for van Meer and Simons's hypothesis (Brown and Rose, 1992). They noted that PLAP was soluble in the detergent Triton-X-100 (TX-100) immediately after synthesis but became insoluble in the Golgi apparatus. The authors suggested that the change in solubility of PLAP might be due to a change in its

membrane environment. To test this hypothesis they devised a method for isolating detergent insoluble complexes on a sucrose density gradient. These complexes contained PLAP as well as other GPI-anchored proteins (GPI-APs) and were rich in sphingolipids, with a lipid composition of 1:1:1 sphingolipid to cholesterol to glycerophospholipid, similar to the composition of the apical membrane. These results were taken to support the concept of sphingolipid-rich microdomains in the Golgi apparatus involved in the targeting of lipids and proteins to the apical plasma membrane. The authors suggested sorting signals in the proteins might target vesicles formed from these domains to the apical membrane. Other studies also found that GPI-anchored proteins were insoluble in non-ionic detergents (Cinek and Horejsi, 1992; Fiedler et al., 1993; Hoessli and Rungger-Brandle, 1985; Low, 1989; Vitetta et al., 1973). This work established the standard method for isolation of detergent resistant membranes (DRMs): extraction in cold TX-100 followed by floatation on a sucrose density gradient. DRMs were hypothesized to correspond to *in vivo* lipid rafts (Simons and Ikonen, 1997).

## 1.1.2. Lipid rafts and detergent resistant membranes

Prior to further discussion of the lipid raft field it is important to emphasize the distinction between lipid rafts and DRMs. Lipid rafts are hypothetical entities: $L_o$ phase microdomains, rich in cholesterol and sphingolipids, postulated to exist as dispersed domains in the plasma membrane of most cells (Simons and Ikonen, 1997). The bulk plasma membrane is thought to be in the $L_d$ phase. A schematic diagram of the lipid raft model is shown in figure 1.3. DRMs are the product of detergent extraction procedures based on the method of Brown and Rose (Brown and Rose, 1992) and are believed to represent clustered lipid rafts. The following sections discuss the relationship of DRMs to $L_o$ phase domains and the composition of DRMs.

Before considering the properties of DRMs it is worth mentioning the relationship of lipid rafts to another membrane microdomain, caveolae. Like lipid rafts caveolae are

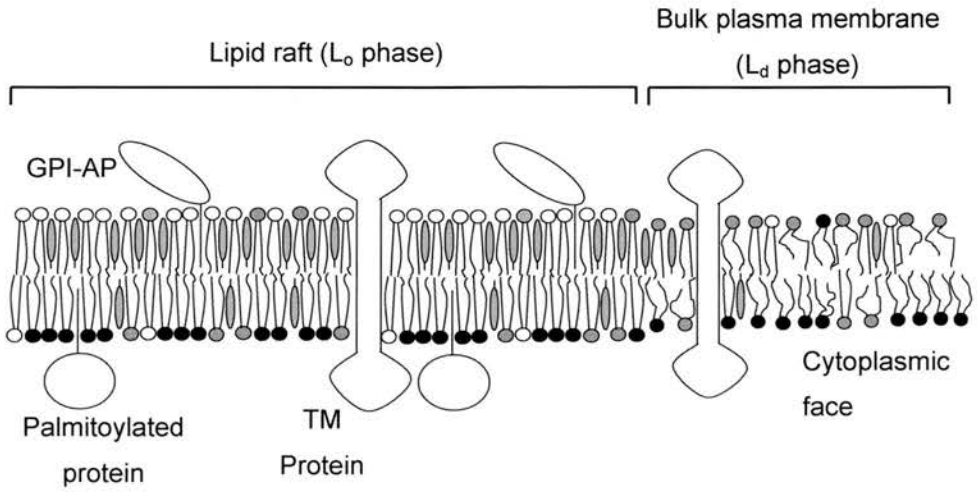


**Figure 1.3. The lipid raft model**

Schematic diagram illustrating the original lipid raft hypothesis. Lipid rafts are suggested to be $L_o$ domains rich in sphingolipids (white circles), saturated PCs (grey circles) and cholesterol (grey ovals). GPI-anchored proteins (GPI-APs), palmitoylated proteins and particular transmembrane proteins preferentially partition into rafts. The bulk plasma membrane is in the $L_d$ phase in this model. The inner leaflet of the plasma membrane is enriched in phosphatidylserine and phosphatidyl ethanolamine (black circles) and depleted in cholesterol compared to the outer leaflet.

suggested to be rich in cholesterol and sphinolipids. Caveolae are sensitive to depletion of cholesterol (Parton, 2003) and caveolin, the essential protein component of caveolae, has been demonstrated to bind cholesterol (Murata et al., 1995). Colocalisation of the glycosphingolipid ganglioside GM1 with caveolae has been reported (Fra et al., 1995; Parton and Richards, 2003) and caveolin was identified in DRMs (Fiedler et al., 1993; Sargiacomo et al., 1993), leading Lisanti et al to suggest that DRMs are in fact caveolae (Lisanti et al., 1994). However, DRMs rich in GPI-anchored proteins can still be isolated from cell types that do not express caveolin (Fra et al., 1994; Gorodinsky and Harris, 1995; Mirre et al., 1996) showing that DRMs derive from a membrane domain that does not require caveolin. It should be pointed out though that caveolin does reproducibly associate with DRMs in cells that express this protein, i.e. the detergent extraction procedure appears to isolate caveolae in addition to other caveolin-independent membrane domains. One important difference between caveolae and lipid rafts is that caveolae are morphologically identifiable, whilst lipid rafts are not. The necessity of using lipid raft markers makes the study of lipid raft biology particularly challenging.

#### 1.1.2.1. Detergent resistant membranes may represent $L_o$ domains

The DRM isolation method devised by Brown and Rose relies on the insolubility of DRMs in non-ionic detergent and their low buoyant density. The $L_o$ domains that DRMs are believed to represent are also likely to exclude detergent molecules due to the hydrophobic interactions that promote tight packing of cholesterol with saturated acyl chains. If the bulk plasma membrane is in the $L_d$ phase then this should be preferentially solubilised by detergent, leaving $L_o$ domains intact (London and Brown, 2000; Shogomori and Brown, 2003). Support for this hypothesis was obtained in model membranes. Model liposomes with a DRM composition (1:1:1 molar ratio of glycerophospholipids to sphingolipids to cholesterol) were compared with $L_d$ phase (7:1 PC to cholesterol) and $L_o$ phase (2:1 DPPC to cholesterol) liposomes (Schroeder et al., 1994). GPI-anchored PLAP inserted into the model liposomes was fully solubilsed from the $L_d$ phase by TX-100 extraction but the model DRMs and $L_o$ phase liposomes were more resistant to solubilisation. In further

studies the dequenching of an $L_o$ phase-preferring fluorescent probe was used to monitor the formation of $L_o$ phase domains as it segregated away from an $L_d$ phase-preferring quencher molecule (Ahmed et al., 1997; Schroeder et al., 1998). When the molecular ratio of cholesterol and SM to unsaturated PC was altered the extent of dequenching, reporting the degree of $L_o$ phase separation, correlated well with the proportion of insoluble lipid recovered following detergent extraction. Other studies also reported that the degree of $L_o$ phase formation correlated with detergent insolubility (Xu et al., 2001; Xu and London, 2000).

An ESR study by Ge and co-workers strengthened the argument that DRMs are $L_o$ phase membranes (Ge et al., 1999). DRMs isolated from RBL-2H3 mast cells were compared with liposomes of pure SM or DPPC (in gel and $L_d$ phases) or a 1:1 molecular ratio of cholesterol to DPPC as a model for the $L_o$ phase. Spin labelled lipids reported on the rotational diffusion, acyl chain ordering and lateral mobility of lipids in each system. The mast cell-derived DRMs produced results that were similar to the $L_o$ phase liposomes and differed from the $L_d$ and gel phase liposomes in the expected way (e.g. rotational diffusion rates were greater in the DRMs than in the gel phase liposomes). These model membranes produced encouraging evidence for a connection between $L_o$ phase domains and detergent insolubility.

### 1.1.2.2. Protein composition of DRMs

A large number of proteins with a wide variety of functions have been identified as DRM-associating proteins and mass spectrometry studies have attempted to define the raft proteome in several cell types. Inconsistencies between studies are a cause for concern but can perhaps be explained by considering the possibility of heterogeneity within the lipid raft population.

Early studies established the TX-100 insolubility of GPI-anchored proteins (Brown and Rose, 1992; Chatterjee and Mayor, 2001; Cinek and Horejsi, 1992; Fiedler et al., 1993; Hoessli and Rungger-Brandle, 1985; Low, 1989; Vitetta et al., 1973) and implicated the GPI-anchor in targeting of the attached protein to DRMs (Rodgers et

al., 1994). Tyrosine kinases of the Src family were also found to be concentrated in DRMs (Davy et al., 2000; Draberova and Draber, 1993; Field et al., 1995; Field et al., 1997; Robbins et al., 1995; Rodgers et al., 1994; Shenoy-Scaria et al., 1994; Wu et al., 1997). These studies and further investigations of palmitoylated proteins indicated that palmitoylation might cause proteins to preferentially partition into DRMs due to the saturated acyl chain of this lipid modification (Melkonian et al., 1999). More importantly these studies added to the list of cell signalling related proteins associated with DRMs and caveolae, establishing caveolae and lipid rafts as signalling platforms (Simons and Ikonen, 1997; Zajchowski and Robbins, 2002). It was suggested that lipid rafts might enhance cell signalling by locally concentrating components of a signalling pathway or excluding interfering proteins. Signalling pathways might be modulated by altering the localisation of a protein between raft and non-raft compartments, thereby changing its access to other signalling proteins.

Mass spectrometry has been used to analyse the protein composition of DRMs isolated from cell types including Jurkat T cells (von Haller et al., 2001), human umbilical vein endothelial cells (Sprenger et al., 2004) and hippocampal neurons (Ledesma et al., 2003), amongst others (Blonder et al., 2004; Foster et al., 2003; Nebl et al., 2002). All these studies reported the presence of raft markers such as caveolin, the palmitoylated protein flotillin-1 and GPI-anchored proteins as confirmation that their DRM preparations were successful. Furthermore, all studies describe a group of proteins that are particularly rich in signal transduction proteins such as Src family kinases (Blonder et al., 2004; Foster et al., 2003; Nebl et al., 2002), heterotrimeric G-proteins (Blonder et al., 2004) and even some cytoplasmic signalling proteins (Foster et al., 2003; Sprenger et al., 2004). Cytoskeletal proteins were also particularly abundant in all the DRM preparation but Ledesma *et al* speculate that this might be due to the high abundance of cytoskeletal proteins in cells rather than a specific association with DRMs (Ledesma et al., 2003).

Though these proteomic studies all found broadly similar classes of proteins to be enriched in DRMs the detailed protein composition of the DRMs differed between studies. In a recent review, Edidin also points to conflicting reports concerning the

DRM localisation of specific proteins (Edidin, 2003). These discrepancies could be due to cell type differences or slight differences in the detergent extraction procedures employed. For example, the detergent to protein ratio has been found to affect the localisation of proteins to DRMs. Increasing the detergent to protein ratio decreases the overall recovery of protein in the DRMs (Chamberlain and Gould, 2002; Ostermeyer et al., 1999) and the association of specific proteins, including the raft marker caveolin, reduces with increasing detergent concentration (Chamberlain and Gould, 2002; Shogomori and Brown, 2003). This indicates that lipid rafts may be partially solubilised at high detergent concentrations and/or the bulk plasma membrane may not be fully solubilised at low detergent concentrations. It is clear then that it is extremely important to consistently use the same detergent to protein ratio for a set of experiments, but choosing this ratio is difficult. Ostermeyer *et al* found that the recovery of protein in DRMs was fairly stable at detergent to protein ratios of 5:1 w/w and above (Ostermeyer et al., 1999) so this maybe a good guide. However, the detergent to protein ratio is rarely explicitly stated in publications and the importance of the parameter does not seem to be widely appreciated.

An attractive explanation for inconsistencies produced by different DRM isolation protocols is the that lipid rafts are a heterogeneous population of microdomains (Pike, 2004). Pike suggests that different rafts may consist of slightly different lipid and protein components and therefore be differently insoluble. This would explain the different solubilsation profiles of lipid raft markers observed following extraction with various alternative detergents (Schuck et al., 2003). Support for the theory of distinct lipid raft sub-populations comes from immunoaffinity purifications of DRMs. The detergent Brij 96 was used to extract DRMs from rodent brain homogenate (Madore et al., 1999). GPI-anchored proteins prion protein (PrP) and Thy-1 were both present in the DRMs. However, addition of a strong ionic deteregent fully solubilised PrP but not Thy-1. Immunoaffinity purification of DRMs with anti-PrP antibodies successfully isolated all the PrP but only recovered about 10% of Thy-1 in the total DRMs. The authors concluded that the two proteins were in separate microdomains with different solubility profiles. Analysis of lipid composition showed that PrP DRMs had higher levels of cholesterol, SM and a

particular glycosphingolipid than the Thy-1 DRMs (Brugger et al., 2004). Other studies have also managed to immunopurify subsets of DRMs with different protein compositions (Drevot et al., 2002).

The lack of a universally accepted protocol for detergent extraction and cell type differences may result in different isolation of proteins due to the varied solubility of distinct lipid raft sub-populations (Chamberlain, 2004; Pike, 2004; Taylor et al., 2002). Considering the complexity of cell signalling, lipid raft heterogeneity seems to be a very reasonable proposal if lipid rafts indeed function in modulation of signalling processes.

## 1.1.3. Visualisation of lipid rafts

DRM isolation provides a convenient method for investigating membrane microdomains and insolubility correlates with the presence of $L_o$ phase domains. However, concerns about whether DRMs represent physiological membrane domains (Edidin, 2003; Munro, 2003) led researchers to explore techniques for visualisation of lipid raft-like domains in intact cells. Labelling of proteins with fluorescent molecules is often used to assess the localisation of a DRM-associating protein compared with established lipid raft markers. Information about the size and density of microdomains in cell membranes has been gained from studies employing Förster resonance energy transfer (FRET), a technique that reports on the proximity of molecules. Single particle tracking (SPT) continues to play an important role in assessing the size and stability of membrane microdomains. Accumulating evidence from imaging studies has led to modifications of the original lipid raft hypothesis, particularly with respect to the size and stability of rafts. Alternative models for membrane compartmentalisation have also been presented as an explanation for some of the data.

### 1.1.3.1. Localisation of fluorescent lipid raft markers

Fluorescent protein constructs have been used extensively to investigate the distribution of lipid raft markers (usually designated as such by association with DRMs) on the cell surface. Fluorescently labelled cholera toxin subunit B (CTXB) that binds to ganglioside GM1 (a glycosphingolipid) is particularly useful as a marker for saturated lipids (Critchley et al., 1982; Holmgren, 1973). The co-clustering of two raft markers after crosslinking of one or both of them provides evidence for the association of both proteins with the same membrane microdomains. Many such studies generated support for the lipid raft hypothesis but they do not agree that all DRM/lipid raft markers colocalise with each other (Kusumi and Suzuki, 2005). Recent studies involving a lipid probe for membrane order also

provide evidence for the presence of membrane microdomains (Gaus et al., 2005; Gaus et al., 2003).

Initial studies with fluorescently tagged GPI-APs mainly showed a diffuse distribution of these proteins on the plasma membrane (Jacobson and Dietrich, 1999). Following these negative results, crosslinking studies were employed to aid the search for segregated membrane domains. Growth hormone fused to a GPI anchoring signal was efficiently crosslinked into clusters on the surface of MDCK cells by a short (nm scale) chemical crosslinker (Friedrichson and Kurzchalia, 1998). Cholesterol depletion is frequently employed to demonstrate the dependence of a protein or process on lipid rafts. In this study cholesterol depletion abrogated crosslinking, providing support for cholesterol dependent rafts rich in GPI-APs.

Following the success of these chemical crosslinking experiments the technique was transferred to imaging studies. Antibody mediated crosslinking of fluorescently labelled GPI-APs revealed colocalisation between pairs of proteins in intact cell membranes. Cholera toxin B subunit has also been extensively employed as a natural crosslinker of the GSL ganglioside GM1 as it is pentavalent (Merritt et al., 1998). The co-clustering of pairs of proteins was followed in live fibroblast BHK-21 cells (Harder et al., 1998). Thy-1, PLAP (GPI-APs), influenza haemagglutinin (HA, a transmembrane DRM-associated protein) and GM1 all co-clustered with each other when simultaneously crosslinked. Transferrin receptor (TfR), a transmembrane protein that is generally excluded from DRMs, segregated from PLAP when both were crosslinked. However, co-clustering of the lipid raft markers was more variable when only one of them was crosslinked. Other studies also found that antibody mediated crosslinking of Thy-1 did not recruit the GPI-AP folate receptor (Mayor et al., 1994) or CTXB-labelled GM1 (Fra et al., 1994) to Thy-1 clusters. In direct contrast, studies in T cells have demonstrated recruitment of components of the T cell signalling machinery to GM1 crosslinked with CTXB (Janes et al., 1999; Parmryd et al., 2003) and complimentary recruitment of GM1 following T cell receptor (TCR) engagement (Viola et al., 1999). Crosslinking of the immunoglobulin E (IgE) receptor (FcεRI) following antigen recognition induced transient

redistribution of FcεRI to GM1 clusters (Stauffer and Meyer, 1997). In Jurkat T cells, crosslinking of GM1 or GPI-AP, CD59 caused co-clustering of cyan fluorescent protein (CFP) attached to the cytosolic face of the cell membrane by a dual palmitoyl and myristoyl anchor (Gri et al., 2004). This last study is of particular interest because it implies coupling of microdomains in the outer leaflet of the plasma membrane with microdomains in the inner leaflet. Whether the two leaflets are coupled is a very important question for lipid raft function.

A recent interesting development in the visualisation of microdomains is the use of the fluorescent lipid probe Laurdan. In contrast to the marker proteins discussed above, Laurdan reports directly on the order of its membrane environment according to studies in model membranes (Parasassi et al., 1990; Parasassi et al., 1991). The emission spectrum of Laurdan inserted into gel phase membranes differs from that in $L_\alpha$ phase (Parasassi et al., 1999; Parasassi et al., 1998). Gaus *et al* used Laurdan imaging to separate more ordered from more disordered regions on the plasma membrane of live cells (Gaus et al., 2003). They observed a decrease in the ordering of the membrane in response to cholesterol depletion and increasing temperature, in line with the expected characteristics of $L_o$ domains. Isolated DRMs had a similar level of membrane order as the more ordered regions of live cell membranes. These authors went on to show that lipids in and around the TCR complex are more ordered than bulk T lymphocyte plasma membrane (Gaus et al., 2005).

Many of the lipid raft marker crosslinking studies and Laurdan imaging provide support for the presence of membrane microdomains enriched in particular proteins. However, the crosslinking studies where no recruitment of lipid raft markers was observed suggest that all DRM associated proteins do not necessarily reside in the same microdomains in intact cell membranes.

### 1.1.3.2. The use of FRET in the study of membrane microdomains

The resolution of conventional fluorescence microscopy is constrained to the optical diffraction limit of 250 nm. FRET involves excitation of an acceptor fluorophore by emission from an excited donor fluorophore. FRET microscopy can provide information about promixity of molecules on a nanometre scale because the fluorophores must be less than 10 nm apart for detectable FRET to occur (Stryer, 1978). FRET has been employed to study the distribution of lipid raft markers on the cell surface. FRET efficiency independent of the density of donor and acceptor fluorophores on the cell surface is taken to demonstrate clustering of the labelled proteins. If the FRET efficiency is altered by changes in protein density this suggests a random distribution of the proteins (Lagerholm et al., 2005).

FRET was detected between yellow fluorescent protein (YFP) and CFP when both were attached to the plasma membrane by the addition of palmitoyl and myristoyl anchors (Zacharias et al., 2002). Importantly the efficiency of FRET was saturable suggesting clustering of the proteins. In another study Varma and Mayor detected homo-FRET between GPI-anchored folate receptor molecules via the loss of fluorescence anisotropy (Varma and Mayor, 1998). Light emitted immediately following excitation is polarised in the same direction as the laser but when homo-FRET occurs the light emitted by the indirectly excited fluorophores is not polarised. Thus, as homo-FRET increases the anisotropy of the emitted light decreases. Fluorescence anisotropy values from GPI-anchored folate receptor were unchanged by incresing receptor density suggesting that the receptors were present as clusters. In both studies FRET became dependent on protein density following cholesterol depletion, implying that clustering is dependent on cholesterol.

All FRET studies do not correlate directly with the lipid raft hypothesis. In two studies Kenworthy *et al* presented results that are inconsistent with clustering of GPI-APs and GM1 (Kenworthy and Edidin, 1998; Kenworthy et al., 2000). Labelled GPI-APs and CTXB-labelled GM1 were studied on the surface of various cell types. Hetero-FRET between like proteins and between combinations of the proteins was

dependent on surface density, suggesting a random distribution of these molecules. Sharma and co-workers carried out time resolved homo-FRET and deduced that > 10 % of GPI-anchored GFP molecules were in high density structures in which the molecules were < 4 nm apart (Sharma et al., 2004). They suggest that 20 – 40 % of GPI-GFP molecules are in nanoscale clusters whilst the rest are present as monomers. Clearly this does not support a simple model where all GPI-APs are present in large scale lipid rafts, though homo-FRET was decreased by cholesterol depletion. In addition Sharma *et al* noted that the ratio of monomers to clusters did not change with increase expression of GPI-GFP (Sharma et al., 2004). Plowman *et al* made the same observation in a different system (Plowman et al., 2005). They were studying GFP attached to the membrane by dual palmitoylation and farnesylation, using immunogold labelling and electron microscopy. They also reported that the ratio of clusters to monomers was unchanged with increasing protein expression. This result was at odds with a mathematical model where protein molecules partition into a fixed number of stable, pre-existing microdomains.

According to Hancock and Mayor and Rao the apparent inconsistencies between these FRET studies can be reconciled if the microdomains with which GPI-APs associate are viewed as very small structures with short life times (Hancock, 2006; Mayor and Rao, 2004). If each domain contained only a few protein molecules, perhaps only one of a particular type of protein, then this would explain the inability of Kenworthy *et al* to detect clustering (Hancock, 2006). If domains were unstable, dispersing and reforming all the time, this might explain the results concerning the unchanged ratio of clusters to monomers in response to increased protein expression (Plowman et al., 2005; Sharma et al., 2004). However, other results are more consistent with all GPI-AP molecules being in stable domains (Varma and Mayor, 1998; Zacharias et al., 2002).

### 1.1.3.3. The size of membrane microdomains

Lipid rafts were originally envisaged as large platforms on the scale of hundreds of nanometres that would contain many protein molecules (Simons and Ikonen, 1997). Whilst one study reported 700 nm rafts (Schutz et al., 2000) most studies failed to resolve domains by light microscopy and observed a diffuse distribution of lipid raft markers (Jacobson and Dietrich, 1999). A range of techniques have been employed to attempt to determine the size of lipid rafts but this remains a controversial subject. Most estimates of size agree that steady state lipid raft-like domains are likely to be smaller than the limit of optical diffraction (i.e. < 250 nm) (Rajendran and Simons, 2005).

The FRET studies discussed in the previous section indicate nanometre scale domains. Sharma and co-workers reported that GPI-GFP is likely to be present in 5 nm diameter clusters, containing no more than four molecules of the protein (Sharma et al., 2004). Another study suggested that lipid rafts are less than 70 nm in diameter (Varma and Mayor, 1998) and other results (Kenworthy and Edidin, 1998; Kenworthy et al., 2000) can only be explained by nanometre scale domains (Hancock, 2006) or an absence of domains. Immunogold labelling of GFP targeted to the plasma membrane by dual palmitoylation and farnesylation gave estimates of tens of nanometres for domain size in two separate electron microscopy studies (Plowman et al., 2005; Prior et al., 2003). These domains contained 6 – 20 protein molecules and covered 35 % of the plasma membrane (Prior et al., 2003).

Single particle tracking (SPT) studies have produced estimates of domain size on the scale of fifty to hundreds of nanometres. SPT involves labelling proteins with antibody-coated colloidal gold particles of around 40 nm diameter. The movement of a protein in the plane of the membrane can be tracked due to the light scattering by the gold particle and spatial resolution of a few nanometres can be achieved (Jacobson et al., 1995; Lagerholm et al., 2005). SPT of proteins confined to a 100 nm area of membrane by a laser trap showed that the viscous drag of GPI-APs was greater than that of a transmembrane protein that is excluded from DRMs (Pralle et

al., 2000). This suggests the GPI-APs are part of a larger structure than the transmembrane protein. This study estimated lipid raft size at 52 ± 26 nm in diameter. In another SPT study around a third of Thy-1 and GM1 molecules exhibited confined diffusion in domains of 260 – 330 nm (Sheets et al., 1997). Single molecule tracking of YFP targeted to the membrane by dual palmitoylation and farnesylation also demonstrated confined diffusion of a third of molecules in domains of 200 nm diameter (Lommerse et al., 2004a). The transient confinement of molecules clearly does not agree with the hypothesis that proteins are stably associated with lipid rafts but implies a more dynamic view of membrane microdomains.

These studies demonstrate the range of domain sizes reported. It is possible that the experimental technique employed may influence the size estimate. For example, detectable FRET only occurs if the proteins are < 10 nm apart, thus it is possible that the clusters detected by FRET are present in larger raft structures but are too far apart to produce FRET. The results of SPT studies have been explained by alternative membrane compartmentalisation theories, as discussed below. Furthermore, Kusumi postulates that lipid rafts are very dynamic structures so the time resolution of the technique will be important in determining the results (Kusumi et al., 2004).

### 1.1.3.4. The stability and lifetime of membrane microdomains

The original concept of lipid rafts involved the stable association of protein and lipid molecules due to their preference for the $L_o$ phase over the $L_d$ phase. A more dynamic view of membrane compartmentalisation has emerged from SPT studies. Transient confinement zones (TCZs) have been characterised that share some of the properties that would be expected of $L_o$ domains. However, other evidence suggests that the presence of cytoskeleton-linked membrane fences is the basis for this compartmentalisation or a combination of cholesterol-enriched domains and membrane fences may be involved. The dynamic nature of associations suggests lipid raft-like domains are likely to be small and unstable.

In SPT tracking studies GPI-anchored Thy-1, neural cell adhesion molecule 125 (NCAM125) and also lipid raft marker GM1, showed confined diffusion in 260 – 330 nm domains for periods of 7 – 9 seconds (Sheets et al., 1997; Simson et al., 1995). In support of the idea that these TCZs might represent $L_o$ domains, unsaturated lipid analogues spent less time in TCZs than saturated lipid analogues or lipid raft markers (Dietrich et al., 2002; Schutz et al., 2000; Sheets et al., 1997). Furthermore, inhibition of glycosphingolipid synthesis (Sheets et al., 1997) or depletion of cholesterol (Dietrich et al., 2002) reduced the frequency of transient confinement.

Kusumi and co-workers were able to further dissect the transient confinement of membrane molecules after they achieved the unprecedented SPT time resolution of 25 μs (Fujiwara et al., 2002; Kusumi et al., 2004; Subczynski and Kusumi, 2003). From their observations they developed the concept of hop diffusion. The lipid analogue dioleoyl-phosphatidylethanolamine (DOPE) was transiently confined to 230 nm domains for 11 ms periods before hopping to an adjacent compartment (Fujiwara et al., 2002). These domains appeared to be within larger (730 nm) compartments where molecules were confined for ~ 0.33 seconds. Confinement was dependent on the actin cytoskeleton but not cholesterol. The authors suggest that molecules are confined by fences created by transmembrane proteins anchored to the cytoskeleton, occasionally these fences open enough for a molecule to hop into an adjacent compartment. Confinement of a GPI-AP, CD59 was similar to the unsaturated DOPE and diffusion of both molecules within the TCZs was rapid, which would not be expected if CD59 was part of a large raft structure (Subczynski and Kusumi, 2003). However, crosslinking of CD59 produced a concentration of cholesterol beneath the clusters and a decrease in hop rate. These clusters also appeared to be confined to a different kind of TCZ every 12 hops (every 3.2 seconds). These TCZs were 90 nm in size and dependent on both cholesterol and actin. The authors related these TCZs to those observed by Jacobson and co-workers (Sheets et al., 1997; Simson et al., 1995).

A recent microscopy study employing fluorescence recovery after photobleaching (FRAP) to monitor the diffusion rate of membrane proteins also provided support for the transient interactions with microdomains (Shvartsman et al., 2003). Influenza hemagglutinin (HA) is a transmembrane protein associated with DRMs but wild type HA did not colocalise with a GPI-anchored mutant. However, FRAP reported a decrease in the diffusion rate of wild type HA after crosslinking of GPI-HA. The authors suggest that wild type HA transiently associates with clustered GPI-HA microdomains, retarding its diffusion.

The results of Kusumi and co-workers might appear to disagree with the other SPT and FRAP studies but in fact they report cholesterol dependent confinement of raft marker molecules on the same timescale as observed in other studies (Kusumi et al., 2004). The millisecond timescale hop diffusion described by Kusumi and co-workers is likely to have been missed by previous SPT studies due to limited time resolution. These studies all support a dynamic view of membrane protein compartmentalisation in which both the actin cytoskeleton and transient association with cholesterol-enriched $L_o$ domains may be important.

The results of microscopy studies have led researchers to revise the original lipid raft hypothesis that viewed rafts as large, stable structures that might be up to 1 micron in size (Brown and London, 1997; Brown and Rose, 1992). Reviewers now favour a model in which, consistent with most of the FRET and SPT studies, $L_o$ domains or lipid rafts in the plasma membrane are of the order of nanometres in size, with short (1 ms or less) lifetimes (Hancock, 2006; Kusumi et al., 2004; Kusumi and Suzuki, 2005; Lagerholm et al., 2005; Mayor and Rao, 2004; Subczynski and Kusumi, 2003). Association of membrane proteins with these domains may be random and transient but could be stabilised by clustering of rafts, in response to receptor crosslinking for example (Hancock, 2006; Kusumi et al., 2004; Kusumi and Suzuki, 2005; Lagerholm et al., 2005; Mayor and Rao, 2004; Simons and Vaz, 2004; Subczynski and Kusumi, 2003). The affinity of particular proteins for ordered lipids would still dictate the length of residency in domains and therefore the likelihood of those proteins associating with clustered rafts. In summary, current lipid raft models involve

dynamic microdomains and emphasize the importance of protein-protein interactions in clustering small domains to promote formation of functional signalling platforms.

## 1.1.4. The biological importance of lipid rafts

### 1.1.4.1. Lipid rafts as signalling platforms

The concentration or exclusion of specific signalling proteins in DRMs immediately suggested that lipid rafts could have a role in maintaining signal transduction fidelity (Simons and Ikonen, 1997; Simons and Toomre, 2000; Zajchowski and Robbins, 2002). Early raft models suggested concentration of components of one pathway in a raft and exclusion of negative regulators could increase signal transduction efficiency. More recently raft clustering has emerged as an important concept for explaining how small, transient rafts could be important in organising signalling complexes (Hancock, 2006; Kusumi et al., 2004; Subczynski and Kusumi, 2003).

A vast number of signalling proteins have been reported to associate with lipid raft-like domains, defined by DRM association and/or colocalisation with fluorescent lipid raft markers. Apart from GPI-APs and Src family kinases (discussed in section 1.1.2.2), other examples include G-protein coupled receptors (Chini and Parenti, 2004), voltage gated ion channels (Martens et al., 2004) and components of the insulin signalling pathway (Bickel, 2002; Czech, 2000). Apoptosis regulating proteins Fas and Bad have both been isolated in DRMs and cholesterol depletion affects their functions (Ayllon et al., 2002; Garcia et al., 2003). Lipid raft-like domains also appear to be involved in disease signalling (Simons and Ehehalt, 2002). For example, the GPI-anchored prion protein (PrP) localises to DRMs and disruption of this localisation inhibits the formation of the scrapie PrP isoform (Baron et al., 2002; Marella et al., 2002; Naslavsky et al., 1997; Taraboulos et al., 1995; Vey et al., 1996). Two signalling pathways for which the lipid raft connection has been explored in some detail are highlighted below.

The signalling pathway most comprehensively investigated with respect to lipid raft involvement is T cell receptor (TCR) activation (Harder, 2004; He et al., 2005; Horejsi, 2005; Russell and Oliaro, 2006; Zeyda and Stulnig, 2006). As such it provides a good example of the methodology used to explore the potential role of lipid raft-like domains in a cellular process. Table 1.1 summarises important findings and lists the experimental techniques used in these studies. Both DRM isolation and microscopy have been employed extensively in this research.

The prevailing view of the signalling events initiated by TCR engagement can be summarised as follows (Horejsi, 2005; Zeyda and Stulnig, 2006). When the TCR is engaged by an antigen presenting cell (APC) the tyrosine based activation motifs (ITAMs) in the cytoplasmic tails of the TCR complex become phosphorylated by Src-like kinases Lck and Fyn. The phosphorylated ITAMs recruit ZAP-70 kinase, which in turn phosphorylates Linker for Activation of T cells (LAT). LAT binds several SH-2 domain containing molecules to begin signalling cascades to activate the T cell. Many components of this complex, including the TCR itself, have been isolated in DRMs (see Table 1.1). Both Lyn and LAT are palmitoylated and suggested to rely on this modification for localisation to DRMs and their function in TCR signalling (Harder and Kuhn, 2000; Janes et al., 1999; Kabouridis et al., 1997; Zhang et al., 1998). Microscopy studies have produced more mixed results, some studies have failed to find evidence for TCR complex association with lipid raft markers (Bunnell et al., 2002; Glebov and Nichols, 2004a). More positive results came from a recent study using lipid probe, Laurdan to label ordered membrane domains in the area of the activated TCR complex (Gaus et al., 2005). In addition, a previous study showed that CTXB-mediated clustering of GM1 induced signalling events analogous to those induced by TCR activation, along with co-clustering of TCR components (Janes et al., 1999).

Initial theories about the involvement of lipid rafts in TCR signalling speculated that TCR crosslinking following antigen engagement would lead to clustering with lipid rafts (Horejsi, 2005). Signalling molecules concentrated in rafts could then efficiency

## Table 1.1. Lipid rafts in TCR signalling

| Technique | Observation | Supportive of involvement of lipid raft-like domains? | Reference |
|---|---|---|---|
| DRM isolation | TCR machinery associates with DRMs. | Yes | (Arcaro et al., 2000; Drevot et al., 2002; Janes et al., 1999; Tavano et al., 2004; Xavier et al., 1998) |
| | Engagement or crosslinking of TCR increases its DRM association. | Yes | (Giurisato et al., 2003; Montixi et al., 1998) |
| | Mutant CD45 phosphatase that can not localise to DRMs is incapable of activating Lck. | Yes | (Irles et al., 2003) |
| Cholesterol depletion | Impairment of TCR signalling. | Yes | (Xavier et al., 1998) |
| Mutation of palmitoylation sites | Lck function depends on dual acylation of N-terminus. | Yes | (Janes et al., 1999; Kabouridis et al., 1997) |
| | LAT function impaired. | Yes | (Harder and Kuhn, 2000; Zhang et al., 1998) |
| Immunoisolation of TCR complexes | No enrichment of GM1 or cholesterol in TCR-LAT signalling complexes. | No | (Harder and Kuhn, 2000) |
| Video microscopy | Raft marker GPI-GFP was not incorporated into TCR-LAT complexes following TCR activation. | No | (Bunnell et al., 2002) |
| Fluorescence microscopy | Clustered GM1 colocalised with TCR, Lck and LAT. | Yes | (Janes et al., 1999; Parmryd et al., 2003) |
| | GM1 clustering induced signalling analogous to TCR stimulation. | Yes | (Janes et al., 1999) |
| | TCR engagement caused a redistribution of CTXB-labelled GM1 to the site of engagement. | Yes | (Burack et al., 2002; Viola et al., 1999) |
| FRET | Lipid raft markers did not co-cluster at TCR complex during activation. | No | (Glebov and Nichols, 2004b) |
| Single molecule tracking | CD2 and LAT exhibited confined diffusion but mutation of the LAT palmitoylation site had no effect on diffusion. | No | (Douglass and Vale, 2005) |
| Laurdan imaging | Increased ordering of the membrane around the TCR complex following engagement with APC. | Yes | (Gaus et al., 2005) |

promote signalling cascades, whilst protected from interference by negative regulators such as phosphatases that might partition into non-raft membrane. This view has been revised to accommodate recent results that have emphasized the importance of protein-protein interactions in the formation of the TCR signalling complex (Harder, 2004; Horejsi, 2005; Russell and Oliaro, 2006; Zeyda and Stulnig, 2006). Ordered membrane microdomains (lipid rafts) and cytosketal connections may have roles to play in concentrating components of the complex to increase signalling efficiency.

Whether lipid rafts are large or small, stable or unstable, changing the affinity of a particular protein for $L_o$ domains/lipid rafts could modulate signalling pathways. Several studies suggest that altered affinity for cholesterol dependent microdomains might influence signalling via the small G-protein Ras (Parton and Hancock, 2004). H-Ras and K-Ras are highly homologous but generate distinct signalling effects. The only major difference between the two proteins is their mechanism of anchoring to the inner leaflet of the plasma membrane; H-Ras is farnesylated and dual palmitoylated, whilst K-Ras is farnesylated and has a polybasic sequence that might bind phospholipids. GFP targeted to the membrane via the H-Ras anchor (GFP-tH) was isolated in DRMs and co-clustered with a crosslinked GPI-AP, whilst the GFP targeted by the K-Ras anchor (GFP-tK) was excluded from DRMs (Prior et al., 2001). Electron microscopy studies further demonstrated that immunogold labelled GFP-tK and GFP-tH were in separate clusters on the plasma membrane and only GFP-tH clusters were disrupted by cholesterol depletion (Prior et al., 2003). This segregation appeared to be important in H-Ras function as cholesterol depletion inhibited H-Ras but not K-Ras signalling via Raf (Roy et al., 1999).

It became clear though that simple segregation of H-Ras into lipid raft-like domains and K-Ras into non-raft domains may not be the whole story. Constutively active mutants of H-Ras (H-RasG12V) and K-Ras (K-RasG12V) were excluded from DRMs (Prior et al., 2001) and did not colocalise with GFP-tH (Prior et al., 2003). FRAP studies supported the localisation of GDP-bound H-Ras into cholesterol dependent domains, separate from activated H-Ras (Niv et al., 2002; Prior et al.,

2001; Rotblat et al., 2004). Taken together these data imply that GDP-bound H-Ras is localised in lipid raft-like domains and moves out of these domains on activation (Parton and Hancock, 2004). Importantly, it appears that association with lipid raft like domains has a negative regulatory effect on H-Ras signalling as localisation outside these domains is necessary for efficient signalling (Jaumot et al., 2002).

#### 1.1.4.2. Coupling of lipid rafts between the two leaflets of the bilayer

An extremely important and under investigated question in lipid raft biology is whether lipid rafts in the outer leaflet of the plasma membrane bilayer couple to lipid rafts in the inner leaflet (Brown and London, 1997; Devaux and Morris, 2004; Edidin, 2003; Kusumi et al., 2004; Lommerse et al., 2004b; Rietveld and Simons, 1998). Coupling would clearly be necessary to produce specificity in lipid raft mediated intracellular signalling.

The plasma membrane exhibits asymmetry in the distribution of lipid species between the two leaflets (Op den Kamp, 1979). The inner leaflet is rich in unsaturated phosphophatidylserine (PS) and phosphophatidylethanolamine (PE), which is actively translocated there from the outer leaflet, and sphingolipids are concentrated in the outer leaflet, probably due to passive flipping to replace the lost PE (Devaux, 1991). The partitioning of cholesterol is somewhat unclear but a significant proportion may be present in the inner leaflet (Edidin, 2003). The low concentration of sphingolipids makes it unlikely that $L_o$ domains would occur in the inner leaflet. In a model membrane system mimicking the inner leaflet of the plasma membrane Wang and Silvius failed to find any evidence for $L_o$ domain formation (Wang and Silvius, 2001). However, there is evidence from DRM and microscopy studies to support the localisation of inner leaflet proteins to cholesterol-enriched microdomains, as described in preceeding sections.

How then could coupling of these proteins to lipid rafts in the outer leaflet be achieved? A popular view is that interdigitation of long, extended acyl chains from sphingolipids into the inner leaflet might cause an ordering of inner leaflet lipids

below outer leaflet rafts (Brown and London, 1997; Devaux and Morris, 2004; Kusumi et al., 2004; Rietveld and Simons, 1998). Alternatively, Devaux points out that a mismatch in lipid density between the leaflets has been shown to result in membrane curvature (Baumgart et al., 2003; Devaux and Morris, 2004). Constraints on the membrane due to cytoskeletal attachments might then force the inner leaflet to conform to the higher density, ordered packing of the outer leaflet lipid raft (Devaux and Morris, 2004).

Whilst the mechanism for inner leaflet coupling is a mystery there is some evidence to support its existence. A number of microscopy studies have visualised a co-redistribution of inner leaflet proteins (usually GFP or YFP targeted to the membrane via the dual acylated anchor of H-Ras or Lyn kinase) in response to crosslinking of GPI-APs or GM1 (Baumgart et al., 2003; Gri et al., 2004; Harder et al., 1998; Janes et al., 1999; Stauffer and Meyer, 1997). Pyenta and co-workers used cross correlation spectroscopy to quantify co-redistribution of labelled membrane proteins (Pyenta et al., 2001). Cross correlation spectroscopy correlates spatial and temporal fluctuations in fluorescent signals from multiple probes to follow the movement of groups of labelled molecules in relation to each other (Lagerholm et al., 2005). Pyenta and co-workers demonstrated that GFP anchored to the membrane via the Lyn kinase anchoring signal co-redistributed with crosslinked FcεRI to a greater extent than prenylated GFP (that is not predicted to partition into ordered domains). The redistribution was not specific to FcεRI as crosslinking of GPI-AP, Thy-1 or GM1 via CTXB produced the same result. Janes and co-workers observed stimulation of TCR signalling events mediated by crosslinking of GM1, encouraging evidence that this coupling is functional (Janes et al., 1999).

Rietveld and Kusumi both point out that even if lipid raft clustering brings together GPI-APs and inner leaflet dual-acylated kinases these proteins are still separated from each other across the bilayer (Kusumi et al., 2004; Rietveld and Simons, 1998). They suggest that transmembrane adaptor proteins may be required for GPI-AP signalling. Glial derived neurotropic factor (GNDF) signalling provides an example for this hypothesis (Saarma, 2001; Simons and Toomre, 2000). GDNF is important in

the development of the nervous system and binds the GPI-anchored GDNF receptor α (GFRα). On stimulation with GDNF the transmembrane protein c-Ret translocates into DRMs and brings dual-acylated Src kinase into a complex with GFRα (Paratcha et al., 2001; Tansey et al., 2000). Cholesterol depletion reduces GDNF signalling (Tansey et al., 2000).

### 1.1.4.3. Lipid rafts in membrane trafficking

Studies concerning the preferential sorting of GPI-APs to the apical membrane of polarised epithelial cells provided the first indication that cholesterol and sphingolipid-rich microdomains might have a function in cell biology (Brown and Rose, 1992; Schuck and Simons, 2004). Further studies have implicated raft-like microdomains in apical protein sorting, though other sorting determinants such as N-linked glycans are also important (Benting et al., 1999; Ikonen, 2001; Lipardi et al., 2000; Schuck and Simons, 2004).

More recently caveolae and lipid rafts have been implicated in a clathrin-independent form of endocytosis, that internalises proteins into separate endosomal compartments termed caveosomes (Nabi and Le, 2003; Nichols, 2003; Parton and Richards, 2003). Many molecules demonstrated to be internalised by a clathrin-independent route are also found in DRMs and their internalisation is blocked by cholesterol depletion (Di Guglielmo et al., 2003; Lamaze et al., 2001; Le and Nabi, 2003; Minshall et al., 2000; Nichols et al., 2001; Puri et al., 2001; Venkatesan et al., 2003). Importantly, clathrin-independent endocytosis of DRM-associating proteins (e.g. GPI-APs) has been demonstrated in cells that lack caveolae (Lamaze et al., 2001; Sabharanjak et al., 2002). These results led to the conclusion that other lipid raft-like domains, not just caveolae, could mediate endocytosis.

Phosphorylation by Src-like kinases and the action of the GTPase dynamin have both been reported to be required for caveolar mediated endocytosis. Tyrosine kinase inhibitors (Le and Nabi, 2003; Puri et al., 2001; Tiruppathi et al., 1997) and an

inactive mutant of dynamin (Lamaze et al., 2001; Le and Nabi, 2003; Oh et al., 1998; Puri et al., 2001) both inhibit this pathway. In addition, dynamin has been observed at the necks of caveolae (Henley et al., 1998; Oh et al., 1998). However, not all clathrin-independent endocytosis conforms to these criteria, leading Nichols to suggest that caveolar/lipid raft mediated endocytosis should not viewed as a single pathway as it seems that putative lipid raft proteins are not necessarily constrained to a particular route (Nichols, 2003).

The involvement of lipid rafts and caveolae in exocytosis has not been studied as extensively as their role in endocytosis but some evidence suggests a link (Salaun et al., 2004a). SNARE (soluble NSF (N-ethyl-maleimide-sensitive fusion protein) attachment receptor) proteins are established as essential components in the fusion of membrane vesicles (Chen and Scheller, 2001; Jahn et al., 2003; Lin and Scheller, 2000). Membrane fusion is thought to be driven by the formation of a trans-complex between SNARE proteins that are inserted into the cytoplasmic face of the plasma membrane and those in the vesicle membrane. Stuctural studies have suggested that four coil domains contributed by the three SNARE proteins zip up to form a four α-helix bundle, bringing the two membranes into close apposition (Sutton et al., 1998).

DRM association has been reported for members of the syntaxin and SNAP-25 families of plasma membrane associated SNAREs in a number of cell types (Chamberlain et al., 2001; Chamberlain and Gould, 2002; Foster et al., 2003; Pombo et al., 2003; Predescu et al., 2005; Salaun et al., 2005a; Salaun et al., 2005b) and also brain synaptosomes (Gil et al., 2005; Taverna et al., 2004). DRM association appears to be SNARE isoform specific, for example a larger proportion of SNAP-23 than SNAP-25 localised to DRMs in 3T3-L1 adipocytes (Chamberlain and Gould, 2002) and different syntaxin isoforms associated with DRMs to varying degrees in RBL mast cells (Pombo et al., 2003). Could lipid raft-like microdomains then constitute the site for vesicle fusion at the plasma membrane? Tentative support for this idea came from the findings that cognate SNARE complexes consisting of syntaxin-3, SNAP-23 and vesicle associated membrane protein (VAMP/synaptobrevin) were

enriched in DRMs (Gil et al., 2005; Pombo et al., 2003) and the syntaxin1a/SNAP-25 binary complex was present in PC12 cell DRMs (Chamberlain et al., 2001).

Microscopy studies have demonstrated a high degree of colocalisation between SNAREs and raft markers Thy-1 (Aoyagi et al., 2005) and caveolin-1 (Predescu et al., 2005). However, other studies reported no colocalisation of these markers with syntaxin1a (Lang et al., 2001; Low et al., 2006; Ohara-Imaizumi et al., 2004), though cholesterol depletion was shown to disperse syntaxin1a clusters (Lang et al., 2001), syntaxin3 and SNAP-23 clusters (Predescu et al., 2005). In model membranes syntaxin1a and synaptobrevin (VAMP) segregated away from $L_o$ domains detected by CTXB-labelling or atomic force microscopy (Bacia et al., 2004; Saslowsky et al., 2003).

Cholesterol depletion has been shown to inhibit or reduce regulated exocytosis, providing strong support for the involvement of cholesterol-rich microdomains (Chamberlain et al., 2001; Churchward et al., 2005; Gil et al., 2005; Lang et al., 2001; Ohara-Imaizumi et al., 2004). However, a recent study calls into question the simplicity of this conclusion. Salaun *et al* found that mutation of cysteines at putative palmitoylation sites in SNAP-23 decreased its affinity for DRMs (Salaun et al., 2005a). The ability of various SNAP-25 and SNAP-23 constructs to support exocytosis was then tested in a PC12 cell line stably expressing botulinum neurotoxin that cleaves wild type SNAP-25, inhibiting regulated exocytosis (Salaun et al., 2005b). Mutants with decreased affinity for DRMs had an increased ability to support exocytosis. These results suggest that localisation of SNAREs to DRMs could negatively regulate exocytosis. The localisation of SNAREs to lipid raft-like domains and the role that these domains might play in regulated exocytosis await further clarification.

## 1.2. 14-3-3 PROTEINS

14-3-3 proteins primarily bind phosphoserine or phosphothreonine motifs and are generally classified as signalling adaptor proteins. Since the first identification of a function for this family of proteins in the late 1980s, the investigation of 14-3-3 proteins has expanded to become a very broad field, encompassing studies in an array of eukaryotic organisms and intracellular signalling processes. Numerous functions have been ascribed to 14-3-3 and the list of interacting partners continues to grow. Over one hundred 14-3-3 interacting proteins have been confirmed (Aitken et al., 2002) and two recent proteomic studies each identified around two hundred potential 14-3-3 ligands (Jin et al., 2004; Pozuelo Rubio et al., 2004). This section aims to give a brief introduction to this important family of regulatory proteins and highlight some interesting aspects of their biological function.

### 1.2.1. Identification and characterisation of 14-3-3 proteins

14-3-3 proteins were first identified by Moore and Perez in 1967 from a screen of brain proteins (Moore and Perez, 1967). They are a family of small, acidic proteins with a molecular mass of 28 – 33 kDa. The enigmatic name 14-3-3 derives from their elution fraction numbers from the 2D DEAE-cellulose chromatography and starch gel electrophoresis procedures from which they were first puirfied. However, it was not until much later that any function was identified for 14-3-3. The first property discovered was the ability to activate tyrosine and tryptophan hydroxylases (Ichimura et al., 1987; Yamauchi et al., 1981). Following this, Aitken and co-workers identified 14-3-3 as an inhibitor of protein kinase C (PKC) (Toker et al., 1992). Since these early studies many and varied functions have been ascribed to 14-3-3 proteins, including cell cycle regulation, modulation of transcription, inhibition of apoptosis and regulation of intracellular signalling pathways, to name but a few (Aitken, 2006; Berg et al., 2003; Dougherty and Morrison, 2004; Muslin and Xing, 2000; Rosenquist, 2003).

The five major mammalian brain 14-3-3 isoforms, β, ε, γ, η and ζ, were originally identified by Ichimura and co-workers (Ichimura et al., 1988). This study purified two further isoforms that the authors named α and δ, which were later identified as phosphorylated forms of β and ζ respectively (Aitken et al., 1995b). Two other isoforms, τ and σ were found to be expressed in T cells (Nielsen, 1991) and epithelial cells (Leffers et al., 1993; Prasad et al., 1992) respectively, though τ was also detected in a wide range of tissue including brain. 14-3-3 σ appears to be specific to epithelial cells. The existence of seven mammalian isoforms poses questions about possible isoform specific functions but few studies address this point thoroughly. An important observation in characterisation of 14-3-3 was that it exists as a dimer (Jones et al., 1995a; Jones et al., 1995b), leading to the proposal that 14-3-3 might act as a molecular scaffold to bring together two signalling proteins (Jones et al., 1995a; Morrison, 1994).

#### 1.2.1.1. 14-3-3 ligand binding

The first indication that 14-3-3 proteins bound phosphoserine/threonine (pS/T) motifs came from the observation that 14-3-3 mediated activation of tyrosine hydroxylase required prior phosphorylation by a serine/threonine kinase (Furukawa et al., 1993). Subsequently, it was found that phosphatase treatment inhibited the binding of Breakpoint Cluster Region (BCR) kinase and Raf-1 to 14-3-3 (Michaud et al., 1995). This study also identified serine 259 of Raf-1 as essential for 14-3-3 binding. Muslin and co-workers built on this work with the finding that 14-3-3 ζ bound directly to a peptide encompassing the sequence around the critical Raf-1 S259; importantly PKA phosphorylation of the peptide was necessary for this interaction (Muslin et al., 1996). The authors noted that three 14-3-3 binding partners, Raf-1, Cdc25C and polyoma virus middle T antigen, all contain a sequence based on the motif RSXSXP (where X = any amino acid). A degenerate peptide library was constructed based on the Raf-1 phosphorylated peptide to test the contribution of each amino acid to binding specificity. This led to the definition of RSXpSXP as the consensus sequence for binding to 14-3-3 protein.

The sequence RSXpSXP soon became known as the mode I motif, following a study by Yaffe and co-workers identifying a second consensus motif (mode II) as RXXXpSXP (Yaffe et al., 1997). Degenerate peptide libraries were again employed to define the amino acid preferences at the X positions in both mode I and mode II motifs. Mode I was refined to R-S-(+/Ar)-pS-(L/E/A/M)-P and mode II to the highly related sequence R-X-(Ar)-(+)-pS-(L/E/A/M)-P (Ar = aromatic amino acid, + = positive amino acid). The definition of these motifs was extremely useful in the search for novel potential 14-3-3 interacting proteins. However, it soon became clear that not all 14-3-3 binding partners bind via these optimal motifs. For example, p53 and proto-oncogene Cbl interact with 14-3-3 via serine phosphorylated motifs that deviate from the mode I and II consensus sequences (Liu et al., 1997; Waterman et al., 1998). Very recently a mode III consensus motif was defined as (pS/pT)$X_{1-2}$-COOH, following investigation of 14-3-3 binding to serotonin N-acetyl-transferase (AANAT) (Ganguly et al., 2005). This novel mode of 14-3-3 binding to the C-terminus of a protein is also employed by the potassium channel Kir2.1, with the motif SWpTY at its extreme C-terminus (Coblitz et al., 2005).

Though most 14-3-3 interactions appear to depend on pS/T motifs, non-phosphorylated interaction motifs have also been identified. The adenosine diphosphate-ribosylase exoenzyme S from *Pseudomonas aeruginosa* bound to 14-3-3 with affinity comparable to optimal mode I and II peptides but no phosphorylation sites were identified by mass spectrometry (Masters et al., 1999). Interestingly, the phosphorylated Raf-1 peptide was able to compete with exoenzyme S for binding to 14-3-3, suggesting that this non-phosphorylated motif used the same binding site as phosphorylated motifs. The sequence DALDL was identified as critical for the interaction with 14-3-3 (Henriksson et al., 2002). Screening of a phage display library by Fu and co-workers led to the isolation of a high affinity 14-3-3 binding peptide named R18, which bound via the similar WLDLE motif (Wang et al., 1999). Whilst the binding of 14-3-3 to phosphorylated motifs displays some sequence specificity it seems that the range of sequences able to mediate interactions with 14-3-3 are more diverse that originally suspected.

### 1.2.1.2. 14-3-3 protein structure

The first crystal structures of 14-3-3 protein were solved in 1995, using 14-3-3 τ and ζ isoforms (Liu et al., 1995; Xiao et al., 1995). Since then the structures of all seven isoform homodimers, in complex with bound peptide ligands, have been elucidated. The first crystal structures confirmed the dimeric nature of 14-3-3 proteins and showed that each monomer was cup shaped, with a central channel 35 Å long, 35 Å wide and 20 Å deep (see figure 1.4). The monomers are composed of nine anti-parallel α-helices, the N-terminal four forming the dimer interface and the floor of the central channel. Subsequent studies showed that all isoforms are very similar in structure, as would be expected from the high degree of sequence homology (Gardino et al., 2006).

The general consensus is that all 14-3-3 ligands are likely to bind via the central channel, also known as the amphipathic binding groove. In co-crystal structures with either phosphopeptides (Liu et al., 1995; Petosa et al., 1998; Rittinger et al., 1999; Yaffe et al., 1997) or non-phosphorylated peptides (Petosa et al., 1998), the ligand is always bound within the amphipathic binding groove. Furthermore, mutations within this groove have been shown to disrupt interactions with various proteins (Wang et al., 1998; Zhang et al., 1997). The binding groove contains a basic pocket composed of a lysine residue plus two arginine residues that contact the phosphorylated serine or threonine on the peptide (see figure 1.4). Elkins and co-workers solved the co-crystal structure of 14-3-3 β in the presence of a non-phosphorylated peptide representing the 14-3-3 binding motif from the adenosine diphosphate-ribosylase exoenzyme S (Elkins et al., 2005). This structure showed that an aspartate side chain in this peptide partially mimics the phosphate group, explaining how both phosphorylated and non-phosphorylated peptides can use the same binding site (Gardino et al., 2006). Residues involved in target binding in the amphipathic groove are highly conserved between organisms and also isoforms within a genome, suggesting that the mode of binding is conserved (Gardino et al., 2006; Rosenquist et al., 2000). This also means that any isoform specificity must derive from interactions with residues outside the binding groove that are more variable between sequences.

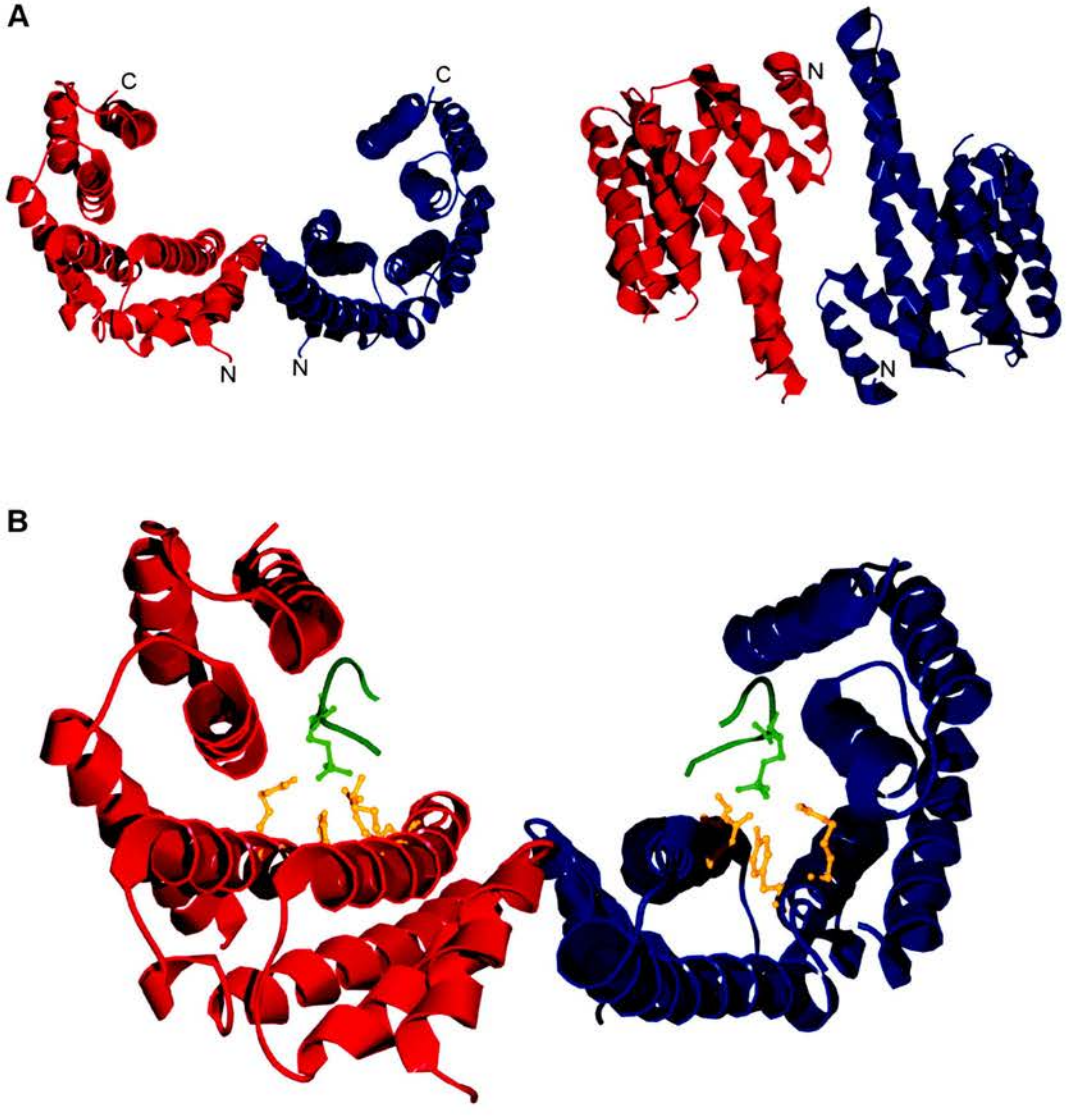


**Figure 1.4. 14-3-3 ζ crystal structure**

Ribbon representations of 14-3-3 ζ dimer with monomer backbones coloured red and blue. **A** Views of the 14-3-3 dimer with the N termini of each monomer labelled. The sequence at the very C-terminus was not resolved but the C-terminal end of the determined structure is labelled. The image on the right is rotated 90° about the horizontal axis relative to the image on the left to show the dimer interface. **B** The 14-3-3 dimer in the presence of bound phosphopeptides (green). The phosphoserine (bright green) is coordinated by lysine 49, arginine 56, arginine 127 and tyrosine 128 (gold), which make up the basic binding pocket. Structure solved by Rittinger *et al* (1999). PDB file 1QJA was obtained from www.rcsb.org/pdb and manipulated using Swiss-Pdb viewer (GSK R&D and the Swiss Institute of Bioinformatics).

One structural study managed to produce a co-crystal structure of 14-3-3 ζ in complex with a protein ligand, serotonin N-acetyltransferase (AANAT) (Obsil et al., 2001). AANAT also binds to 14-3-3 via a phosphorylated motif that contacts the amphipathic binding groove. In all the crystal structures where 14-3-3 is bound to ligand, including the one with AANAT, the 14-3-3 dimer maintains the same structure as in the absence of ligand. Yaffe suggests that the structural rigidity of 14-3-3 protein may constrain binding partners to a more or less active conformation that might otherwise not be favoured (Yaffe, 2002). Dual 14-3-3 binding sites on one protein might aid this process by each binding to one groove on the 14-3-3 dimer. Yaffe's 'molecular anvil' hypothesis is supported by the study of AANAT. Whilst 14-3-3 was unchanged, the conformation of AANAT seems to be stabilised in a more active conformation and its catalytic activity was in fact increased (Obsil et al., 2001). However, this represents only one mechanism by which 14-3-3 might affect protein function; altering the subcellular localisation of proteins also appears to be an important mechanism and will be discussed in later sections.

#### 1.2.1.3. 14-3-3 proteins are evolutionarily conserved

14-3-3 proteins are ubiquitous to all eukaryotic organisms investigated so far and most genomes contain more than one 14-3-3 isoform. Alignment of 153 14-3-3 protein sequences from 48 species showed a high degree of sequence conservation and suggested that all 14-3-3 genes derive from a common ancestor (Aitken et al., 1992; Rosenquist et al., 2000; Wang and Shakes, 1996). Gene duplication events are thought to have produced different isoforms only after the divergence of the four eukaryotic kingdoms. An extremely high degree of sequence homology (96 – 100 %) is observed between the same isoform in different mammalian species, whereas the difference between isoforms within the same genome can be up to 46 % (Rosenquist et al., 2000). This indicates that the divergence of 14-3-3 isoforms took place prior to mammalian speciation and that the isoforms are highly conserved for functional reasons.

Comparison of the sequence alignments with crystal structures of 14-3-3 illustrated that particular residues are conserved for structural reasons (Rosenquist et al., 2000; Wang and Shakes, 1996). Many of the conserved residues are on α-helices facing the interior of the protein and therefore contributing to 14-3-3 monomer stabilisation. Specific residues at the N-terminal dimer interface are also highly conserved. In addition, many residues within the amphipathic binding groove are highly conserved, suggesting that all 14-3-3 proteins bind ligands in a similar fashion.

From phylogenetic trees constructed for the mammalian isoforms it was evident that γ and η are the most highly related isoforms in terms of sequence, probably deriving from a common ancestor (Rosenquist et al., 2000; Wang and Shakes, 1996). The 14-3-3 β, τ, σ and ζ isoforms likely originate from another single common ancestor, though the sequence of 14-3-3 σ is distinct compared with the other three isoforms. 14-3-3 ε shares the least sequence identity with the other mammalian isoforms and in fact is more similar to plant and yeast 14-3-3 proteins at certain positions. 14-3-3 ε is therefore viewed as an ancestral 14-3-3 isoform, presumably conserved because it performs some essential function that can not be fulfilled by the other isoforms (Rosenquist et al., 2000).

#### 1.2.1.4. Localisation of 14-3-3 proteins

14-3-3 protein has been detected in a wide array of mammalian tissues (Celis et al., 1990) but is particularly abundant in brain tissue, where it makes up ~ 1 % of total soluble protein (Boston et al., 1982). Only 14-3-3 σ shows any tissue specific expression, being detected only in epithelial tissues (Leffers et al., 1993). 14-3-3 proteins show a predominantly cytoplasmic localisation (Martin et al., 1994; Muslin and Xing, 2000) but have also been isolated in plasma membrane preparations (Freed et al., 1994; Martin et al., 1994; Mineo et al., 1996) and reported to associate with the Golgi apparatus (Leffers et al., 1993).

The high level of 14-3-3 expression in brain implies that it performs important functions there. Thus it is perhaps not surprising that 14-3-3 might also play a role in aberrant brain function; its involvement in a number of neurodegenerative disorders has been reported (Berg et al., 2003; Dougherty and Morrison, 2004). 14-3-3 was identified in the cerebrospinal fluid (CSF) of Creuzfeldt-Jakob disease (CJD) patients in a screen for surrogate markers to allow pre-mortem diagnosis of CJD (Harrington et al., 1986; Hsich et al., 1996). It was originally suggested that the abundance of 14-3-3 in brain, coupled with tissue destruction might explain its appearance in the CSF. However, the concentration of 14-3-3 in the CSF of CJD patients is significantly higher than in the CSF of patients with other neurodegenerative disorders (Kenney et al., 2000). Furthermore, only 14-3-3 β, ε, γ and η but not 14-3-3 τ or ζ are found in CJD CSF despite similar expression levels in brain (Wiltfang et al., 1999). Many studies support the use of 14-3-3 as a marker for CJD (Beaudry et al., 1999; Lemstra et al., 2000; Zerr et al., 1998) and in 1998 the World Health Organisation included a positive result for 14-3-3 in the criteria for diagnosis of sporadic CJD (Green, 2002). However, the molecular link between 14-3-3 and CJD pathology remains to be elucidated.

14-3-3 has also been identified in Lewy bodies of Parkinson's disease (Kawamoto et al., 2002; Ubl et al., 2002) and the neurofibrillary tangles of Alzheimer's disease (Layfield et al., 1996). 14-3-3 binds to α-synuclein (Ostrerova et al., 1999), one of the main components of Lewy bodies and Berg *et al* suggest that α-synuclein may sequester 14-3-3 in Lewy bodies, preventing 14-3-3 from carrying out its important anti-apoptotic functions (Berg et al., 2003). A recent study indicated the molecular basis of 14-3-3 involvement in Alzheimer's disease (Agarwal-Mawal et al., 2003). The microtubule binding protein tau forms neurofibrillary tangles when hyperphosphorylated. 14-3-3 brings glycogen synthase kinase 3β into association with tau, facilitating phosphorylation of tau. In addition, 14-3-3 may protect tau from dephosphorylation. Lastly, 14-3-3 has been implicated in spinocerebellar ataxia-1 (SCA-1). In SCA-1 the protein ataxin-1 acquires an expanded polyglutamine tract and its accumulation in neurons leads to degeneration. 14-3-3 is reported to stabilise

the mutant expanded ataxin-1 and prevent its normal degradation (Chen et al., 2003a).

## 1.2.2. 14-3-3 Isoforms

### 1.2.2.1. Dimerisation and phosphorylation of 14-3-3 isoforms

The crystal structure of 14-3-3 τ confirmed that 14-3-3 proteins exist as dimers (Xiao et al., 1995), as indicated by earlier biochemical studies (Jones et al., 1995b). Recombinant 14-3-3 proteins are always dimeric, suggesting that the monomeric form is not thermodynamically favourable (Aitken et al., 2002).

Jones and co-workers first showed that 14-3-3 isoforms not only homodimerise but have the capacity to heterodimerise (Jones et al., 1995a). In vitro, bacterially expressed 14-3-3 τ was able to dimerise with itself and the 14-3-3 ζ isoform. In COS cells, myc-tagged 14-3-3 ε co-immunoprecipitated the 14-3-3 ζ isoform when this protein was also overexpressed. Little endogenous 14-3-3 protein could be co-immunoprecipitated with the myc-14-3-3 ε, leading the authors to suggest that 14-3-3 proteins form stable dimers that do not readily exchange. More detailed studies of 14-3-3 dimerisation preferences were therefore carried out in PC12 cell lines stably transfected with myc-tagged 14-3-3 isoforms ε and γ (Chaudhri et al., 2003). 14-3-3 γ mainly formed homodimers, though some heterodimerisation with other isoforms, especially 14-3-3 ε, was also detected. In contrast, 14-3-3 ε showed a preference for heterodimerisation; 14-3-3 β, γ, η and ζ all dimerised with 14-3-3 ε. However, 14-3-3 ε homodimers were not detected. Recent structural studies shed some light on the propensity of 14-3-3 ε to form heterodimers. 14-3-3 ζ homodimers are stabilised by three salt bridges in each half of the dimer interface. However, only one of these salt bridges is present in the ε homodimers. Gardino and co-workers therefore suggest that 14-3-3 ε may preferentially dimerise with other isoforms to increase the number of salt bridges stabilising the dimer interface (Gardino et al., 2006).

The tendancy of 14-3-3 isoforms to heterodimerise appears to be a conserved feature of this protein family as 14-3-3 homologues from *Sacchromyces cerevisiae*, BMH1 and BMH2 were also present mainly as heterodimers (Chaudhri et al., 2003). Aitken and co-workers suggest that heterodimers may function in bringing together two signalling proteins that bind specifically to different 14-3-3 isoforms (Aitken et al., 2002). Homodimers may instead function in altering the cellular localisation or activity of particular proteins.

Phosphorylation of particular 14-3-3 isoforms was first reported when the α and δ isoforms were identified as phosphorylated forms of β and ζ respectively (Aitken et al., 1995b); however, the important functional implications of 14-3-3 phosphorylation have only recently become clear. All seven 14-3-3 isoforms do not contain the same phosphorylation sites; phosphorylation therefore represents an isoform specific regulatory mechanism.

Following their idenitification of phosphorylated 14-3-3 β and ζ in brain tissue Aitken and co-workers found that the phosphorylated forms enhanced the ability of 14-3-3 to inhibit protein kinase C (PKC) two-fold (Aitken et al., 1995a). They went on to define the phosphorylation site as serine 185 in both β and ζ isoforms (Aitken et al., 1995b). Gotoh and co-workers recently discovered that the stress activated Jun N-terminal kinase (JNK) phosphorylates 14-3-3 β, σ and ζ on serine 185 (Tsuruta et al., 2004). This has extremely important consequences for the regulation of apoptosis. Phosphorylation of 14-3-3 σ and ζ by JNK disrupts their interaction with pro-apoptotic proteins Bax, Bad and c-Abl, releasing these proteins from sequestration in the cytoplasm to induce pro-apoptotic signalling (Sunayama et al., 2005; Tsuruta et al., 2004; Yoshida et al., 2005).

Phosphorylation of 14-3-3 τ and ζ, on serine 233 and threonine 233 respectively, is mediated by casein kinase Iα (Dubois et al., 1997) and breakpoint cluster region kinase (Clokie et al., 2005). Phosphorylation of this site appears to be specific to 14-3-3 τ and ζ isoforms. The authors of these studies concluded that phosphorylation of

14-3-3 ζ on T233 is likely to negatively regulate interaction with Raf-1 as only the unphosphorylated form of 14-3-3 ζ bound to Raf-1 in HEK 293 cells (Rommel et al., 1996).

There have been a number of reports of phosphorylation of serine 58 by kinases including protein kinase A (PKA), caspase-cleaved PKCδ and protein kinase B (PKB)/Akt (Hamaguchi et al., 2003; Ma et al., 2005; Megidish et al., 1998; Powell et al., 2002; Woodcock et al., 2003). Serine 58 is buried within the dimer interface and thus would not be expected to be exposed due to the stable nature of the 14-3-3 dimer. However, Woodcock and co-workers provide evidence that phosphorylation of this residue negatively regulates dimer formation (Woodcock et al., 2003). The monomeric versus dimeric status of 14-3-3 is likely to have functional consequences for intact protein ligands.

#### 1.2.2.2. Functional specificities of the different 14-3-3 isoforms

Most organisms so far investigated express more than one homologue of the 14-3-3 family, from two isoforms in *Saccharomyces cerevisiae* to at least twelve in *Arabidopsis thaliana*. The evolutionary conservation of multiple isoforms could be explained in a number of ways, as discussed by Rosenquist (Rosenquist et al., 2000). Firstly, the isoforms may be functionally redundant but provide a mechanism for ensuring availability of high quantities of an extremely important protein. Secondly, the different isoforms may be specifically expressed in different tissues or be targeted to different subcellular locations. Finally, each isoform might interact specifically with a subset of 14-3-3 binding partners, which would help to explain the incredible diversity observed in 14-3-3 functions.

Two studies with *Arabidopsis thaliana* 14-3-3 isoforms provided some initial support for the theory of functional isoform specificity. There were strong differences between the ability of five isoforms to inhibit nitrate reductase (Bachmann et al., 1996) and nine isoforms exhibited different affinities for a peptide from the C-

terminus of plant plasma membrane $H^+$-adenosine triphosphatase (Rosenquist et al., 2000). In direct contrast to the second study, Yaffe and co-workers observed no isoform specificity when investigating the binding of mammalian and yeast isoforms to optimal peptide motifs (Yaffe et al., 1997). However, it may be that isoform specificity is not observed in all interactions. The recent production of a 14-3-3 γ knockout mouse does support at least a degree of functional redundancy within the 14-3-3 family; no differences in behaviour, anatomy or survival rates were reported compared with normal mice (Steinacker et al., 2005). Also, no upregulation of other 14-3-3 genes was detected in the brain tissue. It would perhaps be more interesting to silence or knockout combinations of highly related isoforms, e.g. 14-3-3 γ and η or 14-3-3 β and ζ, that might have overlapping specificities.

The question of isoform specificity has been addressed with respect to particular protein interactions in mammalian cells, listed in table 1.2. The experiments generally involved a combination of yeast two hybrid screens, co-immunoprecipitation and 'pull down' assays to identify 14-3-3 isoform binding. The study of isoform specificity is complicated by the fact that most isoforms appear to be able to heterodimerize, as discussed in section 1.2.2.1. Therefore most studies have chosen to overexpress particular isoforms to produce homodimers. From a functional perspective it would clearly be interesting to investigate the specificity of particular heterodimers but this kind of study is much more challenging. Unfortunately, most of these studies have only investigated a few isoforms, rather than all seven and the majority of reports do not investigate isoform specificity at all. This is certainly a neglected area of 14-3-3 biology but results presented in table 1.2, though incomplete, provide some interesting initial indications about mammalian isoform specificity. Firstly, it is clear that some isoform specificity seems to exist for particular interactions, though usually more than one isoform can bind a certain protein but perhaps with different affinities. This point is illustrated by the studies of A20, A disintegrin and metalloproteinase 22 (ADAM22), calcium/calmodulin-dependent kinase kinase (CAMKK) and protein kinase C ζ (PKCζ).

In table 1.2 the 14-3-3 isoforms are grouped in columns according to the degree of sequence homology, as discussed in section 1.2.1.3. 14-3-3 γ and η are the most highly related isoforms and form a distinct branch from β, τ and ζ on phylogenetic trees. 14-3-3 β, τ and ζ are highly related to each other and less so to the σ isoform. The ε isoform shares the least sequence similarity with the other isoforms. CAMKK and PKCζ show similar levels of binding to 14-3-3 γ and η. However, despite the high degree of sequence similarity between 14-3-3 γ and η, both A20 and ADAM22 bind to 14-3-3 η but not 14-3-3 γ. These proteins instead show some affinity for the 14-3-3 β, ε and ζ isoforms. Thus it appears that 14-3-3 γ and η do not always share functions as might be expected. 14-3-3 β and ζ seem to be more consistent in binding to the same proteins, though PKCζ provides one example where this is not the case. Interestingly, the 14-3-3 ε isoform seems to have properties overlapping with other isoforms with respect to many interactions, though this isoform shows the lowest level of sequence similarity with the others. Perhaps 14-3-3 ε specific functions remain to be discovered.

14-3-3 σ also shows a relatively low level of sequence identity with the other isoforms and appears to have unique functions in cell cycle regulation. 14-3-3 σ co-immunoprecipitates as a complex with Cdc2 and cyclin-B1and knocking out 14-3-3 σ in colorectal carcinoma cells permits inappropriate localisation of Cdc2/cyclin-B1 to the nucleus, leading to cell death by mitotic catastrophe (Chan et al., 1999). Though binding of other 14-3-3 isoforms to cdc2/cyclin-B1 has not been investigated, other isoforms present in 14-3-3 σ -/- cells do not seem to be able to compensate for the loss of 14-3-3 σ. In addition, 14-3-3 σ is unable to bind to CDC25C in contrast to other isoforms (Chan et al., 1999; Dalal et al., 2004). Recent structural studies of 14-3-3 σ provide some explanation for its isoform specific function (Benzinger et al., 2005; Wilker et al., 2005). Wilker and co-workers noted that particular residues that make important contacts in the binding of 14-3-3 ζ to AANAT are conserved in all 14-3-3 isoforms except 14-3-3 σ. Mutation of these divergent residues in 14-3-3 σ to a sequence matching that of the 14-3-3 ζ isoform allowed 14-3-3 σ to bind to CDC25C (Wilker et al., 2005). Thus, these residues

**Table 1.2. Isoform specific 14-3-3 interactions**

| Protein | Function | 14-3-3 isoforms bound | | | | | | | Reference |
|---|---|---|---|---|---|---|---|---|---|
| | | γ | η | β | ζ | τ | σ | ε | |
| A20 | Inhibitor of TNF-induced apoptosis | x | √√√ | √ | √ | - | - | √√ | (Vincenz and Dixit, 1996) |
| ADAM22 | Cell adhesion and spreading | x | √ | √√ | √√ | x | x | √ | (Zhu et al., 2005; Zhu et al., 2003) |
| AKAP-Lbc | PKA-anchoring protein and Rho-GEF | - | - | √ | √ | - | - | √ | (Diviani et al., 2004) |
| Ataxin-1 | Mutated protein in polyglutamine repeat disease, SCA-1 | - | - | √ | √ | - | - | √ | (Chen et al., 2003a) |
| CAMKK | Calcium/calmodulin-dependent kinase kinase | √√ | √√ | - | √ | x | - | x | (Davare et al., 2004) |
| Cdc2/ cyclinB1 | Cell cycle regulation | - | - | - | - | - | √ | - | (Chan et al., 1999) |
| CDC25C | Phosphatase regulating entry into mitosis | √ | - | x | x | - | x | √ | (Chan et al., 1999; Dalal et al., 2004) |
| CLIC4 | Chloride channel | - | - | - | √ | - | - | √ | (Suginta et al., 2001) |
| NFAT | Transcription factor | - | - | - | √ | √√√ | - | - | (Chow and Davis, 2000) |
| Par3α/β | Cell polarity | - | - | √ | √ | √ | - | √ | (Izaki et al., 2005) |
| PKCζ | Protein kinase | √ | √ | √√ | x | √√ | - | - | (Van Der Hoeven et al., 2000) |
| Raf-1 | Protein kinase | - | - | √ | √ | - | - | - | (Fantl et al., 1994; Freed et al., 1994) |

14-3-3 isoforms are grouped into 4 columns on the basis of sequence similarity as discussed in section 1.2.1.3. Where the relative affinity of 14-3-3 isoform binding has been determined it is indicated by the number of ticks: √ = weak, √√ = moderate, √√√ = strong, x = no binding, - = not tested. Single ticks are used where relative strength of binding has not been determined.

Abbreviations: ADAM22 - A disintegrin and metalloproteinase 22, AKAP-Lbc - A-kinase anchoring protein-Lbc, CAMKK - Calcium/calmodulin-dependent kinase kinase, Cdc2 – cell division cycle 2 protein, CDC25C - cell division cycle 25C protein, CLIC4 - chloride intracellular channel 4, NFAT – nuclear factor of activated T cells, PKCζ - protein kinase C ζ.

within the 14-3-3 binding groove clearly have an important role in σ isoform specific interactions. Regarding the other isoforms, Gardino notes some differences in the way the isoforms contact their peptide ligands revealed by the various crystal structures (Gardino et al., 2006). However, the isoform specific functions of the other six 14-3-3 proteins and their structural or other basis require further investigation.

## 1.2.3. 14-3-3 proteins have diverse cellular functions

### 1.2.3.1. 14-3-3 proteins can modulate the localisation or activity of binding partners

14-3-3 functions can be grouped into three main modes of action. Firstly, 14-3-3 can alter the enzymatic activity of its binding partner. The first function ascribed to 14-3-3 was activation of tryptophan and tyrosine hydroxylases (Ichimura et al., 1987; Yamauchi et al., 1981). Serotonin N-acteyltransferase (AANAT) activity is enhanced by 14-3-3, probably due to stabilisation of a more active conformation (Obsil et al., 2001) and 14-3-3 may have a similar role in c-Raf-1 kinase activation (Wilker and Yaffe, 2004). 14-3-3 also inhibits the activity of some binding partners, such as calcium/calmodulin dependent kinase kinase (CAMKK). 14-3-3 binding blocks dephosphorylation of a specific residue to maintain CAMKK in an inactive state (Davare et al., 2004). The second mode of action relies on 14-3-3's dimeric status to bridge two signalling proteins, facilitating their interaction. Three examples of this activity have been reported and all involve c-Raf-1; 14-3-3 mediates the interaction of c-Raf-1 with breakpoint cluster region kinase (Braselmann and McCormick, 1995), PKCζ (Van Der Hoeven et al., 2000) and A20, an inhibitor of tumour necrosis factor (TNF) induced apoptosis (Vincenz and Dixit, 1996).

Lastly, the most prevalent mode of action involves 14-3-3 masking a protein-protein interaction site to modulate the localisation of its binding partner (Muslin and Xing, 2000). 14-3-3 most often sequesters the target protein in the cytoplasm by occluding a nuclear localisation signal (NLS) and many examples of this are given in the

following sections. It was originally suggested that 14-3-3 might act as an attachable nuclear export signal (NES) after a NES consensus sequence was identified (Lopez-Girona et al., 1999; Rittinger et al., 1999). However, it later became clear that export of 14-3-3 from the nucleus relies on the NES of its binding partner as mutation of 14-3-3's basic phosphoserine binding pocket trapped 14-3-3 in the nucleus (Brunet et al., 2002). In addition, 14-3-3 promotes the nuclear localisation of some proteins such as homeodomain transcription factor TLX-2 and the catalytic subunit of teleomerase TERT, probably by obscuring a NES (Seimiya et al., 2000; Tang et al., 1998).

### 1.2.3.2. 14-3-3 proteins in cell cycle regulation

The importance of 14-3-3 in cell cycle regulation has become increasingly apparent with the discovery of numerous roles in progression through G2/M and G1/S transitions and the mediation of proper cell cycle arrest in response to DNA damage. The interactions of 14-3-3 with cell cycle regulatory proteins are summarised below and in figure 1.4. They provide many examples where 14-3-3 regulates subcellular localisation in response to dynamic phosphorylation events. A comprehensive review of this area of 14-3-3 biology has recently been provided (Hermeking and Benzinger, 2006).

The first indication that 14-3-3 has a role in cell cycle regulation came from the observation that 14-3-3 σ is upregulated by ionizing radiation in colorectal carcinoma cells (Hermeking et al., 1997). Overexpression of 14-3-3 σ in cycling cells led to cell cycle arrest in G2, indicating a role for 14-3-3 σ in controlling progression to mitosis. In 14-3-3 σ -/- mutant cells the cyclin dependent kinase Cdc2/cyclin-B1 complex was allowed to translocate to the nucleus following DNA damage, rather than being retained in the cytoplasm, which led to the inappropriate onset of mitosis (Chan et al., 1999). 14-3-3 σ co-immunoprecipitated with Cdc2 and cyclin-B1, suggesting that 14-3-3 σ sequesters this complex in the cytoplasm.

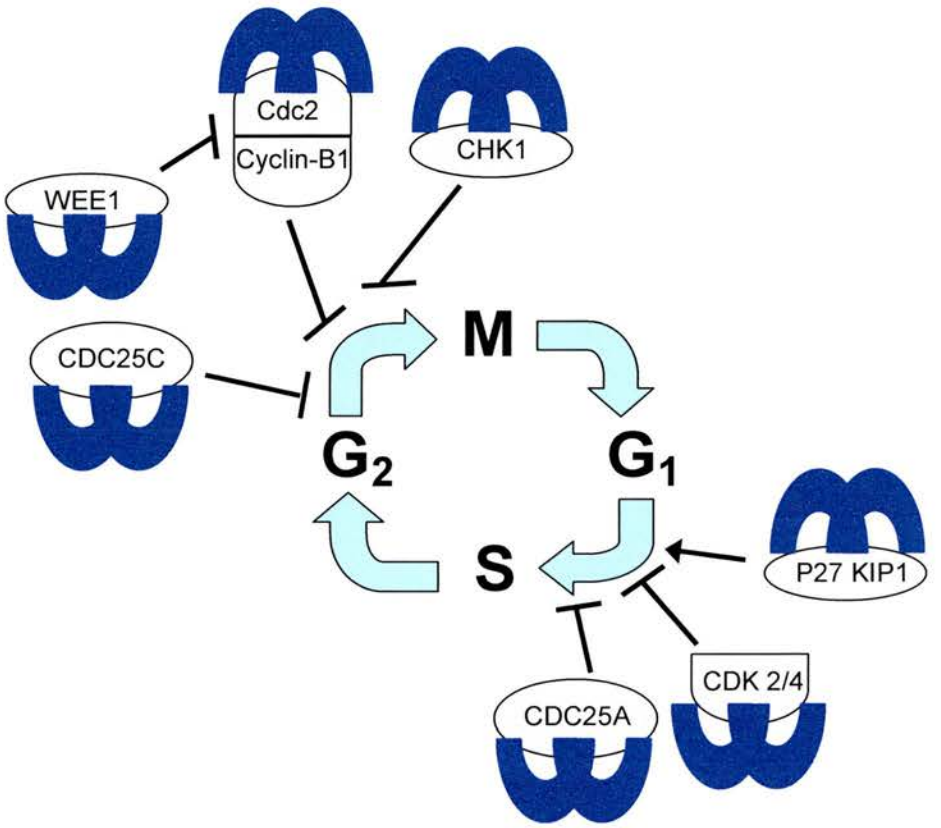


**Figure 1.5. 14-3-3 regulates cell cycle progression**

Summary of some of the important interactions between 14-3-3 and cell cycle regulatory proteins. The interactions are mediated by phosphorylation of the binding partner and mostly alter the subcellular localisation of the protein, as described in detail in the text. M shapes are 14-3-3 dimers. Inhibition of cell cycle progression or kinase activity is shown by ⊥. Promotion of cell cycle progression is shown by ↑. Figure adapted from Hermeking and Benzinger, 2006.

Investigations in fission yeast, Xenopus oocytes and later mammalian cells have revealed that other 14-3-3 isoforms act upstream of Cdc2/cyclin-B1 activation to negatively regulate this complex via multiple mechanisms. The kinases Wee1 and checkpoint kinase 1 (CHK1) and the phosphatase CDC25C have all been found to bind 14-3-3 and point mutations of the critical serine at the 14-3-3 binding sites have elucidated the role of 14-3-3 in each case. In response to DNA damage the checkpoint kinase CHK1 is activated by phosphorylation, creating a 14-3-3 binding site (Jiang et al., 2003; Liu et al., 2000; Zhou and Elledge, 2000). CHK1 is an example of a protein retained in the nucleus by 14-3-3 binding; here CHK1 can phosphorylate Wee1 (Lee et al., 2001) and CDC25C (Peng et al., 1997; Zeng et al., 1998). 14-3-3 binding to both phosphorylated Wee1 and CDC25C serves to negatively regulate Cdc2/cyclin-B1 via two complimentary actions. 14-3-3 bound Wee-1 has an increased kinase activity compared to a 14-3-3 binding deficient mutant; this increases its ability to phosphorylate and therefore inactivate Cdc2/cyclin-B1 (Lee et al., 2001; Rothblum-Oviatt et al., 2001; Wang et al., 2000b). 14-3-3 binding sequesters CDC25C in the cytoplasm and prevents its activation of Cdc2/cyclin-B1 (Kumagai et al., 1998; Zeng et al., 1998). Two studies identified a nuclear localisation signal in CDC25C that is very close to the 14-3-3 binding site and suggest this is masked by 14-3-3 (Kumagai and Dunphy, 1999; Yang et al., 1999). Mutation of the 14-3-3 binding site causes exclusively nuclear localisation of CDC25C and allows cells to escape the G2/M checkpoint following DNA damage (Dalal et al., 2004; Kumagai and Dunphy, 1999; Peng et al., 1997; Zeng and Piwnica-Worms, 1999). Thus 14-3-3 proteins are extremely important in preventing inappropriate initiation of mitosis by controlling the nuclear versus cytoplasmic localisation of CHK1, CDC25C and Cdc2/cyclin-B1 directly, and by altering the activity of Wee1 kinase.

14-3-3 proteins also regulate the G1/S transition by sequestering various regulators in the cytoplasm. CDC25A phosphatase is prevented from activating cyclin dependent kinase 2 (CDK2) in the nucleus when it is bound to 14-3-3 (Chen et al., 2003b). 14-3-3 also competes with importin $\alpha/\beta$ for a binding site on p27(KIP1) (Fujita et al., 2003; Sekimoto et al., 2004). High levels of 14-3-3 therefore sequester p27(KIP1) in

the cytoplasm and prevent its inhibitory action on CDK/cyclin complexes in the nucleus. This 14-3-3 interaction therefore appears to facilitate rather than inhibit cell cycle progression. In contrast, 14-3-3 σ has been reported to prevent the nuclear entry of CDK2 and CDK4 (Laronga et al., 2000). The evidence discussed in this section and the down regulation of 14-3-3 σ in a number of cancer cell types has led to the suggestion that this epithelial cell specific 14-3-3 σ is an important tumour suppressor (Hermeking, 2003; Prasad et al., 1992; Vercoutter-Edouart et al., 2001). However, other 14-3-3 isoforms clearly have important cell cycle roles. The sequestration of CDC25C, for example, can not be performed by 14-3-3 σ, only by other isoforms.

### 1.2.3.3. 14-3-3 proteins in cell survival signalling

The interaction between 14-3-3 and c-Raf-1 is probably the most extensively investigated of 14-3-3's many interactions. Despite this, the role of 14-3-3 in c-Raf-1 activation remains to be fully elucidated due to the complicated nature of 14-3-3's involvement. The current model is summarised below and provides a further example of the diverse effects of 14-3-3 on its target proteins.

The serine/threonine kinase c-Raf-1 is activated by the small GTP-ase Ras, following growth factor stimulation. C-Raf-1 phosphorylates effectors in the mitogen activated protein kinase (MAPK) pathway to promote cell survival. Initial reports of the interaction between 14-3-3 β/ζ and c-Raf-1 noted an increase in kinase activity in response to 14-3-3 overexpression (Fantl et al., 1994; Freed et al., 1994; Fu et al., 1994; Li et al., 1995). However, the picture became more complicated with the identification of three 14-3-3 binding sites on c-Raf-1. Rommel and co-workers discovered that 14-3-3 binds to phosphosphorylated motifs at serine 259 (S259) and serine 621 (S621) (Rommel et al., 1996) and 14-3-3 also appears to bind to the cysteine-rich domain in a phosphorylation independent manner (Clark et al., 1997). Recently a fourth 14-3-3 binding site was identified at phosphorylated serine 233 (Dumaz and Marais, 2003).

In contrast to the initial findings, 14-3-3 binding to pS259 or the cysteine-rich domain appears to negatively regulate c-Raf-1; mutation of these sites increases c-Raf-1 activity (Clark et al., 1997; Jaumot and Hancock, 2001; Light et al., 2002; Michaud et al., 1995; Ory et al., 2003). The Ras binding domain is towards the N-terminus of c-Raf-1 and is close to the cysteine-rich domain and S259. 14-3-3 binding has therefore been suggested to occlude the Ras binding site and maintain c-Raf-1 in an inactive state. Indeed Dhillon and co-workers concluded that dephosphorylation of S259 is the critical event in c-Raf-1 activation and greatly enhances binding to Ras (Dhillon et al., 2002), in agreement with other reports (Dumaz and Marais, 2003; Jaumot and Hancock, 2001; Ory et al., 2003). Though some authors found that S259 dephosphorylation was not necessary for Ras to be able to displace 14-3-3 (Light et al., 2002; Rommel et al., 1996). In either case binding of 14-3-3 to pS259 must be eliminated for proper activation of c-Raf-1.

The positive effect of 14-3-3 on c-Raf-1 activity, observed in early studies, has been confirmed; binding of 14-3-3 to pS621 seems to be essential for proper recruitment of 14-3-3 to the membrane and activation of c-Raf-1 (Light et al., 2002; McPherson et al., 1999; Roy et al., 1998; Thorson et al., 1998; Tzivion et al., 1998; Yip-Schneider et al., 2000). However, there are conflicting reports about whether 14-3-3 remains at the membrane following c-Raf-1 recruitment. Whilst some authors maintain that 14-3-3 is not bound to activated c-Raf-1 at the plasma membrane (Hekman et al., 2004; McPherson et al., 1999; Roy et al., 1998), others have observed 14-3-3 recruitment along with c-Raf-1 (Freed et al., 1994; Mineo et al., 1996) and found that displacement of 14-3-3 inactivates c-Raf-1 (Tzivion et al., 1998). It remains unclear exactly how 14-3-3 binding to pS621 enhances c-Raf-1 activity.

In the current model of 14-3-3 function in c-Raf-1 activation (see figure 1.5), binding to pS259 (possibly in conjunction with binding to pS621) sequesters c-Raf-1 in the cytoplasm and masks the Ras binding site (Dougherty and Morrison, 2004; Fu et al., 2000; Wilker and Yaffe, 2004). 14-3-3 must be displaced from pS259 (and/or pS233 and the cysteine-rich domain) for c-Raf-1 to bind to Ras and dephosphorylation

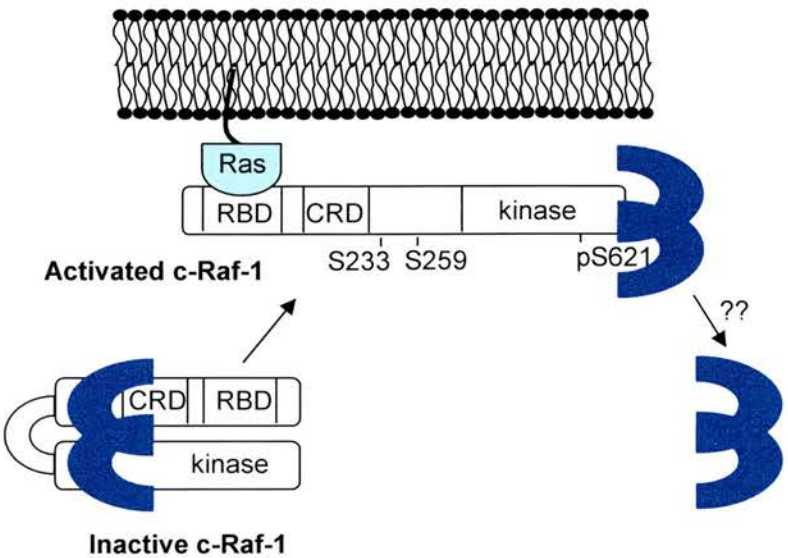


**Figure 1.6. Current model of 14-3-3 function in c-Raf-1 regulation**

The model is explained in detail in the text. Briefly, 14-3-3 maintains c-Raf-1 in an inactive conformation in the cytosol by binding to pS259 and possibly other sites. 14-3-3 must be displaced from pS259 to allow Ras binding. Activation and membrane localisation of c-Raf-1 requires 14-3-3 binding to pS621 but the mechanism for this role is undefined. M shape represents the 14-3-3 dimer. RBD = Ras binding domain. CRD = cysteine-rich domain. Adapted from Fu, Subramanian *et al* (2000) and Wilker and Yaffe (2004).

likely facilitates this process. The interaction of 14-3-3 with the pS621 site is suggested to stabilise the kinase domain of c-Raf-1 or mediate interactions with other proteins. Whilst 14-3-3 does modulate the plasma membrane versus cytosolic localisation of c-Raf-1, in this example the role of 14-3-3 extends beyond simply redistributing its binding partner.

The pro-survival role of 14-3-3 in activating the Ras/Raf/MAPK pathway is complimented by its anti-apoptotic functions (Fu et al., 2000; Masters et al., 2002; Rosenquist, 2003). A recent study by Masters and Fu underlined the importance of 14-3-3 in preventing cell death (Masters and Fu, 2001). These authors designed a high affinity peptide inhibitor specific for 14-3-3 (named difopein) and transfected it into cells to monitor the effect of global 14-3-3 inhibition. Expression of difopein resulted in the induction of apoptosis. This result suggests that 14-3-3 is likely to mediate apoptosis via multiple mechanisms. Indeed a number of interactions with apoptosis regulating proteins have already been documented and others probably await discovery. 14-3-3 interacts with pro-apoptotic proteins Bad and Bax in a phosphorylation dependent manner (Datta et al., 2000; Masters et al., 2001; Nomura et al., 2003; Zha et al., 1996). Whilst bound to 14-3-3 Bad and Bax are unable to heterodimerise with Bcl-2 and Bcl-xL, which would lead to caspase activation and apoptosis. The critical phosphoserine residue in Bad is adjacent to the BH3 domain, which mediates heterodimerisation, providing an example of 14-3-3 masking a protein interaction site to affect the function of a binding partner (Muslin and Xing, 2000). Phosphorylation of apoptosis signal-regulating kinase-1 (ASK-1) also creates a 14-3-3 binding site. ASK-1 mediates apoptosis via activation of JNK, which in turn increases expression of tumour necrosis factor (TNF). This pathway is inhibited by 14-3-3 binding (Masters et al., 2002; Zhang et al., 1999). 14-3-3 has also been reported to bind to an inhibitor of the TNF pathway, A20, but the consequence of this interaction is unclear (Lademann et al., 2001; Vincenz and Dixit, 1996). The cytoplasmic versus nuclear localisation of c-Abl is controlled by 14-3-3 binding, preventing the pro-apoptotic activity of this tyrosine kinase in the nucleus (Yoshida et al., 2005). Lastly, the pro-apoptotic forkhead family transcription factor FKHRL1 is retained in the cytoplasm by 14-3-3 binding to specific phosphorylated motifs

(Brunet et al., 1999; Brunet et al., 2002). Both NLS and NES sequences have been identified in FKHRL1 and disruption of the 14-3-3 binding site or the NES leads to nuclear accumulation. 14-3-3 is proposed to occlude the NLS and expose the NES to mediate export from the nucleus following phosphorylation (Brunet et al., 2002).

#### 1.2.3.4. 14-3-3 proteins in membrane processes

In many of its better characterised functions 14-3-3 mediates the nuclear versus cytoplasmic localisation of the target protein, as described in preceding sections. However, some studies also suggest that 14-3-3 might be involved in regulating the plasma membrane localisation or function of ion channels and receptors. 14-3-3 has also been implicated in the control of calcium regulated exocytosis. These areas have not been studied extensively and therefore await further investigation.

Recently 14-3-3 has been implicated in the regulated trafficking of multimeric ion channels and receptors to the plasma membrane (Michelsen et al., 2005; Nufer and Hauri, 2003). Newly synthesized channel subunits must assemble correctly into oligomers before they travel to the plasma membrane; monomers are retrieved from the secretory pathway back to the endoplasmic recticulum (ER). In many cases this ER retrieval involves the coat protein complex I (COPI) binding to exposed dibasic motifs in the cytoplasmic tails of the channels subunits (Michelsen et al., 2005). In recent studies 14-3-3 has been found to aid the escape of properly assembled multimeric complexes from the ER. 14-3-3 binds to phosphorylated motifs on the cytoplasmic tails of potassium channels KCNK3 and Kir2.1 and the potassium ATPase α subunit Kir6.2 (Coblitz et al., 2005; O'Kelly et al., 2002; Yuan et al., 2003). 14-3-3 appears to mask the dibasic ER localisation signals present in these proteins as the binding of 14-3-3 and COPI are mutually exclusive. Importantly, 14-3-3 only binds to dimeric KCNK3 and dimeric or tetrameric Kir6.2, not the monomers. Thus 14-3-3 is suggested to probe the assembly status of ion channels, allowing only multimeric complexes to translocate to the plasma membrane. 14-3-3 is also necessary for the forward transport of lip35, the invariant chain of major

histocompatibility antigen class II (MHCII), acetylcholine receptor α4 and cell adhesion membrane protein ADAM22 (Godde et al., 2006; Jeanclos et al., 2001; O'Kelly et al., 2002). This again depends on masking of dibasic retention signals. The potassium channels TASK-1 and TASK-3 also require 14-3-3 binding to their extreme C-terminus for proper localisation to the plasma membrane (Rajan et al., 2002). However, it is unknown whether this is due to 14-3-3 occluding dibasic ER localisation motifs.

14-3-3 has been implicated in the insulin signalling pathway; it binds to both insulin-like growth factor-1 receptor (IGF1R) and insulin receptor substrate 1 (IRS-1). Binding to IGF-1 depends on phosphorylation induced by hormone stimulation and may be connected with IGF1R dependent transformation (Craparo et al., 1997; Spence et al., 2003). The interaction of 14-3-3 with IRS-1 is suggested to downregulate insulin signalling by removing IRS-1 from its activation site at the membrane and sequestering it in the cytosol (Kosaki et al., 1998; Ogihara et al., 1997; Xiang et al., 2002). 14-3-3 binding may also modulate the activity of membrane proteins such as the $Na^+/H^+$ exchanger isoform-1 and the $Na^+/K^+$-ATPase (Efendiev et al., 2005; Lehoux et al., 2001). Recruitment of 14-3-3 to the plasma membrane has additionally been reported in response to epidermal growth factor (EGF) stimulation; one study reported transient association of 14-3-3 and c-Raf-1 with caveolae (Mineo et al., 1996; Oksvold et al., 2004).

14-3-3 was identified as a soluble factor that was able to reactivate exocytosis in digitonin-permeabilised adrenal chromaffin cells (Morgan and Burgoyne, 1992a; Morgan and Burgoyne, 1992b; Roth et al., 1994). Burgoyne and co-workers demonstrated that 14-3-3 acts in the magnesium-adenosine triphosphate dependent priming step of exocytosis and may reorganise the cortical actin network to allow vesicle fusion (Chamberlain et al., 1995; Roth et al., 1999; Roth and Burgoyne, 1995). 14-3-3 was also isolated in synaptic membrane preparations (Martin et al., 1994) but its role in exocytosis has not been further explored.

Early reviews of 14-3-3 proposed that its dimeric nature would prove important in bringing two signalling proteins into close proximity. Though a few examples of such scaffolding activity exist, the main function of 14-3-3 proteins appears to involve masking protein-protein interaction sites. Often the interaction site is a NLS or NES; with the result that 14-3-3 modulates the nuclear versus cytoplasmic localisation of the target protein. However, it has recently become clear that 14-3-3 can also mediate the plasma membrane localisation of channels and receptors. In some cases 14-3-3 binding can directly affect the activity of a protein. It remains to be seen whether recruitment of 14-3-3 to the plasma membrane has functions beyond altering protein localisation.

## 1.3. Summary and project aims

14-3-3 proteins are involved in a wide range of cellular signalling processes. They are essential for cell survival as demonstrated by reports that global inhibition of 14-3-3 interactions leads to cell death. 14-3-3 often controls the cytoplasmic versus nuclear localisation of target proteins but recent studies have implicated 14-3-3 in localisation and regulation of membrane anchored proteins. Though 14-3-3 has been isolated in plasma membrane preparations its functions at the membrane are not well chracterised. Where interaction between 14-3-3 and a membrane associated protein has been reported it is often unclear whether the interaction occurs only during transport or recruitment persists at the membrane.

Lipid rafts are hypothesized to be cholesterol and sphingolipid rich domains in the plasma membrane that segregate from the bulk plasma membrane because they form a more ordered membrane phase. Confirmation of the presence of lipid rafts in the plasma membrane remains a challenge. However, biophysical experiments in model membranes support the coexistence of liquid ordered ($L_o$) and liquid disordered phase ($L_d$) phases mediated by physiological concentrations of cholesterol. In addition, there is evidence to suggest that DRMs correspond to $L_o$ domains. Microscopy studies have demonstrated compartmentalisation of membrane proteins that depends, at least to some extent, on cholesterol for the integrity of domains. Current lipid raft models postulate that steady state $L_o$ domains or lipid rafts are likely to be nanometre scale entities with short lifetimes. However, clustering of lipid rafts is suggested to be an important mechanism for creation and stabilisation of larger rafts in response to signalling events.

Preliminary experiments in this laboratory indicated that 14-3-3 might be associated with DRMs, which are believed to represent clustered lipid rafts. Association of 14-3-3 with lipid raft-like domains is interesting from a number of perspectives. Both 14-3-3 and lipid raft-like domains have been implicated in the regulation of cell survival via the Ras/Raf/MAPK pathway and a role for 14-3-3 at the membrane has been suggested. 14-3-3 is also very important in inhibiting a number of apoptotic cell

death pathways, such as the Bad pathway, where the involvement of lipid raft-like domains has been reported. Another interesting aspect of 14-3-3 function is its potential involvement in CJD pathology but the molecular mechanism for this role remains unclear. Lipid raft-like domains are thought to be central to the conversion of cellular PrP to the CJD causing protease resistant form of PrP. The association of 14-3-3 with lipid raft-like domains might be important in its function in all these membrane processes. The potential localisation of 14-3-3 to DRMs is intriguing because 14-3-3 apparently has no structural mechanism for direct membrane attachment and is primarily cytoplasmic. Therefore I would hypothesize that if 14-3-3 functionally associates with DRMs or lipid raft-like domains then it must do so via interaction with other membrane anchored proteins.

In this thesis I initially set out to confirm and characterise the presence of 14-3-3 proteins in DRMs, including the potential for 14-3-3 isoform specificity in this association. Functional specificity of particular isoforms is somewhat under-investigated but some studies support the importance of 14-3-3 isoform dependent interactions. The mode of 14-3-3 recruitment to DRMs was investigated to test the hypothesis that 14-3-3 must bind to another DRM-resident protein to localise to DRMs.

To explore the potential localisation of 14-3-3 proteins to membrane domains in intact cells, confocal microscopy was employed in conjunction with a marker for lipid rafts, cholera toxin subunit B (CTXB). The aim was to determine whether the localisation of 14-3-3 to DRMs correlates with localisation to lipid raft-like microdomains in intact cell membranes. 14-3-3 localisation was compared with that of Thy-1, an established DRM marker protein, and SNAP-25 and syntaxin1a, two proteins anchored to the cytoplasmic face of the plasma membrane and demonstrated to partially reside in DRMs. Though these proteins were initially included as controls, during the course of these studies interesting results were obtained with respect to their membrane domain localisation, leading to further investigations. SNAP-25 and syntaxin1a were of particular interest because lipid raft-like domains have previously been implicated in the regulation of exocytosis.

Cholesterol is central to formation of $L_o$ domains and therefore lipid rafts so cholesterol dependence of the membrane domain localisation of 14-3-3 and the other DRM-associating proteins was investigated in detail. To further explore the relationship between DRMs and membrane domains in intact cells I made a systematic comparison between the effects of cholesterol depletion on DRMs and lipid raft-like domains labelled by CTXB and imaged by confocal microscopy. These experiments aimed to determine whether the observed DRM localisation of the proteins of interest depends on their localisation to pre-existing cholesterol-dependent membrane domains.

# Chapter 2: Materials and Methods

# 2. Materials and Methods

All reagents were purchased from Sigma-Alrich (Poole, UK) unless otherwise stated.

## 2.1. CELL CULTURE TECHNIQUES

All cell culture reagents were Gibco brand products supplied by Invitrogen (Paisley UK) unless otherwise stated.

### 2.1.1. Culture of PC12 cells

PC12 cells (rat adrenal pheochromocytoma derived cell line) were cultured in a humidified atmosphere containing 5 % (v/v) $CO_2$/95 % (v/v) air, at 37°C. The cells were maintained in RPMI 1640 supplemented with 10 % horse serum, 5 % FBS, 100 units/ml penicillin and 100 μg/ml streptomycin. Cells were grown in suspension and passaged every three days. The cells were collected by low speed centrifugation and incubated with 1 ml trypsin-EDTA for two minutes, then resuspended in 10 ml fresh media. Clumped cells were separated by passing through a 19 gauge syringe needle and cells were reseeded at a 1 in 4 dilution.

### 2.1.2. Culture of N2a cells

Mouse neuro-2-a (N2a) cells were cultured in a humidified atmosphere containing 5 % (v/v) $CO_2$/95 % (v/v) air, at 37°C. The cells were maintained in Dulbecco's modified Eagles medium (DMEM) supplemented with 10 % foetal bovine serum (FBS), 2 mM L-glutamine, 100 units/ml penicillin and 100 μg/ml streptomycin. Cells were passaged every two days. Confluent monolayers of cells in 75 $cm^2$ flasks were resuspended in fresh media and reseeded at a 1 in 5 dilution.

## 2.2. MOLECULAR TECHNIQUES

### Table 2.1. Molecular biology buffers

| Buffer | Components | Concentration |
|---|---|---|
| 6 x DNA gel loading buffer | Bromophenol blue<br>Xylene Cyanol FF<br>Glycerol<br>EDTA | 12.6 % (w/v)<br>12.6 % (w/v)<br>30 % (w/v)<br>120 mM |
| Elution buffer for protein purification | Tris-Cl pH 7.5<br>Sodium chloride | 50 mM<br>150 mM |
| Luria Bertani (LB) media | Peptone (GibcoBRL, Paisley, UK)<br>Yeast extract (Oxoid, Basingstoke, UK)<br>Sodium chloride | 10 g/L<br>5 g/L<br>10 g/L |
| LB agar | Bacto-Agar (GibcoBRL, Paisley, UK) in LB media | 15 g/L |
| Lysis buffer for bacterial cells | 1 x PBS<br>DTT<br>EDTA<br>PMSF<br>Complete EDTA-free protease inhibitor tablet (Boehringer Mannheim, Mannheim, Germany) | <br>1 mM<br>1 mM<br>1 mM<br>1 in 50 ml |
| Phosphate buffered saline (PBS) pH 7.4 | Sodium phosphate<br>Potassium phosphate<br>Potassium chloride<br>Sodium chloride | 10 mM<br>1.8 mM<br>2.7 mM<br>137 mM |
| SOC media pH 7.0 (supplied ready made by Promega, Southampton, UK) | Bacto-tryptone<br>Bacto-yeast extract<br>Sodium chloride<br>Potassium chloride<br>Magnesium chloride (hydrated)<br>Magnesium sulphate (hydrated)<br>Glucose | <br><br>10 mM<br>2.5 mM<br>10 mM<br>10 mM<br>20 mM |
| TAE | Tris-acetate<br>EDTA pH 8.0 | 40 mM<br>1 mM |
| TE | Tris-Cl pH 8.0<br>EDTA | 10 mM<br>1 mM |

### 2.2.1. Production of glutathione-S-transferase(GST)-difopein bacterial expression vector

Difopein (**di**meric **fo**urteen-three-three **pe**ptide **in**hibitor) is an inhibitor of 14-3-3 protein interactions, designed by Dr Shane Masters and Professor Haian Fu (Emory University, Atlanta, GA). The plasmid pSCM138, encoding an EYFP-difopein fusion protein, was a gift of Professor Haian Fu. Difopein contains a 20 amino acid sequence that is repeated twice; the full sequence, with the repeated section is brackets, is SADGA (PHCVP RDLSW LDLEA NMCLP) GAAGL DSADG A(PHCV PRDLS WLDLE ANMCL P)GAAG LE. The underlined motif WLDLE binds to the basic pocket in 14-3-3's amphipathic binding groove (Petosa et al., 1998). Due to the sequence repetition, attempts to produce the difopein insert from pSCM138 by PCR were unsuccessful. An alternative strategy was employed involving excision of the difopein insert from pSCM138 and ligation into pGEX-4T1 (GE Healthcare, Buckinghamshire, UK), which had been digested to produce complimentary base pair ends.

#### 2.2.1.1. Restriction enzyme digests

3 µg pGEX-4T1 was digested with 20 units (2 µl) EcoRI (Boehringer Mannheim, Mannheim, Germany) in buffer H (Boehringer Mannheim), in a reaction volume of 60 µl. 6 µg pSCM138 was digested with 40 units (4 µl) EcoRI in buffer H, in a reaction volume of 60 µl. Both restriction digests were incubated at 37°C for 1.5 hours. The digests were then phenol chloroform extracted to remove the enzyme. 60 µl phenol chloroform was added to each digest, vortex mixed for 15 seconds and centrifuged at 13,000 rpm in a bench top centrifuge for 2 minutes. Each upper aqueous phase (~ 45 µl) was removed and retained. 60 µl TE (10 mM Tris-Cl, 1 mM EDTA, pH 8.0) was added to the solvent phase, the mixture was vortex mixed again and centrifuged at 13,000 rpm for 2 minutes. The new aqueous phase (~50 µl) was removed and pooled with the first. 9.5 µl sodium acetate pH 5.2 was added to the total aqueous phase, followed by 200 µl ethanol. This mixture was incubated at -

20°C for 15 minutes and then centrifuged at 13,000 rpm for 30 minutes at 4°C. The supernatant was removed and the pellets were allowed to dry. The pellets were resuspended in 10 mM Tris-Cl pH 8.5.

#### 2.2.1.2. Purification of insert

To purify the difopein insert the phenol chloroform extracted pSCM138 digest was separated on a 1 % agarose gel. The size of the insert (~ 190 base pairs) was confirmed by comparison with DNA molecular weight marker XIV (Roche Diagnostics, Penzberg, Germany). The DNA band corresponding to the difopein fragment was excised from the gel and purified using a QIAquick gel extraction kit (Qiagen, Crawley, UK) according to the manufacturer's instructions. Briefly, three volumes of buffer QG were added to one volume of gel and incubated at 50°C for 10 minutes to dissolve the gel and adjust the pH for binding to the silica membrane in the QIAquick column. One gel volume of isopropanol was added; the sample was mixed and applied to a QIAquick column to bind the DNA. The column was washed with 0.5 ml buffer QG, followed by 0.75 ml ethanol buffer PE and the DNA eluted with 30 µl 10 mM Tris-Cl, pH 8.5.

#### 2.2.1.3. Phosphatase treatment of vector

To reduce re-ligation of the pGEX-4T1 vector with itself the 5' ends of the EcoRI digested vector were dephosphorylated with shrimp alkaline phosphatase (Roche Diagnostics, Penzberg, Germany). Around 3 µg digested pGEX-4T1 was added to 2.5 units (2.5 µl) shrimp alkaline phosphatase in shrimp alkaline phosphatase buffer to give a total reaction volume of 20 µl. The reaction was incubated at 37°C for 20 minutes, following which the shrimp alkaline phosphatase was inactivated by 15 minutes incubation at 65°C.

### 2.2.1.4. Ligation of insert into vector

1.4 µl (~ 200 ng) dephosphorylated, EcoRI digested pGEX-4T1 was added to 2 µl (~ 20 ng) gel purified difopein DNA. This was estimated to give an approximate 1:2 molar ratio of vector:insert DNA. 1 µl T4 DNA ligase (Roche Diagnostics, Penzberg, Germany) and 1 µl 10 x ligase buffer were added and the reaction made up to 10 µl with nuclease free water. The reaction was incubated at ~ 20°C for 16 hours. 1.5 µl of the ligation reaction was transformed into competent JM109 *E.coli* cells (Promega, Southampton, UK). The DNA was added to 30 µl of JM109 cells and incubated on ice for 20 minutes. The cells were then heat shocked by incubation at 42°C for 45 seconds and placed on ice immediately afterwards for a further 2 minutes. 270µl LB media was added to the cells and they were incubated at 37°C, 220 rpm for 1 hour. 100 µl of this culture was spread on a 100 mm diameter LB agar plate containing 50 µg/ml ampicillin. The plate was incubated at 37°C overnight. Colonies were picked into 5 ml LB media containing 50 µg/ml ampicillin and incubated overnight at 37°C, 220 rpm. The plasmid DNA was purified from each culture using Qiagen's mini-prep kit, according to the manufacturer's instructions (see section 2.2.3.1). Restriction digests were then carried out to check for the presence of the difopein insert. 10 µl mini-prep was added to 1 unit (1 µl) EcoRI in buffer H, in a total volume of 20 µl and incubated for 1 hour at 37°C. 10 µl of the restriction digests were separated on a 1 % agarose gel along with molecular weight marker XIV. For reactions where an insert of ~ 190 base pairs was present the corresponding plasmid DNA was sequenced by Cytomyx (Cambridge, UK). A plasmid with the correctly orientated difopein sequence insert was identified and purified on a large scale using Qiagen's maxi-prep plasmid kit (see section 2.2.3.2).

### 2.2.2. Agarose gel electrophoresis

1 % agarose gels were produced by heating 0.6 g molecular biology grade agarose (Bio-rad, Hemel Hempstead, UK) in 60 ml TAE buffer until dissolved. The agarose was allowed to cool before the addition of 1 µl ethidium bromide (Fisher Scientific, Loughborough, UK). The gel was submerged in TAE buffer containing 10 µl ethidium bromide per litre. An appropriate volume of 6 x DNA gel loading buffer was added to each DNA sample and the samples were loaded into the wells. DNA fragments were separated at 60 mA and visualised under ultraviolet light.

### 2.2.3. Purification of plasmid DNA

#### 2.2.3.1. Small scale

One bacterial colony was picked into 5 ml LB media containing the appropriate antibiotic and incubated overnight at 37°C, 220 rpm. The culture was centrifuged at 13,000 rpm in a bench top centrifuge for 2 minutes to pellet the bacteria. Qiagen's QIAquick mini-prep kit was used to purify the plasmid DNA, according to the manufacturer's instructions (Qiagen, Crawley, UK). Briefly, the bacterial pellet was resuspended in 250 µl ribonuclease A containing buffer P1. Cells were lysed in 250 µl alkaline lysis buffer containing sodium dodecyl sulphate (SDS) by gentle mixing. 350 µl of high salt neutralisation buffer was added to precipitate chromosomal DNA, SDS and cellular debris. The sample was then centrifuged at 13,000 rpm for 10 minutes in a bench top centrifuge to pellet the precipitate. The supernatant, containing plasmid DNA, was added to a QIAprep spin column. The column was centrifuged at 13,000 rpm for a minute and the flow through discarded, leaving plasmid DNA bound to the silica membrane. The column was washed with buffer 0.5 ml PB to remove endonucleases. A further wash with 0.75 ml ethanol buffer PE removed salts. The DNA was eluted in 50 µl 10 mM Tris-Cl, pH 8.5.

#### 2.2.3.2. Large scale

One bacterial colony was picked into 5 ml LB media containing the appropriate antibiotic and incubated for 4 hours at 37°C, 220 rpm. This culture was added to 100 ml LB media containing the appropriate antibiotic and incubated overnight at 37°C, 220 rpm. Plasmid DNA was isolated using Qiagen's maxi-prep kit, according to the manufacturer's instructions. Briefly, bacterial cells were pelleted by centrifugation at 3,500 x g for 15 minutes in a JA14 rotor (Beckman Coulter, Fullerton, CA), at 4°C. The pellet was resuspended in 10 ml ribonuclease A containing buffer P1. 10 ml alkaline/SDS lysis buffer was then added and the mixture was incubated for 5 minutes. 10 ml neutralisation buffer was added and mixed gently; following this the lysate was filtered to remove the precipitated chromosomal DNA, proteins and cell debris. The filtrate was applied to an anion exchange resin (the QIAGEN-tip) to bind the plasmid DNA. The resin was washed twice and the DNA eluted. The eluted DNA was precipitated with isopropanol and centrifuged at 15,000 x g for 30 minutes in a Beckman JA20 rotor, at 4°C, to pellet the DNA. The DNA pellet was washed with 70% ethanol. The pellet was allowed to dry and then dissolved in TE buffer. The absorbance of a diluted solution of the plasmid DNA was measured at 260 nm. The DNA concentration in mg/ml was determined using the equation:

$$\text{concentration (mg/ml)} = (\text{Abs}_{260\text{nm}} \times \text{dilution})/20$$

20 is the extinction coefficient for a 1mg/ml solution of DNA.

### 2.2.4. Purification of GST-Difopein fusion protein

#### 2.2.4.1. Transformation of plasmid DNA into competent *E.coli* cells

The GST-difopein DNA construct was transformed into competent BL21 *E.coli* cells (Promega, Southampton, UK). 1 µl GST-difopein DNA was added to 20 µl

competent cells and incubated on ice for 20 minutes. The cells were heat shocked by incubation at 42°C for 30 seconds, then immediately placed on ice for 2 minutes. 120 µl SOC media was added to the cells and 80 µl of this mixture was plated on LB-agar plates containing 50 µg/ml ampicillin. The plates were incubated at 37°C overnight.

### 2.2.4.2. Overexpression of fusion protein

One bacterial colony was picked into 100 ml LB media containing 50 µg/ml ampicillin and incubated at 37°C, 220 rpm overnight. 50 ml of this culture was added to each of two flasks containing 500 ml of LB media with ampicillin and incubated at 37°C, 220 rpm until the absorbance of the culture at 600 nm was between 0.9-1.0. To induce expression of GST-difopein isopropyl-β-D-1-thiogalactopyranoside (IPTG) was added to each flask at a final concentration of 0.5 mM and the cultures were incubated at 37°C, 220 rpm for another 4 hours. The bacterial cells were harvested by centrifugation at 3,500 x g in a Beckman JA14 rotor for 15 minutes, at 4°C. The bacterial pellets were stored at -20°C overnight.

### 2.2.4.3. Purification of fusion protein

The bacterial pellets were resuspended in a total of 40 ml lysis buffer (see table 2.1). The lysate was sonicated six times for 30 seconds at an amplitude of 6 microns, in a Sanyo MSE Soniprep 150. The sonication was carried out on ice and with a cooling period of 90 seconds on ice between each round of sonication. TX-100 was added to a concentration of 1 % and the lysate was incubated turning end over at 4°C for 1 hour. The lysate was centrifuged at 15,000 x g in a Beckman JA20 rotor for 30 minutes, at 4°C. The supernatant was filtered through Millex-HV 0.45 µm filters (Millipore Corporation, Bedford, MA). 1 ml glutathione sepharose bead slurry (GE Healthcare, Buckinghamshire, UK) was washed in 2 x 20 ml PBS. The lysate supernatant was added to the washed beads and incubated overnight at 4°C to bind

the GST-difopein to the beads. The lysate and beads were centrifuged at low speed for 20 seconds to gently pellet the beads and the supernatant was removed. The beads were washed with three changes (20 ml each) of lysis buffer containing 1 % TX-100. They were then washed with two changes (15 ml each) of lysis buffer containing 0.5 M NaCl and 1 % TX-100. They were washed with a further two changes of lysis buffer containing 137 mM NaCl and four changes of PBS. The intact fusion protein was eluted with 8 ml 20 mM glutathione in PBS and dialysed against two changes of 1.5 L 50 mM Tris-Cl pH 7.5, 150 mM sodium chloride at 4°C. The protein concentration was determined by BCA assay (described in section 2.3.6.2). The protein was stored at -70°C with the addition of 30 % glycerol. GST protein for control experiments was produced using the same protocol.

#### 2.2.4.4. Isolation of difopein peptide by thrombin cleavage

The protocol was altered slightly to produce the untagged difopein peptide from the sepharose bead-bound GST-difopein. After washing the beads with PBS they were transferred to a 2 ml tube with 1 ml PBS and 20 units (20 µl) thrombin. The tube was incubated turning end over end at room temperature overnight. The beads were allowed to settle and the eluate was collected. The beads were washed with 3 x 1 ml elution buffer (see table 2.1) and the washes were pooled with the eluate. 0.35 ml Benzamidine sepharose bead slurry (GE Healthcare, Buckinghamshire, UK) was added to a 5 ml column and washed with 15 ml elution buffer. The eluate was passed through the column four times to bind the thrombin and the eluate was collected. 2 ml extra elution buffer was added to the column and collected into the eluate to ensure all the difopein washed through. The presence of difopein peptide in the eluate was assessed by SDS-PAGE and the protein concentration was measured by BCA assay (see section 2.3.6.2). The difopein peptide was stored at 4°C for next day use.

## 2.3. BIOCHEMICAL TECHNIQUES

**Table 2.2. Buffers for membrane isolation procedures**

| Buffer | Components | Concentration |
|---|---|---|
| MES buffered saline (MBS) | MES (morpholinoethane-sulfonic acid) pH 6.5<br>Sodium chloride<br>Complete EDTA-free protease inhibitor tablet (Boehringer Mannheim, Mannheim, Germany) | 25 mM<br>150 mM<br>1 in 50 ml |
| LDM buffer | Sucrose<br>Tricine pH 7.8<br>EDTA | 0.25 M<br>20 mM<br>1 mM |
| Phosphate buffered saline (PBS) pH 7.4 | Sodium phosphate<br>Potassium phosphate<br>Potassium chloride<br>Sodium chloride | 10 mM<br>1.8 mM<br>2.7 mM<br>137 mM |

### 2.3.1. Detergent resistant membrane (DRM) isolation by TX-100 extraction and flotation on a sucrose density gradient

All procedures were carried out at 4°C unless otherwise stated.

#### 2.3.1.1. Isolation of DRMs from whole rat brain

Detergent resistant membranes were prepared based on the method of Chamberlain and co-workers (Chamberlain et al., 2001; Chamberlain and Gould, 2002), similar methods have been employed in numerous other studies (Gil et al., 2005; Martens et al., 2000; Miura et al., 2001; Parkin et al., 1999; Taverna et al., 2004).
Whole rat brain was homogenised on ice in MBS containing 1 % (v/v) TX-100 (see table 2.2), by 30 strokes of a Dounce homogeniser. The homogenate was centrifuged at 1100 x g for 10 minutes, in a Sorvall SS-34 rotor (Sorvall, Thermo Electron, Waltham, MA), to sediment tissue debris. The protein concentration of the cleared

homogenate was assessed by BCA assay (described in section 2.3.6.2 below). The density of TX-100 is 1.07 g/ml so a 1 % (v/v) solution has a detergent concentration of 10.7 mg/ml. The protein concentration was adjusted with additional homogenisation buffer to 2 mg/ml, giving a detergent to protein ratio of 5:1 (w/w). Where a different detergent to protein ratio was used details are given in the text. An equal volume of 80 % (w/v) sucrose in MBS was added to the cleared homogenate and passed through a wide syringe needle five times to thoroughly mix the two components. Discontinuous sucrose density gradients were constructed in thin walled polycarbonate tubes. Where larger tubes were used, 6 ml of 40 % sucrose/homogenate was loaded into the bottom of a tube and overlaid with 18 ml 30 % (w/v) sucrose in MBS, followed by 12 ml 5 % (w/v) sucrose in MBS. Where smaller tubes were employed, 4 ml of 40 % sucrose/homogenate was overlaid with 5 ml 30 % (w/v) sucrose in MBS, followed by 3.5 ml 5 % (w/v) sucrose in MBS. Smaller gradients were centrifuged at 39,000 rpm (~ 190,000 x g) in a Sorvall TH641 swinging bucket rotor for 18 hours. Larger tubes were centrifuged at 27,000 rpm (~ 140,000 x g) in a Beckman SW28 rotor. Twelve 1 ml fractions were collected from the smaller gradients or twenty 2 ml fractions from the larger tubes, fraction 1 being the top of the gradient. Fractions were stored at -20°C.

#### 2.3.1.2. Isolation of DRMs from cultured cells

PC12 cells were seeded onto 100 mm diameter dishes coated with collagen (prepared from rat tail tendons in 10 % (v/v) acetic acid), at a density of ~ 14 x $10^6$ cells per dish, 48 hours prior to lysis and DRM isolation. N2a cells were seeded at a density of ~ 3 x $10^6$ cells per dish in uncoated 100 mm diameter dishes and harvested 24 hours later. Cells were close to confluency when harvested. To determine the distribution of the glycosphingolipid ganglioside GM1 in the sucrose density gradients, cholera toxin B subunit (CTXB) was added to a concentration of 1 μg/ml and incubated at 37°C for 5 minutes prior to cell lysis. Cells were washed with PBS then lysed in 500 μl MBS containing 1 % (v/v) TX-100 and protease inhibitors per dish. The cells were incubated for 20 minutes turning end over end then homogenised with 10

strokes of a Dounce homogeniser. The protein concentration of the lysate was determined by BCA assay (described in section 2.3.6.2 below). The lysates were then diluted with additional MBS containing 1 % (v/v) TX-100 to a concentration of 2 mg/ml (unless otherwise stated), giving a detergent to protein ratio of 5:1 (w/w). An equal volume of 80 % (w/v) sucrose in MBS was added to the lysate and passed through a wide syringe needle five times to thoroughly mix the two components. Discontinuous sucrose density gradients were constructed in thin walled polycarbonate tubes. 5 ml of 40 % sucrose/lysate was overlaid with 5 ml 30 % (w/v) sucrose in MBS, followed by 2.5 ml 5 % (w/v) sucrose in MBS. Gradients were centrifuged at 39,000 rpm (~ 190,000 x g) in a Sorvall TH641 swinging bucket rotor for 18 hours. Twelve 1 ml fractions were collected and fractions were stored at -20°C.

#### 2.3.1.3. Cholesterol depletion of PC12 and N2a cells

Methyl-β-cyclodextrin (MβCD) was dissolved in PBS. For cholesterol depletion of PC12 cells the cell culture media was removed and replaced with either 20 mM MβCD in serum-free RPMI 1640 or an equal volume of PBS in serum-free media. N2a cells were incubated with 5 mM or 10 mM MβCD (or an equal volume of PBS) in serum-free DMEM containing 2mM L-glutamine. Cells were incubated with MβCD for 30 minutes at 37°C, then washed with PBS and lysed. Cell lysis and isolation of DRMs was performed as described above (see section 2.3.1.2).

### 2.3.2. Studies with 14-3-3 binding inhibitor peptide difopein

#### 2.3.2.1. GST 'pull down' with GST-difopein

GST-difopein or GST (~ 160 μg), purified according to the protocol described in section 2.2.4.3, was incubated with ~ 20 μl of washed glutathione sepharose bead slurry in a volume of 500 μl of Tris buffered saline (TBS, 25 mM Tris pH 7.5,

150 mM NaCl) for 1.5 hours, at 4°C with continuous agitation. The GST-difopein or control GST bound beads were collected by low speed centrifugation and divided between four tubes so that each tube contained ~ 40 μg protein. 300 μl rat brain extract (~ 250 μg protein) or 400 μl DRM fraction isolated from rat brain (~ 120 μg protein) was added to each tube and incubated with agitation for 2 hours at 4°C. The beads were then washed 5 times with 0.5 ml TBS containing 1 % Nonidet P40 (Fisher Scientific, Loughborough, UK) plus protease inhibitors. Following the last wash the beads were collected by centrifugation, the wash buffer removed and the beads resuspended in 1 x SDS loading buffer for analysis by polyacrylamide gel electrophoresis and immunoblotting (described in sections 2.3.4 and 2.3.5).

#### 2.3.2.2. Incubation of rat brain tissue with difopein prior to DRM isolation

Whole rat brain was homogenised in MBS containing 1 % (v/v) TX-100 plus protease inhibitors, according to the protocol described in section 2.3.1.1. The protein concentration of the cleared homogenate was adjusted to 2 mg/ml to give a 5:1 detergent to protein ratio. The rat brain extract was split into 2 ml aliquots and each aliquot was incubated for 2 hours at 4°C with 400 μg difopein inhibitor, an unrelated control peptide (peptide 1370), GST or an equal volume of buffer (untreated). The amino acid sequence of peptide 1370 was KQPGFPQPSPDDPS. 400 μg difopein was calculated to be greatly in excess of the amount needed to bind all the 14-3-3 in 2 ml homogenate. Two millilitres of brain homogenate contained 4 mg protein and 14-3-3 protein constitutes ~ 1 % of total brain protein so there was ~ 40 μg 14-3-3 present. The molecular weight of difopein is ~ 7 kDa and that of 14-3-3 is ~ 30 kDa so four times less difopein than 14-3-3 protein in weight will be needed to bind all the 14-3-3 (i.e. ~ 10 μg). Following the incubation period each aliquot of brain extract was mixed with an equal volume of 80 % (w/v) sucrose in MBS and sucrose density centrifugation was performed as described in section 2.3.1.1. The relative localisation of 14-3-3 isoforms to the DRM fraction was compared by immunoblotting and densitometry (described in section 2.3.5).

### 2.3.3. Isolation of low density membranes from rat synaptic plasma membranes by a detergent-free method

Anderson and co-workers isolated low density membranes (LDMs) from cultured cells and synaptic plasma membranes by a combination of sonication and density gradient centrifugation (Smart et al., 1995; Wu et al., 1997). The authors suggest that this method allows the purification of caveolae and lipid raft-like domains in the absence of detergent. LDMs were isolated from synaptic plasma membranes according to the procedure described by these authors (Wu et al., 1997).

All procedures were carried out at 4°C unless otherwise stated. Four whole rat brains were homogenised on ice in 0.3 M sucrose by 20 strokes of a Dounce homogeniser. The homogenate was centrifuged at 800 x g in a Beckman JA20 rotor for 20 minutes to remove tissue debris. The supernatant was then centrifuged at 9000 x g in a Beckman JA20 rotor for 20 minutes to sediment the crude synaptosome pellet. The pellet was washed once in 0.3 M sucrose then lysed in 0.03 M sucrose for 20 minutes. The membranes were collected by centrifugation at 25,000 x g for 20 minutes in a JA20 rotor. The membrane pellet was resuspended in 5 ml distilled water and homogenised with 5 strokes of a Dounce homogeniser, then adjusted to 1.1 M sucrose, 5 mM Tris-Cl pH 7.5 in a volume of 15 ml. This was placed at the bottom of a centrifuge tube and overlaid with 15 ml 0.8 M sucrose, followed by 5 ml 0.3 M sucrose, both in 5 mM Tris-Cl pH 7.5. The resulting sucrose density gradient was centrifuged at 48,000 x g for 2.5 hours in a Beckman SW28 rotor. The opaque band that appeared at the 0.8 M – 1.1 M sucrose interface was collected and designated synaptic plasma membranes (SPM).

The 1 ml SPM fraction was made up to 2 ml with LDM buffer (see table 2.2) and subjected to six 5 second sonication bursts using a 3 mm probe sonicator fitted to a Sanyo MSE Soniprep 150. Between each sonication burst the tube was cooled on ice for 2 minutes. The SPM sonicate was adjusted to 23 % (v/v) Optiprep (60 % (w/v) iodixanol in water, Axis-Shield PoC AS, Oslo, Norway) in LDM buffer, in a volume of 4 ml. This was transferred to a centrifuge tube and overlaid with a 20 – 10 % (v/v)

Optiprep continuous density gradient. The gradient was centrifuged at 52,000 x g for 2.5 hours in a Beckman SW41 rotor and twelve 1 ml fractions were collected. The top 5 ml were mixed with 4 ml 50 % (v/v) Optiprep in LDM buffer and overlaid with 3 ml 5 % (v/v) Optiprep. The resulting gradient was centrifuged at 52,000 x g for 1.5 hours in a Beckman SW41 rotor and twelve 1 ml fractions were collected. The opaque band that appeared at the Optiprep density interface was designated LDMs. Fractions were stored at -20°C prior to analysis.

### 2.3.4. Sodium-dodecyl sulphate polyacrylamide gel electrophoresis (SDS-PAGE)

Two alternative SDS-PAGE buffer systems were employed: Tris-glycine-SDS for the separation of proteins with molecular masses of 25 – 100 kDa and Tris-tricine-SDS for the separation of cholera toxin B subunit, a pentamer with a subunit molecular mass of ~ 12 kDa.

#### 2.3.4.1. Preparation of gradient fractions for SDS-PAGE

For most samples 20 or 25 µl sample was mixed with the appropriate volume of 3 x SDS loading buffer (Laemmli's buffer, see table 2.3), boiled for 3 minutes and loaded onto the gel. Where immunoblotting for Thy-1 was performed the samples were prepared in loading buffer without β-mercaptoethanol as reducing conditions destroy the Thy-1 antibody epitope. In some cases the gradient fractions were concentrated to facilitate detection of the protein of interest. The DRM fraction was routinely concentrated by centrifuging 200 – 900 µl at 100,000 x g in a Beckman TLA 100.3 rotor for 30 minutes at 4°C. This procedure resulted in sedimentation of the DRMs and the resulting membrane pellet was dissolved by resuspension in 1 x SDS loading buffer and 5 minutes incubation in a sonic bath. Following this samples were boiled for 3 minutes and loaded on the gel. Trichloroacetic acid (TCA) precipitation was used as an alternative method for concentrating both membrane and soluble protein fractions. An equal volume of 30 % (w/v) TCA was added to the

sample and incubated for 40 minutes at 4°C. The precipitated protein was collected by centrifugation at 13,000 rpm for 10 minutes in a bench top centrifuge. The resulting pellet was washed once with distilled water then resuspended in 1 x SDS loading buffer, boiled for 3 minutes and loaded onto the gel. Details are given in the figure legends concerning which concentration method was employed and the volume of each fraction loaded.

### 2.3.4.2. Tris-glycine SDS-PAGE conditions

Proteins were separated by denaturing PAGE using a discontinuous buffer system with two phase gels, based on the protocol described by Laemmli (King and Laemmli, 1971). Mini-Protean II PAGE apparatus from Biorad (Hemel Hempstead, UK) was employed for this procedure. Vertical slab gels were produced using 5 ml of resolving gel (components listed in table 2.3), overlaid with 1.5 ml stacking gel (components listed in table 2.3). Gels were fitted into the Mini-Protean II apparatus and the tank reservoirs filled with Tris-glycine running buffer (see table 2.3). Samples were prepared as described above (section 2.3.4.1) with 3 x SDS loading buffer (see table 2.3), boiled for 3 minutes and loaded onto the stacking gel. Pre-stained molecular weight protein markers with a range between 6.5 – 175 kDa (New England Biolabs, Ipswich, MA) were loaded alongside the samples. The samples were run through the stacking gel at 100 V, following which the voltage was increased to 150 V for separation through the resolving gel. Gels were either Coomassie blue stained (see table 2.3 for composition of stain and destain buffers) or transferred to nitrocellulose membrane for immunoblotting as described below (section 2.3.5).

**Table 2.3. Buffers for Tris-glycine SDS-PAGE**

| Buffer | Components | Concentration |
|---|---|---|
| Stacking gel | 37.5:1 Acrylamide: N,N'-methylenebisacrylamide (National Diagnostics, East Riding, UK)<br>Tris-Cl pH 6.8<br>Sodium-dodecyl sulphate (SDS)<br>Ammonium persulphate<br>N,N,N',N'-tetramethylethylenediamine (TEMED) | 5 % (w/v)<br>0.125 M<br>0.1 % (w/v)<br>0.1 % (w/v)<br>0.04 % (v/v) |
| Resolving gel | 37.5:1 Acrylamide: N,N'-methylenebisacrylamide<br>Tris-Cl pH 8.8<br>Sodium-dodecyl sulphate (SDS)<br>Ammonium persulphate<br>TEMED | 10 – 12 % (w/v)<br>0.375 M<br>0.1 % (w/v)<br>0.1 % (w/v)<br>0.1 % (v/v) |
| Tris-glycine running buffer | Glycine<br>Tris<br>SDS | 0.192 M<br>0.025 M<br>0.1 % (w/v) |
| 3 x SDS loading buffer (Laemmli's buffer) | Tris-Cl pH 6.8<br>Glycerol<br>SDS<br>β-mercaptoethanol<br>Bromophenol blue | 0.15 M<br>30 % (v/v)<br>6 % (w/v)<br>15 % (v/v)<br>0.1 % (w/v) |
| Coomassie blue stain | Acetic acid<br>Methanol<br>Coomassie brilliant blue (G250/R250) | 10 % (v/v)<br>45 % (v/v)<br>0.2 % (w/v) |
| Destain | Acetic acid<br>Methanol | 10 % (v/v)<br>30 % (v/v) |

### 2.3.4.3. Tris-tricine SDS-PAGE conditions

To resolve proteins of low molecular mass Schagger and von Jagow developed an alternative Tris-tricine-SDS discontinuous buffer system (Schagger and von Jagow, 1987). Vertical slab gels were prepared with 5 ml of resolving gel and 2 ml stacking gel with the buffer composition described in table 2.4. The gels were fitted into Biometra Minigel-twin apparatus (Goettingen, Germany); the bottom buffer reservoir was filled with anode buffer and the top reservoir with cathode buffer (see buffers

table 2.4). Samples were prepared as described in section 2.3.4.1, with 3 x SDS loading buffer, boiled for 3 minutes and loaded onto the stacking gel. Pre-stained molecular weight markers were run alongside the samples. Proteins were separated at a voltage of 100 V. Gels were transferred to nitrocellulose membrane for immunoblotting as described below (section 2.3.5).

**Table 2.4. Buffers for Tris-tricine SDS-PAGE**

| Buffer | Components | Concentration |
|---|---|---|
| Stacking gel | 29:1 Acrylamide: N,N'-methylenebisacrylamide (National Diagnostics, East Riding, UK) | 3.9 % (w/v) |
| | Tris-Cl pH 8.45 | 0.745 M |
| | SDS | 0.07 % (w/v) |
| | Ammonium persulphate | 0.02 % (w/v) |
| | TEMED | 0.12 % (v/v) |
| Resolving gel | 29:1 Acrylamide: N,N'-methylenebisacrylamide | 14.5 % (w/v) |
| | Tris-Cl pH 8.45 | 1 M |
| | Glycerol | 13.3 % (w/v) |
| | SDS | 0.1 % (w/v) |
| | Ammonium persulphate | 0.016 % (w/v) |
| | TEMED | 0.05 % (v/v) |
| Cathode buffer | Tris | 0.1 M |
| | Tricine | 0.1 M |
| | SDS | 0.1 % (w/v) |
| Anode buffer | Tris-Cl pH 8.9 | 0.2 M |

### 2.3.5. Immunoblotting (Western blotting)

Following SDS-PAGE the separated proteins were transferred from the gel to nitrocellulose membrane at a constant current of 0.2 A for 1.5 hours using Trans-blot SD semi-dry transfer apparatus from Biorad, in the presence of transfer buffer (see table 2.5). The nitrocelluose membrane was washed once in distilled water and Ponceau stained to check the transfer efficiency. Following destaining with distilled water, the membrane was blocked with 5 % non-fat dried milk (Marvel) dissolved in

TBS-T (see table 2.5) for 1 hour on an orbital shaker. The primary antibody was diluted in 5 % milk/TBS-T and incubated with the membrane for 1 hour with continuous agitation. Primary antibodies employed for immunoblotting are listed in table 2.6, along with the dilution factor used for each of them. The membrane was then washed 3 times with TBS-T for 10 minutes per wash and incubated with horse radish peroxidase conjugated secondary antibody diluted in 5 % milk/TBS-T for 1 hour. Anti-rabbit, anti-mouse and anti-goat secondary peroxidase conjugated antibodies were purchased from Biorad, Chemicon International (Temecula, CA) and Sigma-Aldrich respectively and employed at a dilution of 1:2000. Following incubation with secondary antibody, the membrane was again washed 3 times in TBS-T and once with distilled water. Bound secondary antibody was visualised using the enhanced chemiluminescence (ECL) system (GE Healthcare, Buckinghamshire, UK) and the membrane exposed to autoradiographic film (Kodak, Cedex, France) for varying time periods.

**Table 2.5. Buffers for immunoblotting**

| Buffer | Components | Concentration |
|---|---|---|
| Transfer buffer | Glycine<br>Tris<br>Methanol | 0.192 M<br>0.025 M<br>20 % (v/v) |
| Ponceau stain | Ponceau S<br>Trichloroacetic acid | 0.1 % (w/v)<br>3 % (w/v) |
| Tris buffered saline-Tween (TBS-T) | Tris-Cl pH 7.5<br>Sodium chloride<br>Tween 20 | 0.02 M<br>0.137 M<br>0.1 % (v/v) |

**Table 2.6. Primary antibodies for immunoblotting**

| Antibody | Dilution | Host | Supplier/Origin |
|---|---|---|---|
| 14-3-3 (pan) | 1:2000 | Rabbit | Alastair Aitken and co-workers, Edinburgh |
| 14-3-3 β | 1:2000 | Rabbit | Alastair Aitken and co-workers |
| 14-3-3 ε | 1:2000 | Rabbit | Alastair Aitken and co-workers |
| 14-3-3 γ | 1:3000 | Rabbit | Alastair Aitken and co-workers |
| 14-3-3 η | 1:2000 | Rabbit | Alastair Aitken and co-workers |
| 14-3-3 σ | 1:2000 | Rabbit | Alastair Aitken and co-workers |
| 14-3-3 τ | 1:2000 | Rabbit | Alastair Aitken and co-workers |
| 14-3-3 ζ | 1:2000 | Rabbit | Alastair Aitken and co-workers |
| Cholera toxin B subunit (CTXB) | 1:2000 | Goat | Calbiochem, Merck Biosciences, Darmstadt, Germany |
| Flotillin-1 C-20 | 1:500 | Goat | Santa Cruz Biotechnology, Santa Cruz, CA |
| Prion protein, 4F2 | 1:10,000 | Mouse | Gerhard Hunsmann, Goettingen, Germany |
| SNAP-25, SMI81 | 1:10,000 | Mouse | Sternberger Monoclonals, Lutherville, MD |
| Syntaxin-1a, HPC-1 | 1:2000 | Mouse | Sigma Aldrich, Poole, UK |
| Transferrin receptor, H68.4 | 1:500 | Mouse | Zymed laboratories, San Francisco, CA |
| Thy-1, OX7 | 1:1000 | Mouse | Roger Morris, King's College London |

### 2.3.5.1. Densitometry analysis of immunoblots

To quantify the proportion of particular proteins recovered in the DRM fraction immunoblots were analysed by densitometry. Band intensity was measured using ImageJ software (National Institutes of Health, USA) and only non-saturated immunoblots were used for densitometry. The band intensity in the DRM fraction (a) was usually expressed as a percentage of the band intensity of the whole lysate, soluble protein fraction or another loading control (b) to permit comparison between immunoblots and between experiments; i.e. (a / b) x 100 % = c, the proportion of the protein localised to the DRM fraction. For the cholesterol depletion experiments (using MβCD) in Chapter 5 these values were used to calculate the percentage change in recovery of particular proteins in the DRM fraction;

($c_{M\beta CD}$ / $c_{control}$) x 100 % equals the percentage of the protein found in the DRM fraction that remains DRM-associated following MβCD treatment. Subtracting 100 from this value gives the percentage change in DRM recovery of the protein, which is the figure presented in Chapter 5. Mean results from three separate experiments are presented ± the standard error of the mean (SEM).

### 2.3.6. Protein concentration determination

#### 2.3.6.1. Bradford assay

For determination of protein concentration according to the method of Bradford (Bradford, 1976) concentrated Bradford dye reagent (Biorad) was diluted 1:4 in distilled water. Samples were made up to 50 µl with distilled water and 200 µl diluted reagent added to give a 1:4 ratio of sample to diluted reagent. Following 5 minutes incubation at room temperature the absorbance was measured at 595 nm. Samples were analysed in triplicate and compared with a standard curve constructed using serial dilutions of bovine serum albumin (BSA) to allow calculation of protein concentration of samples from absorbance.

#### 2.3.6.2. Bicinchoninic acid (BCA) assay

The BCA assay kit was purchased from Pierce (Rockford, IL) and samples were analysed according to the manufacturer's instructions. Briefly, the samples were made up to a volume of 50 µl with distilled water and incubated with 1 ml working reagent (1:20 ratio) for 30 minutes at 60°C. The working reagent is produced by mixing 50 parts of reagent A (BCA containing solution) with 1 part of reagent B (4 % cupric sulphate). Following the incubation period samples were cooled to room temperature and the absorbance measured at 562 nm. Absorbance values were compared with a BSA standard curve to calculate protein concentrations.

### 2.3.7. Cholesterol assay

Infinity cholesterol liquid stable reagent was purchased from Thermo Electron (Waltham, MA). The assay is based on two sequential enzyme reactions. Cholesterol is converted to cholest-4-en-3-one by cholesterol oxidase. The by-product of this reaction, hydrogen peroxide, combines with hydroxybenzoic acid and 4-aminoantipyrine, in a reaction driven by peroxidase, to form quinoneimine dye, which absorbs at 500 – 550 nm. 10 µl sample was mixed with 1 ml Infinity reagent and incubated at 37 °C for 5 minutes. The absorbance (Abs) was measured at 500 nm and compared with that of a 2 mg/ml cholesterol standard prepared in the same way. Sample cholesterol concentration = (Abs $_{500\ nm}$ sample/Abs $_{500\ nm}$ standard) x 2 mg/ml

## 2.4. IMAGING TECHNIQUES

### 2.4.1. Immunostaining procedure

For imaging following fixation, cells were plated onto 25 mm diameter glass coverslips (thickness 1.0). To aid adhesion of PC12 cells the coverslips were coated with collagen (prepared from rat tail tendons in 10 % (v/v) acetic acid). PC12 cells were resuspended following the passage procedure described in section 2.1.1 and ~ 8 x $10^5$ cells were added to each well of a six well plate containing coated coverslips, in 2 ml complete RPMI media (see section 2.1.1). N2a cells were seeded onto uncoated coverslips, at a density of ~ 3 x $10^5$ cells per well in complete DMEM media (see section 2.1.2). Twenty four hours later, cells were rinsed once in PBS and fixed immediately with 4 % (w/v) paraformaldehyde (PFA) on ice for 30 minutes. Cells were washed twice with PBS then permeabilised with 0.1 % (v/v) TX-100 in PBS for 5 minutes and washed again with PBS to remove the TX-100. Cells were then blocked in 10 % (v/v) FBS in PBS plus 0.2 % (v/v) Tween-20 (PBS-T) for 1 hour at room temperature. The primary antibody was prepared in 10 % (v/v) FBS in PBS-T and incubated with the cells for 3 hours at 4 °C. The dilution factor for each antibody is given in table 2.7. The cells were washed three times for 15 minutes with PBS-T then incubated with fluorescently labelled secondary antibody at a 1:1000 dilution for 1 hour at room temperature. The secondary antibody was either anti-mouse IgG or anti-rabbit IgG conjugated to Alexafluor 647 (Molecular Probes, Invitrogen, Paisley UK). Following three more washes with PBS-T for 15 minutes each and one wash with PBS for 10 minutes, the cells were mounted with Mowiol (Calbiochem, Merck KGaA, Darmstadt, Germany). All washing steps and incubations were carried out on an orbital shaker at a low setting.

**Table 2.7. Primary antibodies for immunostaining**

| Antibody | Dilution | Host | Supplier/Origin |
|---|---|---|---|
| 14-3-3 (pan) | 1:1000 | Rabbit | Alastair Aitken and co-workers, Edinburgh |
| SNAP-25 (SMI81) | 1:2000 | Mouse | Sternberger Monoclonals, Lutherville, MD |
| Syntaxin-1a (HPC-1) | 1:500 | Mouse | Sigma Aldrich, Poole, UK |
| Thy-1 (OX7) | 1:100 | Mouse | Roger Morris, King's College London |

### 2.4.2. Cholesterol depletion and cholera toxin B subunit labelling

For fixed cell imaging, PC12 cells were plated as described in section 2.4.1 above. Twenty four hours later the media was removed and replaced with either 20 mM methyl-β-cyclodextrin (MβCD) in serum-free RPMI 1640 or an equal volume of PBS in serum-free media. Cells were incubated with MβCD for 30 minutes at 37°C. To label ganglioside GM1, cells were then incubated with 1 μg/ml fluorescein-5-isothiocyanate-conjugated cholera toxin B subunit (FITC-CTXB) for 5 minutes, at 37°C. Cells were then rinsed once in PBS, fixed immediately with 4 % (w/v) PFA and immunostained if required (described above in section 2.4.1). The same procedure was followed for N2a cells, except that cells were incubated with 10 mM MβCD (or an equal volume of PBS) in serum-free DMEM supplemented with 2mM L-glutamine.

For live cell imaging ~ 3 x $10^6$ PC12 cells were plated onto 42 mm diameter collagen coated coverslips in 60 mm diameter dishes. The following day cells were incubated with 1 μg/ml FITC-conjugated CTXB in complete medium for between 5 minutes to 30 minutes. The media was replaced to remove excess FITC-CTXB and the cells imaged immediately. Live cells were maintained on a stage heated to 37°C in a chamber containing 5 % (v/v) $CO_2$/95 % (v/v) air during imaging.

### 2.4.3. Cell viability assay

For live cell imaging ~ 3 x $10^6$ PC12 cells were plated on 42 mm diameter collagen coated glass coverslips in 60 mm diameter dishes. N2a cells (~ 8 x $10^5$ cells per dish) were plated onto uncoated 42 mm diameter coverslips. The following day cells were incubated with between 10 – 25 mM MβCD in PBS or an equal volume of PBS (as a control) in serum-free media for 30 minutes at 37°C. Following MβCD treatment, fluorescent dyes propidium iodide and Calcein AM (Molecular Probes, Invitrogen, Paisley, UK) were added to the cells (final concentration 3 μM for both dyes) and incubated for 5 minutes. Cells were then imaged immediately. Live cells were maintained on a heated stage in a chamber containing 5 % (v/v) $CO_2$/95 % (v/v) air during imaging. Propidium iodide stains nuclei but can not penetrate the plasma membrane of live cells so only dead cells are labelled by this dye. Propidium iodide was excited with a helium/neon laser line at 543 nm. Calcein stains live cells and was excited with an argon laser line at 488 nm. The number of live and dead cells in an image was counted using Volocity software (Improvision, Coventry, UK). Volocity was used to count the number of pixels showing propidium iodide or Calcein staining above an intensity threshold (to remove background). To estimate the number of stained cells, the number of stained pixels was divided by the average number of pixels in a propidium iodide stained nucleus or a Calcein stained cell. The percentage of cells that were viable was calculated by dividing the number of Calcein stained (live) cells in an image by the total number of cells (propidium iodide stained cells plus Calcein stained cells).

### 2.4.4. Filipin staining

PC12 and N2a cells were plated onto 25 mm diameter coverslips as for immunostaining. The following day the cells were incubated with either 20 mM MβCD (PC12) or 10 mM MβCD (N2a) or an equal volume of PBS for 30 minutes at 37°C. Cells were then rinsed once in PBS and fixed immediately with 4 % PFA on ice for 30 minutes. Following three washes with PBS, cells were incubated with

filipin at a concentration of 50 μg/ml in PBS with 10 % (v/v) FBS for two hours, at room temperature with gentle agitation. Excess filipin was removed by washing with PBS and the coverslips were mounted in PBS for immediate imaging, which was required due to the instability of filipin. Filipin was excited using a titanium sapphire multi-photon laser at 780 nm. The same photomultiplier tube (PMT) detector settings were employed for all samples on a given day so that their relative staining intensities could be compared. The mean pixel intensity for each image was calculated using Volocity software (Improvision, Coventry, UK), following background subtraction.

### 2.4.5. Image acquisition by confocal laser scanning microscopy (CLSM)

All images were acquired on a Zeiss Axiovert 100M confocal microscope fitted with an LSM510 scanning head, using the Zeiss LSM software.

Immunostained cells fixed in Mowiol were imaged using a Zeiss Plan Aprochomat 63 x oil immersion objective lens, with a numerical aperture (NA) of 1.4. FITC-CTXB labelled live cells were imaged with a Zeiss C-Aprochomat 1.2 NA 63 x water corrected immersion lens. FITC-CTXB was excited with an argon laser line at 488 nm and Alexafluor-647 secondary antibody with a helium/neon laser line at 633 nm. Fluorescence emission was acquired by a multi-track method using a 500 – 550 nm band pass filter to collect FITC emission and a 650 nm long pass filter to collect Alexafluor-647 emission. Using the multi-track approach the two lasers scan sequentially rather than simultaneously so that emissions are acquired separately to avoid bleed through and cross-talk. To permit image restoration (described below) images were sampled at Nyquist sampling frequency to acquire enough information and prevent aliasing effects caused by undersampling (Scientific Volume Imaging, 2006a; Webb and Dorey, 1995). To achieve Nyquist sampling rates the voxel size was set to 49 x 49 x 140 nm and the PMT detector gain and amplifier offset were adjusted so that voxel intensities were spread over the full dynamic range. Particular

care was taken to avoid intensity saturation as this represents a loss of image information.

Filipin stained cells mounted in PBS were imaged with a Zeiss C-Aprochomat 1.2 NA 63 x water corrected immersion lens. Filipin was excited using a titanium sapphire multi-photon laser at 780 nm. A 390 – 465 nm band pass filter was used to acquire the emitted light. Single slice images were obtained and analysed as described in section 2.4.4.

For the cell viability assay the propidium iodide/Calcain stained cells were imaged using a Plan Neofluar 0.3 NA 10 x lens to obtain single slice images of a large field of view. Propidium iodide was excited with a helium/neon laser line at 543 nm and Calcein with an argon laser line at 488 nm. Fluorescence emission was acquired by the multi-track method using a 500 – 550 nm band pass filter to collect Calcein emission and a 560 nm long pass filter to collect propidium iodide emission. Live and dead cells in each image were counted as described in section 2.4.3.

### 2.4.6. Image processing and analysis

Prior to colocalisation analysis image restoration was employed to remove out of focus information, haze and background signals. During the process of image acquisition by the microscope some information is lost and noise is added so the reconstructed image of a point source (described by the point spread function, PSF) is distorted or blurred. The dimensions of the PSF depend on the microscope system. An image can be viewed as composed of small objects each described by their intensity multiplied by the PSF. Image data deconvolution employs the dimensions of the PSF and microscope parameters, coupled with an iterative algorithm to partially restore the true shape of an object (Holmes et al., 1995; Shaw, 1995). It is very important that the raw image, subjected to data deconvolution, has been sampled at a high enough frequency, i.e. enough voxels (volume pixels) per unit volume, to contain sufficient information for this process and avoid aliasing. The necessary sampling rate (Nyquist sampling rate) was employed for all images, as

described in section 2.4.5. Image data deconvolution was carried out on all images using Huygens Essential software (Scientific Volume Imaging, Hilversum, The Netherlands) prior to further analysis, with a theoretical PSF calculated from the microscope parameters. Iterations of the Classical Maximum Likelihood Estimation (CMLE) algorithm were carried out on each image until the set quality threshold was achieved. This greatly improved resolution and removed blur, as illustrated by figure 2.1.

Chromatic aberration was observed in the resulting images, which is a problem for any colocalisation analysis. To correct for this 200 nm fluorescent diameter beads were employed that could be excited at 488, 543 and 633 nm. Bead images were deconvolved and the image from one channel was shifted by one pixel in x and y dimensions relative to the other channels until the position with the highest degree of correlation was found (as assessed by the Pearson's coefficient, discussed below). This gave the channel shift required to correct for chromatic aberration (+5 pixels in x and -5 pixels in y for the 488 nm channel relative to the 633 nm channel). Before colocalisation analysis this channel registration was performed on all images.

In this study the cellular structure of interest was the plasma membrane. However, for data deconvolution it was necessary to acquire 3-dimensional (3D) images of whole cells because emission pertaining to a single point source (i.e. the PSF) extends for some distance in the axial direction. Following data deconvolution 3D images were cropped to a single slice containing emission from the basal plasma membrane of the cells; the purpose being to remove the contribution of intracellular staining to colocalisation calculations. The basal plasma membrane images were further cropped to remove the edges of the cell, which showed particularly intense staining due to edge reinforcement effects (created by the vertical walls of plasma membrane above) and would therefore have artificially increased colocalisation values. The cropped images contained as much of the basal plasma membrane as possible without including edges.

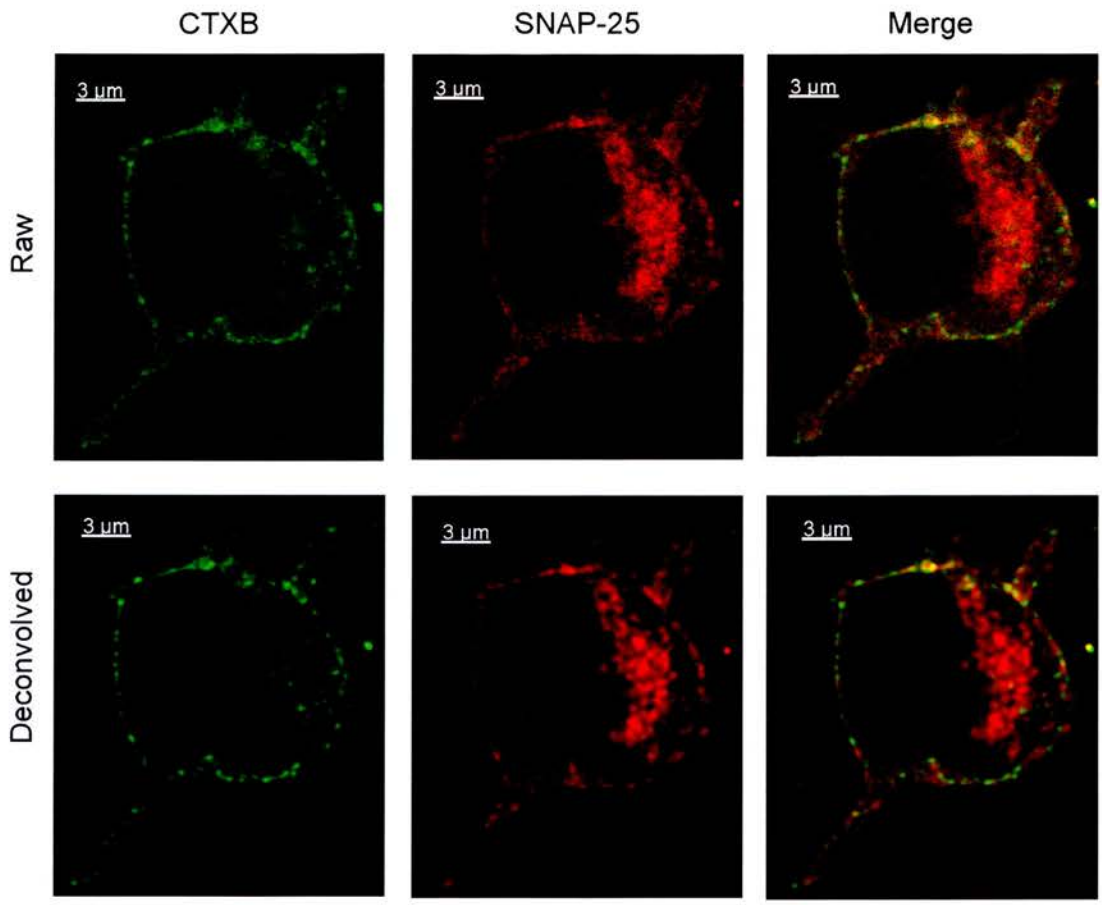


**Figure 2.1. Example of image data deconvolution**

N2a cells were labelled with CTXB following MβCD treatment, fixed and immunostained for SNAP-25. Cells were imaged by confocal microscopy at a sampling frequency that satisfies Nyquist criteria. An equatorial section through a cell is shown before (raw image, top row) and after (bottom row) data deconvolution.

#### 2.4.6.1. Analysis of CTXB and SNARE clusters

All image analysis was carried out after image data deconvolution. The size and plasma membrane density of puncta observed following CTXB-labelling or immunostaining were analysed using the following methods. The full width at half maximum intensity (FWHM) was employed as a measure of punctum or cluster size. Calculation of the FWHM is a standard method for defining cluster size (Lachmanovich et al., 2003; Lang et al., 2001; Ohara-Imaizumi et al., 2004). Images were displayed using Huygens Professional software to allow magnification of clusters so that individual pixels were visible. The FWHM was defined manually by first finding the highest intensity pixel at the centre of a cluster and then finding the two pixels along a line through the centre where the pixel intensity had reduced to half the maximum intensity, as shown in figure 2.2A. The distance between these pixels, the cluster diameter, was measured. The FWHM method for defining cluster size is illustrated by figure 2.2 B and C. At least 100 puncta from 4 – 8 separate images were measured for each sample group.

Cluster density was manually measured by counting the number of clusters in an image of known area. Clusters were defined as separate if the intensity reduced to 25 % of the peak intensity between them. An example image with counted clusters marked is shown in figure 2.2 D and E. Automatic methods for cluster counting were explored but all require thresholding to identify and separate clusters. The broad range of cluster peak intensities made it difficult to threshold an image and retain all low intensity clusters whilst keeping higher intensity clusters separate. For CTXB labelling the total intensity per unit area was also calculated using Huygens Professional software to determine the sum of all voxel intensities in an image of known area. At least 10 images from at least two separate experiments were analysed for calculation of cluster density and total intensity per unit area.

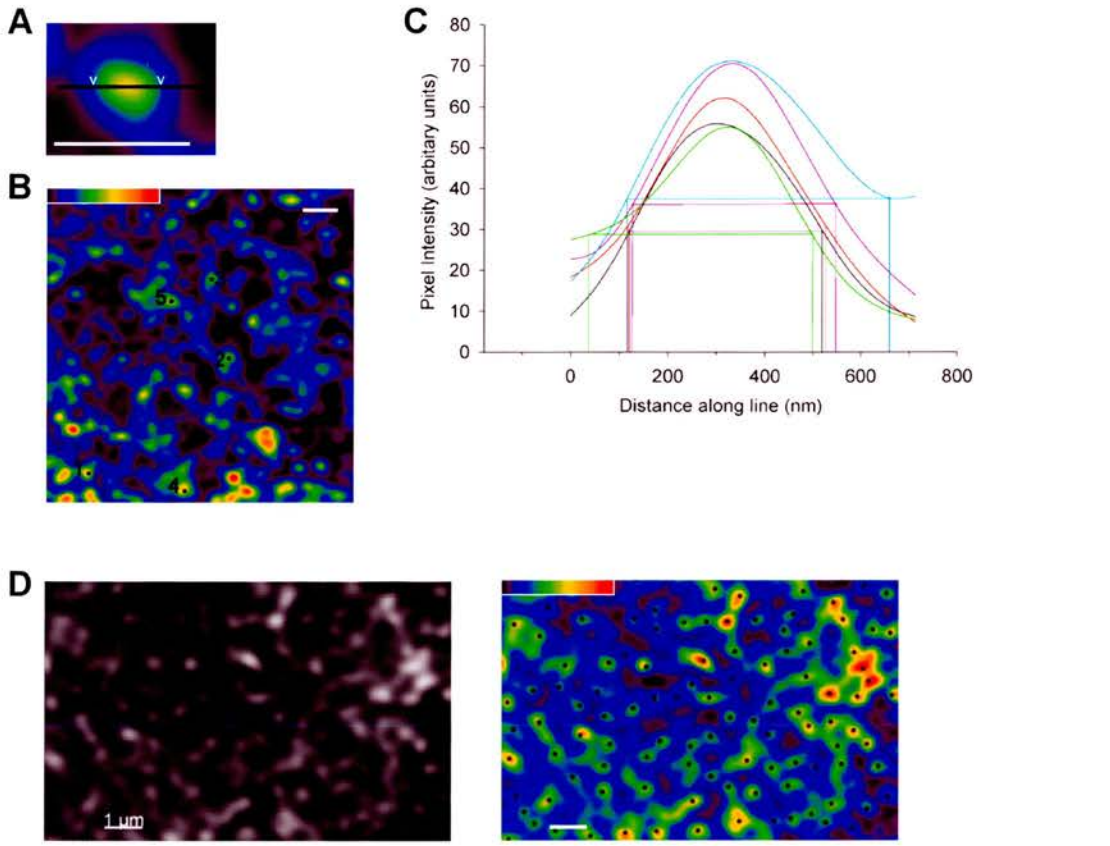


**Figure 2.2. Analysis of cluster size and density**

**A** Magnified cluster from the image in B. The cluster FWHM was determined by finding the two pixels along the line, to either side of the centre, where the intensity was equal to half the peak intensity (shown by two white arrows). The distance between these pixels is the FWHM size. **B** False colour image of CTXB staining on the plasma membrane of an untreated N2a cell. Lines were drawn through the clusters labelled 1 – 5, similar to panel A, and the intensity along these lines measured. **C** Visual representation of the FWHM method of determining cluster size. Intensity line plots along lines through clusters 1 – 5 show cluster centre peak intensities. Horizontal lines are drawn across each plot at the half maximal intensity and dropped lines show the cluster width on the x axis. The FWHM for these 5 spots ranged between 430 – 570 nm. **D** Image of SNAP-25 staining on the plasma membrane of an untreated N2a cell in greyscale and false colour. Each object counted as a cluster for calculation of cluster density is marked by a black dot on the false colour image. False colour scale from 0 (black) to 255 (red) intensity units is shown by the coloured bars in B and D. All white scale bars = 1 µm.

### 2.4.6.2. Quantification of colocalisation and image correlation

Analysis of coincident staining in fluorescent two channel images is central to this study. Simple visual inspection of merged red and green channel images for yellow overlapping areas fails to provide the quantitative information necessary for comparing images. Therefore two alternative methods will be presented throughout this study to quantify the amount of overlap between the red and green channels: Pearson's correlation coefficient and percentage colocalisation based on Manders' coefficients. Implementation and interpretation of these parameters is discussed below, along with some of their limitations.

Pearson's coefficient, R describes the intensity dependent correlation between the two channels, giving a value between -1 and 1. R = 1 represents perfect correlation, when R = 0 there is no correlation between the images and R = -1 represents perfect negative correlation. R was calculated from deconvolved image data using Imaris software (Bitplane AG, Zurich, Switzerland). For ease of interpretation, $R^2$ x 100 % gives the percentage of the red channel variance that can be explained by variation in the green channel (Scientific Volume Imaging, 2006b). Pearson's coefficient, R, is calculated using the following equation:

$$R = \frac{\sum((r_i - r_{avg})(g_i - g_{avg}))}{\sqrt{\sum(r_i - r_{avg})^2 \sum(g_i - g_{avg})^2}}$$

Where $r_i$ = intensity of each voxel in the red channel, $r_{avg}$ = mean intensity in the red channel, $g_i$ = intensity of each voxel in the green channel, $g_{avg}$ = mean intensity in the green channel. Summations of voxel intensities with an index $i$ include all voxels over the entire image.

Pearson's coefficient and other correlation analysis procedures provide a good method for statistically comparing the coincidence of two fluorphores between images (Demandolx and Davoust, 1997; Li et al., 2004; Manders et al., 1992; Parmryd et al., 2003). However, R gives no indication of the relative contribution of

the red and green channels to colocalisation. To overcome this shortcoming, Manders devised an alternative method for quantifying colocalisation (Manders et al., 1993). Manders coefficients describe the fraction of total red signal that is colocalised with green signal ($M_1$) and the fraction of total green signal that is colocalised with red signal ($M_2$) to assess percentage overlap.

$$M_1 = \frac{\sum r_{i,\,coloc}}{\sum r_i} \qquad\qquad M_2 = \frac{\sum g_{i,\,coloc}}{\sum g_i}$$

Where $r_i$ = intensity of each voxel in the red channel, $g_i$ = intensity of each voxel in the green channel. $\sum r_{i,coloc}$ = sum of intensities in the red channel of all voxels for which $g_i > 0$. $\sum g_{i,coloc}$ = sum of intensities in the red channel of all voxels for which $r_i > 0$. Summations of voxel intensities with an index $i$ include all voxels over the entire image.

Using this method a pixel registers as colocalised if the intensity in both the red and the green channel is greater than 0. This creates a problem if background pixels have an intensity greater than 0 as all pixels will appear colocalised and results will not be meaningful. Therefore some mode of thresholding must be employed. Choosing the thresholds involves user bias so an automatic thresholding method was sought. Costes and co-workers devised an automatic thresholding algorithm that has been incorporated into Imaris software (Bitplane AG, Zurich, Switzerland) and into ImageJ software (National Institutes of Health, USA) (Costes et al., 2004). This method and the resulting colocalisation mask are illustrated for an example image in figure 2.3 A-C. The example two channel image and merge is shown in figure 2.3A. Figure 2.3B shows a scatter plot where the red intensity in each pixel (y-axis) has been plotted against the corresponding green intensity (x-axis) for every pixel in the image. Costes' algorithm uses Pearson's coefficient (R) as a measure of correlation.

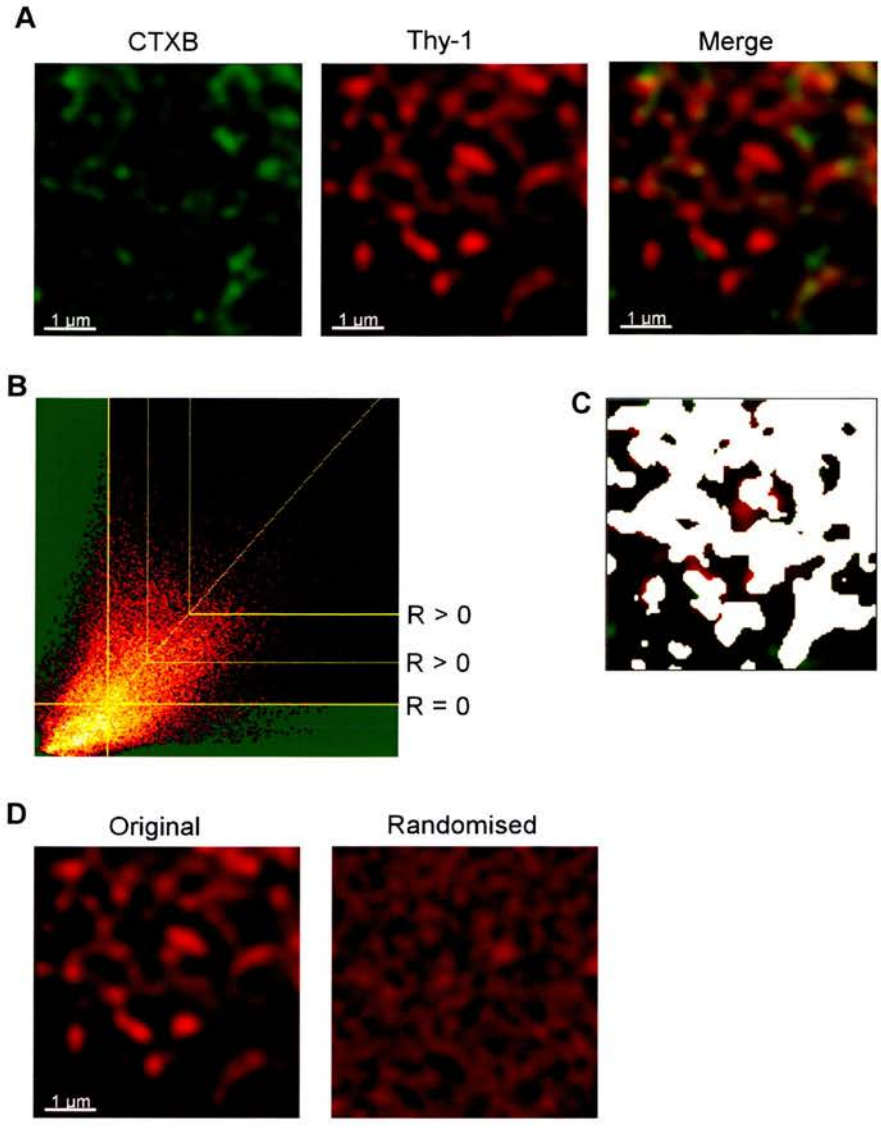


**Figure 2.3. Analysis of colocalisation and correlation**

PC12 cells were labelled with CTXB, fixed and immunostained for Thy-1. **A** Image from the base of a representative cell, showing CTXB staining in green and Thy-1 staining in red and the merged image. **B** Scatter plot of red pixel intensity against green pixel intensity for each pixel in the image in panel A. The diagonal line represents perfect correlation, the tighter the distribution of points around this line the higher the correlation described by R. Costes' algorithm incrementally lowers the threshold (represented by yellow vertical and horizontal lines) until a threshold is reached below which R = 0 (represented by the green area). **C** Mask showing all the pixels above the threshold in B. **D** The Thy-1 image from A alongside an example randomised image created by Costes randomisation test in ImageJ.

The algorithm incrementally lowers the thresholds starting at the highest intensity until it reaches the threshold below which R = 0, i.e. there is no correlation between the intensities from each channel (see figure 2.3B). The colocalisation mask in figure 2.3C shows all the pixels above the threshold in white. The percentage colocalisation of the red channel with the green channel and vice versa were calculated, based on the Manders method. The sum of red pixel intensities in the colocalisation mask was divided by the sum of all red pixel intensities from the whole image. The same procedure was employed for the green channel. The sum of intensities in each channel and the mask were calculated using Huygens Professional software.

The percentage correlation ($R^2$ x 100% or Pearson's coefficient) and the percentage colocalisation calculated from the Costes threshold mask are complimentary methods for describing overlap. The Pearson's coefficient is informative because it describes intensity dependent correlation, i.e. the degree to which the localisation of green signal or objects depends on the localisation of red signal or objects. The main disadvantage of Manders's method is that it does not take into account whether areas of high red intensity overlap with areas of high green intensity as all pixels above the threshold contribute to the measurements. However, the colocalisation mask created by the Costes thresholding process provides a useful visual representation of overlap, whilst percentage correlation is much more difficult to transform into an image map because the value R is calculated over the whole image. Because the Costes thresholding process employs R to set the thresholds the colocalisation mask relates to the degree of correlation in the whole image. Pixels within the mask show some degree of intensity dependent correlation, whereas those outside the mask show no correlation. Thus it is useful to present the colocalisation mask alongside $R^2$ x 100% and the percentage colocalisation values that estimate the contribution of each channel to coincident staining.

Another advantage of Pearson's correlation analysis over Manders colocalisation analysis is that no thresholding of the images is required. However, a degree of positive correlation might be expected between randomly distributed membrane puncta due to chance. Therefore some method is required to assess whether the

observed R value demonstrates significant correlation between the two channels above random level. Costes and co-workers also devised a method for randomising the signal in one channel so that a value for random correlation can be obtained (Costes et al., 2004). Rather than randomising all pixels separately this method divides the red channel image into tiles the size of the PSF to retain some of the structure from the image and calculates R with respect to the original green channel image. An example original image and corresponding randomised image are shown in figure 2.3D. For each image fifty iterations of the randomisation procedure were carried and the original R value compared with the mean R(random) value (by paired T-test) to determine whether the original red channel showed significantly more correlation with the green channel than would be expected due to random variation. As an alternative to Costes randomisation test, random correlation was calculated by flipping the red channel image through 180° in the x or y dimensions (using Imaris software) and recalculating R with respect to the original green channel.

In summary, for each set of images the percentage correlation between the channels ($R^2$ x 100%) was calculated and the significance of this value determined by Costes randomisation test. The percentage colocalisation of the red with the green channel and the percentage colocalisation of the green with the red channel were calculated following automatic thresholding of the images. Mean values are presented along with example colocalisation masks produced by the automatic thresholding procedure. Statistical analysis was performed using the SigmaStat software package (Systat software, London, UK). Values of correlation or colocalisation provide a method for quantitatively comparing the effect of two treatments or labelling of two different proteins on coincident staining.

# Chapter 3: 14-3-3 associates with detergent resistant membranes

# 3. 14-3-3 associates with detergent resistant membranes

Cholesterol and sphingolipid-rich membrane microdomains, termed lipid rafts, have been extensively investigated as signaling platforms. 14-3-3 proteins are also important regulators of numerous intracellular signaling processes. Both 14-3-3 proteins and lipid rafts have been implicated in the regulation of the Ras/Raf/MAPK signaling pathway and apoptotic cell death pathways. The importance of these pathways in cellular regulation and survival provided grounds for the investigation of whether 14-3-3 proteins associate with lipid rafts.

Though it is over 15 years since cholesterol and sphingolipid-rich $L_o$ domains were first hypothesized to exist in the plasma membrane, *in vivo* identification of these domains is still a challenge. Current theories ascribe this to the probable nanometre scale size of steady state lipid rafts (Hancock, 2006; Kusumi et al., 2004; Lagerholm et al., 2005; Mayor and Rao, 2004; Subczynski and Kusumi, 2003). The TX-100 extraction procedure is an established biochemical method for isolating detergent resistant membranes (DRMs) that are believed to represent clustered lipid rafts (Brown and Rose, 1992; London and Brown, 2000; Shogomori and Brown, 2003; Simons and Ikonen, 1997). In this chapter the association of 14-3-3 proteins with DRMs isolated from rat brain, where 14-3-3 protein is particularly abundant, is investigated. The mode of interaction of 14-3-3 with DRMs was investigated using a peptide inhibitor of 14-3-3 interactions. DRMs were also purified from two cell lines that are often used as models for neuronal cell types: Neuro-2a (N2a, a mouse neuroblastoma derived cell line) and PC12 (a rat adrenal pheochromocytoma derived cell line). In these cell lines the cholesterol and temperature dependence of 14-3-3 association with DRMs was studied. Detergent free methods have also been reported to isolate cholesterol and sphingolipid-rich membranes and such an approach was explored with respect to 14-3-3 association.

## 3.1. Isolation of DRMs from whole rat brain

### 3.1.1. DRMs isolated from rat brain possess the characteristics of lipid rafts

DRMs were isolated from rat brain homogenate on a sucrose density gradient (illustrated in figure 3.1A), as described in Chapter 2, section 2.3.1.1. An opaque band was observed at the 5 % - 30 % sucrose interface, corresponding to fraction 8 and designated the DRM fraction. The majority of the cellular protein remained in the 40% sucrose layer, contained in fractions 16 – 20 (see figure 3.1B) and termed the TX-100 soluble protein fractions.

To confirm that the DRMs had lipid raft characteristics the cholesterol concentration and presence of protein markers in the DRM fraction was determined. The cholesterol concentration of each sucrose density gradient fraction was measured using a colorimetric assay (see Chapter 2, section 2.3.7). Figure 3.1B shows the distribution of cholesterol and total protein across the gradient. It is clear that most of the cholesterol resides in the DRM fraction (fraction 8). The mean cholesterol concentration in the DRM fraction (number 8) was 1.0 mg/ml, whereas in fraction 20 it was less than 0.05 mg/ml. In contrast the protein concentration is almost ten-fold higher in the soluble protein fractions (mean of 2.6 mg/ml in fraction 20) than in the DRM fraction (mean of 0.3 mg/ml). This shows that only a small proportion of the total protein resides in the DRMs. This enrichment of cholesterol versus protein concentration is characteristic of DRM preparations (Brown and Rose, 1992; Prinetti et al., 2000). Lipid rafts are suggested to be rich in cholesterol relative to the bulk plasma membrane (Silvius, 2003a; Simons and Ikonen, 1997).

The peak of total protein concentration in fraction 8 led me to analyse the protein composition of the fractions. Figure 3.2A demonstrates that the protein composition of

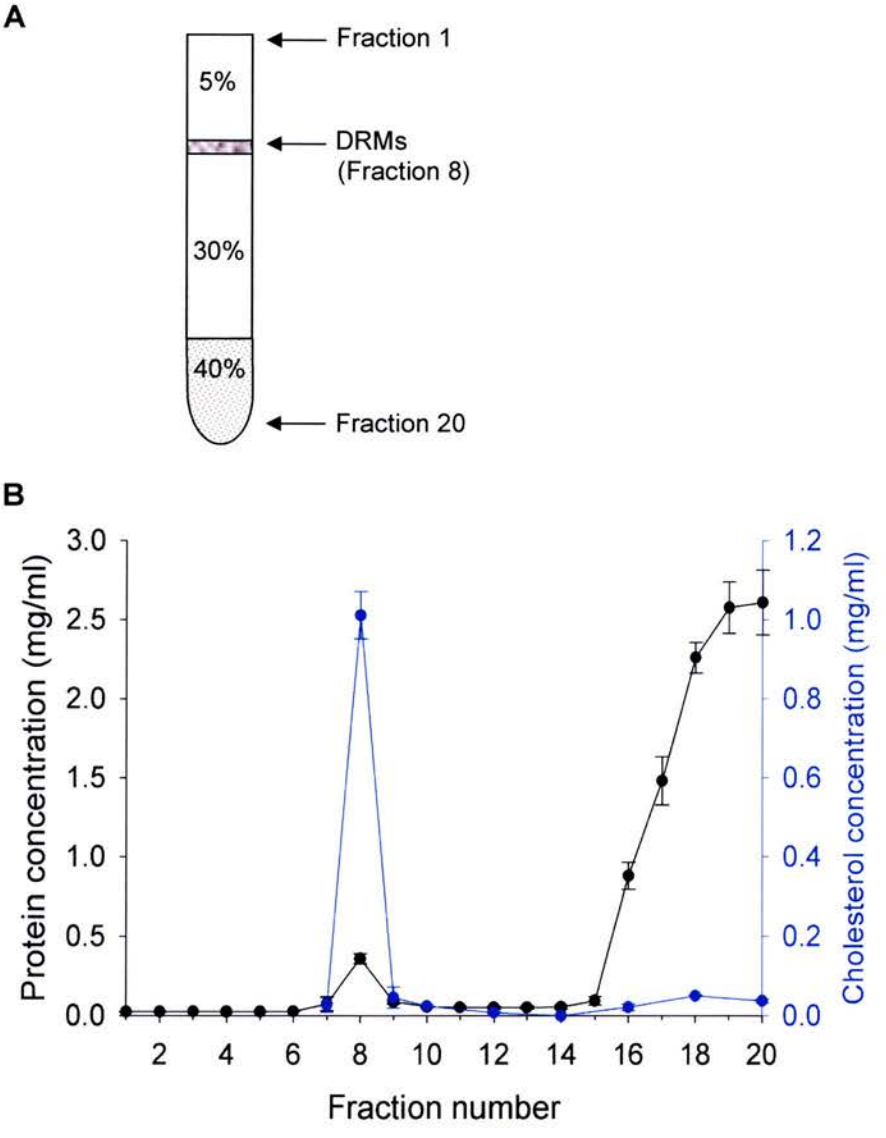


**Figure 3.1 The detergent resistant membrane (DRM) fraction isolated from rat brain is enriched in cholesterol**

DRMs were isolated from rat brain by TX-100 extraction, followed by flotation on a sucrose density gradient, as described in Chapter 2, section 2.3.1.1. **A** A schematic representation of the discontinuous sucrose gradient used, with the percentage sucrose in each layer labelled. The gradient was collected as 20 fractions and fraction 8 contained the DRMs. **B** The protein (black line) and cholesterol (blue line) concentrations (mg/ml) of each fraction are shown. Each point represents the mean ± SEM, n = 3.

the DRM fraction was different from that of the soluble protein fractions. The Coomassie blue staining pattern of fraction 8 is different from that of fraction 17 – 20. For example, the strongest band in fraction 20 is at ~ 50 kDa but this band does not appear as strong, relative to the other bands, in fraction 8. Two strong bands around 60 - 65 kDa in fraction 8 are not as prominent in fractions 17 - 20. It is also apparent from figures 3.1B and 3.2A that the protein concentration of fractions 1 – 7 and 9 – 15 was very low. This shows that the DRMs were concentrated at the 5% - 30% sucrose interface and were well separated from the soluble protein fractions.

The sucrose gradients were immunoblotted with antibodies against two lipid raft markers: flotillin-1 and prion protein (PrP). Bickel *et al* demonstrated that flotillin-1 associates specifically with caveolae from murine lung and lipid raft-like membranes from murine brain, isolated by three different methods (Bickel et al., 1997). It has since been determined that flotillin-1 associates with DRMs via palmitoyl and myristoyl modifications (Morrow et al., 2002; Neumann-Giesen et al., 2004). Flotillin-1 is frequently used as a lipid raft marker (Abrami et al., 2003; Chamberlain et al., 2001; Fallon et al., 2002; Kokubo et al., 2003; Salaun et al., 2005a). PrP is also enriched in DRMs due to its GPI-anchor (Naslavsky et al., 1997; Vey et al., 1996). In this DRM preparation flotillin-1 and PrP were both enriched in the DRM fraction and undetectable in the soluble protein fractions (see figures 3.2 B and C). The three bands detected by the anti-PrP antibody in figure 3C are likely to correspond to differently glycosylated forms of the protein (Korth et al., 2000; Rudd et al., 2001).

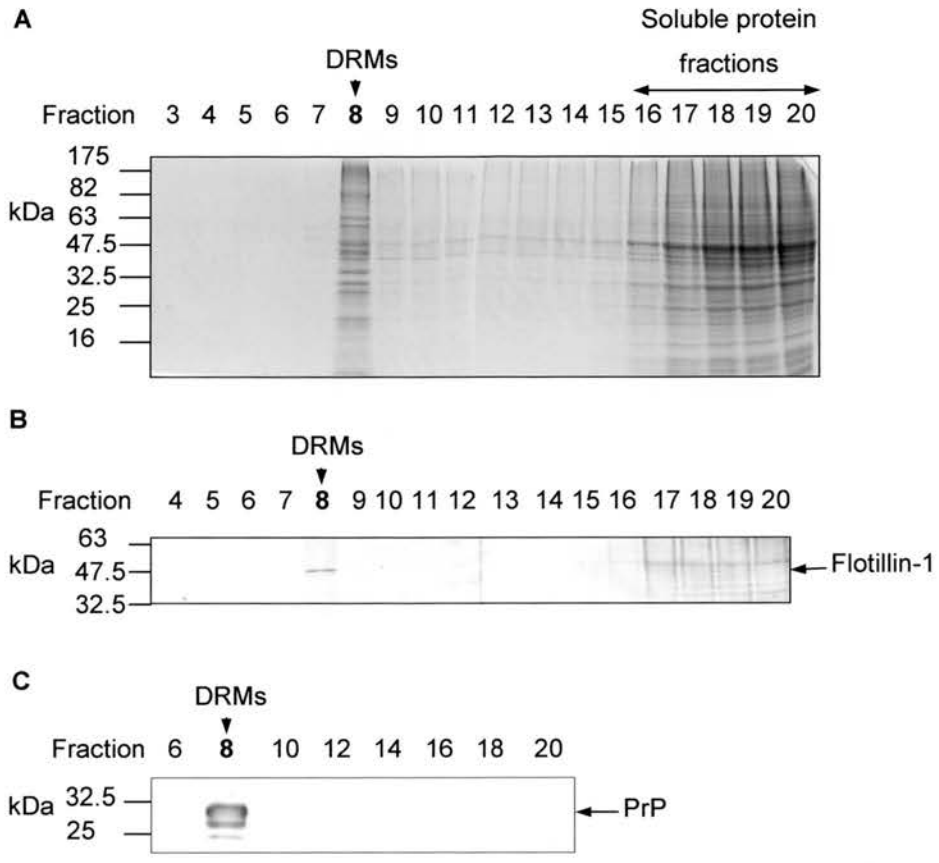


**Figure 3.2 The protein composition of the DRM fraction differs from the rest of gradient and contains lipid raft markers**

DRMs were isolated from rat brain on a sucrose density gradient, as described in Chapter 2, section 2.3.1.1. 20µl of each fraction from the gradient was separated by SDS-PAGE. Gradient fraction numbers are indicated, fraction 20 is the bottom of the gradient. **A** Coomassie blue stained gel of the gradient fractions. **B** Immunoblot with anti-flotillin-1 antibody. **C** Immunoblot with anti-PrP antibody.

### 3.1.2. Transferrin receptor also associates with DRMs

The membrane resident protein transferrin receptor (TfR) is frequently used as a negative control for DRMs and is described as a 'non-raft' protein that localises exclusively to the soluble protein fractions of the gradient (Chamberlain et al., 2001; Harder et al., 1998; Magee et al., 2005; Roper et al., 2000; Salaun et al., 2005a; Takeda et al., 2003; Taverna et al., 2004). The popularity of TfR as a non-raft control can probably be attributed to a study by Smart and co-workers where they developed a detergent-free method for isolating caveolae (Smart et al., 1995). They showed by immunoblotting that whilst TfR was very abundant in their plasma membrane fraction it was absent from the caveolar membrane fraction.

Though not all DRM studies include such a negative control, for completeness of the present study the localisation of TfR in the density gradients was assessed. Figure 3.3 shows that transferrin receptor was detected in the DRM fraction isolated from rat brain homogenate. A similar amount of each fraction was loaded on the gels in figure 3.3 as in the gels in figure 3.2, in which rat brain DRMs were immunoblotted with anti-flotillin-1 and anti-PrP antibodies. The immunoblots were also exposed for similar lengths of time (around 5 minutes) so it is not the case that a particularly long exposure or an increased amount of DRM fraction was required to detect TfR. However, it is clear from figure 3.3 that the majority of TfR protein resides in the soluble protein fractions of the gradient; it is certainly not concentrated in the DRM fraction as observed for flotillin-1 and PrP (figure 3.2).

Despite the fact that TfR is usually dismissed as a non-raft protein, Batista and co-workers found that ~50% of the TfR redistributes to the DRM fraction in Jurkat T-cells on stimulation with anti-CD3 antibodies (Batista et al., 2004). They went on to use immunofluorescence microscopy to show TfR colocalisation with DRM-associated protein Lck after stimulation. In addition, there appears to be a weak TfR signal in the

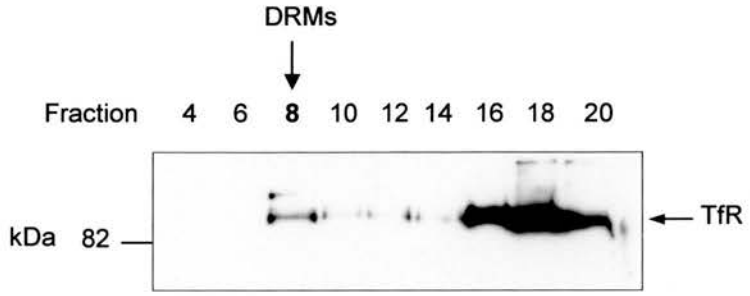


**Figure 3.3 Transferrin receptor is present in DRMs isolated from rat brain**

Detergent resistant membranes were isolated from whole rat brain homogenate by TX-100 extraction, followed by flotation on a sucrose density, as described in Chapter 2, section 2.3.1.1. 25µl of alternate fractions 4 - 20 was immunoblotted with anti-TfR antibody.

DRM fraction from unstimulated cells, though the authors do not comment on it. This study demonstrates that the localisation of TfR is not strictly non-raft.

The appearance of TfR in DRM fraction could also be due to incomplete solubilisation of the bulk plasma membrane. To explore this possibility DRMs were prepared from rat brain at increasingly high detergent to protein ratios and the distribution of TfR was monitored. Whole rat brain was homogenised in 1% (v/v) TX-100 and the protein concentration was determined, as described in Chapter 2, section 2.3.1.1. The homogenate was then diluted with additional homogenisation buffer to protein concentrations between 1 – 8 mg/ml and incubated with agitation for an hour to ensure thorough mixing. The density of TX-100 is 1.07 g/ml so a 1% by volume solution of TX-100 has a detergent concentration of 10.7mg/ml. Therefore 1 mg/ml protein in 1 % (v/v) TX-100 gives a detergent to protein ratio of around 10:1 (w/w). 8 mg/ml protein in 1 % TX-100 gives a detergent to protein ratio of around 5:4 (w/w). Figure 3.4A shows the DRM fractions from each of the gradients resulting from the 1 – 8 mg/ml homogenates, immunoblotted for TfR. It is clear that even at a detergent to protein ratio of 10:1 (w/w) (1 mg/ml protein) some TfR localises to the DRM fraction. In figure 3.4B the results of a similar experiment are shown, here the TX-100 concentration was varied instead of the protein concentration. 1 % (v/v) and 2 % (v/v) TX-100 correspond to detergent to protein ratios of 5:1 (w/w) and 10:1 (w/w) respectively. At 2 % (v/v) TX-100 TfR still partially associates with DRMs, along with lipid raft marker PrP. It should be noted that it was necessary to concentrate the DRM fractions by centrifugation at 100,000 x g (described in Chapter 2, section 2.3.4.1) to detect TfR at the highest detergent to protein ratio. This suggests that the detection of TfR in DRMs in other studies may have been hindered by low protein concentration and antibody sensitivity. A study by Parkin and co-workers illustrates this point. Whilst they detected no amyloid precursor protein by immunoblotting of mouse cerebral cortex DRMs prepared at 2 mg/ml protein and 1 % (v/v) TX-100, concentration of the DRMs showed that amyloid precursor protein was in fact present (Parkin et al., 1999).

Figure 3.4 demonstrates that at detergent to protein ratios between 5:4 and 10:1 (w/w) some TfR associates with the DRM fraction. Ostermeyer and co-workers found a stable level of protein association with DRMs at detergent to protein ratios of 5:1 (w/w) and above. This lends some support to the assertion that the presence of TfR in the DRM fraction is not due to incomplete solubilsation of cellular protein, but unfortunately no reliable method is available to confirm full solubilisation of the bulk phase of the plasma membrane.

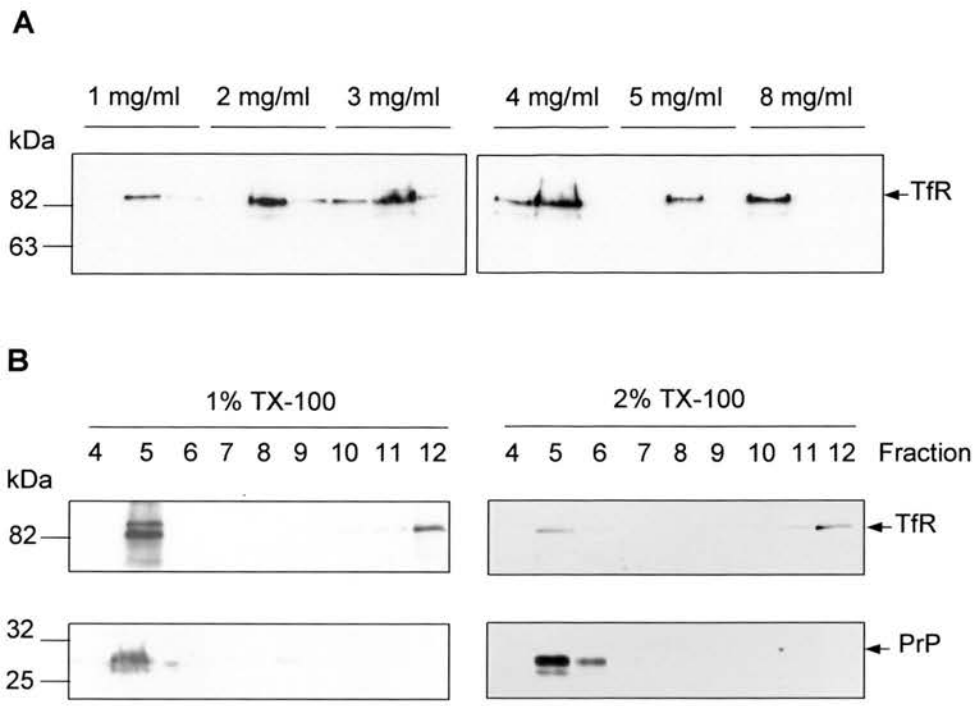


**Figure 3.4 Transferrin receptor associates with DRMs at a range of detergent to protein ratios**

Whole rat brain extract was prepared with increasing concentrations of TX-100 and the localisation of TfR in the gradient was monitored. **A** Rat brain was homogenised in 1 % (v/v) TX-100 at between 1 – 8 mg/ml protein and DRMs were isolated on a sucrose density gradient. For 1 – 4 mg/ml protein 400 µl of each DRM fraction 3 – 5 was concentrated (as described in Chapter 2, section 2.3.4.1) and separated by SDS-PAGE. For 5 – 8 mg/ml protein 25 µl of fractions 3 - 5 was separated by SDS-PAGE. Immunoblotting was carried out using anti-TfR antibody. **B** Rat brain at a concentration of 2 mg/ml protein was homogenised in either 1 % (v/v) or 2 % (v/v) TX-100 and DRMs isolated. 400 µl of concentrated DRM fraction (fraction 5) or 25 µl of each other fraction were separated by SDS-PAGE and immunoblotted with anti-TfR or anti-PrP antibodies.

### 3.1.3. 14-3-3 proteins associate with DRMs isolated from rat brain

Having verified that the cholesterol rich fractions contained classical DRM markers it was then possible to investigate the presence of 14-3-3 proteins in the DRM fraction. Rat brain was solubilised in either 1 % or 2 % (v/v) TX-100, giving detergent to protein ratios of 5:1 and 10:1 (w/w) respectively. Following isolation of the DRMs by flotation on a sucrose density gradient, the DRM fractions were concentrated by centrifugation to sediment the membrane and analysed by immunoblotting. Figure 3.5A shows that at both detergent to protein ratios a proportion of the total 14-3-3 localised to DRMs.

Antibodies demonstrated to be highly specific for each 14-3-3 isoform have been raised (Martin et al., 1993; Martin et al., 1994), making it possible to investigate which of the individual 14-3-3 isoforms associated with DRMs from rat brain. 14-3-3 β, ε, γ, η and ζ isoforms are very abundant in mammalian brain, whereas 14-3-3 τ is only expressed at a low level and 14-3-3 σ is virtually undetectable (Leffers et al., 1993; Patel et al., 1994). In agreement with these reports, preliminary experiments failed to detect 14-3-3 σ or τ in the gradient fractions so only the five brain abundant isoforms were further investigated. Figure 3.5B shows the distribution of 14-3-3 isoforms β, ε, γ, η and ζ across the sucrose density gradient, equal volumes of each fraction were separated here. Most of the 14-3-3 protein is localised to the detergent soluble fractions (fractions 16 – 20). However, a small proportion of each isoform is localised to fraction 8, which contains the DRMs. 14-3-3 proteins are clearly not exclusively present in the DRMs, unlike raft markers PrP and flotillin-1. From figure 3.5B there appears to be some difference between the distributions of each of the brain abundant isoforms across the density gradient. 14-3-3 β and η seem to be more evenly distributed across the middle part of the gradient than 14-3-3 ε and γ. 14-3-3 β and η are present in fractions 10 - 15 at a similar level to the DRM fraction. 14-3-3 ε and γ are more concentrated in the DRM fraction. 14-3-3 ζ was the isoform most difficult to detect, though long exposure of the blots showed it was present. It is not possible to compare the signal intensity in the DRM

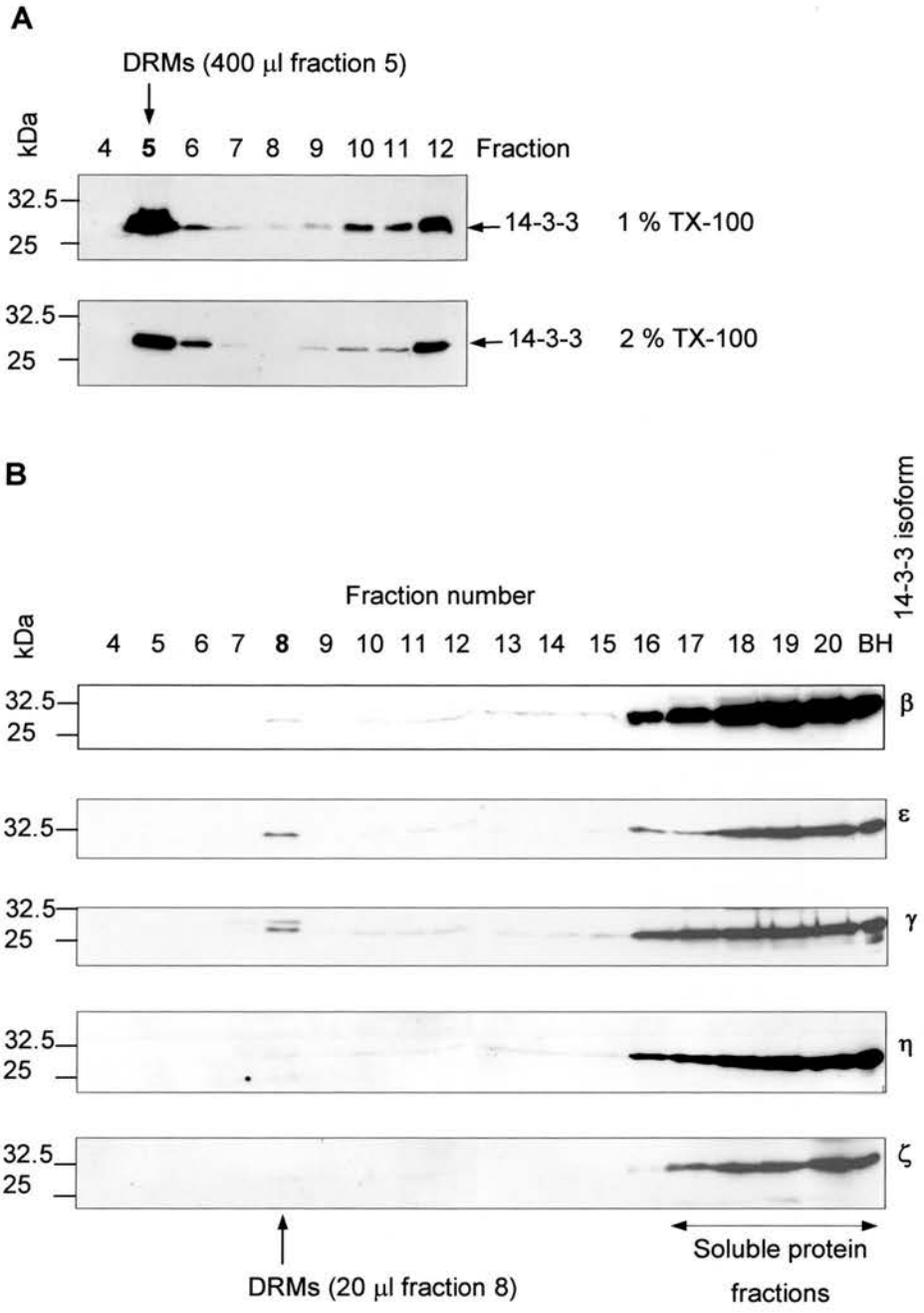


**Figure 3.5 14-3-3 proteins associate with DRMs isolated from rat brain**

fraction directly between isoforms because of the intrinsic variability between immunoblots and antibodies. The proportion of each isoform in DRMs compared with the soluble protein fraction also could not be determined from the results in figure 3.5B as the signal in fraction 16 - 20 is clearly saturated. This point is addressed in section 3.1.4.

### 3.1.4. The extent of association with DRMs differs between 14-3-3 isoforms

The existence of seven mammalian 14-3-3 isoforms presents the possibility of isoform specific functions. Despite the high sequence homology between 14-3-3 isoforms, isoform specificity has been reported for a number of protein interactions (as discussed in Chapter 1, section 1.2.2.2). Thus the potential isoform specificity of 14-3-3 protein association with DRMs is of interest.

The isoform specific 14-3-3 antibodies have different titres and there is likely to be variation between transfer efficiency and exposure, therefore it was not possible to quantitatively compare immunoblots carried out with the different antibodies. Instead the 14-3-3 signal from the DRM fraction was compared against the signal from a soluble protein fraction (fraction 11 from small (12 ml) gradients) to estimate the relative partitioning of each isoform into DRMs versus the soluble material. DRMs were again isolated from rat brain homogenate by extraction in 1 % TX-100 and flotation on 12 ml sucrose density gradients.

In figure 3.6, five-fold less fraction 11 than DRM fraction was loaded to produce well exposed immunoblots for quantification by densitometry. The aim here was to compare partitioning into DRMs between the isoforms, rather than produce a value for the percentage of each isoform associated with DRMs. The DRM band intensity was similar to the soluble protein (fraction 11) band intensity for 14-3-3 $\gamma$ and $\eta$, whilst the DRM

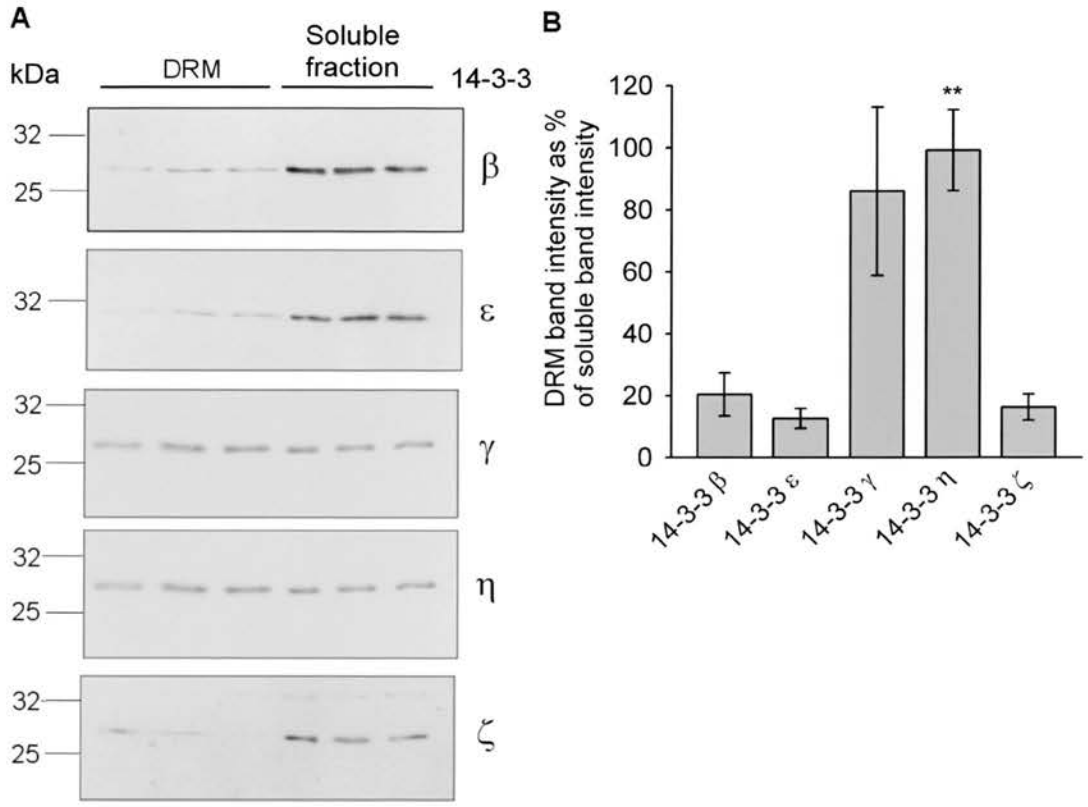


**Figure 3.6 14-3-3 isoforms associate with DRMs to different extents**

Rat brain homogenate was solubilised in 1% TX-100 at a protein concentration of 2mg/ml (5:1 detergent to protein ratio) and DRMs were isolated on 12 ml sucrose density gradients. **A** 20 µl DRM fraction (in triplicate) and 4 µl soluble fraction 11 (in triplicate) were separated by SDS-PAGE and immunoblotted with 14-3-3 isoform specific antibodies. **B** The intensity of the bands was quantified (as described in Chapter 2, section 2.3.5.1) and the mean DRM band intensity is expressed as a percentage of the mean fraction 11 band intensity. The bars represent mean values ± SEM, n = 3.
** 14-3-3 η mean DRM band intensity was significantly greater than all other isoforms except 14-3-3 γ (Student's T-test, $p < 0.05$.)

band intensity was much lower than the soluble protein band intensity for 14-3-3 β, ε and ζ, as shown by the example immunoblots in figure 3.6A. This suggests that more of the total 14-3-3 γ and η is present in DRMs than total 14-3-3 β, ε and ζ. In figure 3.6B quantification of band intensities from three similar experiments is presented. The mean DRM band intensity is expressed as a percentage of the mean soluble protein (fraction 11) band intensity. However, this value does not represent the proportion of total 14-3-3 isoform associated with the DRMs because the detergent soluble 14-3-3 protein is distributed between at least four fractions (fractions 8 – 12) and five times less fraction 11 was loaded than DRM fraction. Therefore the percentage of each isoform associated with the DRMs is at least 20-fold lower than figure 3.6B suggests. For example, less than 5 % of the total 14-3-3 η is likely to be associated with DRMs according to these calculations. Figure 3.6 is instead intended to compare the relative localization of each 14-3-3 isoform to the DRMs versus detergent soluble material. The data in figure 3.6B confirms that a significantly greater proportion of total 14-3-3 η is localized to DRMs than 14-3-3 β, ε or ζ (Student's T-test, $p < 0.05$, $n = 3$). The association of 14-3-3 γ with DRMs was not significantly different to any of the other isoforms and was more variable between experiments as shown by the larger error bars. There was no statistical difference between the relative localization of 14-3-3 β, ε and ζ to the DRMs.

These results suggest some 14-3-3 isoform specificity in DRM association. Under these experimental conditions 14-3-3 η associates with DRMs to a greater extent than the 14-3-3 β, ε and ζ isoforms and 14-3-3 γ shows a similar trend though the difference was not significant.

## 3.2. 14-3-3 DRM localisation is reduced by a peptide inhibitor of 14-3-3 interactions

Direct membrane attachment has not been reported for 14-3-3; therefore any membrane association would be expected to occur via interaction with another transmembrane or lipid-anchored protein. In the following experiments 14-3-3 interactions were disrupted to test the hypothesis that 14-3-3 requires a binding partner to achieve DRM localization.

The majority of 14-3-3 interactions are predicted to occur via its conserved amphipathic groove. The crystal structures of 14-3-3 protein in complex with a variety of different phosphorylated and non-phosphorylated peptide ligands indicate that the amphipathic groove is the primary ligand binding site (Gardino et al., 2006; Petosa et al., 1998; Rittinger et al., 1999; Wilker et al., 2005; Wurtele et al., 2003; Yaffe et al., 1997; Zhang et al., 1997). The only protein that has so far been crystallized in complex with 14-3-3 protein, serotonin N-acetyltransferase, also utilizes the same binding groove (Obsil et al., 2001). Furthermore, mutations in the binding groove have been found to decrease 14-3-3 protein interaction with binding partners (Wang et al., 1998; Yang et al., 2001; Zhang et al., 1997).

Fu and co-workers used a phage display library to isolate a peptide ligand (named R18) that bound to all 14-3-3 isoforms with high affinity, blocking 14-3-3 association with binding partner Raf-1 (Wang et al., 1999). R18 also binds the amphipathic groove (Petosa et al., 1998). The researchers went on to design a dimeric R18 peptide (named difopein: **di**meric **fo**urteen-three-three **pe**ptide **in**hibitor) to bind to both amphipathic grooves of a 14-3-3 dimer and thus antagonize 14-3-3 protein interactions (Masters and Fu, 2001). Difopein is suggested to be a competitive inhibitor of 14-3-3 protein interactions. It prevents binding of Raf-1 to 14-3-3 protein (Masters and Fu, 2001), has been used to affinity isolate 14-3-3 protein (Lalle et al., 2006) and inhibits the global cell survival functions of 14-3-3 protein (Masters and Fu, 2001; Peluso and Pappalardo,

2004). In the present study difopein was employed to disrupt 14-3-3 interactions in rat brain extract and the effect on the association of 14-3-3 isoforms with DRMs was monitored.

### 3.2.1. Purification of GST-difopein and difopein peptide

A difopein-EYFP expression plasmid was obtained from Professor Haian Fu and difopein was sub-cloned into the pGEX-4T1 bacterial expression vector. GST-difopein was expressed in *E.coli* and purified on a glutathione sepharose column (as described in Chapter 2, section 2.2.4). To produce free difopein peptide the GST moiety was cleaved off using thrombin. The purified GST-difopein and difopein peptide is shown on the Coomassie stained gel in figure 3.7A. Difopein appeared as a diffuse band due to its low molecular weight (~ 7 kDa). GST-difopein was able to specifically pull down 14-3-3 from rat brain homogenate or DRM fraction, as illustrated by figure 3.7B. 14-3-3 was not detected in 'pull down' experiments where GST-bound sepharose beads were used in place of GST-difopein.

### 3.2.2. Difopein reduces the localisation of 14-3-3 proteins to DRMs

As the purified difopein peptide can bind 14-3-3 it was possible to assess its ability to disrupt 14-3-3 association with DRMs. Whole rat brain was homogenised in 1 % (v/v) TX-100 and the protein concentration adjusted to give a 5:1 (w/w) detergent to protein ratio. Aliquots (2 ml) of rat brain extract were incubated for two hours with 400 μg difopein inhibitor, an unrelated peptide (peptide 1370), GST or an equal volume of buffer (untreated), as described in Chapter 2, section 2.3.2.2. Sucrose density centrifugation was then performed (see Chapter 2, section 2.3.1.1).

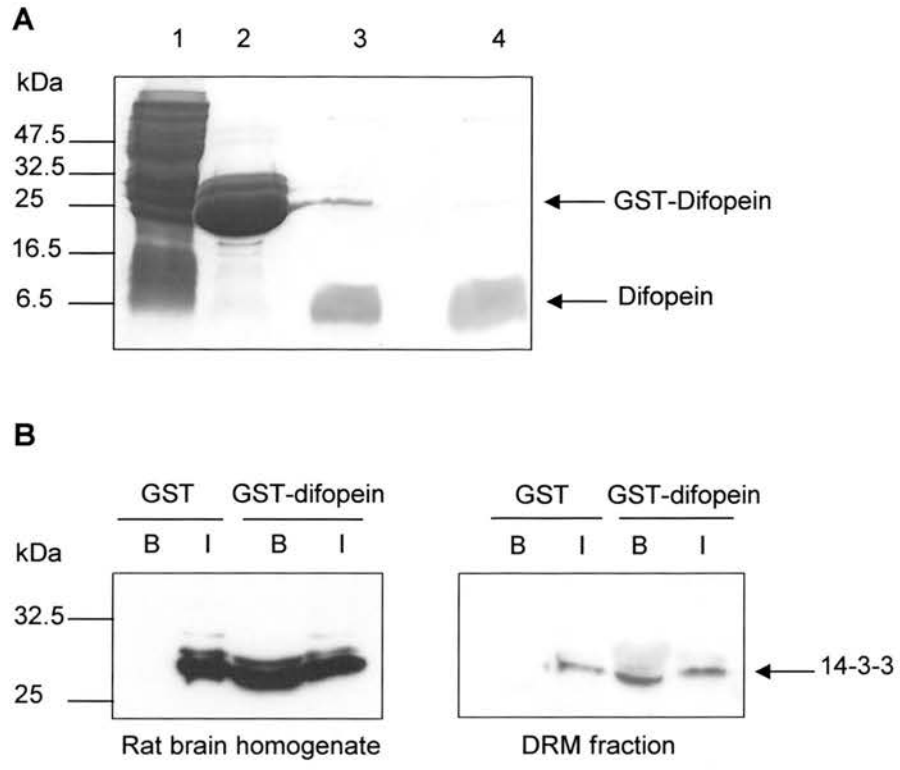


**Figure 3.7 14-3-3 protein binds specifically to GST-difopein**

GST-difopein was purified on glutathione sepharose beads as described in Methods. Difopein was cleaved off the GST using thrombin, which was then removed by passing the solution through a benzamidine sepharose column. **A** Samples from this procedure were separated by SDS-PAGE and Coomassie stained. The lanes 1 – 4 were loaded with 20 µl flow through from the glutathione column (lane 1), 5 µl glutathione sepharose beads (lane 2), 20 µl column eluate following thrombin cleavage (lane 3), 20 µl column eluate from benzamidine column (lane 4). Difopein is the low molecular weight diffuse band. **B** 40 µg GST-difopein or GST bound to glutathione beads was incubated for 2 hours with 300 µl rat brain homogenate (~ 250 µg protein) or 400 µl DRM fraction isolated from rat brain (~ 120 µg protein.) Following extensive washing, the sepharose beads (B) were boiled in Laemmli's buffer and separated by SDS-PAGE, along with 20 µl of input material (I). Immunoblots were performed with anti-14-3-3 (pan) antibody.

An equal volume of the DRM fraction from each gradient was separated by SDS-PAGE and immunoblotted first for SNAP-25. SNAP-25 is a palmitoylated protein that has been reported to associate with DRMs (Chamberlain et al., 2001; Salaun et al., 2005a; Salaun et al., 2004a). SNAP-25 was used as a control to demonstrate that the peptide incubations did not affect the localisation of other proteins to DRMs and that equal amounts of protein were loaded from each fraction. The immunoblots were then stripped and reprobed with isoform specific 14-3-3 antibodies (figure 3.8). Figure 3.8 shows that the amount of SNAP-25 associated with the DRM fraction was similar for all treatments. However, the amount of 14-3-3 ε (figure 3.8A), 14-3-3 γ (figure 3.8B) and 14-3-3 η (figure 3.8C) present in the DRM fraction appears to decrease in response to difopein incubation, compared with all three control treatments (untreated, peptide 1370 and GST).

The 14-3-3 isoform band intensities were quantified as described in Chapter 2, section 2.3.5.1 and expressed as a percentage of the SNAP-25 loading control band intensities. The results are presented alongside the representative immunoblots in figure 3.8 A - C. Significantly less 14-3-3 ε, γ and η was associated with the DRM fraction following difopein treatment compared with both the untreated DRMs and the controls where difopein was replaced with an unrelated peptide or GST (Student's T-test, $p < 0.05$.) The implication is that these 14-3-3 isoforms associate indirectly with DRMs via binding to another protein.

The results of the 14-3-3 γ quantification are intriguing. 14-3-3 γ association with DRMs was significantly increased by incubation with the control peptide 1370 or GST relative to the untreated control (figure 3.8B). It is unclear why a general increase in protein concentration should affect localisation of this particular isoform and not the others. Altering the detergent to protein ratio has been shown to change the amount of protein associated with DRMs but this is suggested to be due to poor solubilisation of non-raft membrane at low detergent to protein ratios, or solubilisation of lipid rafts at high ratios

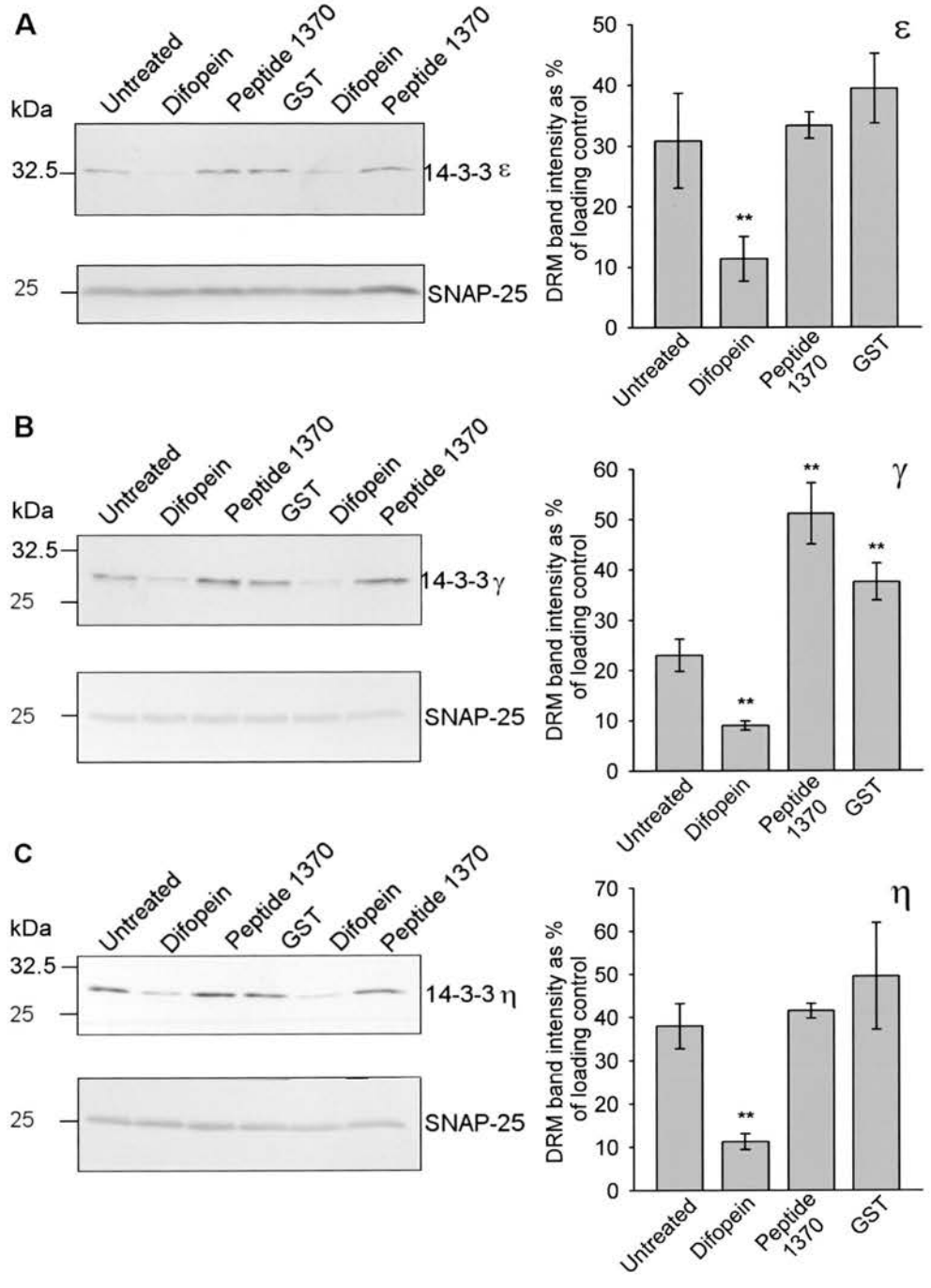


**Figure 3.8 Difopein significantly decreases the association of three 14-3-3 isoforms with DRMs**

(Ostermeyer et al., 1999). In that case protein concentration is really being used as an estimate of relative lipid concentration.

The same DRM preparations were also analysed with respect to 14-3-3 β and ζ localisation (figure 3.9). From the immunoblots in figure 3.9 it seems that less 14-3-3 β and ζ are associated with difopein incubated DRMs than DRMs from the three control treatments. However, quantification and statistical analysis of band intensities demonstrated that 14-3-3 β and ζ association with difopein treated DRMs was not significantly different from untreated control DRMs at $p < 0.05$ (Student's T-test). Interestingly, 14-3-3 β and ζ show a similar trend to 14-3-3 γ with respect to peptide 1370 and GST. More 14-3-3 protein appears to be associated with DRMs incubated with control peptide 1370 or GST. Whilst these results were not significantly different with respect to the untreated control DRMs, the association of 14-3-3 ζ with difopein treated DRMs is significantly reduced compared to the peptide 1370 and GST treatments. Peptide 1370 and GST were originally included as controls to confirm that simply increasing the protein concentration of the homogenate did not reduce 14-3-3 protein association with DRMs. Quite the opposite seems to occur, at least for 14-3-3 isoforms γ and ζ. One could speculate that GST and peptide 1370 both non-specifically associate with DRMs and 14-3-3 γ and ζ, bringing these proteins to DRMs. However, GST did not bind any 14-3-3 protein from rat brain homogenate or indeed DRMs in an in vitro 'pull down' assay (figure 3.7B). It remains puzzling then that increasing the general protein concentration specifically increases the localisation of 14-3-3 γ and ζ but not 14-3-3 isoforms ε, η or SNAP-25 to DRMs.

In summary, the 14-3-3 interaction inhibitor difopein significantly reduces the association of 14-3-3 ε, γ and η with DRMs but the decrease in 14-3-3 β and ζ association is not significant. The implication is that at least a proportion of 14-3-3 presence in DRMs is due to its interaction with another DRM-resident protein via the 14-3-3 amphipathic binding groove.

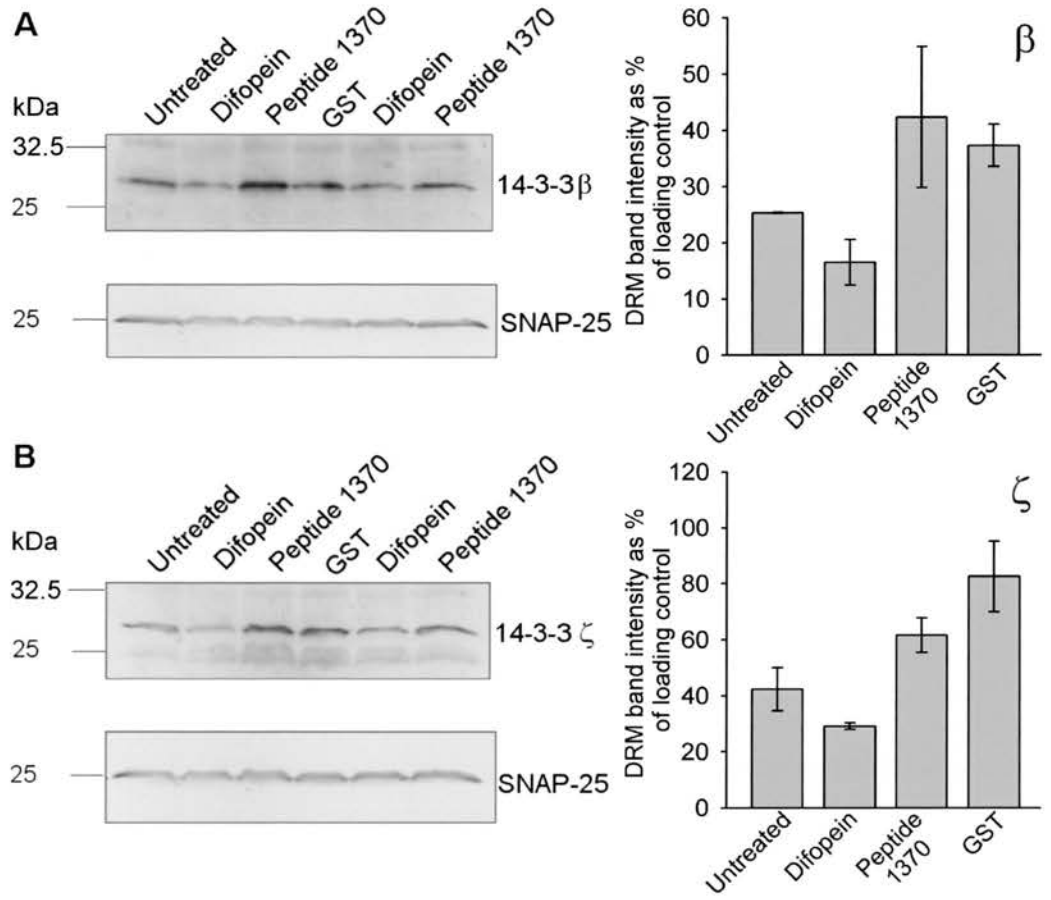


**Figure 3.9 Difopein does not significantly decrease the association of 14-3-3 β and ζ with DRMs**

Rat brain extract was solubilised in 1% TX-100 (5:1 detergent to protein ratio) for 30 minutes. 400 μg Difopein, peptide 1370 or GST per milliliter of homogenate was then added and incubated for 2 hours, following which DRMs were isolated (as described in Chapter 2, sections 2.3.1.1 and 2.3.2.2). The DRM association of 14-3-3 β (**A**) and 14-3-3 ζ (**B**) was analysed. 120 μl of the DRM fraction was concentrated, separated by SDS-PAGE and immunoblotted for SNAP-25. The blots were stripped and re-probed for the 14-3-3 isoform. The intensity of the bands was quantified as described in Chapter 2, section 2.3.5.1. The 14-3-3 band intensity is expressed as a percentage of the corresponding SNAP-25 loading control band intensity. The bars represent the mean DRM band intensity ± SEM (n = 3).

## 3.3. Isolation of DRMs from N2a cells

The mouse neuroblastoma derived cell line, N2a was employed to further investigate the potential association of 14-3-3 proteins with DRMs in neuronal type cells. Cultured cells also provided the possibility of depleting the cell membranes of cholesterol prior to detergent extraction. In numerous studies cholesterol depletion has been shown to reduce the association of proteins with the DRMs. This effect is attributed to disruption of lipid rafts, in which cholesterol is thought to be an essential component. Cholesterol dependent DRM association is taken as good evidence that a protein localizes to cholesterol-rich membrane microdomains *in vivo*.

### 3.3.1. Lipid raft markers associate with DRMs isolated from N2a cells

DRMs were isolated from N2a cells by TX-100 extraction, followed by centrifugation through a sucrose density gradient (described in Chapter 2, section 2.3.1.2). The isolation was performed on 12 ml gradients, from which 1 ml fractions were collected. The opaque band around the 5 – 30 % sucrose interface was diffuse and the DRMs collected into fractions 3 – 5. Due to the low protein concentration in the N2a cell gradients it was necessary to concentrate the fractions before SDS-PAGE analysis.

The Coomassie stained gel of the N2a cell gradient in figure 3.10A shows that as in the rat brain gradient the DRM fraction protein composition appears to differ from that of the soluble protein fractions. The distribution of lipid raft marker proteins flotillin-1 and PrP in the gradient was analysed by immunoblotting (figure 3.10B). These proteins were again enriched in the DRM fraction and undetectable in the soluble protein fractions (fractions 8 – 12). The concentration of cholesterol in the N2a cell fractions was not high enough to be detected by the available cholesterol assay but the evidence presented in figure 3.10 suggests that the N2a DRM fractions had similar characteristics to the rat brain derived DRMs.

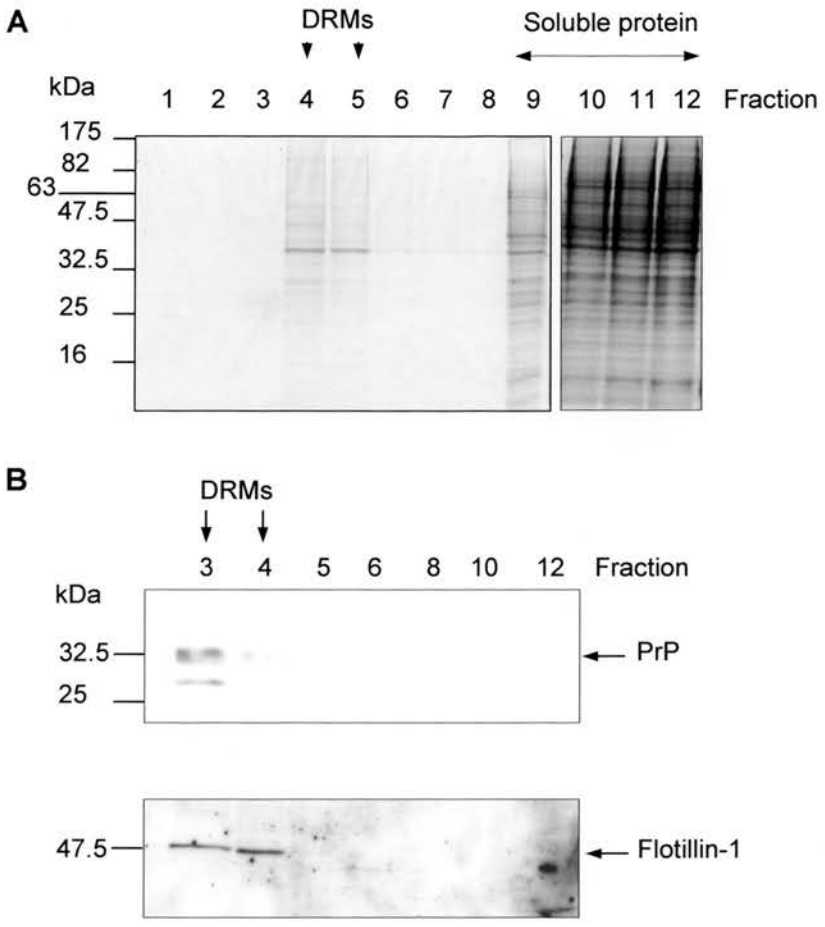


**Figure 3.10 The protein composition of the N2a cell derived DRMs differs from the rest of gradient and contains lipid raft markers**

Detergent resistant membranes were isolated from N2a cells by TX-100 extraction followed by flotation on a sucrose density gradient (described in Chapter 2, section 2.3.1.2). The gradient was collected as twelve fractions and the DRMs were contained in fractions 3 – 5. **A** 20µl of each fraction was separated by SDS-PAGE and Coomassie blue stained. **B** 200µl of fractions 3 – 12 were TCA precipitated (as described in Chapter 2, section 2.3.4.1), separated by SDS-PAGE and immunoblotted with anti-PrP or anti-flotillin-1 antbodies.

### 3.3.2. 14-3-3 proteins associate with DRMs derived from N2a cells

The N2a cell gradients were immunoblotted using each of the isoform specific 14-3-3 antibodies (figure 3.11). All of the brain abundant isoforms (β, ε, γ, η and ζ) were present. However, 14-3-3 σ and τ were undetectable in N2a cell gradients or the cell lysates. The volume of soluble protein fractions loaded was 10-fold less than for the DRM fraction so that the intensity of signal on the immunoblot would not be too bright for the soluble protein fractions. Despite the 10-fold lower volume the signal intensity in the soluble protein fractions is greater than in the DRMs, demonstrating that only a small proportion of each 14-3-3 protein localizes to DRMs and the majority resides in the soluble protein fractions. Qualitative comparison of all the isoforms implies that less 14-3-3 β and ζ localise to DRMs relative to the soluble protein fraction. It is interesting that 14-3-3 γ and η appear to show elevated DRM association compared with 14-3-3 β and ζ; a similar pattern was observed when the isoform specificity of 14-3-3 protein association with rat brain DRMs was investigated (see figure 3.6).

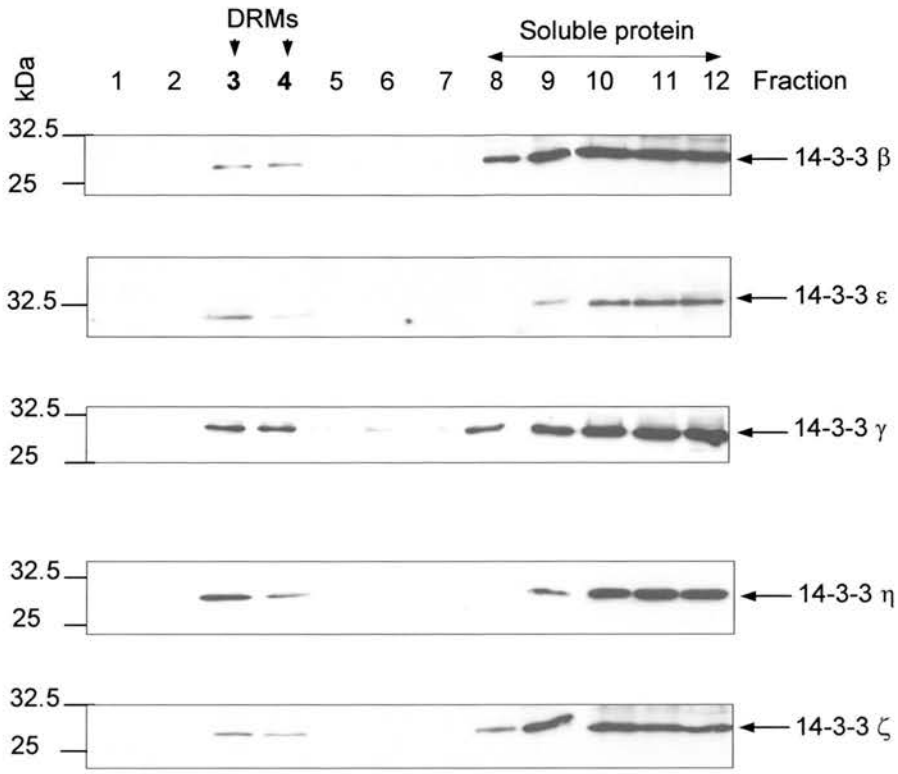


**Figure 3.11 The five brain abundant 14-3-3 isoforms associate with DRMs isolated from N2a cells**

Detergent resistant membranes were isolated from N2a cells by TX-100 extraction, followed by flotation on a sucrose density gradient. The gradient was collected as twelve fractions (numbered). The DRMs were visible as an opaque band that was contained in fractions 3 and 4. 200µl (TCA precipitated) of fractions 1 - 8 or 20µl of fractions 9 – 12 were separated by SDS-PAGE and immunoblotted with isoform specific anti-14-3-3 antibodies against 14-3-3 β, ε, γ, η and ζ as indicated.

### 3.3.3. The localization of 14-3-3 isoforms to N2a cell DRMs is cholesterol dependent

Cholesterol is believed to be an integral component of lipid rafts (Silvius, 2003a; Simons and Ikonen, 1997) and DRMs are described as cholesterol-rich (Brown and Rose, 1992; Pike et al., 2002). Cholesterol depletion has been used in numerous studies to demonstrate the dependence of a protein or process on lipid rafts. For example, removal of cholesterol was found to decrease conversion of normal PrP into the scrapie prion isoform, leading the authors of this study to suggest that the process is dependent on lipid rafts (Marella et al., 2002; Taraboulos et al., 1995). The same treatment was found to affect tyrosine phosphorylation in Jurkat T-cells (Kabouridis et al., 2000) and reduce MAP kinase activation in response to ligand binding to DRM-associated protein GFRα (glial cell line-derived neurotrophic factor receptor, (Tansey et al., 2000)). Cholesterol depletion has also been shown to reduce the association of various DRM proteins with the DRM fraction (Foster et al., 2003; Remacle-Bonnet et al., 2005; Taverna et al., 2004; Vial and Evans, 2005).

Cholesterol depletion is usually achieved using methyl-β-cyclodextrin (MβCD). β-cyclodextrins are cyclic heptasaccharides with β (1-4)-glucopyranose units. They are water soluble but the ring of glucopyranose units has a hydrophobic interior cavity that can solubilise hydrophobic molecules such as cholesterol (De Caprio et al., 1992; Kilsdonk et al., 1995; Yancey et al., 1996). It has been demonstrated that β-cyclodextrins can modulate the cholesterol content of cells causing depletion of cholesterol by increasing the rate of cholesterol efflux (Kilsdonk et al., 1995; Yancey et al., 1996). Rapid cholesterol efflux is observed and cholesterol may diffuse directly from the cell membrane into the hydrophobic core of the cyclodextrin molecule (Yancey et al., 1996).

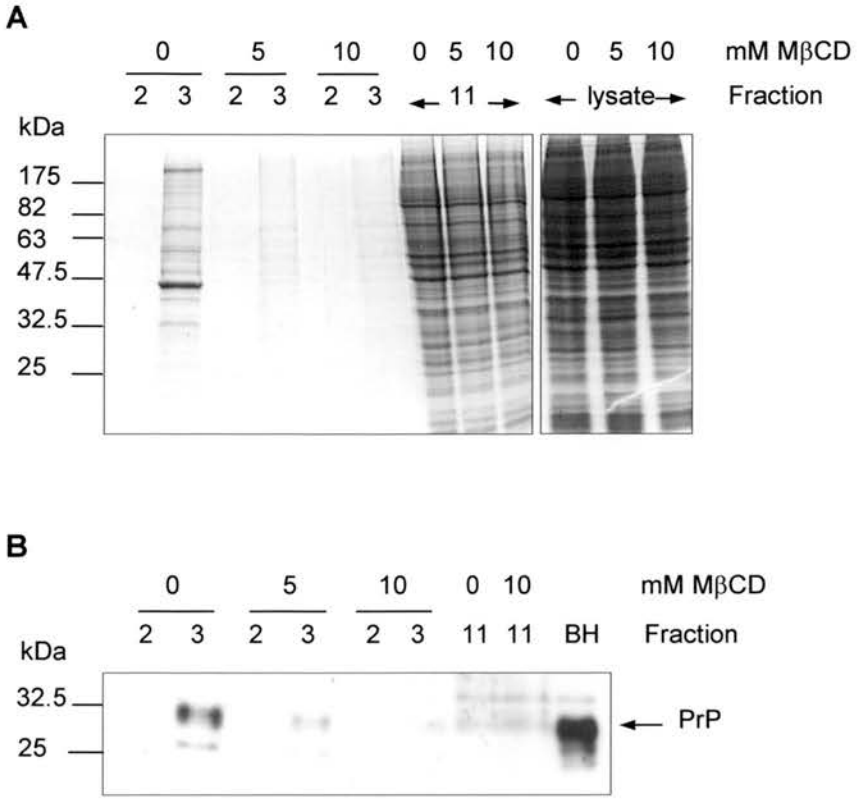


**Figure 3.12 Cholesterol depletion reduces the overall protein content of DRMs and attenuates the association of lipid raft marker PrP**

N2a cells were incubated for 30 minutes in the presence of 5 mM or 10 mM methyl-β-cyclodextrin (MβCD) or PBS (0 mM) as a vehicle control (as described in Chapter 2, section 2.3.1.3). The cells were lysed and DRMs were prepared by separation on a sucrose density gradient. The DRMs collected into fractions 2 and 3. 30µl DRM fractions 2 and 3 and soluble protein fraction 11 (and 10µl pre-separation lysate in A) were separated by SDS-PAGE. **A** Coomassie blue stained. **B** Immunoblot with anti-PrP antibody. The last lane is 20 µg whole brain homogenate (BH) as a control for PrP detection.

Cell culture studies investigating lipid rafts generally use MβCD at between 2 – 20mM for incubation periods from 15 minutes to 1 hour (Abrami et al., 2003; Foster et al., 2003; Kabouridis et al., 2000; Tansey et al., 2000; Taverna et al., 2004). It has been demonstrated that at MβCD concentrations ≤ 1mM net cholesterol efflux from cells does not take place (Atger et al., 1997). N2a cells were therefore treated with 5 or 10mM MβCD for 30 minutes at 37°C, followed by DRM isolation (as described in Chapter 2, sections 2.3.1.2 and 2.3.1.3).

Figure 3.12A shows that treatment with MβCD induces a large reduction in the total protein associated with the DRM fraction compared to the vehicle control (0 mM MβCD). Importantly MβCD also specifically reduces the association of lipid raft marker PrP with the DRM fraction as would be predicted if MβCD disrupts lipid rafts (see figure 3.12B). The right hand 3 lanes of figure 3.12A show that similar amounts of total protein were present in the control and MβCD treated cell lysates (this was confirmed by Bradford assay). Additional protein might have been expected to appear in the soluble protein fractions (including fraction 11) when cells were MβCD treated, due to redistribution of protein away from the DRM fraction. However no such redistribution is apparent from the Coomassie blue stained gel in figure 3.12A. This is probably because the protein displaced from the single DRM fraction is diluted into five soluble protein fractions and each soluble protein fraction contains at least five times more protein that the control DRM fraction (determined by Bradford assay). The five-fold dilution into the soluble fractions may also explain why PrP is undetectable in fraction 11 even though the majority is displaced from DRMs by MβCD (figure 3.12B).

I next analysed the effect of MβCD treatment on 14-3-3 presence in DRMs. Figure 3.13 shows sucrose gradients from MβCD treated or control N2a cells immunoblotted with isoform specific 14-3-3 antibodies. It is clear that whilst all four 14-3-3 isoforms associate with the DRM fraction (fractions 2 and 3) in the control gradient

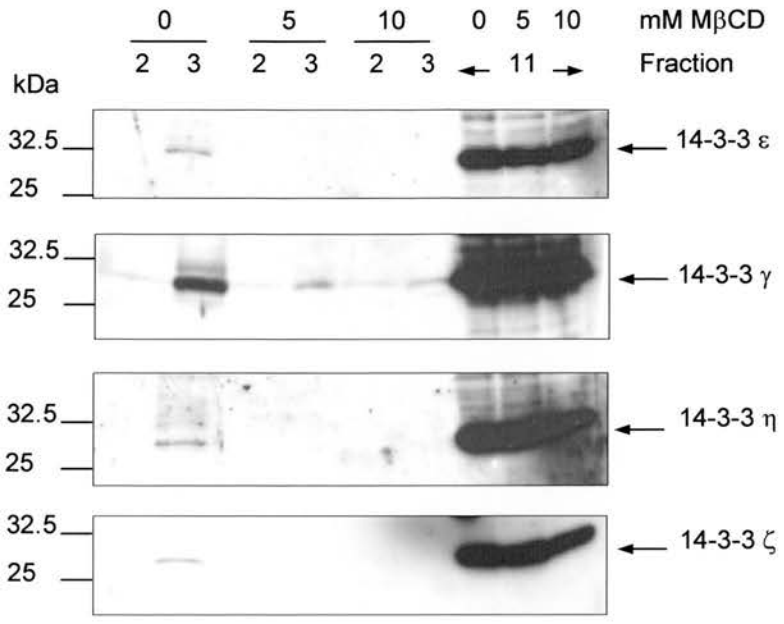


**Figure 3.13 Cholesterol depletion reduces the association of 14-3-3 proteins with DRMs**

N2a cells were incubated for 30 minutes in the presence of 5 mM or 10 mM methyl-β-cyclodextrin (MβCD) or PBS (0 mM MβCD) as a vehicle control (as described in Chapter 2, section 2.3.1.3), following which DRMs were isolated (as described in Chapter 2, section 2.3.1.2). 30 µl DRM fractions 2 and 3 and 5 µl soluble protein fraction 11 were separated by SDS-PAGE and immunoblotted with isoform specific 14-3-3 antibodies.

(0mM MβCD); association with the DRM fraction is greatly reduced by treatment with 5 mM or 10 mM MβCD. The three right hand lanes in each panel of figure 3.13 demonstrated that 14-3-3 proteins are very abundant in fraction 11 (soluble protein fraction) from both control and MβCD treated cells.

## 3.4. Isolation of DRMs from PC12 cells

The PC12 cell line was isolated from a rat adrenal pheochromocytoma and responds to nerve growth factor (NGF) by ceasing to multiply and producing neuronal-like processes (Greene and Tischler, 1976). PC12 cells are often used as a model for neuronal or secretory cell types. DRMs were first isolated using the standard TX-100 extraction procedure to determine whether 14-3-3 associates with DRMs derived from PC12 cells, as well as N2a cells and rat brain extract.

The extraction procedure was then carried out at 25°C instead of the standard 4°C to ascertain whether 14-3-3 remained associated with DRMs at elevated temperature. One of the criticisms often made about the standard DRM preparation is that lowering the temperature of the cells or tissue to 4°C should not be necessary to isolate lipid rafts if they are present in living organisms at 37°C. In one review, London and Brown suggest that lowering the temperature may allow isolation of rafts that are already present at 37°C by stabilising lipid-lipid interactions that would be too weak at 37°C to resist detergent solubilisation, i.e. lipid rafts exist but are not necessarily detergent insoluble at 37°C (London and Brown, 2000). However they do concede that lowering the temperature of membranes might lead to increased formation of liquid ordered ($L_o$) phase domains. The work of Heerklotz indicates that cooling biological membranes to 4°C might increase the presence of the $L_o$ phase (Heerklotz, 2002). Cold DRM preparations might then overestimate the proportion of the cellular membranes present as lipid rafts ($L_o$ domains) and therefore the protein content of these rafts. It was therefore of interest to determine whether DRMs could still be prepared above 4°C by

the method employed here and if so whether raft markers and 14-3-3 protein could still be detected in the DRMs.

### 3.4.1. 14-3-3 protein and raft marker flotillin-1 associate with DRMs isolated from PC12 cells

DRMs were isolated from PC12 cells using TX-100 extraction procedure, at 4°C (described in Chapter 2, section 2.3.1.2). The DRMs were visible as an opaque band at the 5 – 30% sucrose interface (fractions 3 and 4) and the TX-100 soluble material was present in fractions 8 – 12. Figure 3.14A shows that raft marker flotillin-1 appeared exclusively in the DRM fractions but was undetectable in the soluble protein fractions. 14-3-3 was also detected in the DRM fractions. Again 14-3-3 was distributed between the soluble protein fractions and the DRMs, with the majority of 14-3-3 apparently present in the soluble protein fractions. The fractions were also immunoblotted for transferrin receptor (TfR). Figure 3.14A shows that whilst most of the TfR was present in the soluble protein fractions, a small proportion was also localised to the DRM fraction. The distribution of these three proteins in the gradient agrees with the results obtained from DRM preparations from rat brain tissue and N2a cells.

After confirming that 14-3-3 protein and raft marker flotillin-1 were present in PC12 derived DRMS prepared at 4°C, the TX-100 DRM preparation (described in Chapter 2, section 2.3.1.2) was carried out at 25°C. At no point during the procedure was the cell lysate cooled. After centrifugation DRM material was again visible as a low density opaque band in the gradient. When the gradient fractions were separated by SDS-PAGE and immunoblotted for flotillin-1 there was a clear signal in the DRM fraction (see figure 3.14B) but not in the soluble protein fractions (fractions 8 - 12). Figure 3.14B also shows that 14-3-3 protein was present in the DRM fraction as well as in the soluble protein fractions. These results demonstrate that it is not necessary to cool the cell extract to 4°C to prepare DRMs of characteristic low density, enriched in the raft marker

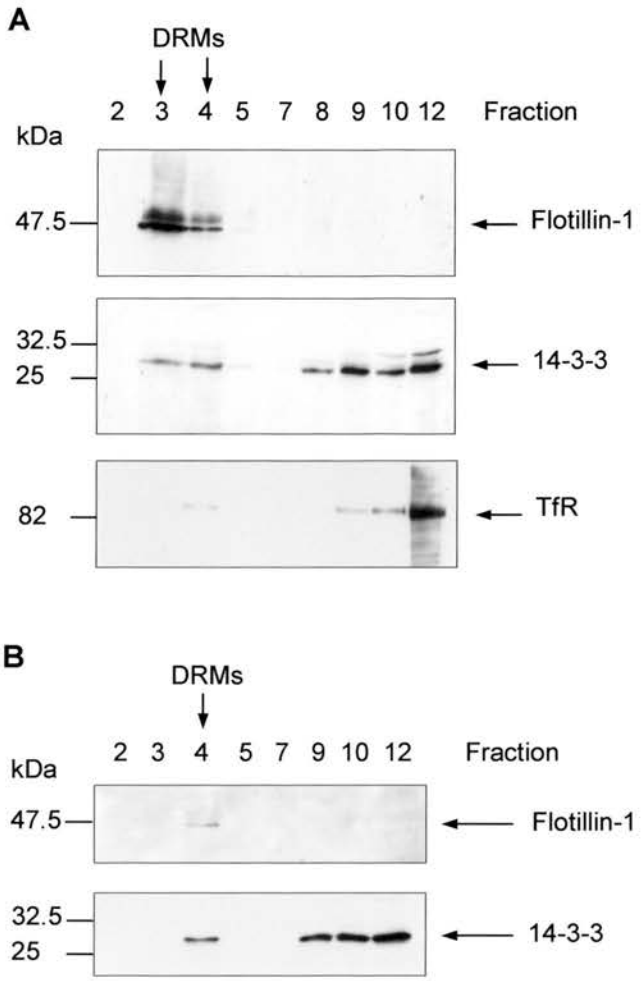


**Figure 3.14 14-3-3, lipid raft marker flotillin-1 and TfR all associate with DRMs prepared from PC12 cells**

Detergent resistant membranes were isolated from PC12 cells by TX-100 extraction at 4°C (**A**) or 25°C (**B**) followed by flotation on a sucrose density gradient (described in Chapter 2, section 2.3.1.2). The gradient was collected as twelve fractions. The DRMs were visible as an opaque band that collected into fractions 3 and 4. 850 µl of fractions 3 and 4 was concentrated by centrifugation at 100,000 x g. The resulting membrane pellets were separated by SDS-PAGE along with 25 µl of each other fraction and immunoblotted with anti-14-3-3 (pan), anti-flotillin-1 or anti-TfR antibodies.

flotillin-1. They also indicate that 14-3-3 association with DRMs is not induced by the process of cooling the cell extract to 4°C but occurs at higher temperatures.

## 3.5. 14-3-3 proteins associate with 'lipid raft' fractions isolated by a detergent-free procedure

Probably the most controversial aspect of the lipid raft purification methodology is the use of Triton-X-100 to extract detergent resistant membranes (DRMs) that are suggested to represent *in vivo* lipid rafts in terms of their protein and lipid composition. Despite numerous studies using resistance to TX-100 as the main criterion to assign a protein lipid raft-associated status, many in the lipid raft field are sceptical of this interpretation and point to potential flaws in the use of this detergent (Edidin, 2003; Munro, 2003; Pike, 2003; Simons and Vaz, 2004). In their reviews of lipid rafts Edidin and Pike both point to conflicting reports about the DRM association of particular proteins (Edidin, 2003; Pike, 2003). Differences in the detergent to protein ratios between studies may be the cause of these discrepancies but it is difficult to determine which detergent to protein ratio fully solubilises the bulk plasma membrane whilst leaving lipid rafts intact. The TX-100 extraction procedure may increase the formation of liquid ordered phase domains (Heerklotz, 2002) and would in that case overestimate the amount and possibly composition of lipid and protein associated with pre-existing lipid raft-like domains. These problems cast some doubt over the robustness of the TX-100 extraction method for consistent, reliable preparation of lipid rafts. In response to these concerns, alternative procedures have been explored using different detergents (Schuck et al., 2003) or detergent-free protocols (Luria et al., 2002; Macdonald and Pike, 2005; Smart et al., 1995; Song et al., 1996; Wu et al., 1997) to purify lipid raft-like membranes.

The most established detergent-free purification method was devised by Anderson and co-workers (Liu et al., 1996; Mineo et al., 1996; Smart et al., 1995; Wu et al., 1997). The procedure was originally employed to purify caveolae from fibroblast plasma

membrane but was extended to the isolation of lipid raft-like, low density membranes (LDMs) from synaptic plasma membranes (Wu et al., 1997). LDMs are enriched in cholesterol, sphingomyelin (Pike et al., 2002; Wu et al., 1997) and lipid raft markers ganglioside GM1 and PrP (Wu et al., 1997), compared with whole plasma membrane. In addition, Fyn kinase and Ras, both of which have been identified as DRM associating proteins (Henke et al., 1996; Parton and Hancock, 2004; Shenoy-Scaria et al., 1994), were concentrated in the LDMs (Wu et al., 1997). LDMs therefore seem to share the properties of DRMs and the expected properties of cholesterol and sphingolipid-rich lipid rafts. Furthermore, it has been proposed that LDMs may be more representative of bilayer lipid rafts than DRMs; LDMs were found to contain a higher proportion of inner leaflet lipids such as PE and PS, which are depleted in DRMs (Pike, 2003; Pike et al., 2002). The LDM isolation procedure was used to investigate whether 14-3-3 proteins associate with lipid raft-like membranes purified in the absence of detergent, as well as DRMs.

### 3.5.1. PrP and flotillin-1 associate with LDMs prepared by a detergent-free method

The first step in the LDM procedure is purification of plasma membrane. Sonication is then employed to break up the plasma membrane in place of detergent and the resulting sonicate is placed at the bottom of an Optiprep density gradient (gradient 1) as illustrated in figure 3.15. Following ultracentrifugation of gradient 1, the top five fractions are collected, mixed with 50 % Optiprep and placed at the bottom of another Optiprep gradient (gradient 2). Gradient 2 concentrates LDMs at the 5 – 25 % Optiprep interface (see figure 3.15). Smart and co-workers suggest that their method allows the purification of caveolae and lipid rafts based on the unique low buoyant density of these membrane compartments, which they believe is due to the low protein versus lipid content (Smart et al., 1995).

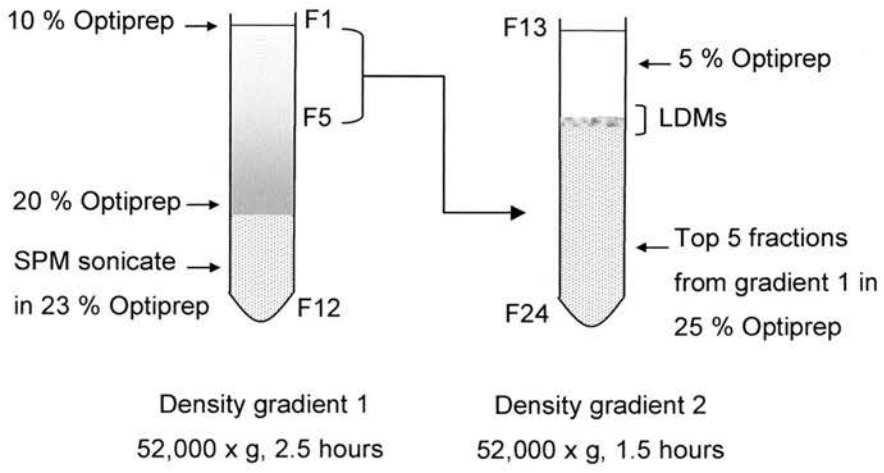


**Figure 3.15 Detergent-free protocol for the isolation of lipid raft-like domains**

Low density membranes (LDMs) were prepared from synaptic plasma membranes (SPM) as described in Chapter 2, section 2.3.3. The SPM sonicate was mixed with Optiprep to a final concentration of 23 % (v/v) Optiprep and overlaid with a continuous 20 – 10 % (v/v) Optiprep gradient (gradient 1). Gradient 1 was centrifuged at 52,000 x g for 2.5 hours and collected as twelve 1ml fractions from the top of the tube (as indicated, Fraction 1 – Fraction 12). The top 5 fractions were mixed with 4 ml 50 % (v/v) Optiprep (to give a final concentration of ~ 25 %) and overlaid with 5 % (v/v) Optiprep (gradient 2). Gradient 2 was centrifuged at 52,000 x g for 1.5 hours and collected as 1 ml fractions: Fraction 13 to Fraction 24 from the top of the gradient. An opaque band was present at the 5 – 25 % (v/v) Optiprep interface and collected into Fraction 16.

Synaptic plasma membranes were purified according to Wu *et al* (1997) and used as the starting material for LDM isolation. An opaque band was visible at the 5 – 25 % Optiprep interface in gradient 2. This band was designated LDMs and collected into fraction 16 (figure 3.15 shows the fraction numbering used in subsequent figures). Fractions from both gradients and the original synaptic membrane preparation were separated by SDS-PAGE and immunoblotted for lipid raft markers flotillin-1 and PrP. Both proteins were recovered in LDM fraction (fraction 16) and were visible in the original synaptic membrane preparation (see figure 3.16).

Only the low density fractions 1 – 5 from gradient 1 contribute to gradient 2. However, some PrP and flotillin-1 were also detected in high density fraction 9 from gradient 1 and PrP was present in fractions 6 and 7 (see figure 3.16). Anderson and co-workers also observed that caveolin-1, PrP and GM1 were distributed throughout gradient 1 and caveolin-1 appeared to be particularly concentrated around fractions 8 – 11 (Smart et al., 1995; Wu et al., 1997). This may reflect the localization of these proteins to different membrane domains, which would agree with current theories on membrane compartmentalization suggesting that protein association with steady state lipid rafts is transient (Hancock, 2006; Kusumi et al., 2004; Subczynski and Kusumi, 2003). Alternatively, the LDM procedure may not isolate all lipid raft-like membranes. In contrast, following TX-100 DRM isolation from rat brain or N2a cells, PrP and flotillin-1 appear to be concentrated in the low density DRM fraction and are undetectable in the higher density fractions (see figures 3.2 and 3.10).

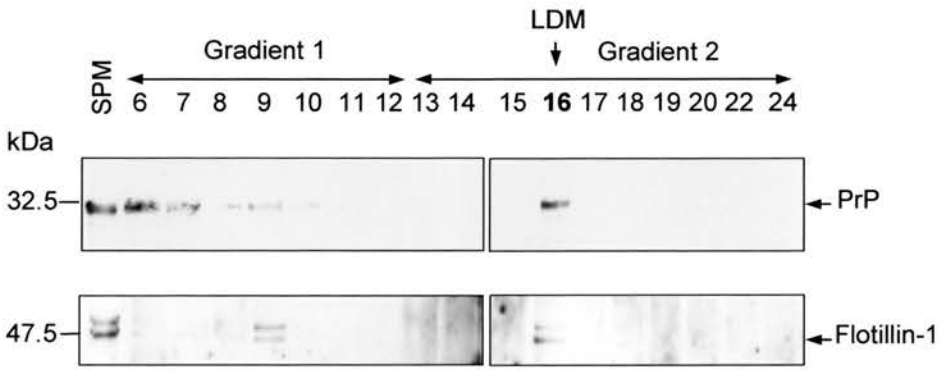


**Figure 3.16 Lipid raft markers flotillin-1 and PrP associate with LDMs prepared from synaptic plasma membranes**

LDMs were prepared from synaptic plasma membranes (SPM) as described in Chapter 2, section 2.3.3. The two density gradients used to separate the LDMs are labelled and the fractions are numbered. The LDMs appeared as an opaque band in fraction 16 (gradient 2). 5 µl of SPM fraction or 25 µl of the other fractions were separated by SDS-PAGE and immunoblotted with anti-PrP or anti-flotillin-1 antibodies.

### 3.5.2. 14-3-3 proteins associate with LDMs prepared by a detergent-free procedure

Having isolated LDMs from rat brain I then investigated whether 14-3-3 isofroms were associated with this membrane fraction. Immunoblotting with isoform specific antibodies revealed that 14-3-3 ε, γ, η and ζ were all present in synaptic plasma membranes and purified LDMs (see figure 3.17). 14-3-3 β was not detected in the LDM fraction but it should be noted that detection of this isoform in synaptic plasma membranes required long exposure. The 14-3-3 isoforms localized to high density fraction 9 of gradient 1, as observed for flotillin-1 and PrP (see figure 3.16). Unlike the lipid raft markers however, 14-3-3 isoforms were also detected in fractions 10 – 12, the highest density membrane fractions. This result is in agreement with the distribution of 14-3-3 on the density gradient following TX-100 extraction, where much of the 14-3-3 remains in the high density, soluble protein fractions (see figure 3.5). Association of 14-3-3 with high density fractions isolated from synaptic membranes implies that some of the TX-100 soluble 14-3-3 could also be membrane associated. 14-3-3 protein might localise to both lipid raft-like domains and non-raft plasma membrane.

In summary, the gradient distribution of 14-3-3 proteins following LDM isolation is distinct from the distribution of lipid raft markers, in agreement with TX-100 extraction results. 14-3-3 protein, flotillin-1 and PrP all localise to LDMs and DRMs but a large proportion of 14-3-3 protein resides in the highest density fractions. The association of 14-3-3 proteins with cholesterol-rich membranes isolated by two alternative procedures advocates their localization to lipid raft-like domains *in vivo*.

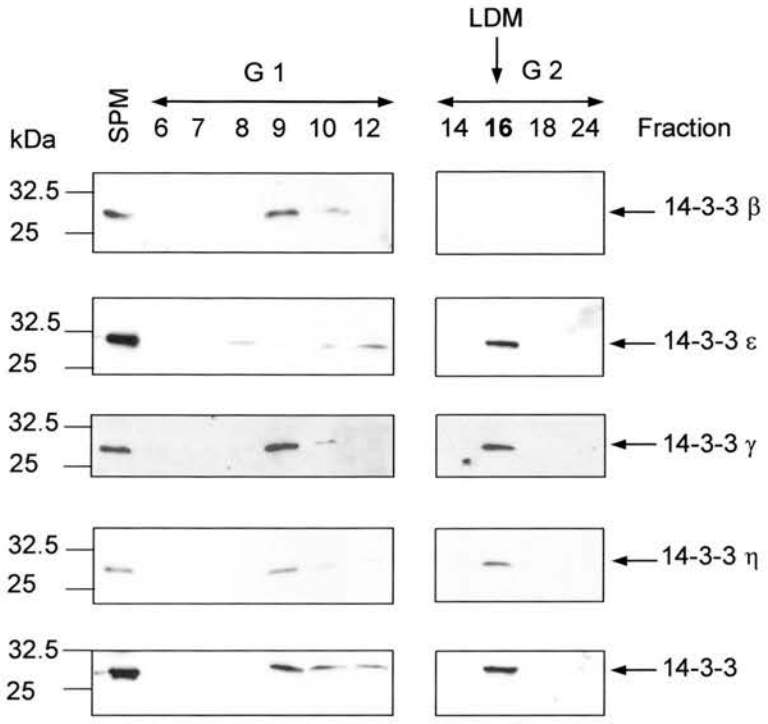


**Figure 3.17 14-3-3 isoforms associate with LDMs derived from synaptic plasma membranes**

LDMs were prepared from synaptic membranes (SPM) as described in Chapter 2, section 2.3.3. The two density gradients used to separate the LDMs are labelled G1 and G2 and the fractions are numbered. The LDMs were contained in fraction 16 (gradient 2). 5 µl of SPM fraction or 25 µl of the other fractions were separated by SDS-PAGE and immunoblotted with isoform specific 14-3-3 antibodies.

## 3.6. Summary and discussion

In this chapter the association of 14-3-3 with DRMs, which are believed to represent clustered lipid rafts, was investigated. A small proportion of the total 14-3-3 protein from rat brain tissue, N2a and PC12 cells was found to reside in DRMs. Enrichment of 14-3-3 in lipid rafts would be unexpected as most of the reported functions of 14-3-3 occur in the cytosol (Aitken, 2006; Muslin and Xing, 2000). Analysis of rat brain derived DRMs implied isoform specificity in the localization of 14-3-3 proteins to DRMs; a significantly greater proportion of 14-3-3 η partitioned into DRMs relative to 14-3-3 β, ε and ζ and 14-3-3 γ showed a similar trend. Interestingly, 14-3-3 γ and η have higher sequence homology with each other than with the other isoforms, suggesting that they are evolutionarily closely related (Aitken et al., 1992; Berg et al., 2003; Wang and Shakes, 1996). These isoforms might then be expected to perform similar or overlapping functions. The isoform specific functions of 14-3-3 have not been studied in detail (as discussed in Chapter 1, section 1.2.2.2). However, CAMKK has been demonstrated to preferentially interact with 14-3-3 γ and η rather than other 14-3-3 isoforms (Davare et al., 2004). In contrast, both A20 (an inhibitor of TNF-induced apoptosis) and ADAM22 (cell adhesion protein) bind to 14-3-3 η but not 14-3-3 γ (Vincenz and Dixit, 1996; Zhu et al., 2005; Zhu et al., 2003). Thus it seems that 14-3-3 γ can not always substitute for 14-3-3 η.

The isolated DRMs were characteristically enriched in lipid raft markers flotillin-1 and the GPI-anchored PrP and also cholesterol. TfR, a transmembrane protein that is often cited as a non-raft marker, was also detected in DRMs isolated at a range of detergent to protein ratios. It was necessary to concentrate the DRM fraction to allow detection of TfR, which was possibly hindered in previous studies by low protein concentration or low antibody sensitivity. Indeed, one other DRM study did report DRM association of TfR (Batista et al., 2004). TfR, like 14-3-3, is certainly not enriched in DRMs relative to detergent soluble material but this does not preclude a functional interaction.

14-3-3 is a very abundant protein so it was important to investigate whether it could be a contaminant in the DRM preparation. Two lines of evidence indicate that 14-3-3 association with DRMs is not due to contamination. Firstly, 14-3-3 protein localization to DRMs was dependent on cholesterol as shown by cholesterol depletion of N2a cells. Foster and co-workers suspected contamination of their DRM preparation with nuclear and mitochondrial proteins but found that whilst cholesterol depletion reduced the association of lipid raft markers it did not affect the suspected contaminants (Foster et al., 2003). Secondly, the DRM association of three 14-3-3 isoforms was disrupted by incubation of rat brain extract with difopein (an inhibitor of 14-3-3 interactions), prior to DRM isolation. Direct membrane attachment has not been reported for 14-3-3 so functional localization to DRMs was predicted to occur via binding to another DRM-resident protein. In all cases some 14-3-3 was still detected in the difopein treated DRM fraction, despite the fact that much more difopein was added than would be required to bind all the 14-3-3 estimated to be present. Some 14-3-3 interactions may not be dissociated by difopein if the binding partner in question has a higher affinity than difopein for the 14-3-3 binding groove. Alternatively, some of the 14-3-3 may be associating non-specifically with DRMs. However, the fact that difopein can dissociate a proportion of 14-3-3 from DRMs supports the specific localization of 14-3-3 to lipid raft-like domains mediated by interaction with another protein. Moreover these results strengthen the argument that the highly abundant 14-3-3 is not present in DRMs solely due to non-specific contamination. Nevertheless the results do not rule out the possibility that the binding of 14-3-3 to a DRM-resident protein occurs during the extraction process, but does not happen *in vivo*.

The results discussed so far endorse the potential association of 14-3-3 with lipid raft-like membrane domains. However, some researchers have raised concerns about whether the TX-100 DRM isolation procedure reports the physiological association of proteins in lipid raft-like microdomains (Edidin, 2003; McMullen et al., 2004; Munro, 2003). Non-physiological association of proteins with DRMs during the extraction procedure has been implicated as a source of contamination. For example, the

immunoglobulin E (IgE) receptor FcγRII has been shown to localize to DRMs. When DRMs that were free of FcγRII (due to inclusion of TX-100 in the density gradient) were mixed with a soluble protein fraction containing FcγRII and the DRMs re-isolated on another gradient, FcγRII appeared in the DRMs (Korzeniowski et al., 2003). This suggests that soluble proteins can spuriously associate with DRMs during the extraction procedure. However, this result is at odds with an earlier study which showed that GPI-anchored proteins inserted into $L_d$ phase liposomes do not become detergent insoluble when mixed with model DRMs, i.e. proteins do not artificially associate with DRMs during the extraction procedure (Schroeder et al., 1998). The propensity of a protein to artificially associate with DRMs seems likely to depend on the properties of the particular protein.

Biophysical experiments in model membranes have suggested that TX-100 could increase formation of $L_o$ domains or even induce phase separation in initially homogeneous membranes (Heerklotz, 2002). When the effect of TX-100 on cell membranes at 4°C was directly observed by light microscopy large holes in a mainly intact membrane were observed (Hao et al., 2001) and detergent also led to clustering of a fluorescent GPI-anchored protein that was initially diffusely distributed in the membrane (Mayor and Maxfield, 1995). These studies indicate that there maybe problems with the use of TX-100 extraction to purify membrane microdomains that retain their *in vivo* structure and protein composition.

In response to the apparent concerns regarding the TX-100 extraction procedure detergent-free lipid raft isolation methods have been devised and some researchers have investigated the isolation of DRMs at physiological temperature. The detergent-free methods mainly employ sonication in place of detergent to break up the membrane. 14-3-3 and lipid raft markers flotillin-1 and PrP were also found to associate with the LDMs isolated by one of these detergent-free methods, lending further support to the potential lipid raft association of 14-3-3. However, the raft markers were not

concentrated solely in the LDM fraction calling into question the efficiency of this procedure. In addition, it is unclear exactly what effect sonication has on the membrane.

To investigate whether association of 14-3-3 with DRMs relies on cooling the cell lysate to 4°C, DRMs were extracted from PC12 cells using the standard procedure except that all steps were carried out at 25°C. Flotillin-1 demonstrated exclusive localisation to the DRMs at both 4°C and 25°C. 14-3-3 was also still detected in the DRMs isolated at elevated temperature, suggesting that cooling the extract to 4°C does not induce DRM association of 14-3-3. Other studies where DRMs have been isolated at temperatures above 4°C have produced mixed results. In three studies lipid raft markers PrP, Thy-1 and flotillin-1 remained enriched in the DRM fraction following incubation of TX-100 extract at 37°C prior to density gradient centrifugation (Madore et al., 1999; Naslavsky et al., 1997; Parkin et al., 1999). However, redistribution of DRM proteins to the soluble protein fractions has also been reported when the preparation temperature has been raised from 4°C to 37°C (Baron et al., 2002; Taylor et al., 2002).

The results presented in this chapter provide good evidence for the cholesterol dependent localization of 14-3-3 proteins to DRMs, which are widely represented as corresponding to *in vivo* lipid rafts. However, two points warn against the further use of the TX-100 procedure in isolation to study 14-3-3 membrane localization. Firstly, the concerns about this subcellular fractionation procedure discussed above and secondly, the possibility that 14-3-3 protein might associate with a DRM-resident protein only during the extraction procedure. Rather than continuing with functional studies in DRMs, in the next chapter further confirmation of 14-3-3 association with membrane microdomains was sought via the study of intact cells.

# Chapter 4: Imaging-based studies of lipid raft markers and 14-3-3

# 4. Imaging-based studies of lipid raft markers and 14-3-3

In the previous chapter the association of 14-3-3 with DRMs was established and this interaction was found to be dependent on cholesterol and access to the 14-3-3 binding groove. These results point to a functional interaction between 14-3-3 and DRMs, mediated by binding to a membrane anchored protein. However, it is possible that the association of 14-3-3 with a DRM-resident protein is an artefact of the extraction procedure, rather than a physiological interaction. Furthermore, there are concerns about the validity of the TX-100 extraction procedure for isolating pre-existing microdomains (Edidin, 2003; Heerklotz, 2002; Munro, 2003). This chapter aims to investigate localisation of 14-3-3 to membrane microdomains in intact cells.

Detection of lipid raft-like microdomains is only possible through the use of markers as lipid rafts are not morphologically identifiable. Cholera toxin B (CTXB) is frequently used as a marker for lipid rafts (Fra et al., 1994; Harder et al., 1998; Janes et al., 1999; Locke et al., 2005; Magee et al., 2005; Mitchell et al., 2002; Stauffer and Meyer, 1997; Stuermer et al., 2001; Yi et al., 2005). The B subunit binds to a glycosphingolipid, ganglioside GM1 (Critchley et al., 1982; Holmgren, 1973), which allows the toxin to gain entry to the cell. The native toxin is internalised along with GM1 into the Golgi apparatus and then traffics to the endoplasmic reticulum where unfolding of the toxin allows release of the active peptide from subunit A (Fishman and Orlandi, 2003; Fujinaga et al., 2003; Lencer et al., 1995; Parton and Richards, 2003). Cholera toxin entry was found to occur via non-coated invaginations that were identified as caveolae (Montesano et al., 1982; Parton, 1994; Parton et al., 1994; Parton and Richards, 2003). In cells that lack caveolin cholera toxin was also internalised in a cholesterol dependent manner, suggesting that the toxin binds lipid raft-like microdomains (Orlandi and Fishman, 1998; Shogomori and Futerman, 2001b).

In support of these studies, glycosphingolipids such as ganglioside GM1 are predicted to partition into $L_o$ phase domains due to their saturated acyl chains. Localisation of GM1 to the $L_o$ phase has been confirmed in giant unilamellar vesicles and supported bilayers composed of equimolar cholesterol, SM and DOPC, via labelling with fluorescent CTXB (Bacia et al., 2004; Dietrich et al., 2001a; Dietrich et al., 2001b; Kahya et al.,

2005; Kahya et al., 2003; Wang and Silvius, 2003). The $L_o$ phase was independently defined by exclusion of liquid disordered phase markers or a decrease in the diffusion coefficient of probes. Therefore, CTXB is not only an established caveolae and lipid raft marker but importantly, also a marker for the $L_o$ phase.

The size of lipid raft microdomains remains a controversial issue. Many current estimates suggest that lipid rafts are nanometre scale structures that would be impossible to resolve by light microscopy (Plowman et al., 2005; Prior et al., 2003; Rajendran and Simons, 2005; Sharma et al., 2004; Varma and Mayor, 1998). With respect to this problem CTXB is a useful marker because it is a pentamer and each subunit binds one GM1 molecule (Merritt et al., 1998). CTXB therefore has the potential to crosslink small rafts to aid visualisation of other raft components.

In the studies described in this chapter PC12 cells were labelled with fluorescently tagged CTXB as a marker for lipid raft-like $L_o$ domains. Confocal laser scanning microscopy (CLSM) of immunostained cells was undertaken to determine whether 14-3-3 and CTXB colocalise in puncta on the plasma membrane. Immunostaining for the GPI-anchored protein Thy-1 was performed to determine whether CTXB reliably colocalises with an established DRM-enriched protein. The coupling of lipid rafts across the bilayer is a contentious issue as it is unclear exactly how coupling would occur. CTXB and Thy-1 are both present on the exoplasmic leaflet of the bilayer, whereas 14-3-3 would be predicted to interact with the cytoplasmic leaflet. Therefore, colocalisation between CTXB and two inner leaflet membrane anchored proteins, syntaxin1a and SNAP-25, was also investigated. Syntaxin1a is anchored in the membrane by a transmembrane domain, whilst SNAP-25 is palmitoylated (Hess et al., 1992). Both proteins have been established as DRM residents (Chamberlain et al., 2001; Chamberlain and Gould, 2002; Foster et al., 2003; Gil et al., 2005; Pombo et al., 2003; Predescu et al., 2005; Salaun et al., 2005a; Salaun et al., 2005b; Taverna et al., 2004). The membrane distribution of these established DRM-associating proteins was compared with that of 14-3-3, with respect to the $L_o$ phase marker CTXB, to explore the hypothesis that 14-3-3 localises to lipid raft-like membrane domains, as implied by the DRM studies in Chapter 3.

## 4.1. Characterisation of lipid raft markers in PC12 and N2a cells

In Chapter 3 association of 14-3-3 with DRMs derived from both N2a and PC12 cells was established. PrP and flotillin-1 were employed as lipid raft markers but unfortunately the available antibodies against these proteins were unsuccessful in immunostaining tests, so Thy-1 was chosen as an alternative marker. A number of studies have reported DRM association of both Thy-1 (Brugger et al., 2004; Draberova and Draber, 1993; Fra et al., 1994; Madore et al., 1999; Naslavsky et al., 1997; Rege and Hagood, 2006) and CTXB (Badizadegan et al., 2000a; Badizadegan et al., 2000b; Shogomori and Futerman, 2001a; Wolf et al., 1998). However, it was necessary to verify the DRM localisation of Thy-1 and CTXB in PC12 and N2a cells in this investigation before beginning microscopy studies with these proteins.

Following this, the distribution CTXB in live and paraformaldehyde (PFA) fixed cells was characterised by confocal microscopy. To study the localisation of endogenous 14-3-3, fixation and immunostaining of the cells is necessary. This approach is preferable to overexpression of a fluorescent fusion protein construct as the partitioning of a protein into lipid raft-like domains and its overall localisation may be sensitive to expression levels. CTXB staining was compared in live and fixed cells to assess the impact of fixation. The expected plasma membrane localisation of Thy-1 was also investigated by immunostaining.

### 4.1.1. DRM association of CTXB and Thy-1

DRMs were isolated from PC12 and N2a cells as described in Chapter 2, section 2.3.1.2. To assess the localisation of GM1 in the gradient, cells were incubated with 1 μg/ml CTXB for 5 minutes prior to lysis and isolation of DRMs. The gradients were collected as twelve fractions and DRMs were observed at the 5 – 30 % sucrose interface, corresponding to fractions 3 and 4.

In PC12 cells, Thy-1 and CTXB were both enriched in DRM fractions 3 and 4 and barely detectable in the soluble protein fractions (fractions 8 – 12), as shown in figure 4.1A. This agrees with previous reports of Thy-1 enrichment in DRMs derived from

PC12 cells (Aoyagi et al., 2005; Herreros et al., 2001). CTXB was also concentrated in DRMs derived from N2a cells (figure 4.1B) but the Thy-1 distribution was reproducibly different. Thy-1 appears to be concentrated in fraction 6, which indicates a higher density than the DRM fractions as it corresponds to the middle of the 30 % sucrose layer (see figure 4.1B). The localisation of Thy-1 in flotation gradients loaded with N2a cell lysate has not previously been reported. However, this result is at odds with studies that show Thy-1 enrichment in DRMs isolated from other cells and tissues. Indeed it is rather unusual for a protein to be concentrated in the middle fractions of the gradient instead of the DRMs or soluble protein fractions (8 – 12). Whilst the reason behind this aberrant localisation is unclear, we could speculate that, in N2a cells, Thy-1 localises to DRMs with a higher density. Because Thy-1 association with DRMs in N2a cells could not be confirmed, PC12 cells were chosen as the focus of subsequent microscopy experiments.

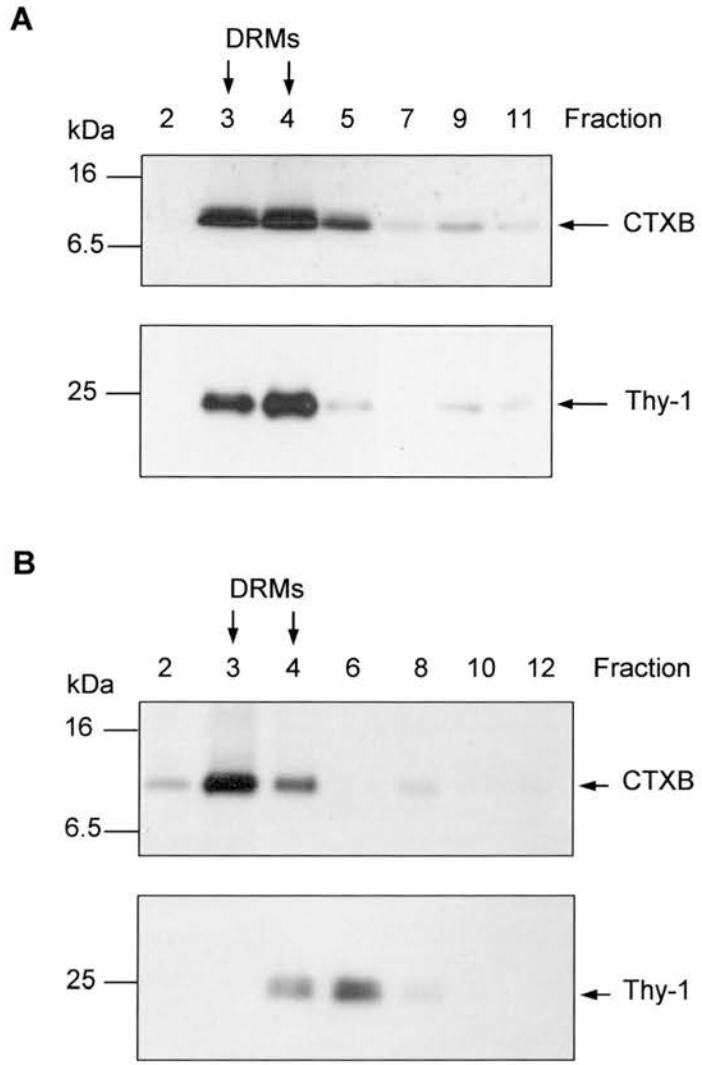


**Figure 4.1 CTXB and Thy-1 are enriched in PC12 cell DRMs but Thy-1 exhibits a different distribution in N2a cell gradients**

PC12 and N2a cells were incubated with 1 μg/ml CTXB for 5 minutes at 37°C, followed by isolation of DRMs (see Chapter 2, section 2.3.1.2). The sucrose density gradient was collected as twelve fractions, fraction 1 being the top of the gradient and fraction 12 the bottom. DRMs corresponded to fractions 3 and 4. For analysis of CTXB distribution each fraction was concentrated and separated by SDS-PAGE. For analysis of Thy-1 distribution, 20 μl of each fraction was separated by SDS-PAGE. **A** PC12 cell gradients were immunoblotted for CTXB and Thy-1. **B** N2a cell gradients were immunoblotted for CTXB and Thy-1.

### 4.1.2. Characterisation of CTXB staining in PC12 cells

Previous studies have employed fluorescently labelled CTXB at concentrations ranging from 0.1 – 10 μg/ml (Harder et al., 1998; Kenworthy et al., 2000; Locke et al., 2005; Naslavsky et al., 1997; Nichols, 2003; Nichols et al., 2001). PC12 cells were incubated with 1 μg/ml FITC-labelled CTXB at 37°C for periods of 5 to 30 minutes. Cells were then washed once to remove excess CTXB and imaged immediately. An incubation period of only 5 - 10 minutes was found to be optimum for achieving plasma membrane staining. After 15 minutes high intensity staining was observed in an internal compartment and this interfered with detection of the signal form the plasma membrane. Rapid trafficking of CTXB to the Golgi apparatus has been reported (Nichols et al., 2001).

Figure 4.2 shows sequential horizontal sections through a PC12 cell stained with 1 μg/ml CTXB. Plasma membrane staining can clearly be seen in the mid-sections and at the base of the cell, exhibiting a punctate appearance. Strong staining of an internal compartment is already visible after only 10 minutes incubation with CTXB. CTXB staining was also visualised following fixation of PC12 cells. Live cells were incubated with 1 μg/ml CTXB for 10 minutes and fixed immediately in 4 % (w/v) PFA on ice. Fixed cells (figure 4.3) showed a similar subcellular distribution of CTXB as observed in live cells (figure 4.2). The plasma membrane and partly internal localisation of CTXB is again evident.

CTXB staining of live and fixed cells was compared in detail by analysing the full width at half maximum intensity (FWHM) size of the CTXB clusters and the density of clusters on the plasma membrane (described in Chapter 2, section 2.4.6.1). Areas from the plasma membrane at the base of cells were analysed and representative examples are displayed in figure 4.4A. CTXB clusters were of a similar size and surface density in live and fixed cells, as shown in figure 4.4 B and C. Whilst the distribution of cluster sizes in fixed cells was slightly different from that of live cells (figure 4.4B), the mean FWHM sizes were not significantly different between live and fixed cells, according to the Student's T-test. The mean FWHM sizes were 635 nm ± 21 nm (SEM) in live cells and 646 nm ± 20 nm (SEM) in fixed cells.

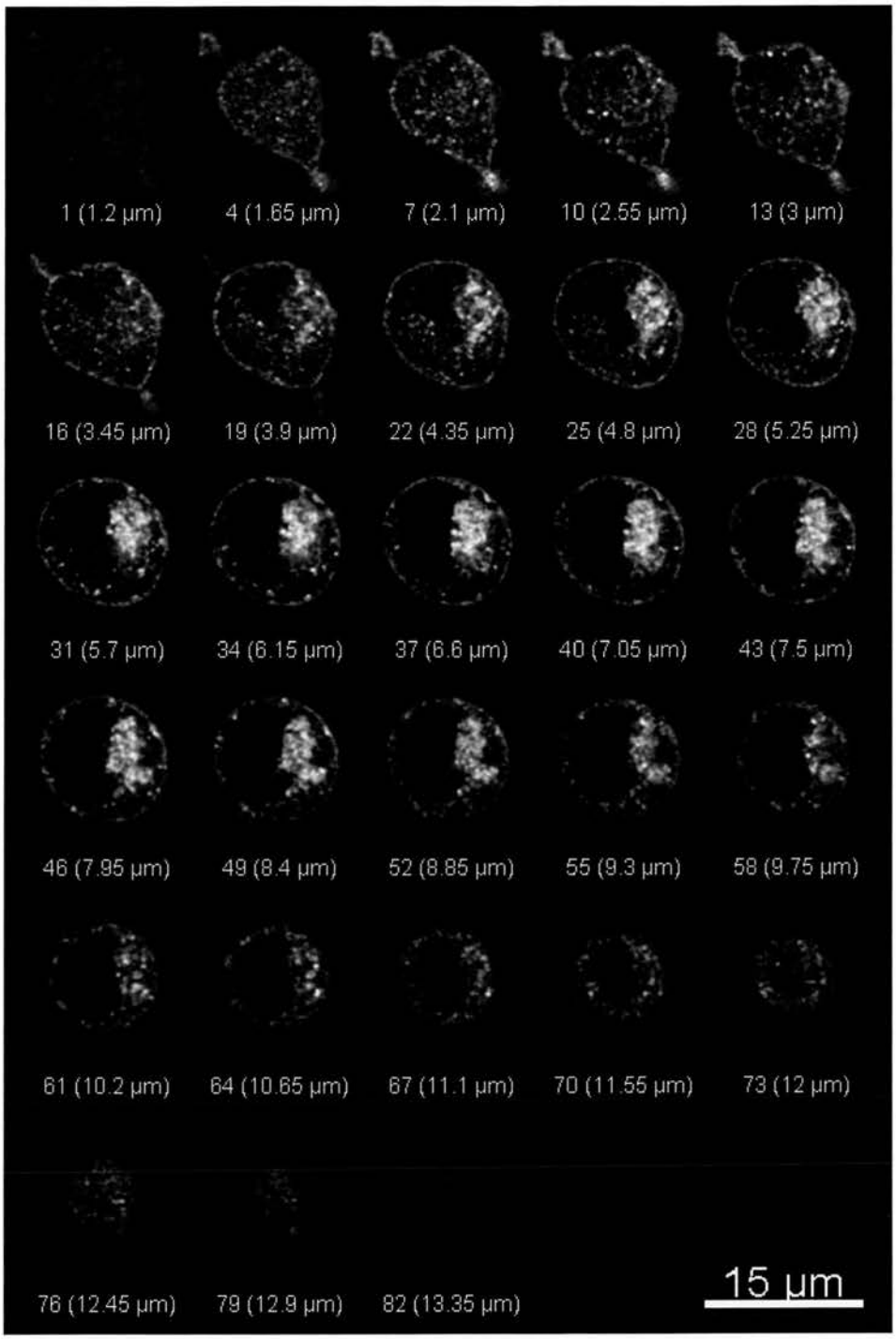


**Figure 4.2 Horizontal sections through a live PC12 cell stained with CTXB**

PC12 cells were labelled for 10 minutes with 1 µg/ml FITC-CTXB, at 37°C, washed once and imaged immediately. CLSM was employed to image horizontal sections through cells. An image was acquired every 140 nm, every third section is displayed. Section numbers and distance through the image stack are shown below each image.

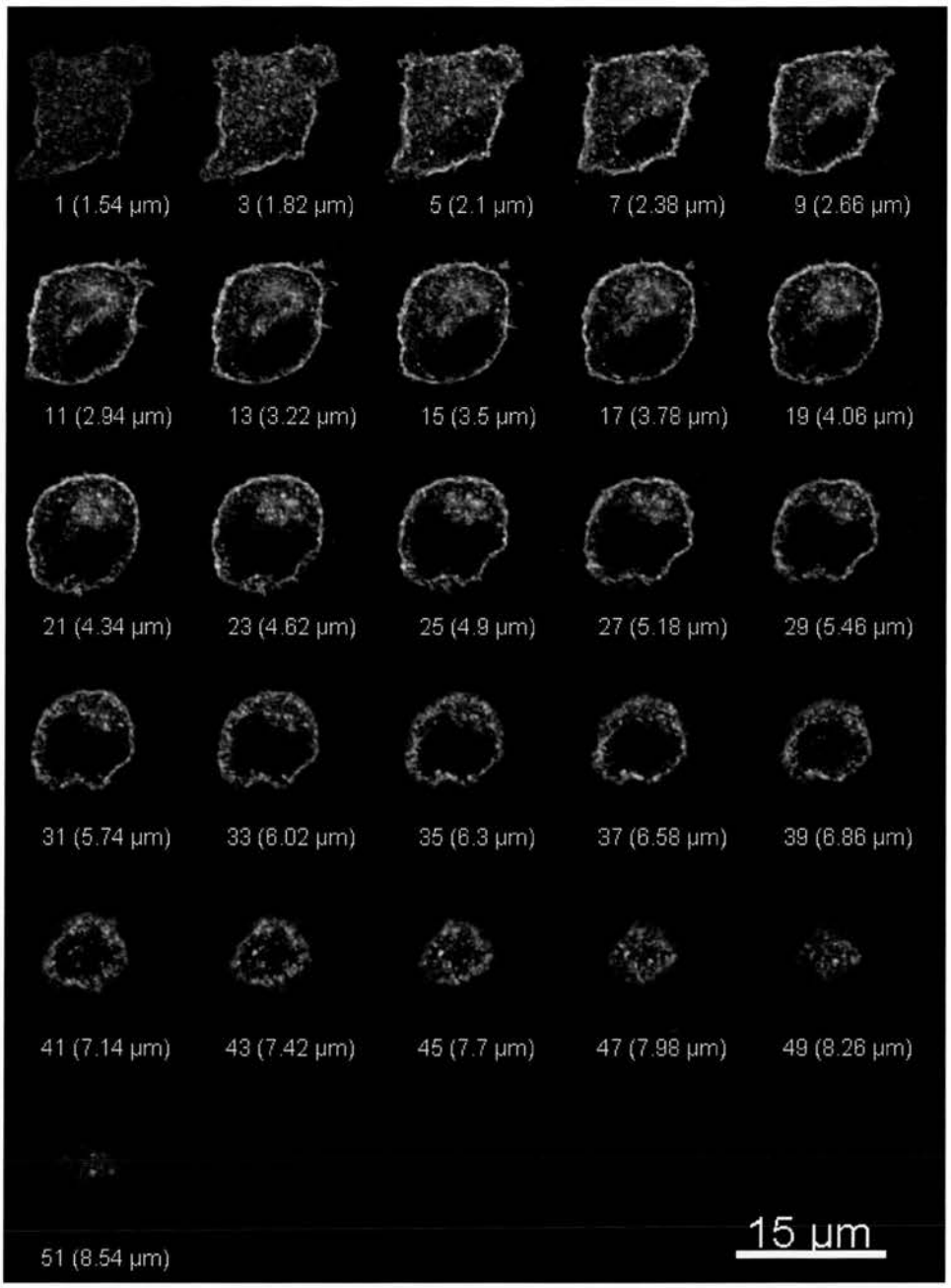


**Figure 4.3 Horizontal sections through a fixed PC12 cell stained with CTXB**

PC12 cells were labelled for 10 minutes with 1 µg/ml FITC-CTXB, at 37°C, then washed once with PBS and fixed immediately with 4 % (w/v) PFA on ice, for 30 minutes. Following mounting of the cells, CLSM was employed to image horizontal sections through cells. An image was acquired every 140 nm, every second section is displayed. Section numbers and distance through the image stack are shown below each image.

The cluster density was also very similar in live and fixed cells (figure 4.4C). The mean cluster density was 1.39 ± 0.04 (SEM) clusters per $\mu m^2$ in live cells and 1.38 ± 0.04 (SEM) clusters per $\mu m^2$ in fixed cells. Thus it appears that the fixation process does not significantly alter the CTXB distribution on PC12 cell membranes.

### 4.1.3. Thy-1 is localised to the plasma membrane in PC12 cells

Thy-1 is a GPI-anchored protein in the external leaflet of the plasma membrane bilayer (Homans et al., 1988; Rege and Hagood, 2006) and is widely expressed in the mammalian nervous system (Morris, 1985). PC12 cells were immunostained with anti-Thy-1 (OX7) antibody to observe the plasma membrane localisation of Thy-1. Figure 4.5 shows the distribution of Thy-1 staining in sequential horizontal sections through two representative PC12 cells. Bright Thy-1 staining can be seen at the plasma membrane on the middle section images, with some Thy-1 staining inside the cells. Thy-1, like CTXB, showed a punctate appearance on the cell surface as can be seen at the base of the cell in figure 4.5. Many studies have reported a diffuse plasma membrane distribution for GPI-anchored proteins, including Thy-1, visualised by immunostaining (Fra et al., 1994; Harder et al., 1998; Kenworthy et al., 2000; Mayor et al., 1994; Stuermer et al., 2001). However, in PC12 cells specifically, two studies confirmed that immunostaining for Thy-1 reveals a punctate distribution (Aoyagi et al., 2005; Herreros et al., 2001). In addition, when Thy-1 was detected by immunostaining or immunogold labelling and electron microscopy in primary neurons, a clustered surface distribution was apparent (Brugger et al., 2004; Ledesma et al., 1998; Madore et al., 1999). Madore *et al* point out that image data deconvolution (as employed for the image in figure 4.5) was necessary to resolve separate Thy-1 puncta on neurons following immunostaining (Madore et al., 1999).

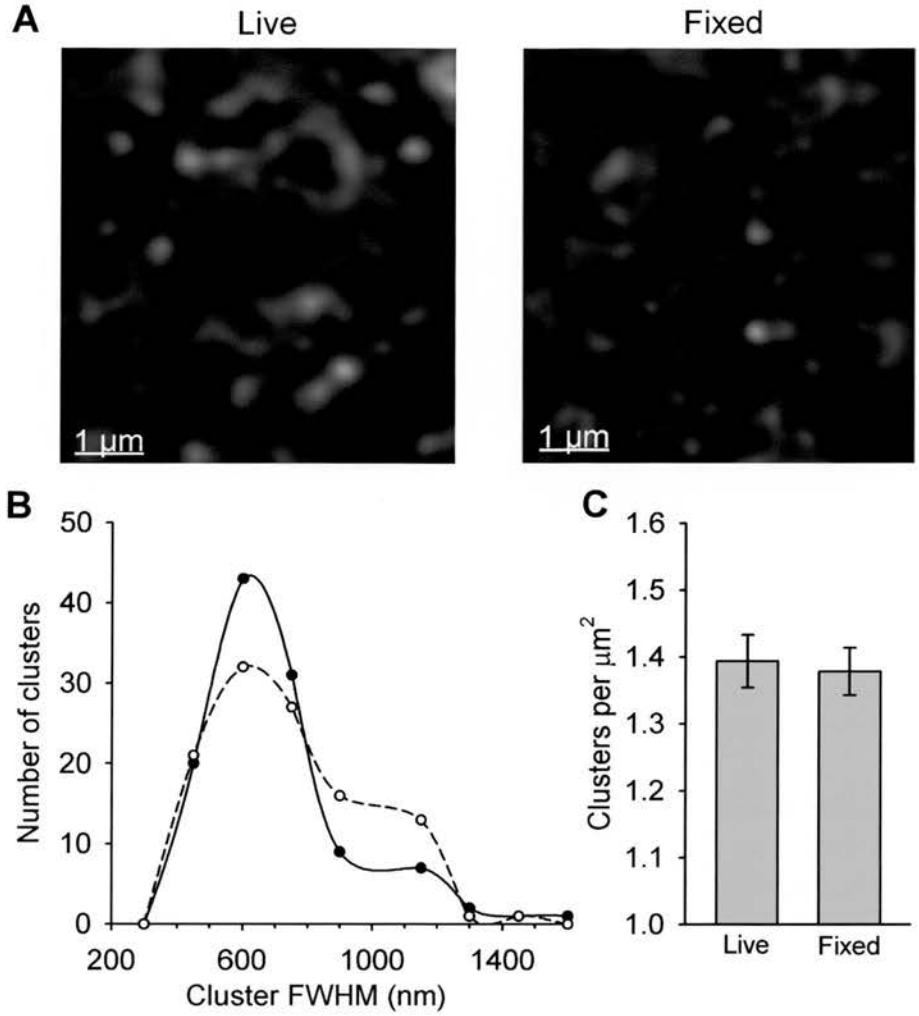


**Figure 4.4 CTXB clusters are of a similar size and density in live and fixed PC12 cells**

PC12 cells were labelled with 1 µg/ml FITC-CTXB, at 37ºC, then either imaged immediately or fixed with 4 % (w/v) PFA on ice, for 30 minutes and imaged following mounting of the cells (as described in Chapter 2, sections 2.4.1 and 2.4.2).

**A** Representative images from the base of a live and a fixed PC12 cell used for cluster analysis. **B** The FWHM cluster size was measured for a total of 120 clusters from at least 4 separate images. The distribution of cluster sizes is shown in a frequency histogram of cluster size. Filled circles/solid line = live cells, open circles/dashed line = fixed cells. **C** The mean density of clusters per $\mu m^2$ ± SEM, n = 6 images.

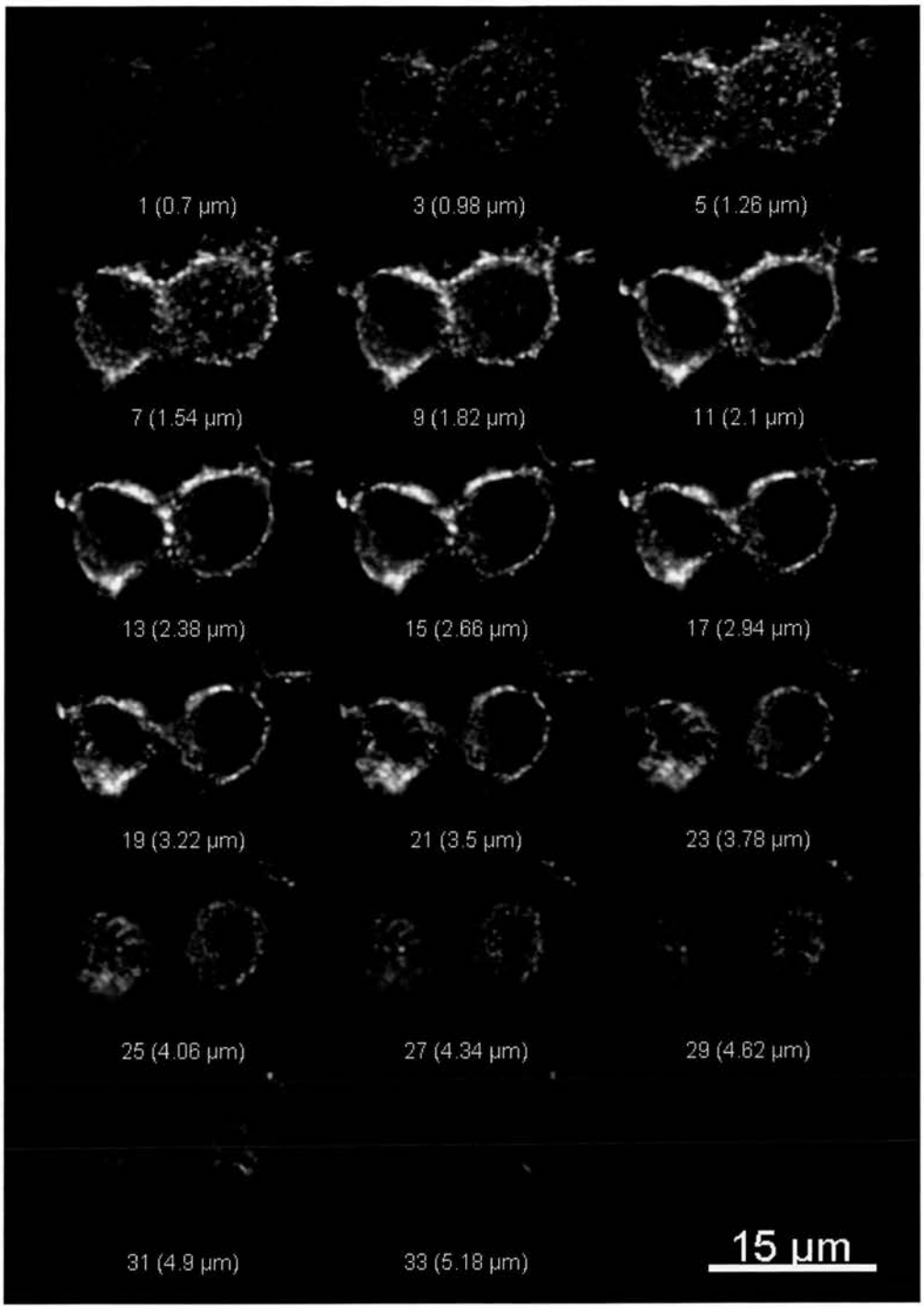


**Figure 4.5 Horizontal sections through a PC12 cell immunostained for Thy-1**

PC12 cells were fixed on ice with 4 % (w/v) PFA, immunostained with anti-Thy-1 antibody and imaged by CLSM, taking horizontal sections through the cells. An image was acquired every 140 nm, every second section is displayed. Section numbers and distance through the image stack are shown below each image.

## 4.2. Colocalisation of DRM proteins with the lipid raft marker CTXB

CTXB and Thy-1 were both enriched in DRMs and both exhibited a punctate distribution on the surface of PC12 cells. If DRMs represent pre-existing membrane microdomains then CTXB and Thy-1 puncta would be predicted to overlap if cells were co-stained for the two molecules. To test this hypothesis, Thy-1 immunostaining of CTXB-labelled PC12 cells, followed by CLSM and image analysis, was performed to examine the extent of colocalisation between these two lipid raft markers. The same procedures were then used to assess the extent of colocalisation between 14-3-3 and CTXB.

### 4.2.1. Colocalising puncta of Thy-1 and CTXB are visible on the plasma membrane in dual labelled PC12 cells

PC12 cells were labelled with CTXB for five minutes at 37°C, fixed and immunostained for Thy-1, figures 4.6 displays sections through representative dual labelled cells. CTXB labelling does not change the overall localisation of Thy-1. The middle section view shows that Thy-1 (red) is concentrated at the plasma membrane, as observed when Thy-1 immunostaining was performed without CTXB labelling (figure 4.5). The punctate distribution of both Thy-1 and CTXB is again evident from the base and top images in figure 4.6. Some colocalisation between Thy-1 and CTXB puncta is visible in the merged images; examples of overlapping puncta are indicated by arrowheads.

### 4.2.2. 14-3-3 is distributed throughout the cytosol in PC12 cells

Before investigating colocalisation of 14-3-3 with CTXB, the overall localisation of 14-3-3 in PC12 cells was determined. PC12 cells were fixed and immunostained using anti-14-3-3 (pan), which recognises all 14-3-3 isoforms. Unfortunately the 14-3-3 isoform specific antibodies were not successful in immunostaining tests. This is probably because these antibodies were raised against a peptide at the N-terminus of 14-3-3 (Martin et al., 1993) and the crystal structures of 14-3-3 show that the N-terminus of each monomer is buried in the dimer interface (Gardino et al., 2006). Thus, whilst the

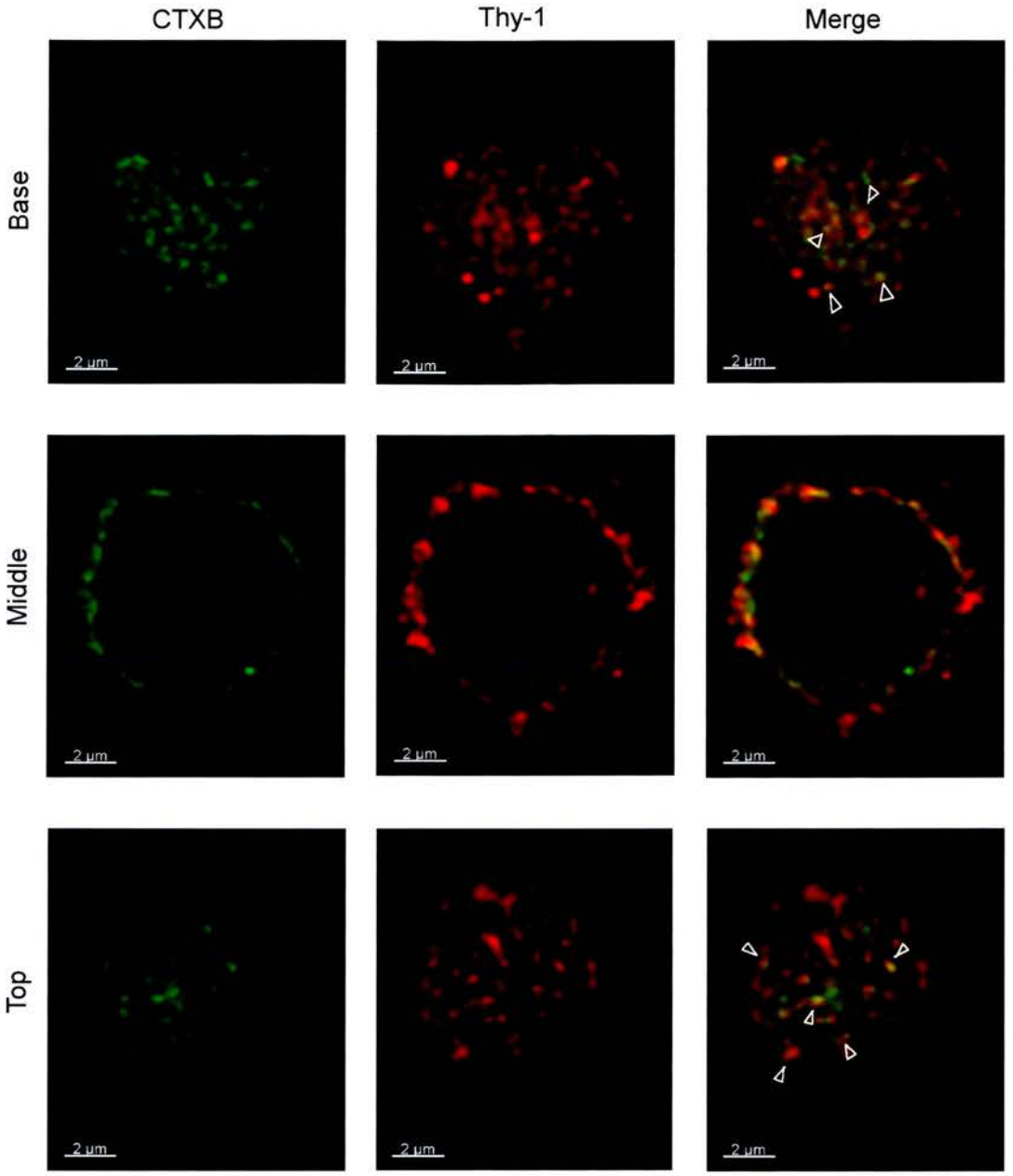


**Figure 4.6 Thy-1 localises to the plasma membrane in CTXB-labelled PC12 cells**

PC12 cells were incubated with FITC-CTXB for 5 minutes at 37°C, fixed and immunostained for Thy-1 (see Chapter 2, sections 2.4.1 and 2.4.2). CTXB (green) and Thy-1 (red) were visualised by CLSM, taking horizontal sections at 140 nm intervals through the cells. Sections from the base, middle and top of a representative cell are displayed. Scale bars = 2 µm. Arrowheads indicate overlapping Thy-1 and CTXB puncta.

antibodies recognise denatured 14-3-3 on an immunoblot they would be less likely to recognise native 14-3-3.

Sequential horizontal sections through representative immunostained cells are shown in figure 4.7, demonstrating that 14-3-3 was distributed throughout the cytosol. The nucleus of each cell is visible as a dark hole where little 14-3-3 staining is detected compared to the strong signal from the cytosol. The cytosolic staining is not uniform with variations in the local concentration of 14-3-3. Predominantly cytosolic 14-3-3 staining agrees with previous reports (Beguin et al., 2005; Carreno et al., 2005; Cavet et al., 2003; Oksvold et al., 2004; Strochlic et al., 2004), with most of the functions so far ascribed to 14-3-3 protein occuring in the cytosol (Aitken, 2006; Muslin and Xing, 2000).

Following visualisation of the mainly cytosolic distribution of 14-3-3, PC12 cells were again immunostained for 14-3-3 but this time incubated with CTXB prior to fixation. Horizontal sections from the base, middle and top of representative cells are displayed in figure 4.8. The middle section image demonstrates that 14-3-3 (red) retains its cytosolic distribution following CTXB staining. 14-3-3 protein is also observed at the top and base of the cells, in the same section where CTXB staining is concentrated and in the middle section images 14-3-3 staining reaches into the periphery of the cell where CTXB labels the membrane. Considering CTXB as a plasma membrane marker, these observations suggest that some 14-3-3 is present in the plasma membrane proximal region of the cells. Inspection of the merged images in figure 4.8 suggests that, in contrast to Thy-1, little CTXB staining overlaps with 14-3-3 at the top and base of these cells. In the following section the apparent difference between the extent of colocalisation of Thy-1 and 14-3-3 with CTXB is analysed quantitatively.

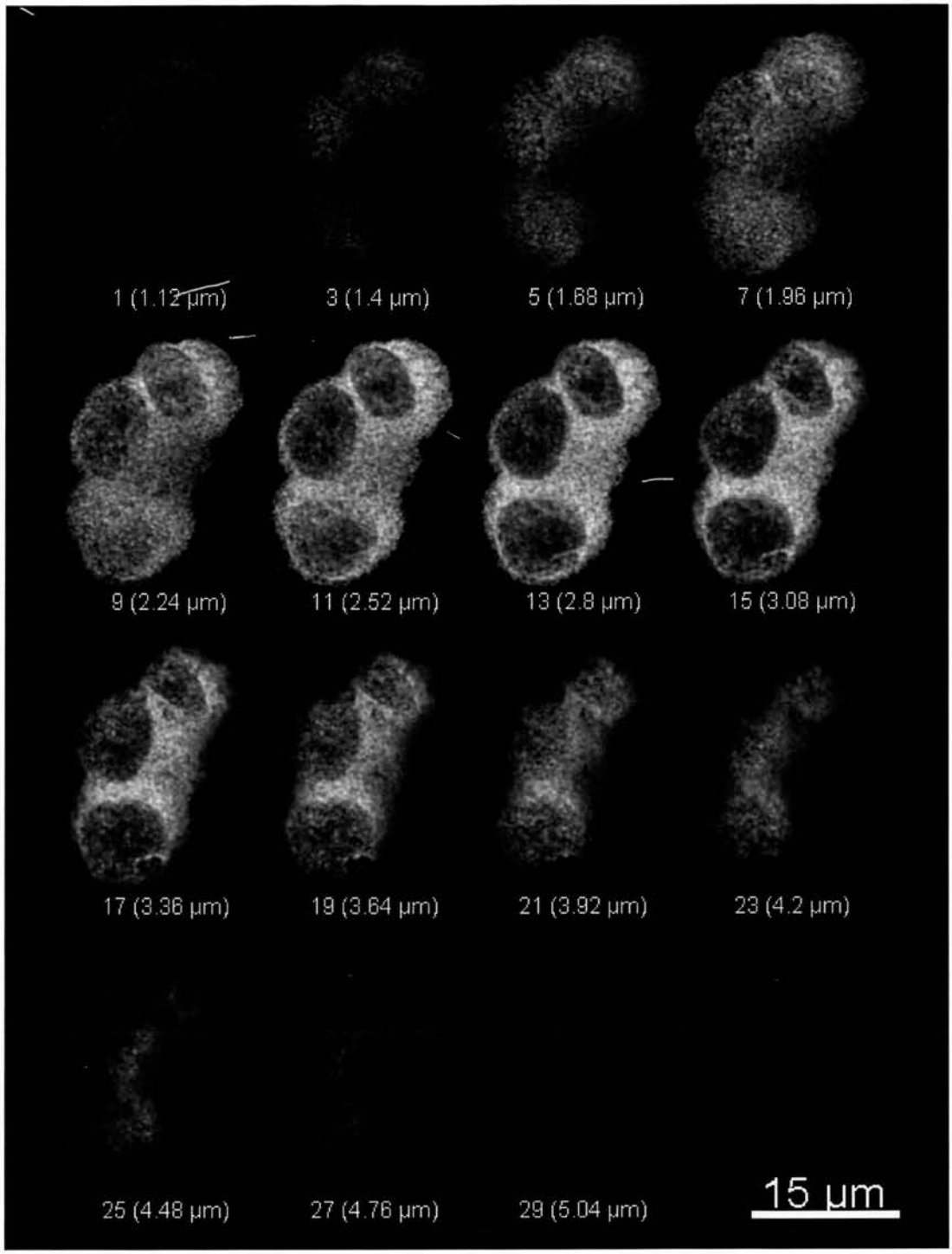


**Figure 4.7 Horizontal sections through PC12 cells stained for 14-3-3**

PC12 cells were fixed on ice with 4 % (w/v) PFA, immunostained with anti-14-3-3 (pan) antibody and imaged by CLSM, taking horizontal slices through the cells. An image was acquired every 140 nm. Section numbers and distance through the image stack are shown below each image.

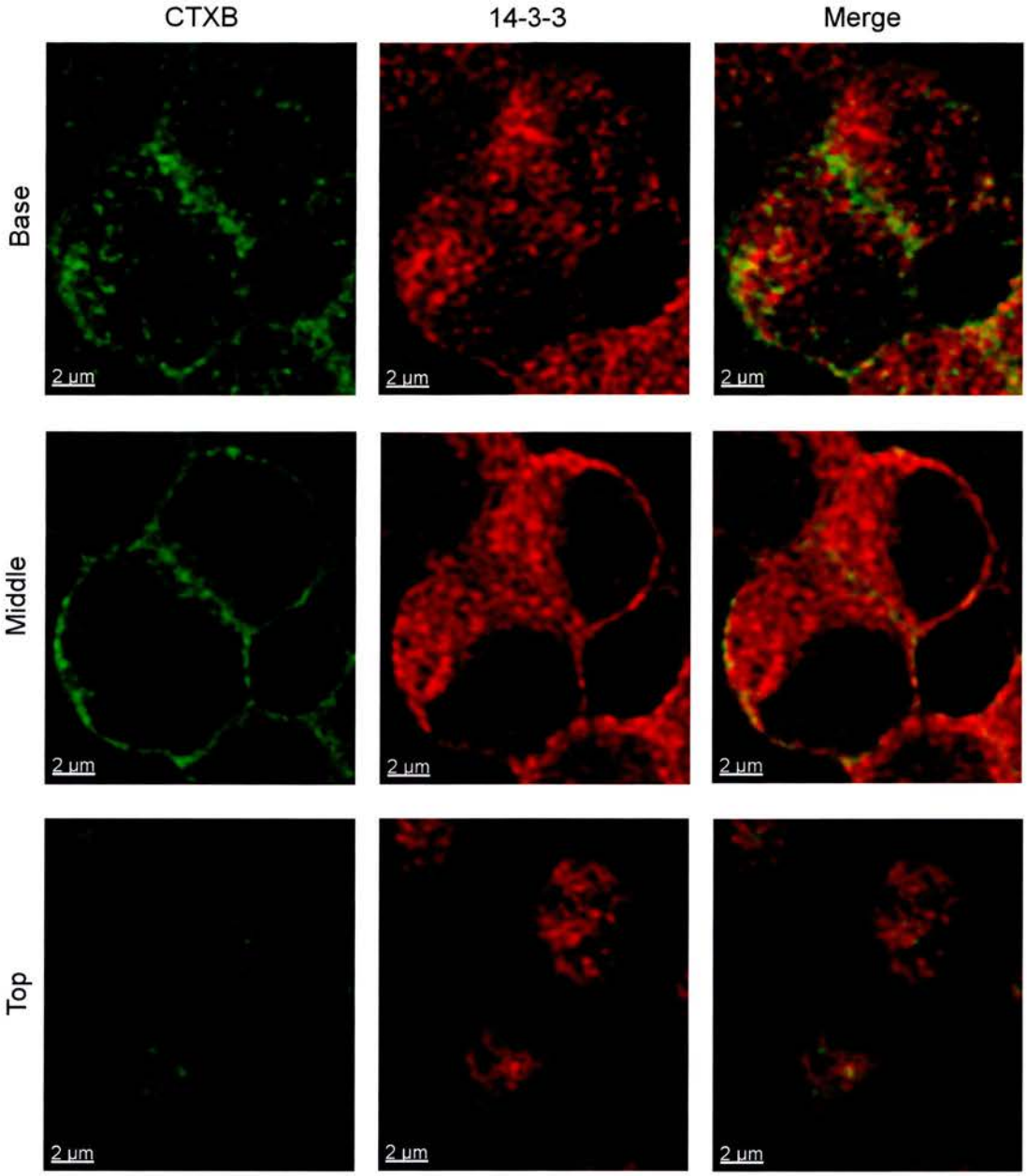


**Figure 4.8 14-3-3 is present in the cytosol and periphery of CTXB-labelled PC12 cells**

PC12 cells were incubated with FITC-CTXB for 5 minutes at 37°C, fixed and immunostained for 14-3-3 (see Chapter 2, sections 2.4.1 and 2.4.2). CTXB (green) and 14-3-3 (red) were visualised by CLSM, taking horizontal sections at 140 nm intervals through the cells. Sections from the base, middle and top of representative cells are displayed. Scale bars = 2 µm.

### 4.2.3. Thy-1 colocalises with CTXB to a greater extent than 14-3-3

In many studies two proteins are presented as colocalised if the merged image of the red and green channels shows yellow (overlapping) regions. However, this technique is clearly not quantitative and relies on unbiased visual inspection of the image. Various methods have been devised for a more rigorous analysis of the extent of colocalisation. In this study the percentage colocalisation of each channel (based on the Manders coefficients (Manders et al., 1993)) and the percentage correlation between the channels ($R^2$ x 100, where R = Pearson's coefficient) will be reported alongside each other. Calculation and interpretation of these parameters is explained in detail in Chapter 2, section 2.4.6.2. Measurement of percentage colocalisation has the advantage of producing a separate value for each channel, whereas Pearsons correlation coefficient (R) describes the relationship between the two channels (Manders et al., 1992; Scientific Volume Imaging, 2006b). However, calculation of percentage colocalisation requires thresholding of each channel to remove the contribution of low intensity background signal. Manually assigning thresholds could introduce bias, so an automatic thresholding algorithm, devised by Costes *et al* (Costes et al., 2004), was used (see Chapter 2, section 2.4.6.2). This automatic thresholding provides a useful way of visualising colocalisation by producing a mask of all voxels that contribute to the colocalisation calculation. However, the percentage correlation ($R^2$ x 100) supplies valuable information because it gives an intensity dependent measurement of the extent to which the red and green signals are covariant.

To quantitatively examine the coincidence of Thy-1 and 14-3-3 with CTXB, images from the base of at least twelve cells were analysed for the percentage colocalisation of each protein and the degree of intensity dependent correlation ($R^2$ x 100) between the red and green channels. The mean results are presented in figure 4.9, along with two further examples of Thy-1 and 14-3-3 protein staining at the base of CTXB-labelled PC12 cells. From the merged images in figure 4.9A it appears that more Thy-1 than 14-3-3 overlaps with CTXB. However, it is clear from the Thy-1 and CTXB stained images that not all Thy-1 resides in the same clusters as CTXB and vice versa, as might be expected if both proteins localise to the same membrane microdomains. Quantification of the colocalisation, following automatic thresholding, agrees with these conclusions.

**Figure 4.9 Thy-1 colocalises with CTXB to a greater extent than 14-3-3 on the plasma membrane of PC12 cells**

PC12 cells were incubated with FITC-CTXB, fixed and immunostained for Thy-1 or 14-3-3. CTXB (green) and Thy-1 or 14-3-3 (red) were visualised by CLSM. **A** Images from the base of representative cells. Scale bars = 1 μm. The right hand panels are scatter plots of the red intensity plotted against the green intensity for each voxel in the image. **B** Colocalisation masks for the merged images in A, generated by automatic thresholding (described in Chapter 2, section 2.4.6.2). **C** The mean percentage colocalisation of CTXB with Thy-1 or 14-3-3 (colocalisation of the green channel with the red channel) and mean percentage colocalisation of Thy-1 or 14-3-3 with CTXB (colocalisation of the red channel with the green channel). **D** Mean percentage correlation ($R^2$ x 100) of the green channel (CTXB) with the red channel (Thy-1 or 14-3-3 protein). All error bars represent SEM, n = 12. ** 14-3-3 values were significantly different from Thy-1 values (Student's T-test, $p < 0.001$).

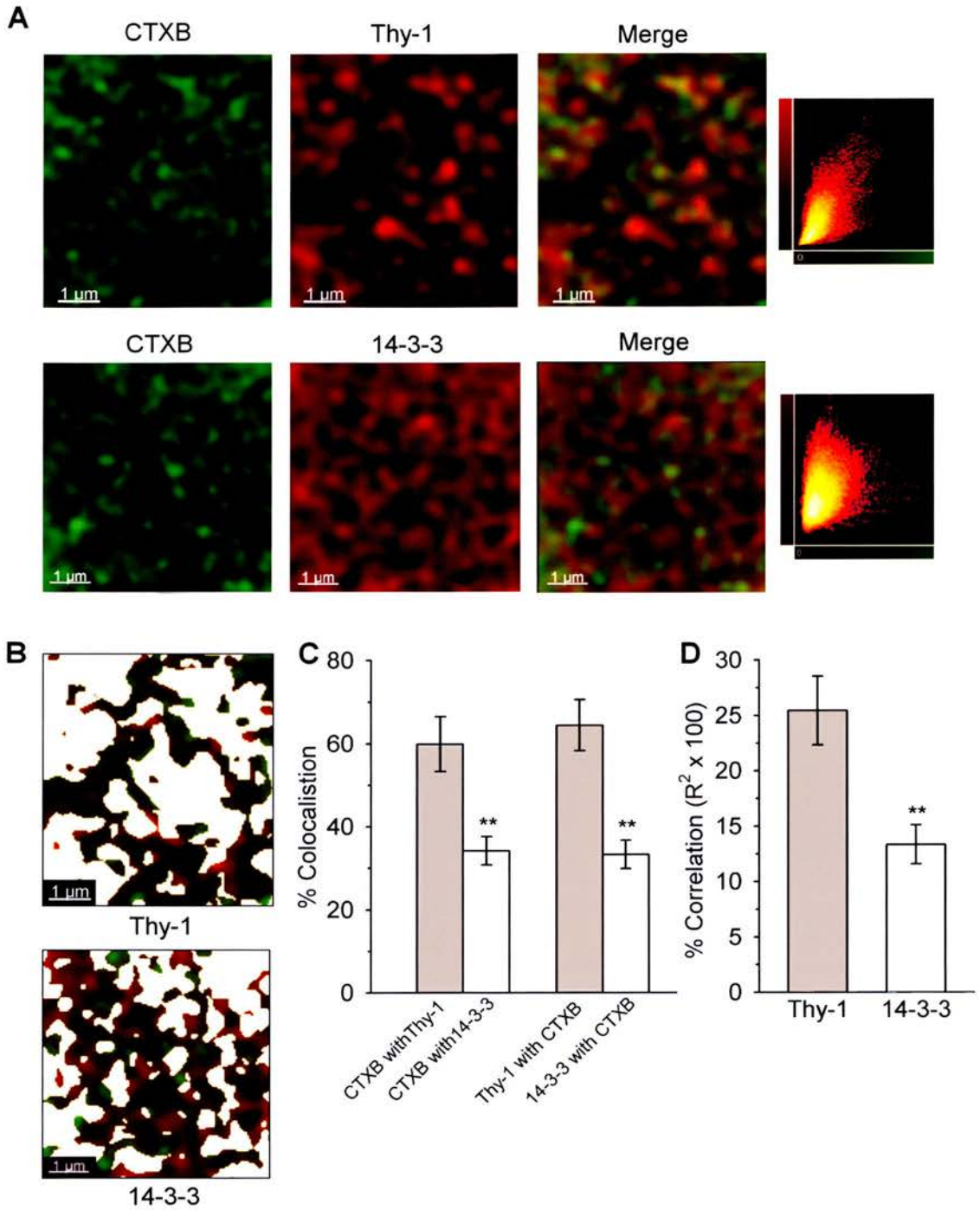


**Figure 4.9 Thy-1 coincides with CTXB to a greater extent than 14-3-3 on the plasma membrane of PC12 cells**

Of the total Thy-1 signal intensity, 64 ± 6 % (SEM) colocalised with CTXB signal and 60 ± 7 % of the CTXB signal colocalised with Thy-1 signal. For 14-3-3, only 33 ± 3 % of 14-3-3 signal intensity colocalised with CTXB signal and 34 ± 3 % of CTXB signal colocalised with 14-3-3 signal. These results are illustrated by the colocalisation masks produced by automatic thresholding (figure 4.9B) and the bar chart in figure 4.9C. Colocalisation of 14-3-3 protein with CTXB was significantly lower than colocalisation of Thy-1 with CTXB (Student's T-test, $p < 0.001$).

The scatter plots in the right hand panels of figure 4.9A show the red signal intensity plotted against the green signal intensity for each voxel in the image. These scatter plots therefore give some visual indication of correlation between the channels. Perfect intensity dependent correlation would produce a straight diagonal line, originating at zero. In the CTXB/Thy-1 scatter plot (top) the points are clustered closer to the diagonal than in the CTXB/14-3-3 scatter plot (below), where the spread is wider. Calculation of the mean correlation ($R^2$ x 100) from a set of similar images confirmed that CTXB and Thy-1 staining showed significantly more correlation than CTXB and 14-3-3 staining (Student's T-test, $p < 0.001$). A mean of 25 ± 4 % (SEM) correlation was observed between CTXB and Thy-1, whereas only 13 ± 2 % correlation was observed between CTXB and 14-3-3 (figure 4.9D).

The correlation between the intensity of CTXB and 14-3-3 staining certainly appears very low from figure 4.9A. Is it in fact below expected random correlation? Two different methods were employed to estimate the contribution of random variation to the correlation coefficient. First, the red channel (14-3-3 protein or Thy-1) was repeatedly randomised (using Costes' randomisation algorithm, see Chapter 2, section 2.4.6.2) and $R^2$ calculated with respect to the original green (CTXB) channel. In the second procedure, the red channel was flipped through 180° (in either the x or y dimension) and $R^2$ calculated with respect to the original green channel. Costes' randomisation algorithm carries out 50 iterations where the image is split into tiles, randomised differently and a mean $R^2$(random) is calculated. The red channel flipping produces a single value but the complete structure of the image is maintained. Table 4.1 shows the mean results when these procedures were performed with at least twelve images. Both methods produced similar random correlation values for each data set but whereas the random correlation calculated for 14-3-3 staining was ~5 – 6 %, the random correlation in Thy-1 images was

lower at ~ 2 %. However, a paired t-test showed that the correlation observed between 14-3-3 protein and CTXB in the original images was significantly greater than random values ($p < 0.005$). According to these data the correlation observed between both Thy-1 and CTXB and 14-3-3 protein and CTXB is not due to random variation. This implies that a very small proportion of 14-3-3 protein reproducibly colocalises with CTXB.

**Table 4.1 Random correlation tests – Thy-1 and 14-3-3**

| Red Channel | Mean $R^2$ x 100% | SEM | Paired T-test versus original |
|---|---|---|---|
| Thy-1 original | 25.5 | 3.6 | - |
| Thy-1 randomised | 2.9 | 1.5 | $P < 0.001$ |
| Thy-1 flipped 180° in x | 2.5 | 1.1 | $P < 0.001$ |
| Thy-1 flipped 180° in y | 0.33 | 1.3 | $P < 0.001$ |
| 14-3-3 original | 13.3 | 1.8 | - |
| 14-3-3 randomised | 6.5 | 1.0 | $P = 0.004$ |
| 14-3-3 flipped 180° in x | 4.8 | 1.0 | $P < 0.001$ |
| 14-3-3 flipped 180° in y | 5.4 | 1.1 | $P < 0.001$ |

In summary, 14-3-3 staining coincides with CTXB staining to a much lesser degree than Thy-1 staining coincides with CTXB staining. However, the low level coincidence observed between 14-3-3 and CTXB appears not to be due solely to random variation.

## 4.3. Comparison of DRM association and membrane localisation of inner leaflet lipid raft markers

It is unclear how lipid rafts in the outer leaflet of the bilayer couple with lipid rafts in the inner leaflet. However, many inner leaflet membrane proteins and signalling functions reportedly associate with DRMs. It is interesting then that the intracellular protein 14-3-3 appears to show a degree of non-random overlap with a lipid raft marker present in the outer leaflet of the bilayer, CTXB-labelled GM1. Is this true of other established DRM-associating proteins that are anchored to the inner leaflet of the plasma membrane? This would further validate the conclusions inferred from 14-3-3 colocalisation with CTXB.

SNAP-25 and syntaxin1a are anchored to the inner leaflet by palmitoylation and a single transmembrane domain respectively. Both have been reported to partially associate with DRMs (Chamberlain et al., 2001; Chamberlain and Gould, 2002; Foster et al., 2003; Gil et al., 2005; Pombo et al., 2003; Predescu et al., 2005; Salaun et al., 2005a; Salaun et al., 2005b; Taverna et al., 2004). Furthermore, these proteins are essential mediators of regulated exocytosis and cholesterol depletion has been reported to inhibit exocytosis (Chamberlain et al., 2001; Churchward et al., 2005; Gil et al., 2005; Lang et al., 2001; Ohara-Imaizumi et al., 2004). Their potential localisation to $L_o$ domains is therefore of interest.

In this section the initial aim was to confirm the previously reported DRM association of these proteins in PC12 cells. Imaging studies were then carried out to determine whether SNAP-25 and syntaxin1a colocalise with CTXB. The results were compared with those obtained for Thy-1 and 14-3-3.

### 4.3.1. SNAP-25 and syntaxin1a associate with PC12 cell DRMs

DRMs were isolated from PC12 cells (see Chapter 2, section 2.3.1.2). Sucrose density gradient fractions were separated by SDS-PAGE and immunolotted for SNAP-25 and syntaxin1a. SNAP-25 and syntaxin1a were both detected in DRM fractions (figure 4.10), though the majority of both proteins reside in soluble protein fractions (fractions 8 – 12.) Figure 4.10 indicates that a greater proportion of total SNAP-25 than total syntaxin1a localises to DRMs. A similar result was presented by Gil and co-workers when they isolated DRMs from rat brain synaptosomes (Gil et al., 2005). However, Chamberlain and co-workers calculated that similar proportions of total SNAP-25 (24 %) and syntaxin1a (22 %) were associated with DRMs derived from PC12 cells (Chamberlain et al., 2001).

The proportion of SNAP-25 associated with PC12 cell DRMs in this study was quantified to find out whether similar results would be observed. The relative partitioning of Thy-1 and SNAP-25 into DRMs was compared as Thy-1 represents a protein concentrated in DRMs and barely detectable in other fractions.
Serial dilutions of the DRM fractions and original lysates were separated by SDS-PAGE and immunoblotted. Figure 4.11A shows that a 5-fold dilution of the DRM fraction contained a similar amount of SNAP-25 as a 50-fold dilution of the lysate (this was confirmed by densitometry). Therefore,

$$[\text{SNAP-25}]_{\text{lysate}} = 10 \times [\text{SNAP-25}]_{\text{DRMs}}$$

The volume of lysate (mixed with 80 % sucrose) loaded onto the gradient was 6 ml and the volume of the DRM fraction containing detectable SNAP-25 was 1 ml. Thus,

$$\text{volume of lysate} = 6 \times \text{volume of DRMs}$$

Therefore the amount of SNAP-25 in the DRMs equalled,

$$\frac{\text{Amount SNAP - 25 in lysate}}{6 \times 10} = \frac{\text{Total SNAP - 25}}{60} = < 2\ \%\ \text{total SNAP-25}$$

Thus, < 2 % of the total SNAP-25 was present in the DRMs. The same rationale was employed to calculate that DRM fraction 3 contains 33 % of the total Thy-1 and fraction 4 contains 17 %. All together 50 % of the total Thy-1 resides in DRMs. This is less than would have been predicted from the gradient immunoblot in figure 4.1A but the rest of the Thy-1 could plausibly be spread out over the gradient or trapped in the insoluble pellet. It is interesting that quantification of DRM partitioning reveals that only 50 % of

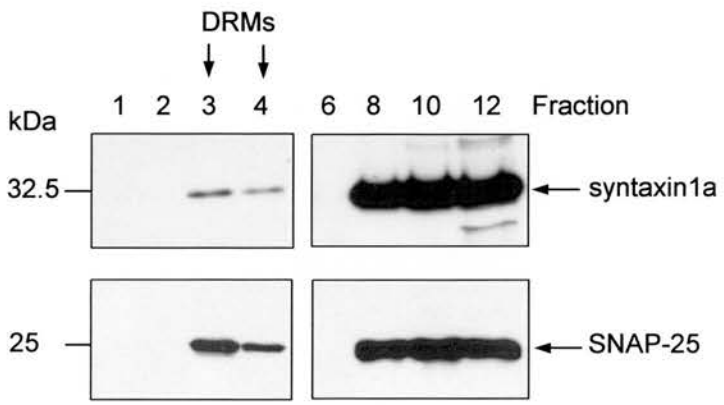


**Figure 4.10 SNAP-25 and syntaxin1a associate with PC12 cell DRMs**

DRMs were isolated by TX-100 extraction at a detergent to protein ratio of 5:1, followed by flotation on a sucrose density gradient (as described in Chapter 2, section 2.3.1.2). The DRMs were contained in fractions 3 and 4. 25 µl each fraction was separated by SDS-PAGE and immunoblotted using anti-syntaxin1a (HPC-1) or anti-SNAP-25 (SMI81) antibodies.

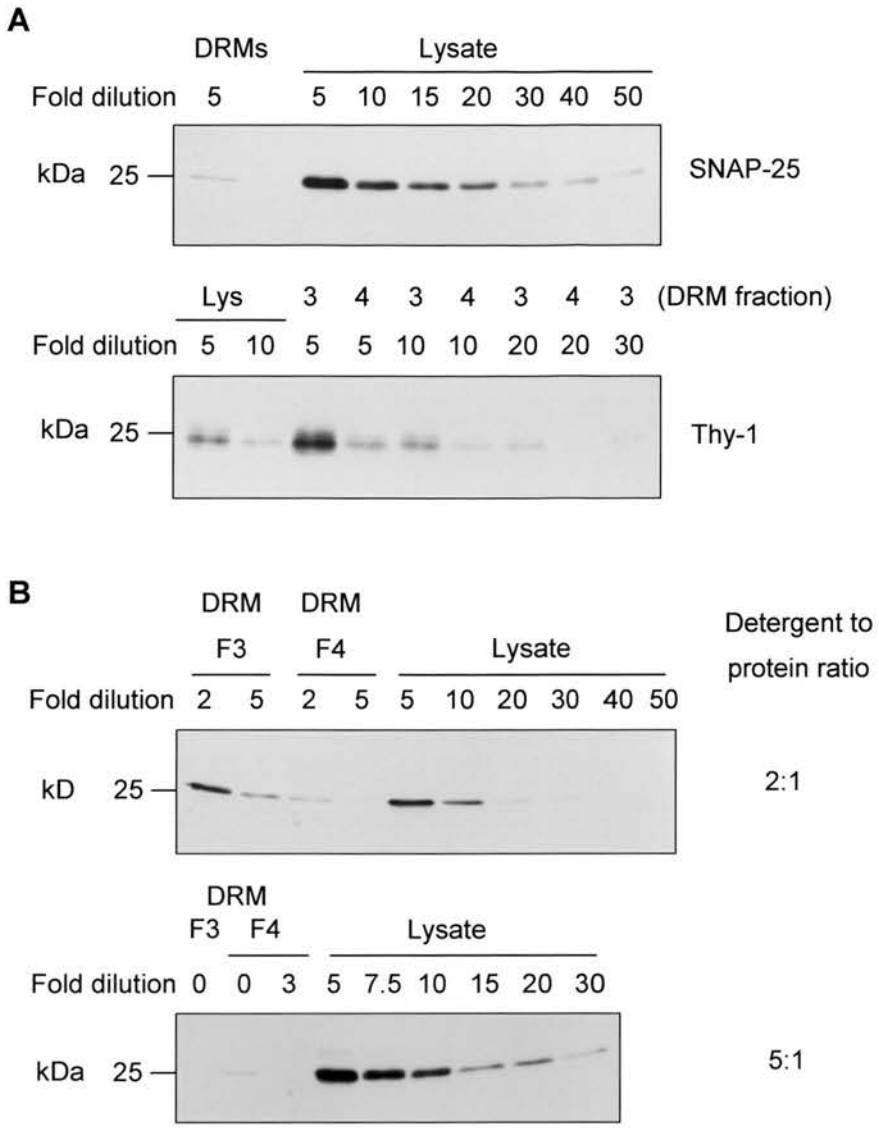


**Figure 4.11 Less SNAP-25 than Thy-1 localises to DRMs but SNAP-25 localisation is sensitive to the detergent to protein ratio**

**A** DRMs were isolated from PC12 cells by TX-100 extraction, at a detergent to protein ratio of 5:1. The cell lysate and DRM fractions were diluted between 5 and 50-fold and 20 µl of each dilution was separated by SDS-PAGE (fold dilution is indicated above each lane) and immunoblotted using anti-SNAP-25 (SMI81) or anti-Thy-1 (OX7) antibodies. **B** DRMs were isolated by TX-100 extraction at a detergent to protein ratio of 2:1 or 5:1. Dilutions of the cell lysate and DRM fractions were again separated by SDS-PAGE and immunoblotted for SNAP-25.

Thy-1 resides in DRMs, in agreement with the observed partial colocalisation of Thy-1 with CTXB (figure 4.9).

Less than 2 % of SNAP-25 associating with DRMs is very different from the 24 % association calculated by Chamberlain and co-workers. It seems that slight differences in the DRM isolation protocol may significantly alter protein localisation in the gradient. For example, changing the detergent to protein ratio employed for TX-100 extraction had a marked effect on SNAP-25 association with DRMs. DRMs were prepared from PC12 cells at a detergent to protein ratio of 5:1 (as used for figure 4.11A) or a ratio of 2:1. Serial dilutions of lysate and DRM fractions were again compared by immunoblotting to estimate the relative partitioning of SNAP-25 into DRMs. It is immediately clear from figure 4.11B that a greater proportion of SNAP-25 associates with DRMs at a ratio of 2:1 than at a ratio of 5:1. At a 2:1 detergent to protein ratio a two-fold dilution of DRM fraction 3 contains a similar amount of SNAP-25 as a five-fold dilution of lysate, which corresponds to ~ 10 % of the total SNAP-25 residing in the DRMs. Thus altering the detergent to protein ratio increased SNAP-25 association with DRMs greater than five-fold (from < 2 % to ~10 %). Altered protein localisation in response to changing the detergent to protein ratio has been observed by others (Chamberlain and Gould, 2002; Ostermeyer et al., 1999). Unfortunately there is no reliable method for determining which detergent to protein ratio fully solubilises the bulk plasma membrane, whilst leaving lipid rafts intact.

In light of these results, percentage partitioning of a protein into DRMs should not be taken as an indication of the absolute amount of protein residing in $L_o$ domains or lipid rafts in intact cells. However, when comparing the effect of two treatments or conditions on DRM localisation of a particular protein, this sort of quantitation might be useful. The results should be valid if the detergent to protein ratio is kept constant. Analysis of colocalisation with CTXB in intact cells provides an alternative method, devoid of such artefacts, for estimating relative partitioning into $L_o$ domains.

### 4.3.2. SNAP-25 and syntaxin1a localise predominantly to the plasma membrane in PC12 cells

SNAP-25 and syntaxin1a are expected to localise predominantly to the plasma membrane, this subcellular localisation was confirmed by immunostaining PC12 cells. Sequential horizontal sections through PC12 cells stained for SNAP-25 and syntaxin1a are shown in figures 4.12 and 4.13 respectively. The mainly plasma membrane localisation of both proteins is evident. Observing the base of each cell we can see that both proteins show a punctate distribution on the plasma membrane, in agreement with previous reports (Aoyagi et al., 2005; Lang et al., 2001; Ohara-Imaizumi et al., 2004; Rickman et al., 2004; Sieber et al., 2006).

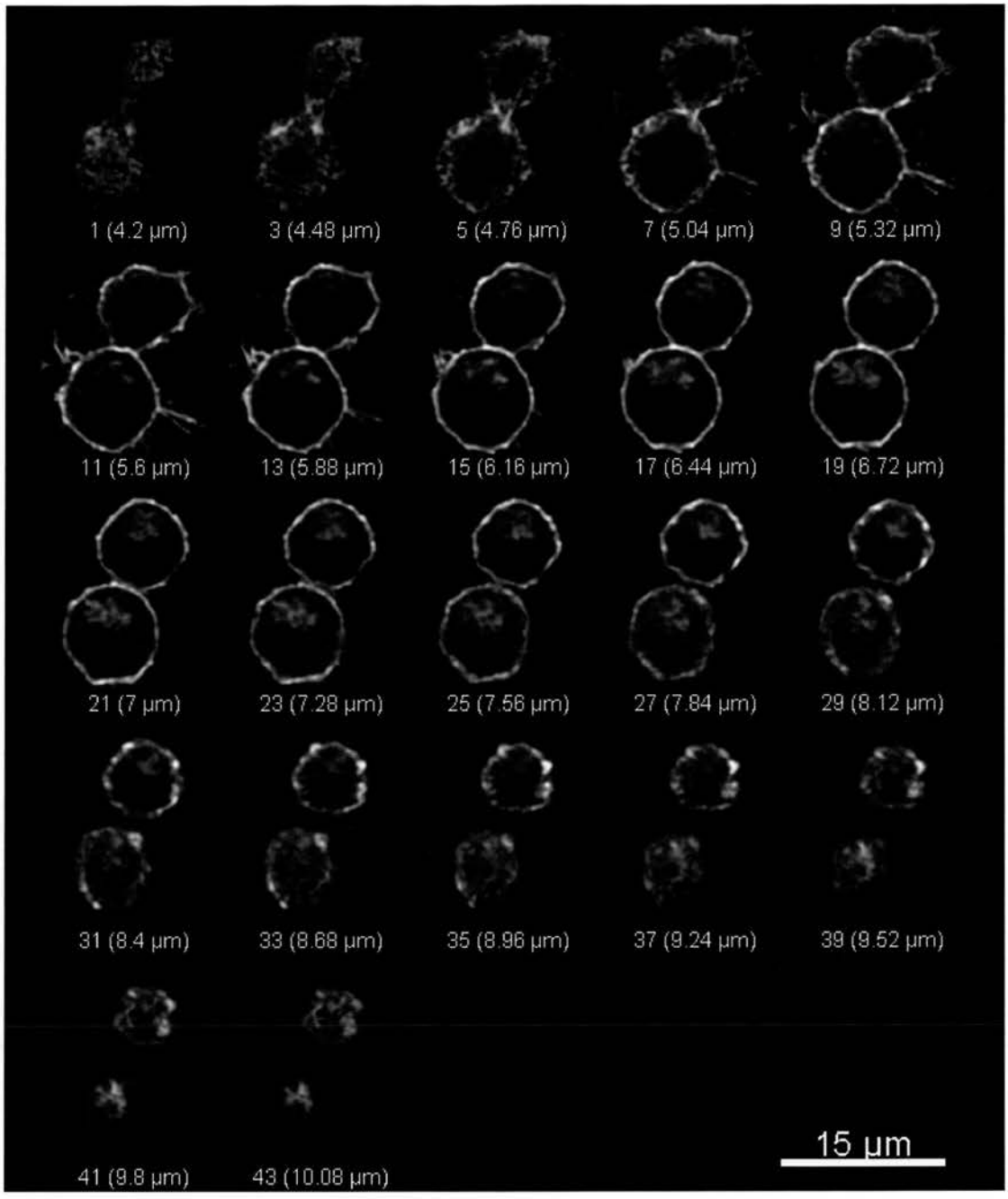


**Figure 4.12 Horizontal sections through PC12 cells immunostained for SNAP-25**

PC12 cells were fixed on ice with 4 % (w/v) PFA, immunostained using anti-SNAP-25 (SMI81) antibody and imaged by CLSM, taking horizontal slices through the cells. An image was acquired every 140 nm, every second slice is displayed. Section numbers and distance through the image stack are shown below each image.

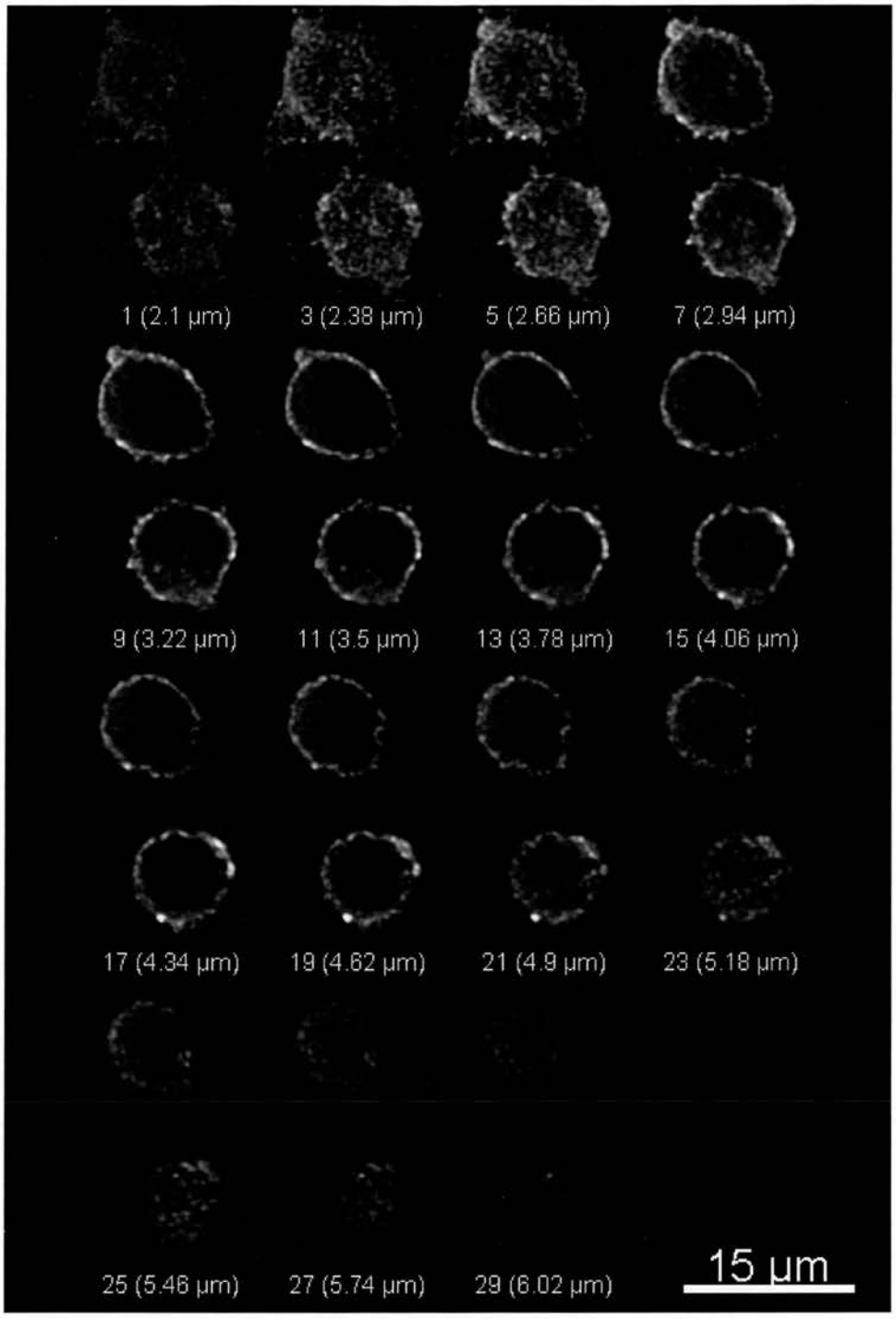


**Figure 4.13 Horizontal sections through PC12 cells immunostained for syntaxin1a**

PC12 cells were fixed on ice with 4 % (w/v) PFA, immunostained using anti-syntaxin1a (HPC-1) antibody and imaged by CLSM, taking horizontal slices through the cells. An image was acquired every 140 nm, every second slice is displayed. Section numbers and distance through the image stack are shown below each image.

### 4.3.3. SNAP-25 colocalises with CTXB to a greater extent than syntaxin1a

PC12 cells were again labelled with FITC-CTXB, then fixed and immunostained for SNAP-25 or syntaxin1a. Figure 4.14A shows regions from the base of two representative cells. Close inspection of the merged images suggests that some CTXB puncta overlap with some SNAP-25 and syntaxin1a puncta. However, much of the SNARE (red) and CTXB (green) signal appears separate in both cases and quantification was necessary to assess the degree of overlap. Costes automatic thresholding (see Chapter 2, section 2.4.6.2) was employed to create the colocalisation masks presented in figure 4.14B. Similar colocalisation masks were generated for at least fourteen separate images to permit calculation of the mean percentage colocalisation that is presented in figure 4.14C. In the SNAP-25 images, the colocalisation mask contained on average 57 ± 4 % (SEM) of the SNAP-25 signal and 58 ± 4 % of the CTXB image. In contrast, in Syntaxin1a images a mean of only 35 ± 3 % of syntaxin1a signal contributed to the colocalisation mask and 36 ± 3 % of CTXB signal. The difference between SNAP-25 and syntaxin1a colocalisation with CTXB was found to be significant (Mann Whitney U test, $p < 0.005$). However, the SNAP-25 colocalisation mask in figure 4.14B registers more of the signal as colocalised than would be estimated by eye. Therefore intensity dependent correlation between the two channels was also calculated as an alternative measure of coincidence.

The scatter plots at the righthand side of figure 4.14A show the red signal intensity plotted against the green signal intensity for each voxel in the example images. In the syntaxin1a image scatter plot the points are spread out towards the two axes suggesting a low level of covariance between syntaxin1a and CTXB staining. The SNAP-25 scatter plot shows a tighter distribution of points indicating a higher level of intensity dependent correlation between red and green signals in this image. This observation is reflected in the results of correlation analysis. Whilst the mean correlation ($R^2$ x 100%) for syntaxin1a and CTXB was only 12 ± 2 % (SEM), the mean correlation between SNAP-25 and CTXB was 23 ± 5 % (as illustrated in figure 4.14D). These correlation values were significantly different (Mann Whitney U test, $p = 0.005$).

**Figure 4.14 SNAP-25 and syntaxin1a colocalise with CTXB to different extents on the plasma membrane of PC12 cells**

PC12 cells were incubated with FITC-CTXB, fixed and immunostained for SNAP-25 or syntaxin1a. CTXB (green) and SNAP-25 or syntaxin1a (red) were visualised by CLSM. **A** Images from the base of representative cells. Scale bars = 1 μm. The scatter plots show the red intensity plotted against the green intensity for each voxel in the image. **B** Colocalisation masks for the merged images in A, generated by automatic thresholding (described in Chapter 2, section 2.4.6.2). **C** The mean percentage colocalisation of CTXB with SNAP-25 or syntaxin1a (colocalisation of the green channel with the red channel) and mean percentage colocalisation of SNAP-25 or syntaxin1a with CTXB (colocalisation of the red channel with the green channel). **D** Mean correlation ($R^2$ x 100) of the green channel (CTXB) with the red channel (SNAP-25 or syntaxin1a). All error bars represent SEM, n = 14. ** Significantly different from SNAP-25 values (Mann Whitney U test, $p < 0.005$).

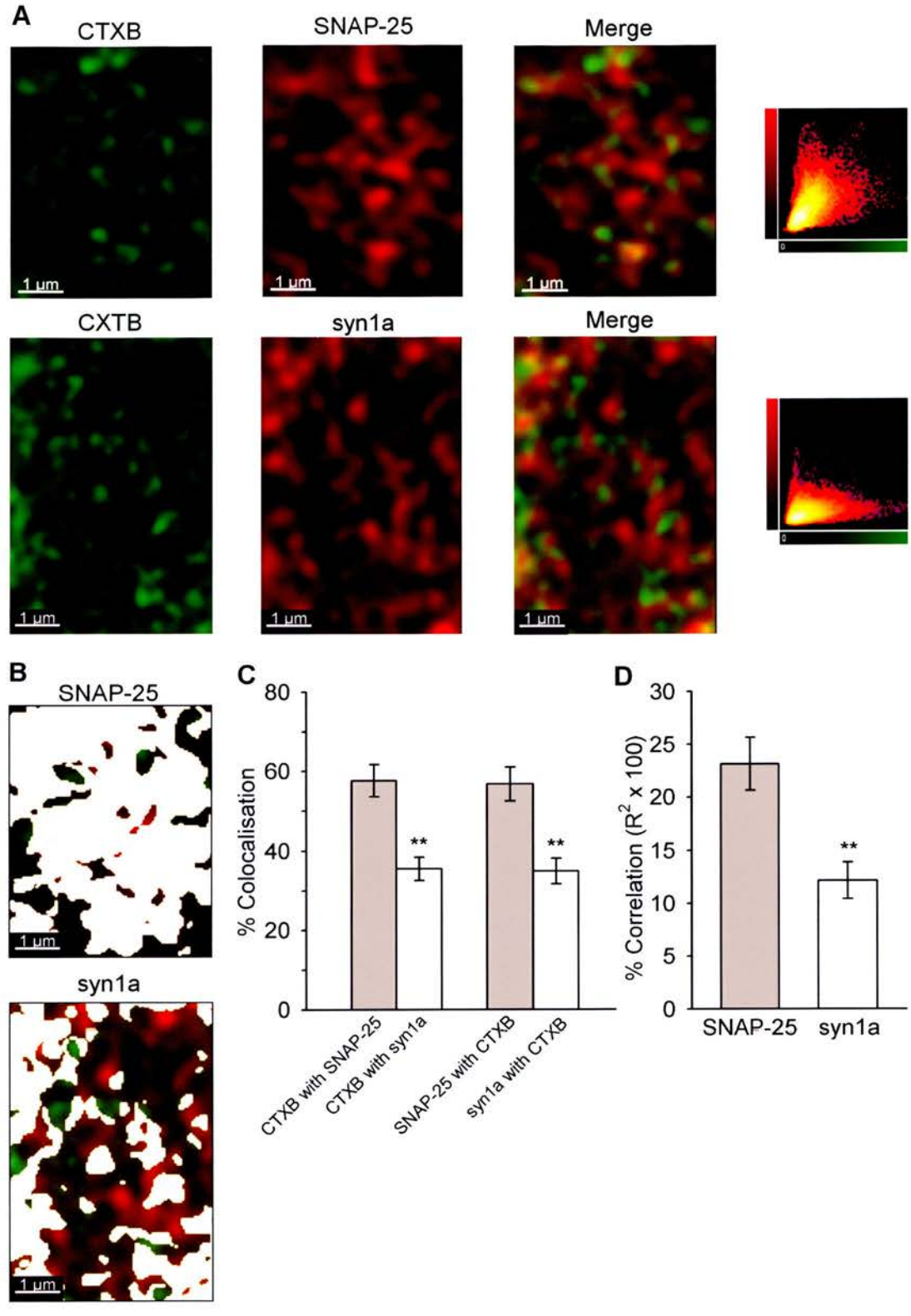


**Figure 4.14 SNAP-25 and syntaxin1a colocalise with CTXB to different extents of the plasma membrane of PC12 cells**

To determine whether the correlation observed in the images could be due to random variation, randomisation tests were performed as in section 4.2.2. Table 4.2 compares the observed correlation with the mean random correlation value calculated by Costes' randomisation algorithm and the correlation values produced by flipping the red channel image through 180°. Each value represents the mean of at least fourteen images.

**Table 4.2 Random correlation tests – SNAP-25 and syntaxin1a**

| Red Channel | Mean $R^2$ x 100% | SEM | Paired T-test versus original |
|---|---|---|---|
| SNAP-25 original | 23.2 | 2.5 | - |
| SNAP-25 randomised | 8.0 | 1.5 | $p < 0.001$ |
| SNAP-25 flipped 180° in x | 5.0 | 1.1 | $p < 0.001$ |
| SNAP-25 flipped180° in y | 4.6 | 1.8 | $p < 0.001$ |
| syntaxin1a original | 11.5 | 1.7 | - |
| syntaxin1a randomised | 10.8 | 1.7 | $p = 0.727$ |
| syntaxin1a flipped 180° in x | 4.0 | 1.3 | $p = 0.005$ |
| syntaxin1a flipped 180° in y | 2.2 | 0.7 | $p < 0.001$ |

These randomisation tests confirm that the correlation observed between SNAP-25 and CTXB is not due to random variation, as demonstrated by the results of paired T-tests presented in table 4.2. However, the two randomisation procedures do not agree about the significance of the observed correlation between syntaxin1a and CTXB staining. The syntaxin1a images randomised by Costes' algorithm and the original syntaxin1a images show a similar level of correlation with the original CTXB image (paired T-test, $p = 0.727$). Flipping the syntaxin1a images produces lower values of random correlation that are significantly different from the observed correlation. Channel flipping may produce unrealistically low $R^2$ values if staining is unevenly distributed over the whole image; Costes' randomisation algorithm overcomes this problem by cutting the image into tiles and sampling fifty different configurations. Thus, the correlation observed between syntaxin1a and CTXB is probably due to random variation rather than any dependent localisation of the two proteins.

## 4.4. Summary and discussion

The primary aim of this chapter was to further investigate the potential interaction of 14-3-3 with lipid raft-like membrane microdomains, suggested by the DRM studies in Chapter 3. These microdomains were defined in intact cells by the GM1 ligand CTXB; immunostaining permitted visualisation of DRM associating proteins, including 14-3-3. Thy-1, SNAP-25 and syntaxin1a were included as controls to confirm that other established DRM residents colocalise with CTXB.

Initial characterisation of CTXB staining demonstrated a punctate distribution on the plasma membrane. Could each spot be due to light emitted from a single FITC-CTXB molecule or do the spots represent clustering of CTXB? When deconvolved images of 200 nm fluorescent beads were analysed, the FWHM of a single bead was found to be ~ 280 nm. However, the mean FWHM for CTXB puncta was 635 ± 21 nm (see figure 4.4), indicating that each punctum does not originate from a single, sub-resolution point source. CTXB clustering could represent binding of many CTXB molecules to rafts of hundreds of nanometres in size. In the alternative view of nanometre scale rafts, it has been suggested that crosslinking of rafts could lead to their stabilisation and recruitment of other mobile rafts (Hancock, 2006; Kusumi et al., 2004; Subczynski and Kusumi, 2003). Thus pentameric CTXB could cluster small rafts and recruit other CXTB-labelled rafts to the cluster. Clustering of CTXB, and indeed Thy-1, SNAP-25 and syntaxin1a, could also be due to alternative modes of membrane compartmentalisation, including protein-protein interactions (as discussed in Chapter 1, Section 1.1.3.4).

Both CTXB and Thy-1 appeared to be present exclusively in DRMs (see figure 4.1), as previously reported. If the CTXB and Thy-1 clusters indeed correspond to the $L_o$ domains from which DRMs are believed to originate, then complete overlap of these clusters would be expected. In fact only ~ 60 % colocalisation was observed between CTXB and Thy-1 and only 25 % correlation between the distributions of the two markers. Quantification of the amount of Thy-1 in DRMs suggested that only about half the total Thy-1 was present in DRMs (as discussed in section 4.3.1 and see figure 4.11A), which agrees with the observed partial colocalisation of Thy-1 with CTXB. However, whilst comparing the degree of association of Thy-1 and SNAP-25 with

DRMs it became clear that the level of association can be dramatically altered by small changes in the DRM isolation protocol, such as changing the detergent to protein ratio. Reducing the detergent to protein ratio from 5:1 to 2:1 increased the association of SNAP-25 with DRMs > 5-fold (as demonstrated in figure 4.11B). Therefore DRMs should not be used to estimate the absolute amount of a protein present in lipid raft-like domains. It is still reasonable though to quantitatively compare the effect of two treatments on DRM association of a particular protein, as long as the detergent to protein ratio is carefully controlled.

Imaging provides an alternative method for exploring the relative association of different proteins with membrane microdomains. Before discussing the imaging results from this chapter it would be productive to consider what values of partial colocalisation or correlation actually mean for the biological system. If a voxel contributes to colocalisation or overlap then its red and green channel intensities are both above the respective thresholds. However, it is not possible to separate objects that are less than 200 nm away from each other by light microscopy and in practice the resolution obtained is usually less. During the process of image acquisition by the microscope some information pertaining to the object is lost and noise is added so the image of an object is distorted or blurred. Image data deconvolution, employed throughout this project, uses an iterative algorithm to partially restore the true shape of the object, much improving on the resolution achieved from raw confocal microscope images. However, the emission from a single fluorophore will still be spread over a number of 50 x 50 x 140 nm voxels and in addition, each voxel may contain signal originating from a number of fluorophores. Therefore, if a voxel registers as colocalised it really means that the concentration of red and green fluorophores in and around that voxel is high enough for the intensities to exceed the threshold. However, high red intensity/moderate green intensity and high red intensity/high green intensity voxels contribute equally to colocalisation even though the density of green fluorophores is different in each case.

Whilst percentage colocalisation (based on Manders coefficients) provides a simple measure of red and green signal overlap and can easily be visualised, intensity dependent correlation analysis may be more informative. Pearson's coefficient, R (from which the percentage correlation, $R^2$ x 100, was calculated) describes the degree of correlation between two variables. In the case of perfect correlation, variation in red intensity

depends linearly on variation in green intensity and perfect overlap would be observed. Values of correlation < 100 % but greater than random correlation show that variation in red intensity partially depends on variation in green intensity. This suggests that the localisation of a proportion of red fluorophores depends on the localisation green fluorophores. Whilst this value is not very meaningful for a single image, it is very useful for comparing the degree to which the localisation of two flurophores depends on each other in two conditions or two sets of images.

Table 4.3 and figure 4.15 compare the coincidence of Thy-1, 14-3-3, SNAP-25 and syntaxin1a with lipid raft marker CTXB, as revealed by immunostaining experiments in this chapter. Table 4.3 shows that results from the colocalisation and correlation analyses are in good agreement with respect to the relative localisation of each protein with CTXB. In addition, for all four proteins, the percentage colocalisation of CTXB with the immunostained protein of interest is very similar to the value for colocalisation of the protein of interest with CTXB. This may be because all the proteins, including CTXB, present a similar punctate appearance. If the staining distribution was very different between the red and green channels then a large difference in the percentage colocalisation of each channel with the other would be more likely; for example, if one channel was punctate and the other showed a diffuse distribution.

For simplicity I will concentrate on the results of the correlation analysis in this discussion, these results are illustrated by figure 4.15. The same level of correlation was observed between CTXB and Thy-1 and CTXB and SNAP-25. The correlation of 14-3-3 with CTXB was significantly lower than the correlation of Thy-1 or SNAP-25 with CTXB (Student's T-test, $p < 0.01$), as was correlation of syntaxin1a with CTXB (Student's T-test, $p < 0.05$). These results agree broadly with DRM preparations where 14-3-3 protein (see Chapter 3) and Syntaxin1a (see figure 4.10) localise predominantly to the detergent soluble fractions and only a small proportion partitions into DRMs. Thy-1 though, was found to be highly concentrated in DRMs (see figure 4.1 and 4.11), whilst SNAP-25 appeared much less so (see figure 4.10 and 4.11). However, considering the difficulties concerned with quantification from DRMs discussed above, the discrepancy between the imaging results and DRMs is not very surprising. It is very interesting in fact that SNAP-25, which is anchored to the cytoplasmic leaflet of the plasma

**Table 4.3 Summary of coincidence of DRM proteins with CTXB**

| Red channel | % colocalisation of CTXB with red channel | % colocalisation of red channel with CTXB | % channel correlation ($R^2$ x 100) | Paired t-test $R^2$ x 100 (random) vs $R^2$ x 100 (original) |
|---|---|---|---|---|
| Thy-1 | 60 | 64 | 25.5 | $p < 0.001$ |
| SNAP-25 | 57 | 58 | 23.2 | $p < 0.001$ |
| 14-3-3 | 34 | 33 | 13.3 | $p = 0.004$ |
| syntaxin1a | 35 | 36 | 11.5 | $p = 0.727$ |

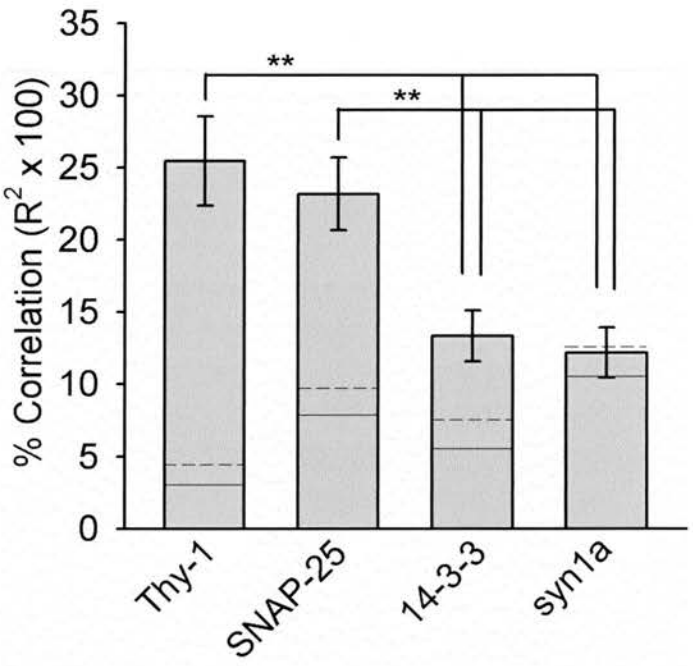


**Figure 4.15 Summary of correlation observed between CTXB and four DRM-associated proteins**

Summary of data presented in figures 4.9D and 4.14D. The bars represent the mean percentage correlation with CTXB for Thy-1, 14-3-3, SNAP-25 and syntaxin1a, ± SEM, shown by the error bars. The solid line on each bar represents the mean random correlation calculated for that set of images using Costes' randomisation test, the dashed line represents the SEM. ** The percentage correlation of 14-3-3 and syntaxin1a with CTXB was significantly lower than the correlation of Thy-1 or SNAP-25 with CTXB (Student's t-test, $p < 0.05$, $n = 12$).

membrane, showed the same level of CTXB dependent localisation as Thy-1, which is GPI-anchored in the external leaflet.

The correlation observed between 14-3-3 and CTXB (13.3 %) was not significantly greater than the correlation between syntaxin1a and CTXB (11.5 %). However, Costes' randomisation test suggested that the correlation between syntaxin1a and CTXB was below random levels, whilst 14-3-3/CTXB correlation was not (see table 4.3). The mean random correlation was calculated by randomising the red channel (see Chapter 2, section 2.4.6.2) in each separate set of images and calculating $R^2$ x 100 with respect to the original green (CTXB) channel, this value is shown as a solid line across each bar in figure 4.15. It is evident from this figure that each set of images produced a different random correlation value, that of syntaxin1a images being the highest. This difference probably arises from slight differences in the staining pattern for each protein. It seems sensible to compare observed correlation values with random values generated from the same set of images; then random distributions of that particular immunostaining pattern are being used. Flipping the red channel image through 180°, instead of randomising it as tiles (Costes' method), produced slightly lower values of $R^2$ x 100 (see table 4.2). Random correlation values calculated by Costes' randomisation test might then represent a more stringent test of whether the observed correlation could be due to random variation.

If we accept the results of the Costes' randomisation test then it would appear that syntaxin1a localisation is independent of CTXB. The observed overlap must arise from the relatively high concentrations of both proteins in the plasma membrane.
This is clearly at odds with recovery of syntaxin1a in DRMs (figure 4.10). Perhaps syntaxin1a only associates with DRMs during the extraction procedure or DRMs may not represent intact membrane microdomains as some researchers suggest. The colocalisation of syntaxin1a or SNAP-25 with CTXB has not previously been investigated in any cell type. However, syntaxin1a failed to colocalise with two other lipid raft markers; Thy-1 in PC12 membrane sheets (Lang et al., 2001) and flotillin-1 in MIN6β cells (Ohara-Imaizumi et al., 2004). In contrast, Chintagari and co-workers reported colocalisation of the related SNARE syntaxin4 and SNAP-23 with raft marker CD44 (a GPI-anchored protein) in alveolar epthithelial cells (Chintagari et al., 2006).

There are conflicting reports concerning the colocalisation of Thy-1 with CTXB-crosslinked GM1. In Jurkat T-cells co-patching of Thy-1 and GM1, with antibody and CTXB respectively, caused colocalisation of the two raft markers (Harder et al., 1998). In addition, both Thy-1 and CTXB colocalised with another raft marker, flotillin-1, in PC12 cells (Stuermer et al., 2001). On the other hand, patching of GM1 by addition of CTXB, followed by anti-CTXB antibody and secondary antibody, did not cause co-redistribution of Thy-1 in a lymphocyte cell line (Fra et al., 1994). Furthermore, in RBL-2H3 mast cells, immunogold electron microscopy detected separate clusters of Thy-1 and CTXB, whose distribution was independent of each other (Wilson et al., 2004). Herreros and co-workers also failed to detect significant FRET between CTXB and Thy-1 in fixed PC12 cells (Herreros et al., 2001). This last result does not necessarily preclude co-clustering of Thy-1 and CTXB; fluorophores must be < 10 nm apart for FRET to occur so clusters may still contain both molecules but at a density too low for FRET.

Most of the immunostaining studies discussed above did not attempt to quantify the degree of colocalisation. However, it is clear that a range of results have been obtained regarding CTXB colocalisation with Thy-1. These results contrast with each other and the detection of partially dependent localisation of Thy-1 and CTXB in this chapter. Kusumi and Suzuki postulate that discrepancies between immunostaining studies arise due to the dynamic nature of lipid rafts (Kusumi and Suzuki, 2005). According to their theory, nanometre scale steady-state lipid rafts are constantly clustering and dispersing and protein molecules are moving in and out of these rafts. Single molecule tracking studies have monitored the transient confinement of Thy-1 and GM1 to 200 – 300 nm domains, suggesting that these molecules indeed show a dynamic partitioning into plasma membrane microdomains (Dietrich et al., 2002; Sheets et al., 1997). The correlation of ~ 25 % observed between CTXB and Thy-1 or SNAP might then represent an increased residence time in $L_o$ domains compared with 14-3-3, which shows only 13 % correlation with CTXB localisation. In other words, the different levels of correlation may reflect the different affinity of each protein for $L_o$ domains.

In summary, Thy-1 and SNAP-25 showed ~ 60 % colocalisation with CTXB and correlation analysis suggested that their localisation was partially dependent on CTXB localisation. 14-3-3 and syntaxin1a exhibited lower levels of correlation with CTXB, in

line with their low level of partitioning into DRMs. According to Costes' randomisation test the correlation observed between syntaxin1a and CTXB may be due to random variation rather than dependent localisation. However, the same test suggested that a very small proportion of membrane associated 14-3-3 is linked to localisation of lipid raft marker CTXB.

# Chapter 5: Cholesterol depletion studies

# 5. Cholesterol depletion studies

The microscopy studies detailed in Chapter 4 indicated that a small proportion of 14-3-3 colocalises with CTXB-labelled clusters, suggested to represent $L_o$ domains. The established lipid raft marker Thy-1 and the DRM-associating protein SNAP-25 also showed coincidence with the $L_o$ domain marker CTXB. However, quantitative analysis of coincidence demonstrated that none of these proteins showed complete overlap with CTXB. This chapter aims to confirm whether or not the observed partial overlap represents association with cholesterol dependent microdomains. Depletion of cholesterol from the plasma membrane by MβCD treatment is widely used to verify that DRM association of a protein relies on cholesterol (Foster et al., 2003; Ilangumaran and Hoessli, 1998; Remacle-Bonnet et al., 2005; Taverna et al., 2004; Vial and Evans, 2005; Xia et al., 2004) and has also been employed in lipid raft imaging studies (Ayllon et al., 2002; Bruses et al., 2001; Goodwin et al., 2005; Launikonis and Stephenson, 2001; Ohara-Imaizumi et al., 2004). This technique was chosen to investigate the cholesterol dependence of the association of 14-3-3, Thy-1 and SNAREs with CTXB-labelled domains.

Some researchers in the lipid raft field propose that DRMs may not correspond to $L_o$ domains present in intact cells and may instead be an artefact of the detergent extraction procedure (Edidin, 2003; Heerklotz, 2002; Munro, 2003). Studies that purport to investigate lipid rafts often rely solely on DRM isolations and few compare DRM and microscopy results. I decided to make a thorough comparison of how cholesterol depletion affects localisation to putative $L_o$ domains in intact cell membranes with its effects on DRM association, for the four proteins studied in Chapter 4.

In this chapter both the DRM isolations and microscopy experiments were carried out in PC12 cells but also extended to N2a cells to examine whether the proteins of interest show similar behaviour in the two cell types. The relatively high level of SNAP-25 coincidence with CTXB-labelled domains in PC12 cells, compared to the

established raft marker Thy-1, is interesting and warranted further investigation. The apparent lack of syntaxin1a coincidence with CTXB, discussed in Chapter 4, was also further explored in N2a cells.

## 5.1. Effect of cholesterol depletion on cellular cholesterol content and cell viability

As cholesterol depletion by MβCD perturbs the cell membrane it may affect cell viability. Cell culture studies investigating lipid rafts generally use MβCD at between 2 – 20 mM (Abrami et al., 2003; Foster et al., 2003; Kabouridis et al., 2000; Lang et al., 2001; Tansey et al., 2000; Taverna et al., 2004). The maximum concentration that could be used without detrimental effects on viability was determined in PC12 and N2a cells prior to extensive use of this technique, by the cell viability assay described in Chapter 2, section 2.4.3. Figure 5.1 compares the viability of PC12 cells that were either untreated or incubated with 20 mM or 25 mM MβCD for 30 minutes. It is immediately evident from inspection of figure 5.1A that many more dead cells (red) are visible following 25 mM MβCD treatment than in the control or 20 mM treated samples. Twenty five millimolar MβCD significantly decreased the percentage of live cells in a field of view from 98 ± 1 % (SEM) to 84 ± 2 % (Student's T-test, $p < 0.001$, $n = 9$), whereas the percentage of viable cells was unchanged by 20 mM MβCD compared with the untreated control.

The morphology of N2a cells appeared to change following application of 20 mM MβCD and the cell viability test confirmed that significantly more dead cells were present in a field of view after 30 minutes incubation with 20 mM MβCD than in the untreated control sample (Student's T-test, $p < 0.001$, $n = 6$), as shown by figures 5.2 A and B. The much lower concentration of 10 mM MβCD was therefore chosen and found not to reduce cell viability significantly, as illustrated by figure 5.2. Thus the maximum concentrations of MβCD that could be employed with PC12 cells and N2a cells were determined to be 20 mM and 10 mM respectively.

**Figure 5.1. 20 mM MβCD treatment of PC12 cells reduces filipin staining but does not alter cell viability**

PC12 cells were incubated in the presence of 20 or 25 mM MβCD or an equal volume of PBS (untreated) for 30 minutes at 37 °C. **A** Cell viability assay was performed as described in Chapter 2, section 2.4.3. Calcein stains live cells green (top row images) and propidium iodide stains the nuclei of dead cells red (bottom row images.) Scale bars = 100 μm. **B** Live (green) and dead (red) cells in a field of view were counted and the percentage of total cells that were viable was calculated. Mean results are presented ± SEM, *** $p < 0.001$, Student's T-test ($n = 9$). **C** Cells were fixed, incubated with 0.05 mg/ml filipin to stain cholesterol and visualised by CLSM. Scale bars = 20 μm.

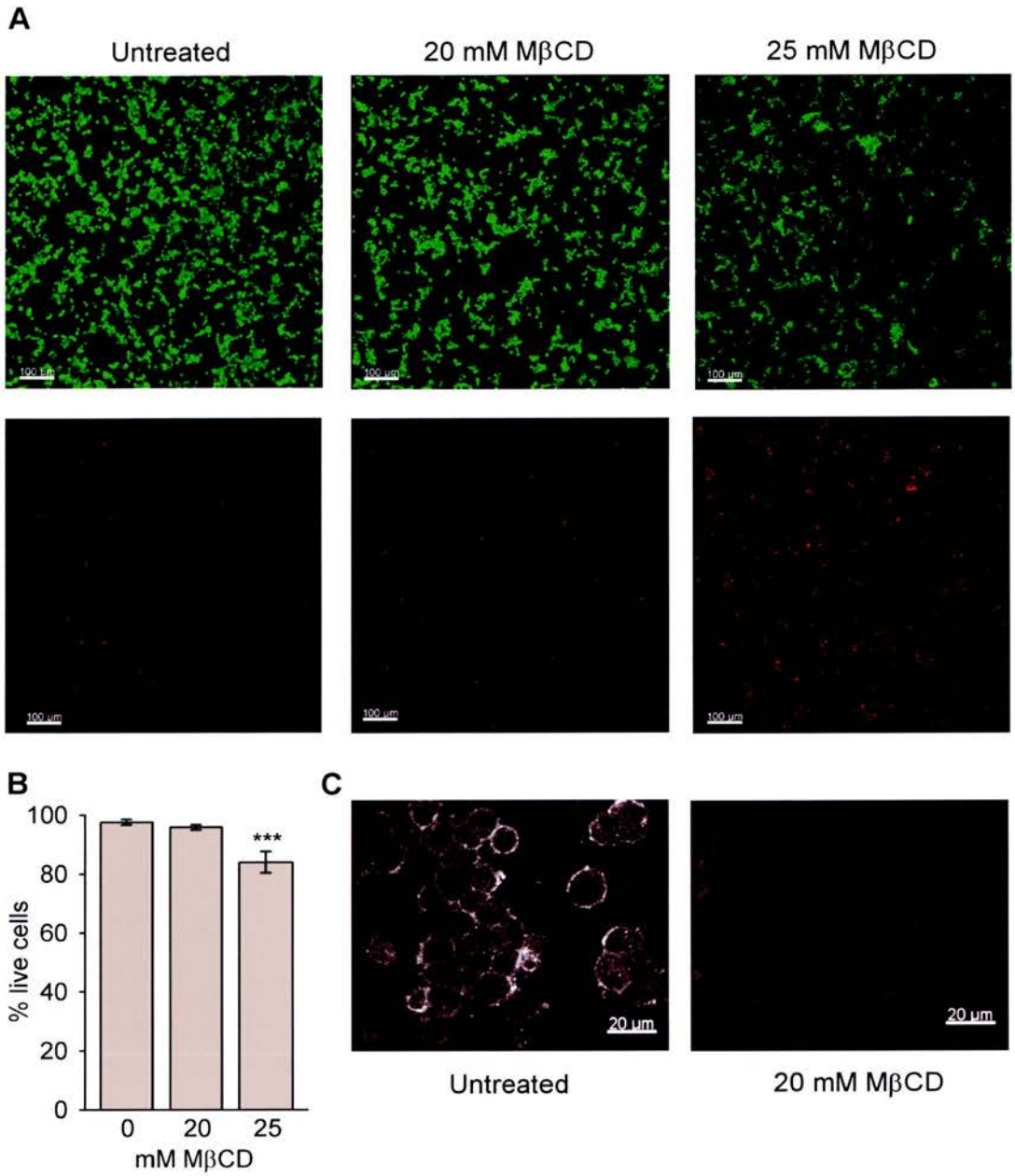


**Figure 5.1. 20 mM MβCD treatment of PC12 cells reduces filipin staining but does not alter cell viability**

**Figure 5.2. 10 mM MβCD treatment of N2a cells depletes cholesterol but does not decrease cell viability**

N2a cells were incubated in the presence of 10 or 20 mM MβCD or an equal volume of PBS (untreated) for 30 minutes at 37 °C. **A** Cell viability assay was performed as described in Chapter 2, section 2.4.3. Calcein stains live cells green (top row images) and propidium iodide stains the nuclei of dead cells red (bottom row images.) Scale bars = 100 μm. **B** Live (green) and dead (red) cells in a field of view were counted and the percentage of total cells that were viable was calculated. Mean results are presented ± SEM, *** $p < 0.001$, Student's T-test ($n = 12$). **C** Cells were fixed, incubated with 0.05 mg/ml filipin to stain cholesterol and visualised by CLSM. Scale bars = 20 μm.

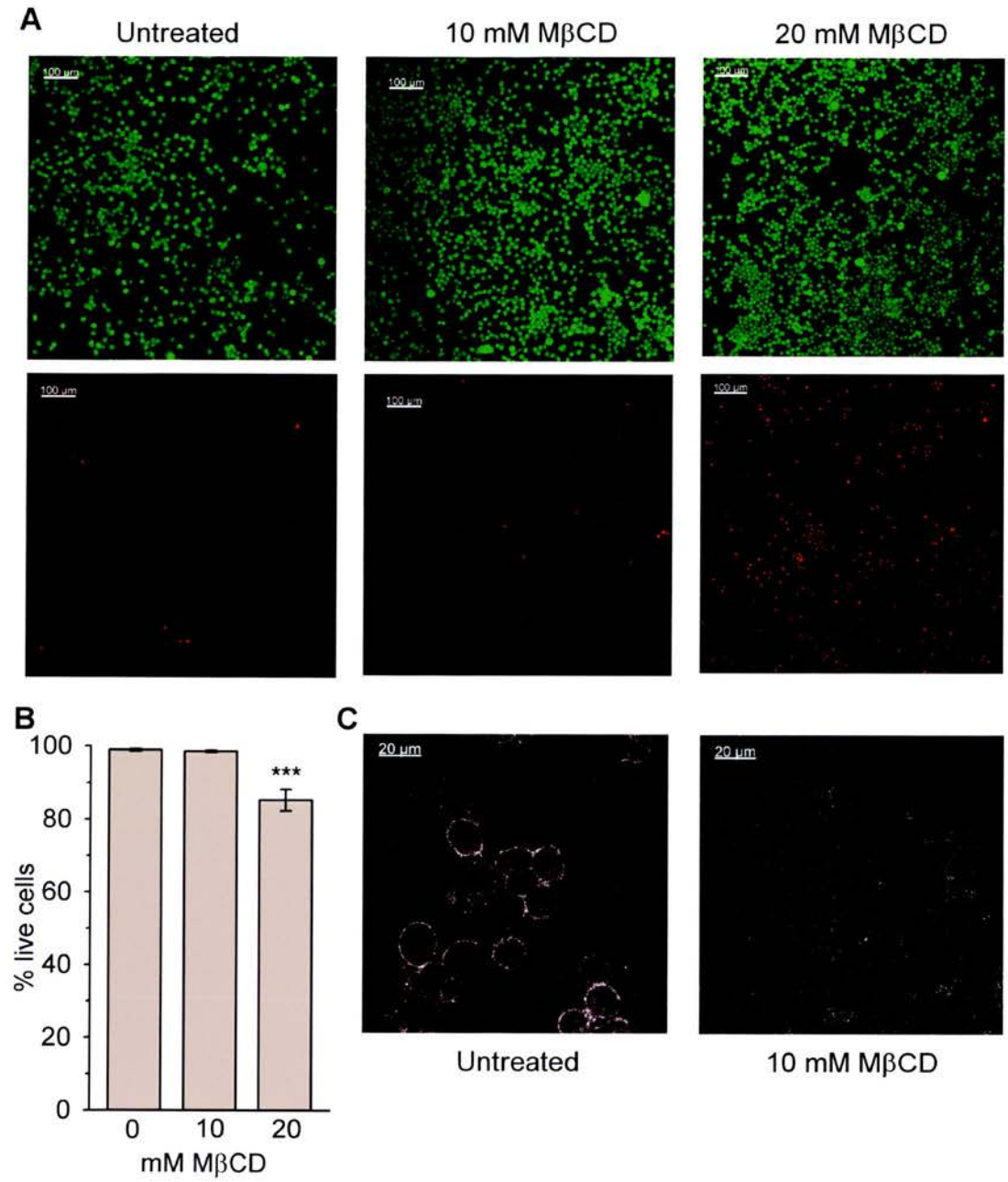


**Figure 5.2. 10 mM MβCD treatment of N2a cells reduces filipin staining but does not alter cell viability**

To confirm that these concentrations of MβCD actually depleted cholesterol from the cell membrane the cholesterol binding agent filipin was employed. Filipin is a fluorescent polyene antibiotic that can conveniently be used to label cellular cholesterol (Blanchette-Mackie et al., 1988; Keller and Simons, 1998; Leventhal et al., 2001; Neufeld et al., 1999). However, filipin staining must be carried out in fixed rather than live cells as it disrupts the cell membrane of live cells. PC12 cells were incubated in the presence or absence of 20 mM MβCD and stained with filipin. From figure 5.1C the intensity of filipin staining appears to be decreased by MβCD treatment. To quantify filipin staining, the mean signal intensity in a field of view was calculated (see Chapter 2, section 2.4.4). All images were acquired with same microscope detector settings and laser power to allow comparison between images collected on the same day. MβCD produced a mean decrease in staining intensity of 31 ± 3 % (SEM) and the mean intensity of MβCD treated images was significantly less than that of untreated images in three separate experiments (Student's T-test, $p < 0.001$, $n = 12$).

In N2a cells a large decrease in filipin staining intensity is also apparent in response to 10 mM MβCD (figure 5.2C). The MβCD treated image (right panel) shows the high background noise associated with filipin staining but the clear plasma membrane staining exhibited by untreated cells (left panel) has disappeared. The mean filipin intensity in MβCD treated images was significantly lower than the mean intensity in untreated cells (Student's T-test, $p < 0.001$, $n = 12$). From these values it was calculated that filipin staining was reduced by 21 ± 3 % (SEM) in response to treatment with 10 mM MBCD. These results confirm that incubation of PC12 and N2a cells with 20 mM and 10 mM MβCD respectively removes a proportion of membrane cholesterol, though not all cellular cholesterol is depleted.

## 5.2. Cholesterol depletion affects the DRM association of five molecules differently

Having established the highest MβCD concentrations that can be used without detrimental effects on cell viability, PC12 and N2a cell DRMs were prepared with or without prior MβCD treatment to evaluate the effect on DRM association of lipid raft markers and 14-3-3. The protein concentrations of the cell lysates from control and MβCD treated cells were adjusted to keep the detergent to protein ratio constant and an equal volume of each cell lysate was loaded onto the sucrose gradients. This procedure allowed comparison of the amount of particular proteins associated with DRMs by SDS-PAGE and immunoblotting.

Representative immunoblots of PC12 cell gradients are presented in figure 5.3. From the top panel of figure 5.3A, CTXB association with DRM fractions (3 and 4) appears to be decreased by MβCD treatment. However, the two left hand lanes of this panel show whole cell lysate from untreated (-) and MβCD treated (+) cells; there also seems to be less CTXB associated with the whole cell lysate following cholesterol depletion. Indeed when the DRM band intensity was measured by densitometry and expressed as a percentage of the lysate band intensity no decrease in relative association of CTXB with DRMs was detected (see figure 5.3C). Thy-1 also consistently showed no decrease in DRM association following MβCD treatment, as illustrated by the second panel in figure 5.3A and figure 5.3C.

The same analysis was carried out for SNAP-25 and syntaxin1a, inner leaflet DRM-associating proteins. From the bottom panel in figure 5.3A it appears that MβCD treatment produces a marked reduction in SNAP-25 association with DRMs. This was confirmed by densitometry analysis of four separate experiments; the mean reduction in DRM association was 59 ± 3 % (SEM). However, more SNAP-25 is not apparent in the detergent soluble fractions (9 and 11) following MβCD treatment. This is probably because the small amount of SNAP-25 from the DRMs was diluted into five fractions and the signal from SNAP-25 already appears saturated in fractions 9 and 11, making additional protein difficult to detect. In contrast to

**Figure 5.3. Cholesterol depletion of PC12 cells reduces the DRM association of SNAP-25 and 14-3-3 but not other lipid raft markers**

PC12 cells were incubated with or without 20 mM MβCD for 30 minutes, followed by 5 minutes incubation with CTXB. DRMs were then isolated as described in Chapter 2, section 2.3.1.2. Fractions 3 and 4 contained the DRMs. **A** 20 μl of each sucrose gradient fraction (fraction numbers above each lane) or 10 μl cell lysate was separated by SDS-PAGE and immunoblotted for CTXB, Thy-1 or SNAP-25. **B** 900 μl DRM fractions 3 and 4 were concentrated, pooled and separated by SDS-PAGE, along with 20 μl of each of the other fractions or 10 μl cell lysate. Immunoblotting for syntaxin1a or 14-3-3 was then performed. **C** Relative localisation of each protein to DRMs was assessed by densitometry (see Chapter 2, section 2.3.5.1) and used to calculate the reduction in DRM association produced by MβCD treatment. The bars represent mean values ± SEM (n = 3).

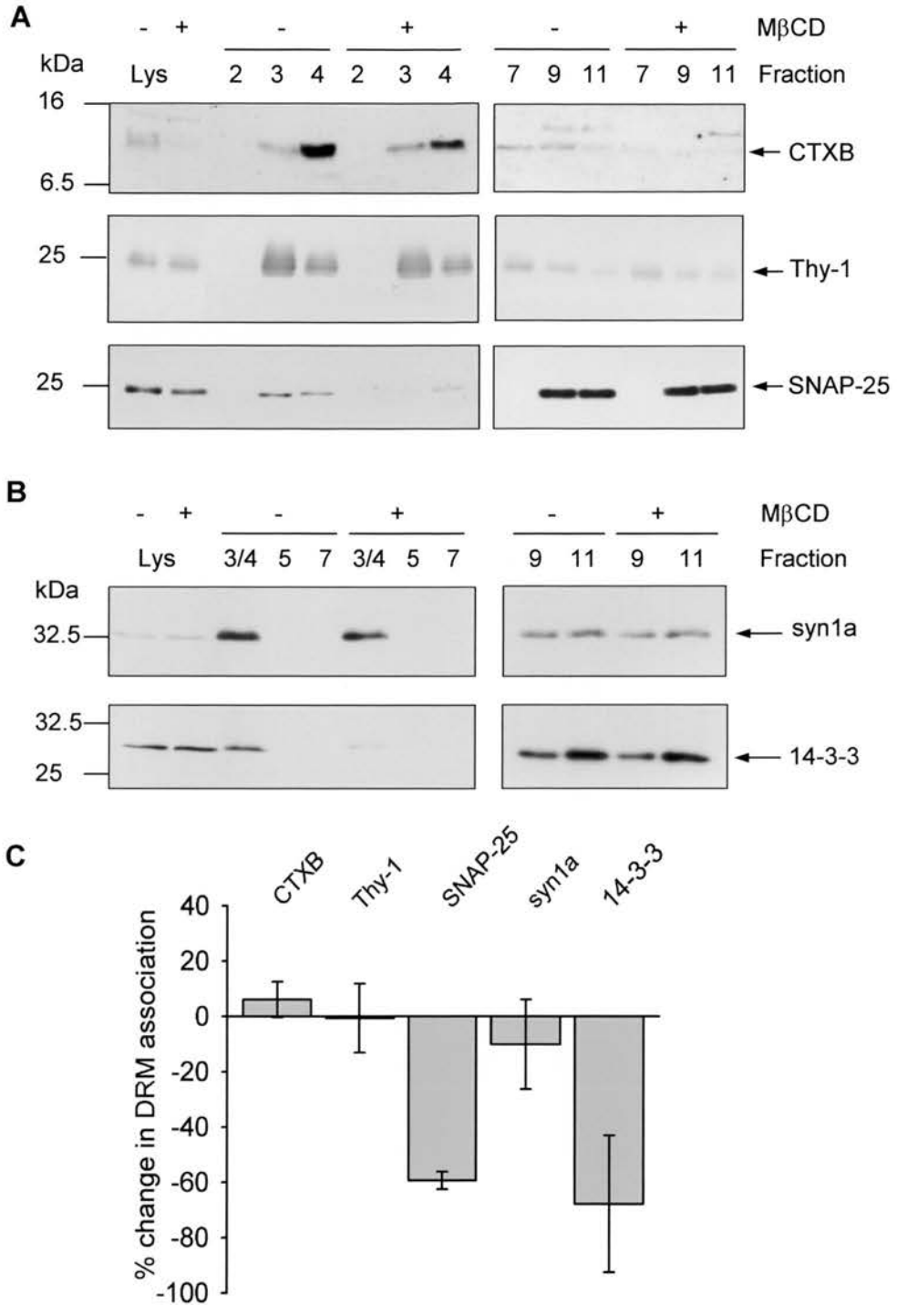


**Figure 5.3 Cholesterol depletion of PC12 cells reduces the DRM association of SNAP-25 and 14-3-3 but not other lipid raft markers**

SNAP-25, syntaxin1a association with DRMs was unaltered by cholesterol depletion (see top panel of figure 5.3B and figure 5.3C). However, immunoblotting for 14-3-3 suggested a decrease in DRM association of this protein following MβCD treatment (bottom panel of figure 5.3B) and quantification of band intensity confirmed that cholesterol depletion reduced the association of 14-3-3 with DRMs by 68 ± 25 % (SEM).

When DRMs were isolated from N2a cells very similar results were obtained as in PC12 cells. There was no reproducible reduction in CTXB association with DRMs, it remained concentrated in the DRM fraction 3 following MβCD treatment and was not detected in the soluble protein fractions (9 and 11), as shown in figure 5.4A. However, a large reduction in DRM association of SNAP-25 (bottom panel, figure 5.4A) and 14-3-3 (bottom panel, figure 5.4B) was again detected in response to cholesterol depletion. Figure 5.4C compares the change in DRM association of all four proteins. The mean reduction in SNAP-25 association was 89 ± 12 % (SEM), whilst the amount of 14-3-3 in DRMs decreased by 36 ± 12 %. This bar chart also shows that cholesterol depletion increased syntaxin1a association with DRMs by 46 ± 4 %. This is not immediately evident from the syntaxin1a immunoblot in figure 5.4B but the amount of syntaxin1a recovered in the lysate seems to be slightly reduced following MβCD treatment. The DRM band intensity was calculated as a percentage of the lysate band intensity so that changes in the overall amount of a protein were taken into account. Densitometry of four similar immunoblots agreed that there was a slight increase in the proportion of total syntaxin1a associated with DRMs. Thy-1 was not investigated in N2a cells due to its unusual localisation in sucrose gradients, discussed in Chapter 4, section 4.1.1.

The PC12 and N2a DRM data mainly agree with respect to the effect of cholesterol depletion. In both cell lines SNAP-25 showed the largest reduction in DRM association and 14-3-3 was also affected but to a lesser extent. Established lipid raft markers Thy-1 and CTXB remained concentrated in the DRMs. Only syntaxin1a exhibited a different response in the two cell types but in neither was it depleted by MβCD.

**Figure 5.4. Cholesterol depletion of N2a cells reduces the DRM association of SNAP-25 and 14-3-3 but not CTXB or syntaxin1a**

N2a cells were incubated with or without 10 mM MβCD for 30 minutes, followed by 5 minutes incubation with CTXB. DRMs were then isolated as described in Chapter 2, section 2.3.1.2. Fractions 3 and 4 contained the DRMs. **A** 20 µl of each sucrose gradient fraction (fraction numbers above each lane) or 10 µl cell lysate was separated by SDS-PAGE and immunoblotted for CTXB or SNAP-25. **B** 900 µl DRM fractions 3 and 4 were concentrated, pooled and separated by SDS-PAGE, along with 20 µl of each of the other fractions or 10 µl cell lysate. Immunoblotting for syntaxin1a or 14-3-3 was then performed. **C** Relative localisation of each protein to DRMs was assessed by densitometry (see Chapter 2, section 2.3.5.1). The mean change in DRM association is plotted ± SEM (n = 3).

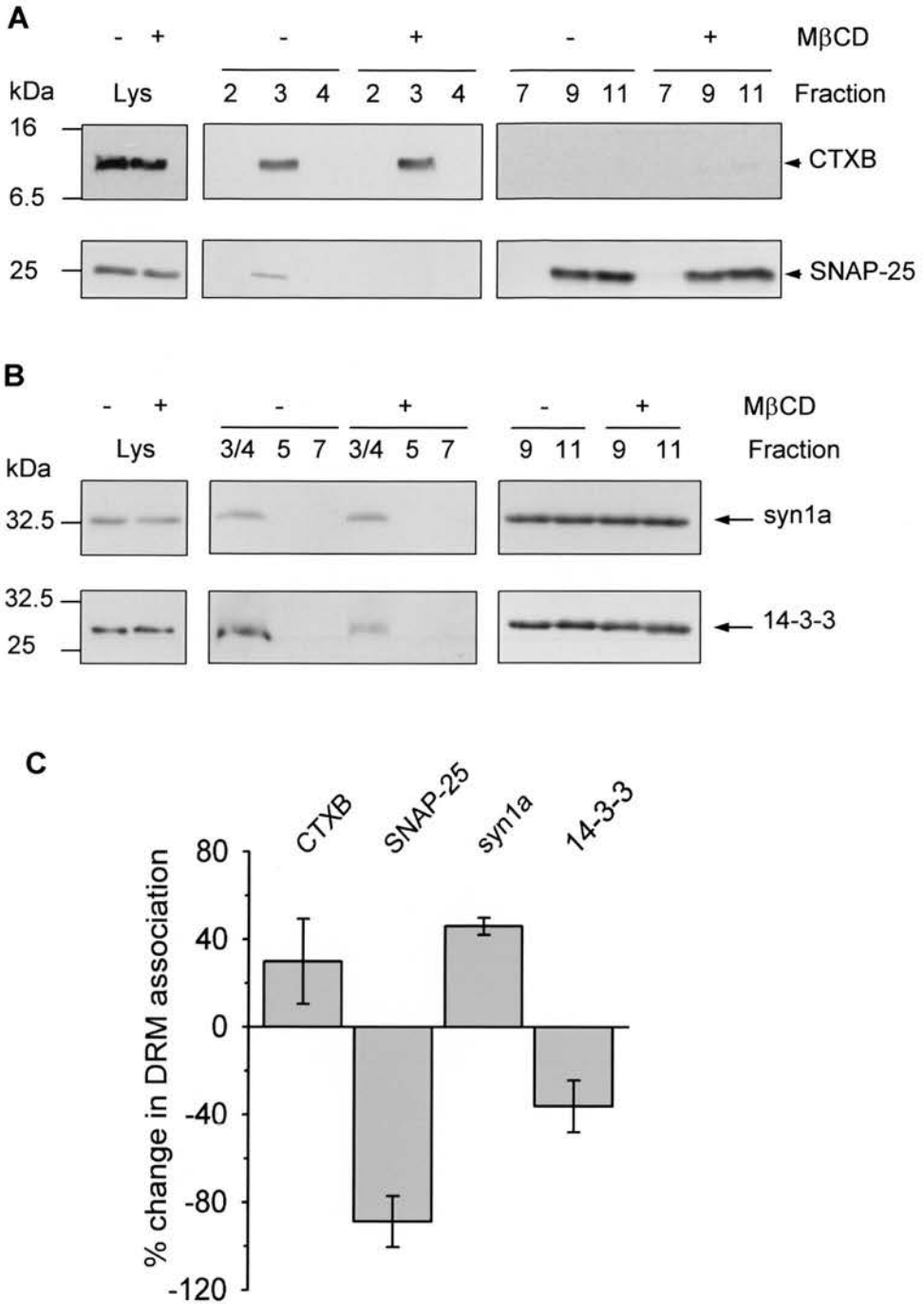


**Figure 5.4. Cholesterol depletion of N2a cells reduces the DRM association of SNAP-25 and 14-3-3 but not CTXB or syntaxin1a**

## 5.3. PC12 cell imaging

### 5.3.1. Cholesterol depletion reduces the intensity of CTXB staining but does not completely disrupt CTXB clusters

In DRM studies less CTXB was recovered in MβCD treated PC12 cell lysates than untreated cell lysates but the proportion of CTXB associated with DRMs was unchanged (see section 5.2). To determine whether these results were reflected by imaging studies I analysed three aspects of CTXB plasma membrane staining; full width at half maximum (FWHM) cluster size, cluster density and staining intensity. Figure 5.5 A and B show examples of the plasma membrane staining of PC12 cells incubated with or without MβCD. It appears that the punctate distribution of CTXB staining is maintained following MβCD treatment. However, there was a small but significant increase in FWHM size in MβCD treated compared with untreated cells (Mann Whitney U test, $p < 0.05$), as illustrated by the cluster size distribution in figure 5.5C. The mean FWHM following MβCD treatment was 585 ± 15 nm (SEM), compared with a mean FWHM of 544 ± 16 nm in untreated cells. The cluster density following MβCD treatment was not significantly different from the untreated control (see figure 5.5D). In agreement with the observation from the DRM preparations in section 5.2, CTXB staining appears to be less intense in cholesterol depleted cells (figure 5.5B) compared with untreated cells (figure 5.5A). Quantification of total signal intensity (see figure 5.5E) revealed that MβCD treatment significantly reduced the overall intensity of CTXB staining (Mann Whitney U test, $p < 0.001$).

The decrease in overall staining intensity suggests that fewer GM1 molecules are present on the surface of PC12 cells. Clusters of 500 – 600 nm in diameter are maintained following MβCD treatment but with presumably fewer CTXB per cluster. This suggests that though microdomains are not dispersed, their lipid composition may be altered and therefore the lipid order is also possibly altered. The increase in cluster size further supports the idea that MβCD in some way perturbs CTXB clusters.

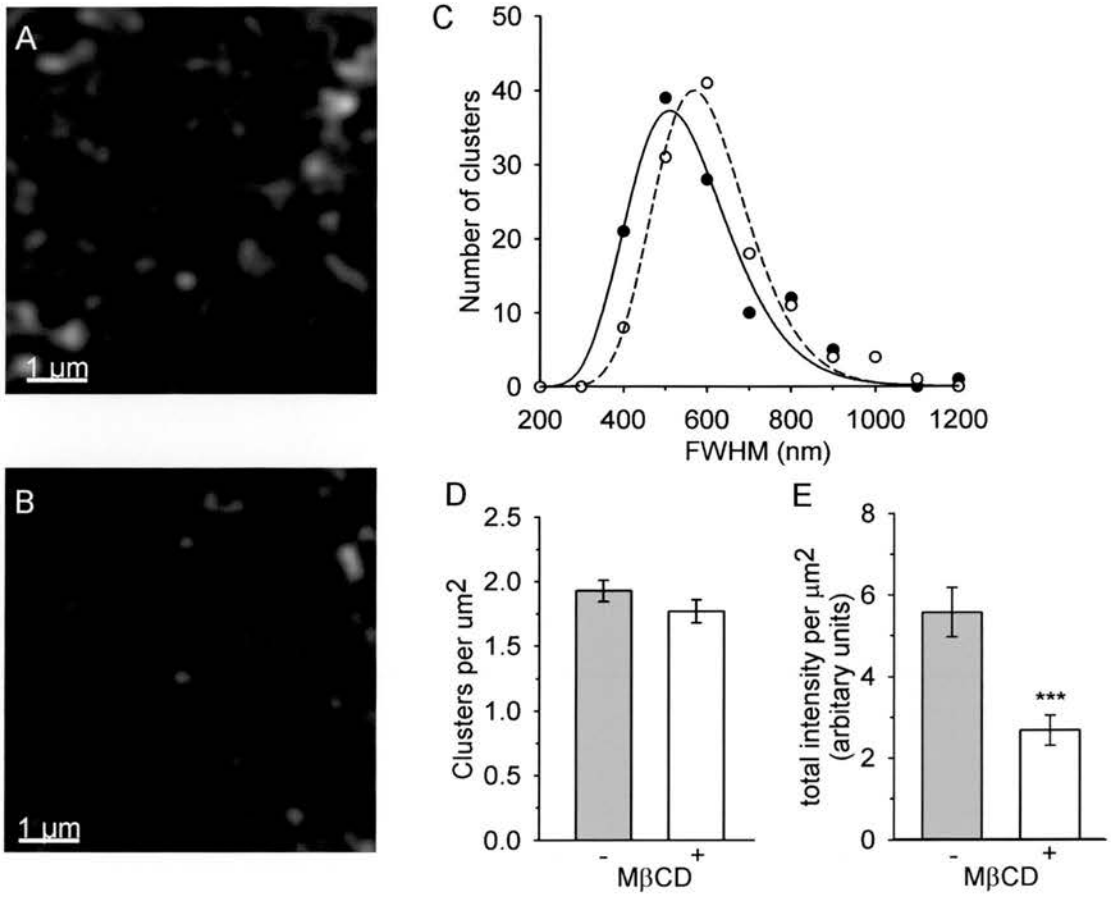


**Figure 5.5. MβCD treatment reduces the intensity of CTXB staining but cluster size and density are not greatly altered**

PC12 cells were incubated with or without 20 mM MβCD for 30 minutes, followed by incubation with FITC-CTXB. Cells were then fixed and imaged by CLSM. Images of the plasma membrane at the base of **A**, a representative untreated cell and **B**, a MβCD treated cell. **C** FWHM cluster size was measured as detailed in Chapter 2, section 2.4.6.1, for in excess of 100 spots from images similar to A and B. Cluster size is plotted against number of clusters of that size ± 50 nm (closed circles/solid line = untreated, open circles/dashed line = MβCD treated). **D** Mean cluster density per $\mu m^2$. **E** Mean total intensity per $\mu m^2$ (calculated as described in Chapter 2, section 2.4.6.1). Error bars correspond to SEM, *** $p < 0.001$, Mann Whitney U test (n = 12 images).

### 5.3.2. Cholesterol depletion does not reduce the coincidence of Thy-1 or 14-3-3 with CTXB in PC12 cells

Having observed that cholesterol depletion alters CTXB staining, implying possible rearrangement of membrane domains, the next step was to determine whether MβCD treatment also changes the coincidence of DRM proteins with CTXB in intact cells. In section 5.2, cholesterol depletion failed to remove the established raft marker Thy-1 from DRMs but 14-3-3 DRM association did decrease; I therefore examined whether these results would be reflected in intact cells. PC12 cells were incubated in the presence or absence of MβCD for 30 minutes, incubated with CTXB and immunostained for Thy-1 or 14-3-3. Image analysis was carried out as in Chapter 4 (described in Chapter 2, section 2.4.6.2). Values of percentage colocalisation or overlap (based on Manders' methods) are presented alongside correlation analysis ($R^2$ x 100, where R = Pearson's coefficient).

Thy-1 plasma membrane staining remained punctate following MβCD treatment and from the merged images in figure 5.6A, it appears that there is still a high level of overlap between CTXB and Thy-1 staining. This was confirmed by colocalisation analysis. Figure 5.6B shows the areas in the images from figure 5.6A that registered as colocalised following automatic thresholding. Twelve similar images were analysed and mean colocalisation was in the region of 60 – 70 % for both colocalisation of CTXB with Thy-1 and Thy-1 with CTXB, as shown in figure 5.6C; there was no significant difference between cholesterol depleted and untreated cells. Intensity dependent correlation analysis of the same images confirmed that MβCD treatment did not reduce the dependence of Thy-1 localisation on CTXB, as might be expected if membrane microdomains were perturbed (figure 5.6D) In fact correlation ($R^2$ x 100) of Thy-1 staining with CTXB staining slightly increased following MβCD treatment, from 25 ± 3 % (SEM) to 35 ± 3 % (Student's T-test, $p < 0.05$). Both values were significantly different from the mean random correlation (Student's T-test, $p < 0.001$), shown by the solid line across each bar in figure 5.4D.

**Figure 5.6. MβCD treatment of PC12 cells did not reduce the coincidence of Thy-1 with CTXB on the plasma membrane**

PC12 cells were incubated with or without 20 mM MβCD for 30 minutes, stained with FITC-CTXB, fixed and immunostained using anti-Thy-1 (OX7) antibody. CTXB (green) and Thy-1 (red) were visualised by laser scanning confocal microscopy. **A** Images from the base of representative cells. The right hand panels are scatter plots of the red intensity plotted against the green intensity for each voxel in the image. **B** Colocalisation masks for the merged images in A, generated by automatic thresholding. **C** The mean percentage colocalisation of CTXB with Thy-1 and Thy-1 with CTXB. **D** Mean correlation ($R^2$ x 100) of the green channel (CTXB) with the red channel (Thy-1). The mean random correlation calculated by Costes' randomisation algorithm (solid line) + SEM (dashed line) are shown on the bars. Error bars correspond to SEM, ** $p < 0.05$, Student's T-test (n = 12). Scale bars = 1 μm.

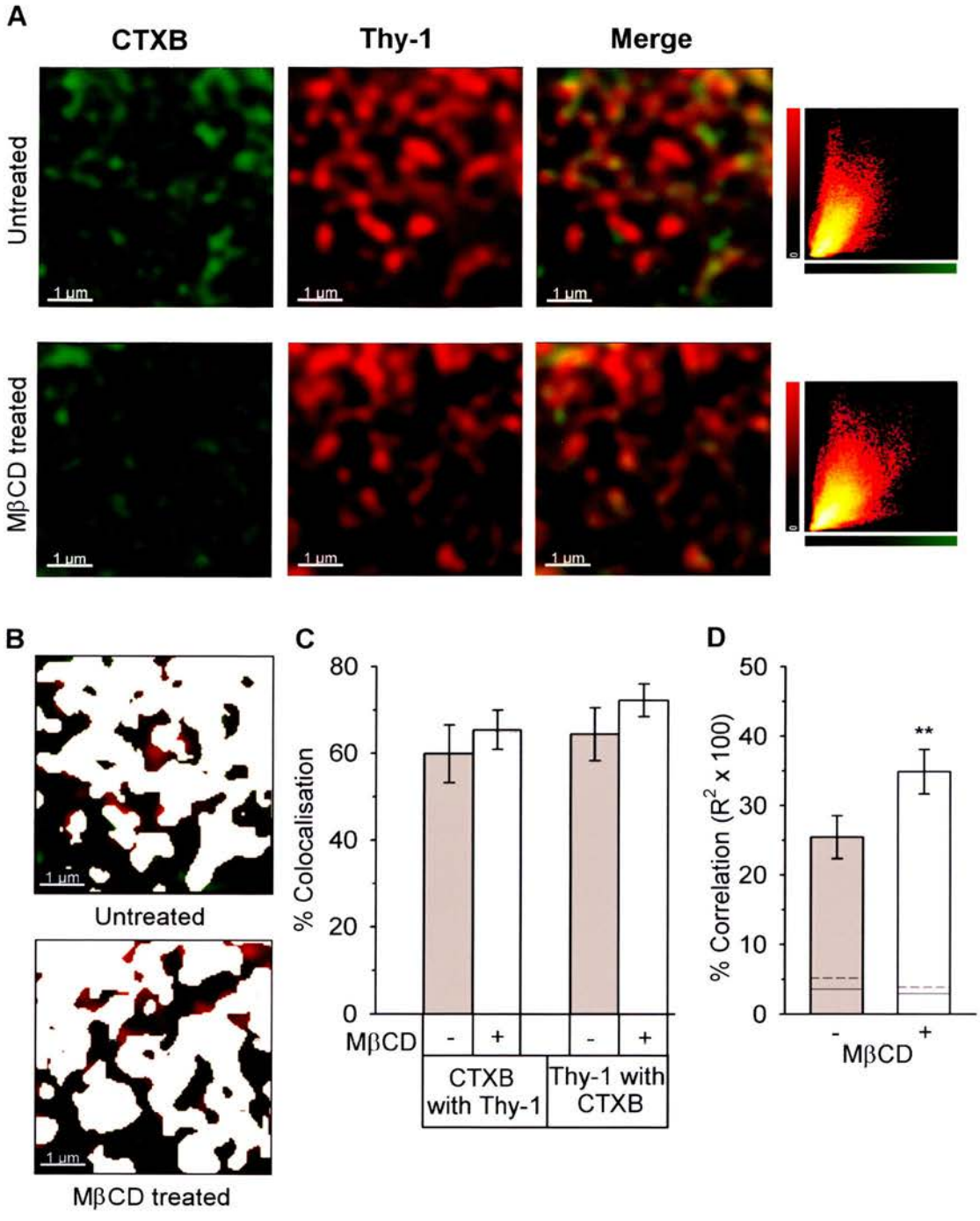


**Figure 5.6. MβCD treatment of PC12 cells did not reduce the coincidence of Thy-1 with CTXB on the plasma membrane**

The contribution of random variation to percentage correlation was assessed by calculating $R^2$ x 100 from red channel images randomised using Costes' method and the original green channel (as described in Chapter 2, section 2.4.6.2).

It is interesting that the correlation analysis disagrees with the colocalisation analysis, which suggests no significant alteration in localisation of Thy-1 relative to CTXB. In Chapter 4 both analysis methods were generally in good agreement. Pearson's correlation analysis is more sensitive to slight changes in the distribution of fluorophores because it describes an intensity dependent variation.

Most of the CTXB remained associated with PC12 DRMs following cholesterol depletion, whilst 14-3-3 was removed from DRMs. It might be expected then that 14-3-3 would segregate away from CTXB following MβCD treatment. However, the imaging results presented in figure 5.7 do not support this hypothesis. MβCD does not alter the distribution of 14-3-3 staining at the plasma membrane (see figure 5.7). Automatic thresholding of images in figure 5.7A produced the colocalisation masks presented in figure 5.7B, from which it is evident that much of the red and green signal does not register as colocalised, according to this thresholding method. When the colocalisation was quantified in 14 such images no significant difference was detected between untreated and MβCD treated cells. Mean colocalisation values, shown in figure 5.7C, are all in the region of 30 – 40 %.

Intensity dependent correlation between 14-3-3 and CTXB was assessed in plasma membrane images such as those in figure 5.7A and found to be unaltered by cholesterol depletion, as illustrated by figure 5.7D. In addition, the correlation observed between 14-3-3 and CTXB following MBCD treatment (12 ± 2 %, SEM) was significantly greater than the mean random correlation value (7 ± 1 %) calculated from Costes randomisation of the same images (paired T-test, $p < 0.05$). The implication is that cholesterol depletion does not affect the observed low level of CTXB dependent 14-3-3 localisation, which remains just above random levels.

**Figure 5.7. MβCD treatment of PC12 cells did not alter the coincidence of 14-3-3 with CTXB on the plasma membrane**

PC12 cells were incubated with or without 20 mM MβCD for 30 minutes, stained with FITC-CTXB, fixed and immunostained using anti-14-3-3 (pan) antibody. CTXB (green) and 14-3-3 (red) were visualised by laser scanning confocal microscopy. **A** Images from the base of representative cells. The right hand panels are scatter plots of the red intensity plotted against the green intensity for each voxel in the image. **B** Colocalisation masks for the merged images in A, generated by automatic thresholding. **C** The mean percentage colocalisation of CTXB with 14-3-3 and 14-3-3 with CTXB. **D** Mean correlation ($R^2$ x 100) of the green channel with the red channel. The mean random correlation calculated by Costes' randomisation algorithm (solid line) + SEM (dashed line) are shown on the bars. Error bars correspond to SEM, n = 12. Scale bars = 1 μm.

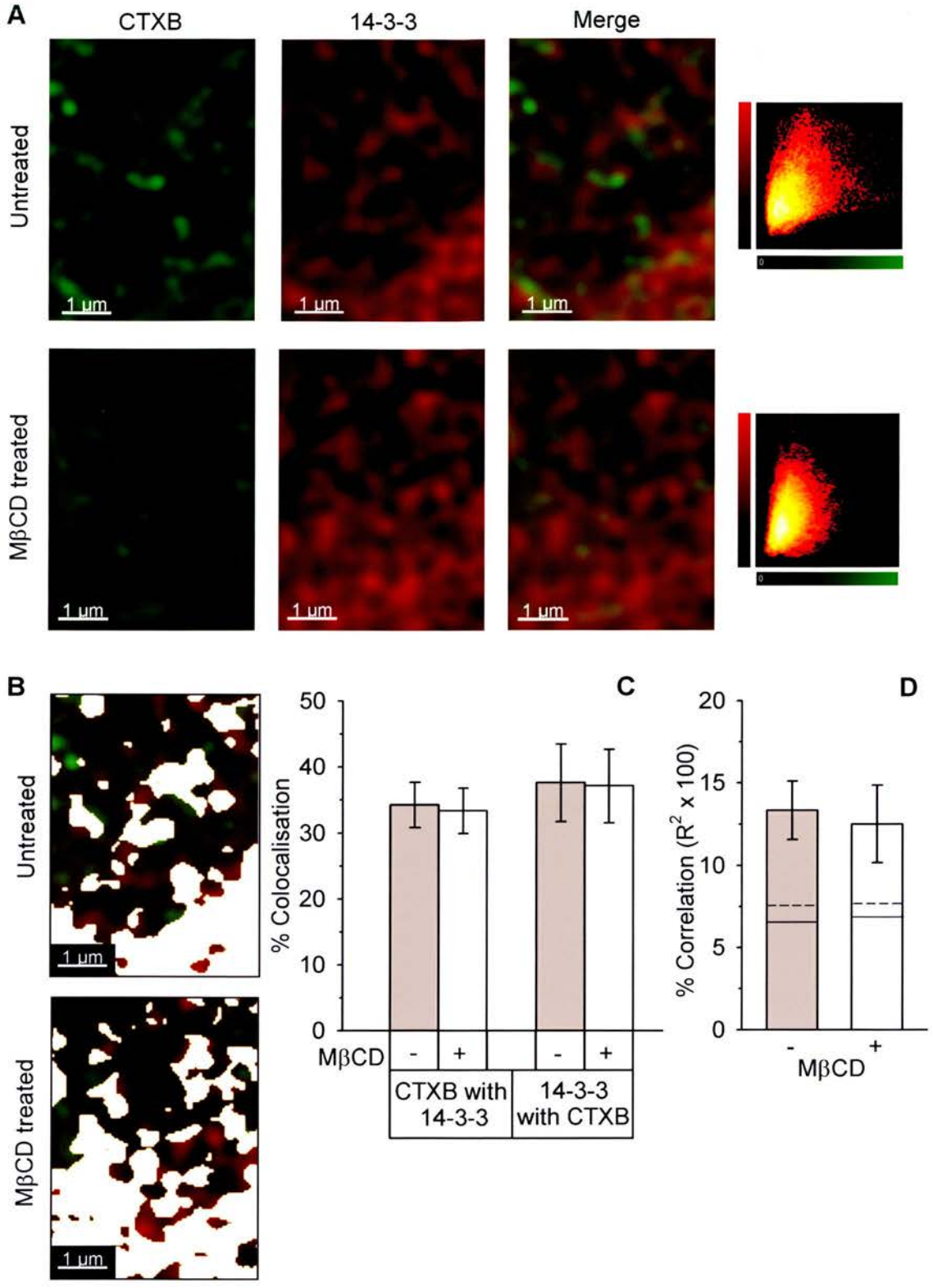


**Figure 5.7. MβCD treatment of PC12 cells did not alter the coincidence of 14-3-3 with CTXB on the plasma membrane**

### 5.3.3. Cholesterol depletion does not alter the coincidence of SNAP-25 or syntaxin1a with CTXB in PC12 cells

In Chapter 4 (section 4.3.3) SNAP-25 coincided with CTXB to a similar extent as the established raft marker Thy-1. However, the correlation observed between syntaxin1a and CTXB was deemed to be due to random variation, rather than dependent localisation of the proteins, upon comparison to Costes' randomisation test. Despite the apparent lack of coincidence I decided to investigate the effect of cholesterol depletion on localisation of syntaxin1a. The correlation of Thy-1 staining with CTXB actually increased slightly following MβCD treatment (figure 5.4D) and the DRM association of both Thy-1 and syntaxin1a is unchanged by MβCD treatment (figure 5.3). Therefore, the possibility of a similar MβCD induced change in correlation of syntaxin1a with CTXB was explored.

Syntaxin1a exhibited a punctate distribution on the plasma membrane of both untreated and MβCD treated cells, as illustrated by figure 5.8A. The merged images of CTXB and syntaxin1a (figure 5.8A) and the colocalisation masks generated by automatic thresholding (figure 5.8B) suggest a similar low level of colocalisation in both untreated and MβCD treated images. Quantitative analysis confirmed that the percentage colocalisation of syntaxin1a with CTXB was similar to that of CTXB with syntaxin1a and the mean of 30 – 40 % colocalisation was preserved following cholesterol depletion (see figure 5.8C). In agreement with the colocalisation analysis, there was also no significant change in intensity dependent correlation ($R^2$ x 100) following cholesterol depletion (see figure 5.8D). Furthermore, the observed mean $R^2$ x 100 of 12 ± 2 % (SEM) in MβCD treated cells was not significantly greater than the mean random $R^2$ x 100 of 10 ± 3 %, calculated from the same set of images with the syntaxin1a staining randomised by Costes' method. Thus cholesterol depletion does not affect the localisation of syntaxin1a with respect to CTXB; the two proteins remain independently distributed on the plasma membrane.

**Figure 5.8. MβCD treatment of PC12 cells did not alter the coincidence of syntaxin1a with CTXB on the plasma membrane**

PC12 cells were incubated with or without 20 mM MβCD for 30 minutes, stained with FITC-CTXB, fixed and immunostained for using anti-syntaxin (HPC-1) antibody. CTXB (green) and syntaxin1a (red) were visualised by laser scanning confocal microscopy. **A** Images from the base of representative cells. The right hand panels are scatter plots of the red intensity plotted against the green intensity for each voxel in the image. **B** Colocalisation masks for the merged images in A, generated by automatic thresholding. **C** The mean percentage colocalisation of CTXB with syntaxin1a and syntaxin1a with CTXB. **D** Mean percentage correlation ($R^2$ x 100) of the green channel with the red channel. The mean random correlation calculated by Costes' randomisation algorithm (solid line) + SEM (dashed line) are shown on the bars. Error bars correspond to SEM, n = 12. Scale bars = 1 μm.

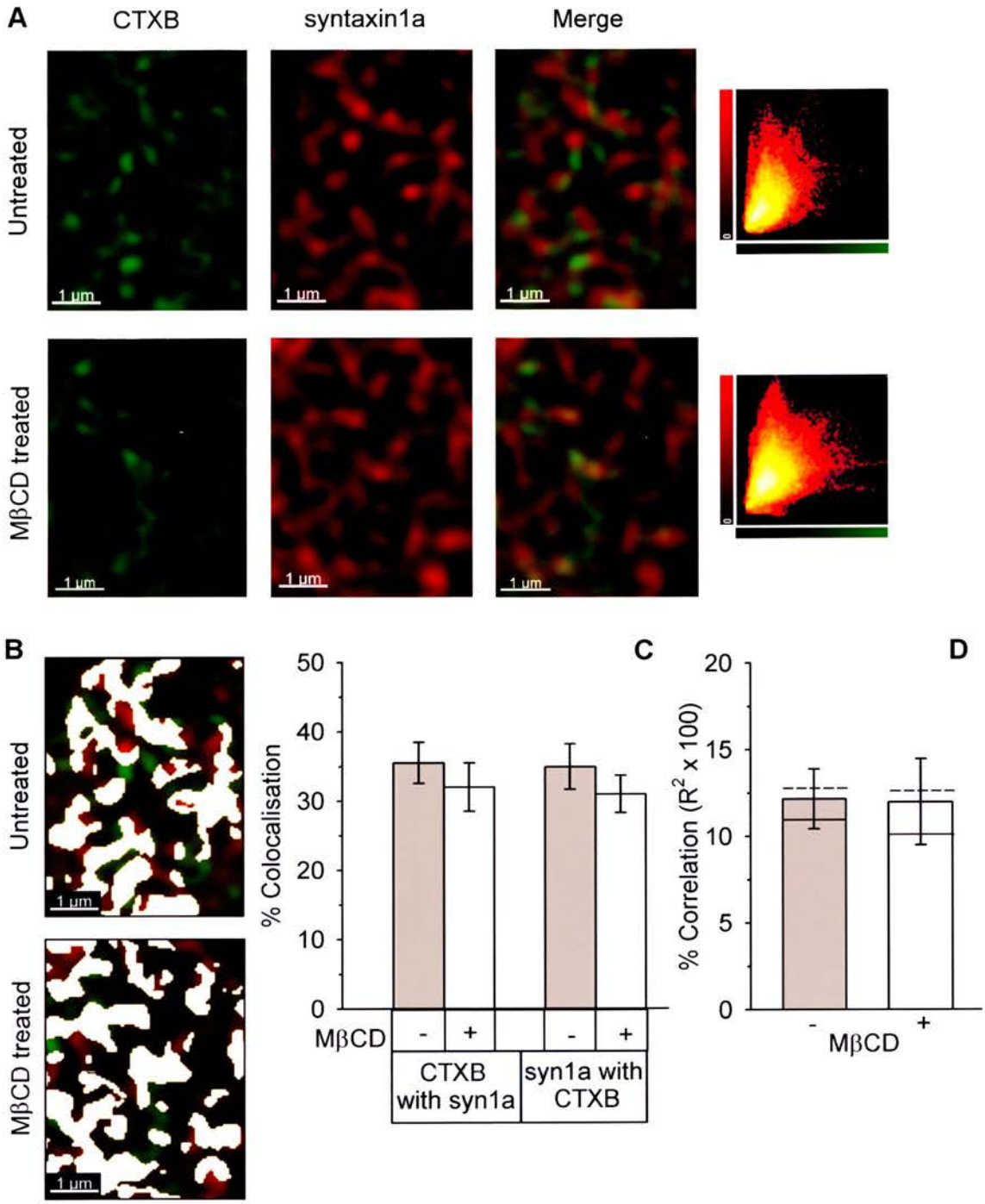


**Figure 5.8. MβCD treatment of PC12 cells did not alter the coincidence of syntaxin1a with CTXB on the plasma membrane**

The distribution of SNAP-25 on the plasma membrane appeared unaltered following MβCD treatment, as shown by images from the base of two representative cells in figure 5.9A. From the merged images it appears that some green puncta overlap with some red puncta in both untreated and MβCD treated cell membrane and the colocalisation masks produced by automatic thresholding (figure 5.9B) confirm this. Again the mean colocalisation of CTXB with SNAP-25 and SNAP-25 with CTXB was very similar and both are virtually unchanged by MβCD treatment, remaining at around 50 - 60 % colocalisation (see figure 5.9C). The scatter plots in figure 5.9A suggest a similar level of correlation between the red and green signal in both images. Intensity dependent correlation between SNAP-25 and CTXB staining is indeed unaltered by cholesterol depletion, as shown by figure 5.9D. The observed 23 ± 3 % (SEM) correlation in MβCD treated images was significantly greater than would be expected due to random correlation, according to Costes' randomisation test (paired T-test, $P < 0.001$). The absence of any alteration in coincidence of SNAP-25 with CTXB disagrees with the DRM data; SNAP-25 was observed to localise predominantly to the detergent soluble fractions following cholesterol depletion, whereas CTXB remained enriched in DRMs.

In summary, cholesterol depletion reduced the binding of CTXB to the plasma membrane of PC12 cells, suggesting some change in the composition of membrane microdomains, though CTXB clusters were not dispersed. However, little change in the localisation of Thy-1, 14-3-3, SNAP-25 or syntaxin1a relative to CTXB was detected in response to cholesterol depletion, by quantitative analysis of co-stained cells.

**Figure 5.9. MβCD treatment of PC12 cells did not alter the coincidence of SNAP-25 with CTXB on the plasma membrane**

PC12 cells were incubated with or without 20 mM MβCD for 30 minutes, stained with FITC-CTXB, fixed and immunostained using anti-SNAP-25 (SMI81) antibody. CTXB (green) and SNAP-25 (red) were visualised by laser scanning confocal microscopy. **A** Images from the base of representative cells. The right hand panels are scatter plots of the red intensity plotted against the green intensity for each voxel in the image. **B** Colocalisation masks for the merged images in A, generated by automatic thresholding. **C** The mean percentage colocalisation of CTXB with SNAP-25 and SNAP-25 with CTXB. **D** Mean correlation ($R^2$ x 100) of the green channel with the red channel. The mean random correlation calculated by Costes' randomisation algorithm (solid line) + SEM (dashed line) are shown on the bars. Error bars correspond to SEM, n = 12. Scale bars = 1 μm.

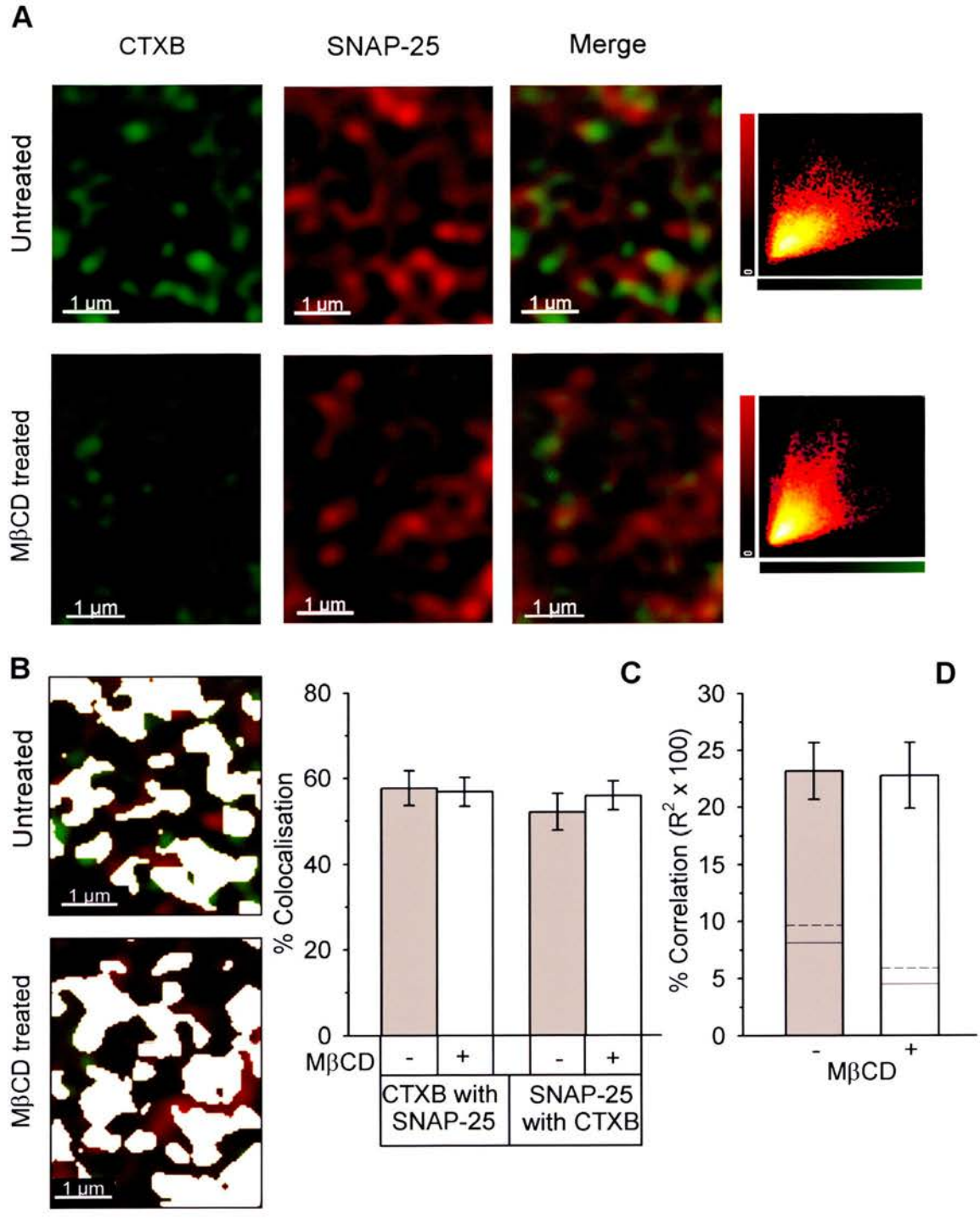


**Figure 5.9. MβCD treatment of PC12 cells did not alter the coincidence of SNAP-25 with CTXB on the plasma membrane**

## 5.4. N2a cell imaging

Previous imaging experiments using the lipid raft marker CTXB in this study have focused on PC12 cells. The following two sections present N2a cells subjected to the same experiments as described for PC12 cells in sections 5.3.2 and 5.3.3 but additional figures are included (figures 5.11, 5.13 and 5.15) to characterise the overall subcellular localisation of the proteins of interest in N2a cells. The experiments presented in the following sections examined whether the coincidence of 14-3-3, syntaxin1a and SNAP-25 with CTXB is affected by cholesterol depletion in N2a cells.

### 5.4.1. Cholesterol depletion disrupts CTXB clusters on the plasma membrane of N2a cells

In PC12 cells cholesterol depletion reduced the binding of CTXB to the plasma membrane as judged by the significant decrease in total intensity of CTXB staining and the cluster size was slightly increased. The analysis of N2a cell DRMs in section 5.2 suggested that cholesterol depletion does not alter the membrane distribution of CTXB in N2a cells. The plasma membrane staining of CTXB was therefore analysed by microscopy to investigate whether the membrane distribution in intact cells concurs with this data.

Images of CTXB stained N2a cells, previously incubated in the presence or absence of MβCD, are presented in figure 5.10A. From the mid-section images the majority of CTXB staining appears to be at the plasma membrane in N2a cells. The images from the base of cells show that CTXB has a punctate distribution, which is not dispersed by cholesterol depletion. However, close inspection of enlarged images of plasma membrane regions from an untreated cell and a MβCD treated cell (figure 5.10B) reveal that the distribution of puncta differs following application of MβCD. CTXB staining was analysed by measuring the cluster FWHM, the cluster

**Figure 5.10. Cholesterol depletion alters the distribution of CTXB on the plasma membrane of N2a cells**

N2a cells were incubated with or without 10 mM MβCD for 30 minutes, followed by 5 minutes incubation with FITC-CTXB and then fixation. **A** Representative untreated and MβCD treated cells (scale bars = 2 μm). **B** Enlarged images of the plasma membrane at the base of an untreated cell and a MβCD treated cell (scale bars = 1 μm). **C** FWHM cluster size was measured (as detailed in Chapter 2, section 2.4.6.1), for in excess of 100 spots from images similar to those in B. Cluster size is plotted against number of clusters of that size ± 50 nm (closed circles/solid line = untreated, open circles/dashed line = MβCD treated). **D** Mean cluster density per $\mu m^2$. **E** Mean total intensity per $\mu m^2$ (calculated as described in Chaper 2, section 2.4.6.1). Error bars correspond to SEM, ** = $p < 0.05$, Student's T-test (n = 16).

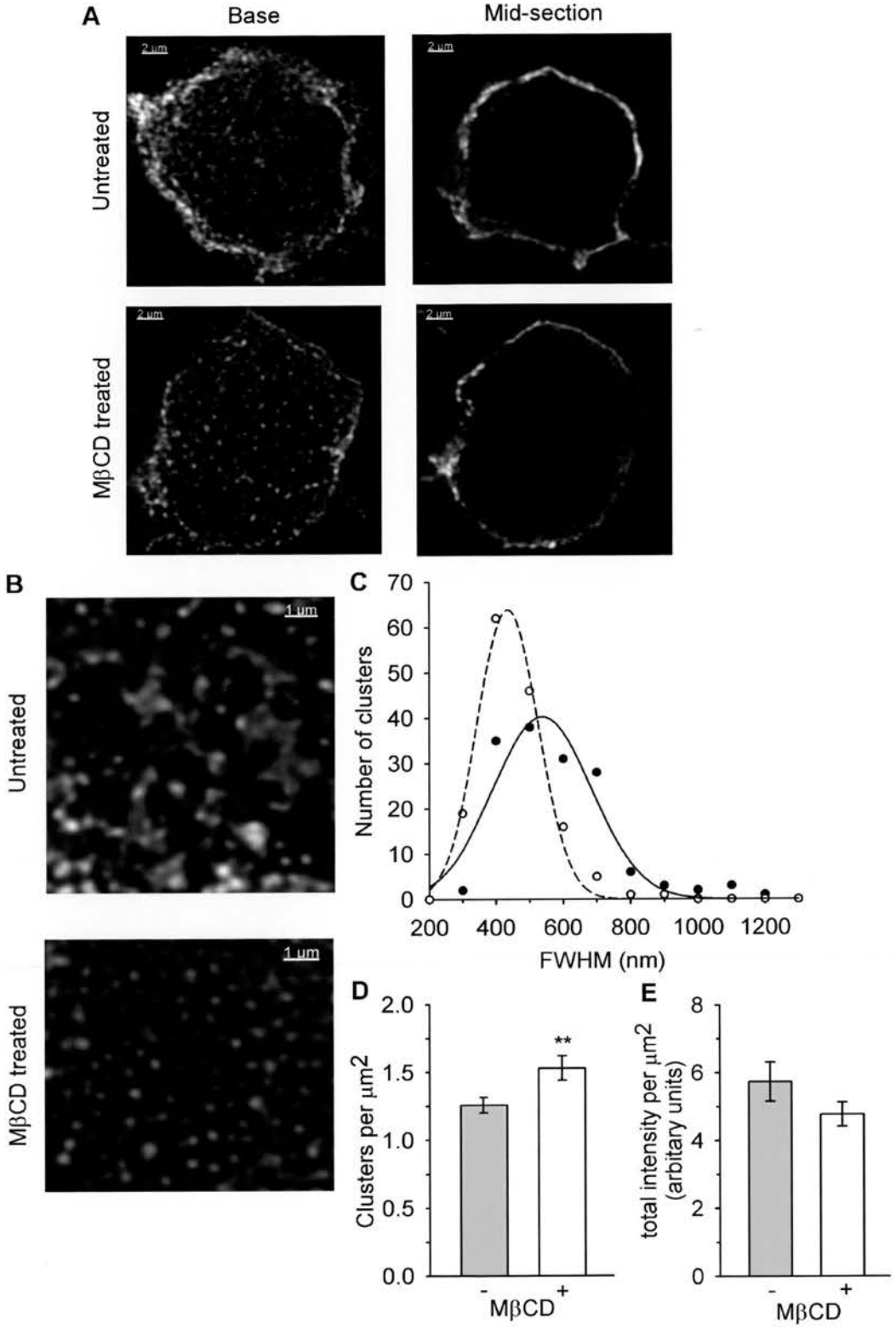


**Figure 5.10. Cholesterol depletion alters the distribution of CTXB on the plasma membrane of N2a cells**

density per $\mu m^2$ and the total intensity per $\mu m^2$ in plasma membrane images from four separate experiments (as described in Chapter2, section 2.4.6.1). The mean cluster FWHM in untreated cells was 527 ± 15 nm (SEM). Figure 5.10C shows the wide range of cluster sizes recorded from untreated cells (solid line); this is reflected by the staining pattern in figure 5.10B. MβCD treated cells exhibited a much narrower distribution of sizes (dashed line, figure 5.10C) and clusters were significantly smaller than clusters in untreated cells (Mann Whitney U test, $p < 0.001$), with a mean FWHM of 407 ± 8 nm. The number of CTXB clusters per $\mu m^2$ was also significantly altered by cholesterol depletion (Student's T-test, $p < 0.02$). The mean cluster density of 1.26 ± 0.06 (SEM) per $\mu m^2$ increased to 1.53 ± 0.09 per $\mu m^2$ following MβCD treatment (shown in figure 5.10D). In PC12 cells MβCD produced a large reduction in total staining intensity. Figure 5.10E suggests that, in N2a cells, the total intensity of CTXB staining tended to decrease slightly in response to cholesterol depletion but this trend was not significant.

In summary, though CTXB remains concentrated in DRMs following cholesterol depletion, microscopy of intact cells revealed that the size of CTXB clusters is decreased and accompanied by an increase in the number of clusters per unit area. Thus MβCD appears to partially disrupt or disperse CTXB clusters in N2a cells. The smaller CTXB puncta observed in cholesterol depleted cells are likely to correspond to clusters rather than single CTXB molecules because their FWHM (~ 400 nm) is larger than that of a single sub-resolution object. Such an object (a 200 nm diameter bead) had a FWHM of 280 nm following data deconvolution (as discussed in Chapter 4, section 4.4), much less than the CTXB puncta. The disruption of CTXB clusters observed in N2a cells contrasts with the effect of cholesterol depletion on CTXB labelling in PC12 cells.

### 5.4.2. Cholesterol depletion does not alter the coincidence of 14-3-3 with CTXB on N2a plasma membranes

Cholesterol depletion appears to have a very different effect on the membrane distribution of CTXB in N2a cells compared with PC12 cells. This treatment might then differently affect the localisation of DRM proteins and their coincidence with CTXB. The original aim of these imaging studies was to explore the possibility that 14-3-3 localises to lipid raft-like domains. The localisation of 14-3-3 in N2a cells was investigated to determine firstly whether 14-3-3 associates with CTXB clusters and then whether this association depends on cholesterol. Sections through a representative N2a cell are presented in figure 5.11 to illustrate the overall distribution of 14-3-3. The mid-section images demonstrate the predominantly cytoplasmic localisation of 14-3-3, both in untreated (panel A) and MβCD treated cells (panel B). As in PC12 cells, 14-3-3 is not uniformly distributed in the cytoplasm; local concentrations of the protein are observed. Images from the base and top of the cells suggest that some 14-3-3 is in the plasma membrane region. From the merged base images it appears that there is little overlap between 14-3-3 and CTXB staining. To investigate this observation, colocalisation and intensity dependent correlation ($R^2$ x 100) were calculated for a set of images. The results are summarised in figure 5.12.

Figure 5.12A presents enlarged images from the base of representative cells and little overlap between CTXB and 14-3-3 is apparent. The colocalisation masks in figure 5.12B confirm that few of the red and green puncta colocalise following the automatic thresholding procedure. Only 20 ± 3 % (SEM) of CTXB signal and 19 ± 3 % of 14-3-3 signal registered as colocalised (figure 5.12C) and these values were unchanged following cholesterol depletion. The spread of points in the scatter plots in figure 5.12A suggests that intensity dependent correlation was also very low in these images. Indeed intensity dependent correlation between 14-3-3 and CTXB staining was only 5 ± 1 % in untreated cells. In agreement with the colocalisation analysis, there was no significant difference between the mean $R^2$ x 100 in untreated

**Figure 5.11. Localisation of 14-3-3 and CTXB in untreated and cholesterol depleted N2a cells**

N2a cells were incubated in the presence or absence of 10 mM MβCD for 30 minutes, followed by 5 minutes incubation with FITC-CTXB, fixation and immunostaining using anti-14-3-3 (pan) antibody. Images from the base, mid-section and top of a representative **A**, untreated cell and **B**, MβCD treated cell, are presented. CTXB is green, 14-3-3 is red. Scale bars = 3 μm.

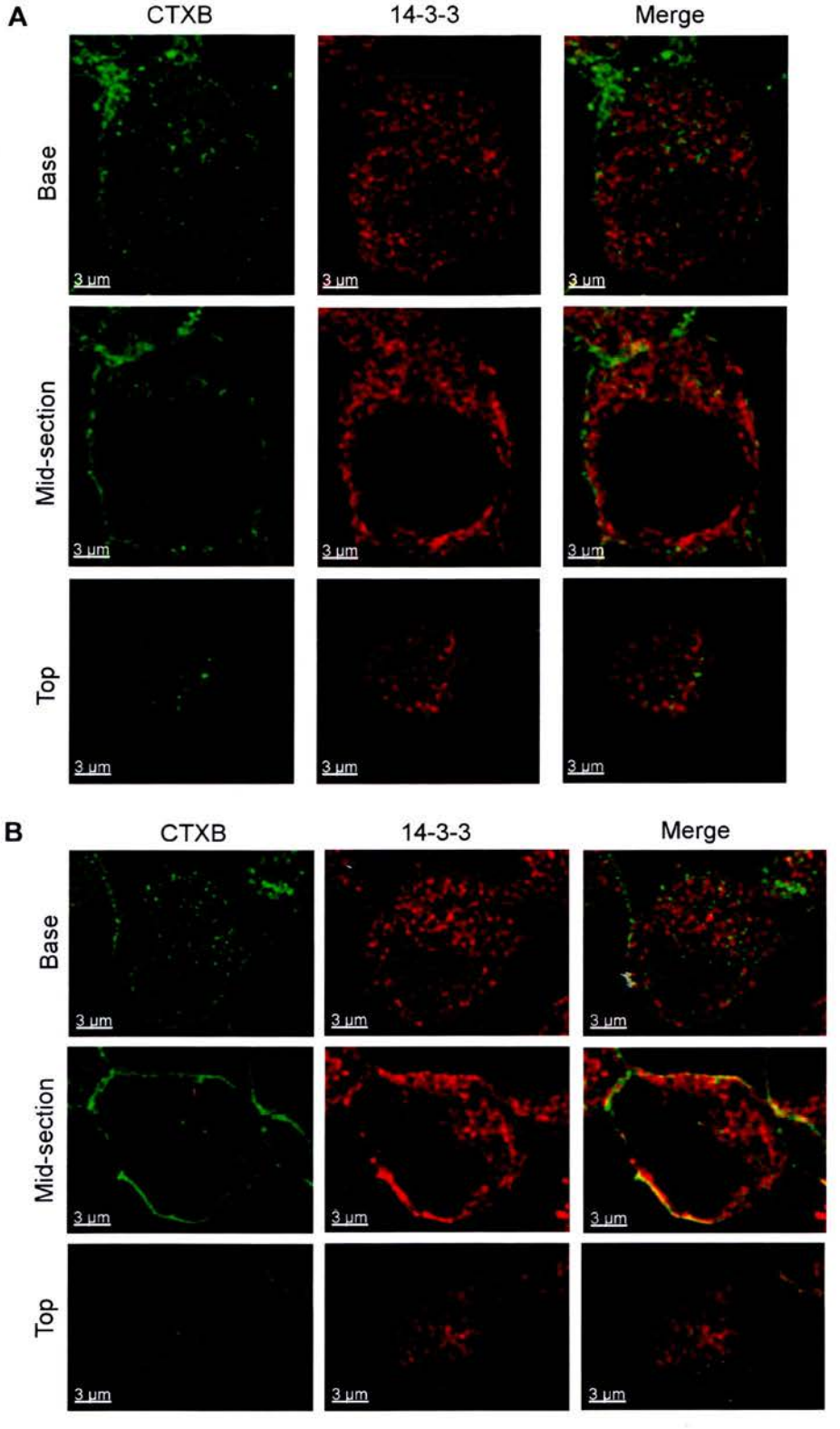


**Figure 5.11. Localisation of 14-3-3 and CTXB in untreated and cholesterol depleted N2a cells**

and MβCD treated cells. However, in both untreated and MβCD treated cells, the observed correlation was calculated to be significantly above random levels (paired T-test, $p < 0.05$). This implies that the observed correlation between 14-3-3 and CTXB staining, albeit low, represents some dependent localisation of the two proteins. A similar situation was described for PC12 cells (section 5.3.2) and in both cell types the association was unaltered by cholesterol depletion.

**Figure 5.12. The coincidence of 14-3-3 with CTXB is not altered by cholesterol depletion in N2a cells**

N2a cells were incubated in the presence or absence of 10 mM MβCD for 30 minutes, followed by 5 minutes incubation with FITC-CTXB (green), fixation and immunostaining using anti-14-3-3 (pan) antibody (red). **A** Images from the base of representative cells. The right hand panels are scatter plots of the red intensity plotted against the green intensity for each voxel in the image. **B** Colocalisation masks for the merged images in A, generated by automatic thresholding. **C** The mean percentage colocalisation of CTXB with 14-3-3 and 14-3-3 with CTXB. **D** Mean correlation ($R^2$ x 100) of the green channel with the red channel. The mean random correlation calculated by Costes' randomisation algorithm (solid line) + SEM (dashed line) are shown on the bars. Error bars correspond to SEM (n = 16). Scale bars = 1 μm.

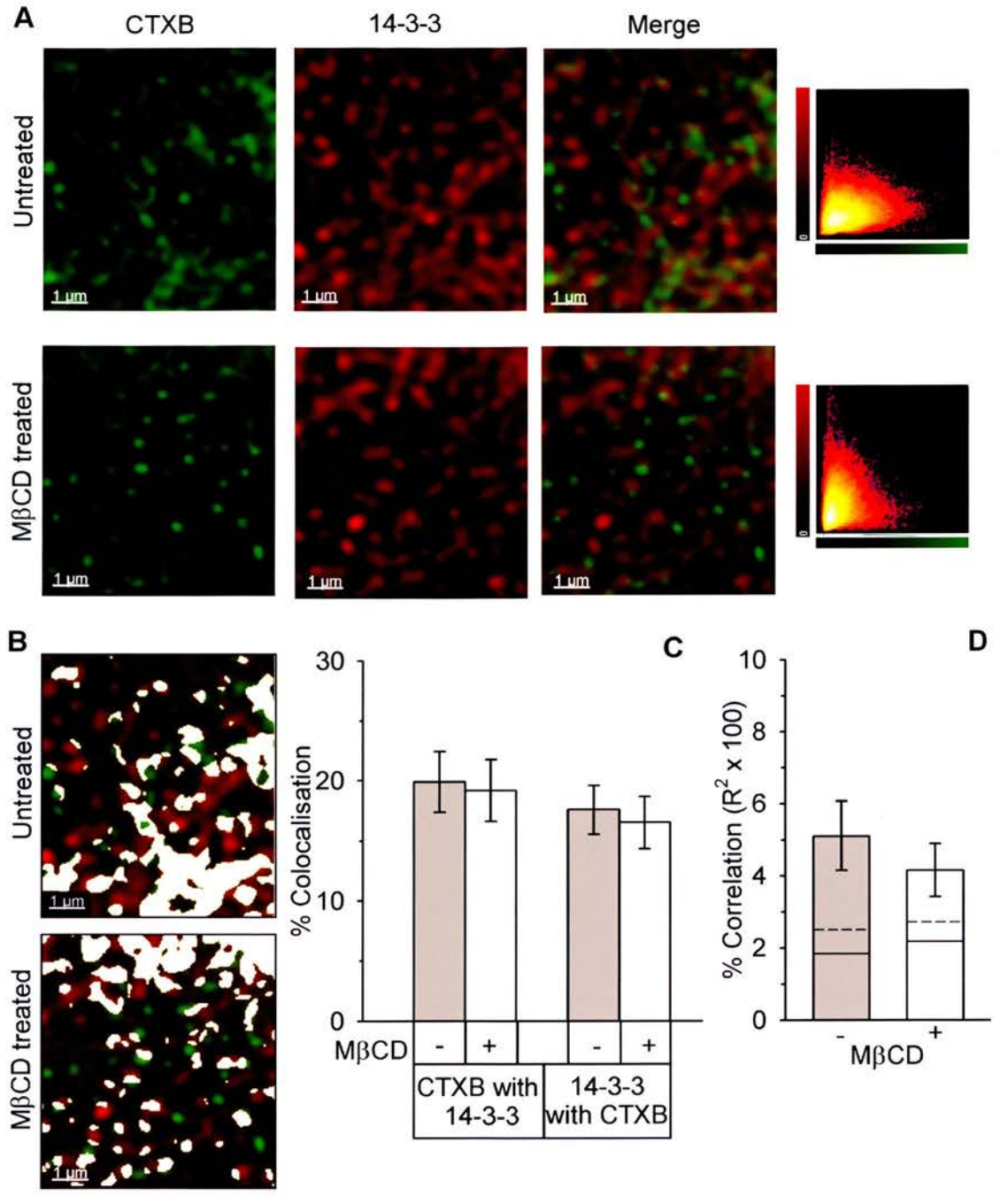


**Figure 5.12. The coincidence of 14-3-3 with CTXB is not altered by cholesterol depletion in N2a cells**

### 5.4.3. Cholesterol depletion does not alter the coincidence of syntaxin1a with CTXB on the N2a plasma membrane

The localisation of syntaxin1a with respect to CTXB was investigated in N2a cells to find out whether the results of PC12 cell imaging would be reproduced in another cell line. Figure 5.13 shows sections through two representative N2a cells that were either untreated or incubated with MβCD prior to staining with CTXB, fixation and immunostaining for syntaxin1a. Immunostaining for syntaxin1a (red) demonstrated that this protein is present at the plasma membrane of N2a cells but also localises to intracellular structures (see mid-section images). Syntaxin1a exhibits a punctate membrane distribution that seems to be maintained following MβCD treatment. The merged images in figure 5.13 suggest there may be less overlap between CTXB and syntaxin1a in response to MβCD treatment. To investigate this hypothesis the colocalisation and intensity dependent correlation ($R^2$ x 100) between the two channels was quantified for a set of images; the results are presented in figure 5.14.

Two further images of the base of representative cells are shown figure 5.14A. However, for these examples the merged images and the colocalisation masks generated by automatic thresholding (figure 5.14B) imply a similar degree of colocalisation in both images. When colocalisation was quantified in 16 similar images a slight decrease was observed following MβCD treatment (see figure 5.14C) but this decrease was not significant. In untreated cells the mean $R^2$ x 100 was 16 ± 2 %; the observed correlation following MβCD treatment was 12 ± 2 % (figure 5.14D). In agreement with the colocalisation analysis, this change in percentage correlation was not significant according to Student's T-test. Importantly, the observed correlation was significantly greater than the mean random correlation calculated by Costes' randomisation test (paired T-test, $p < 0.001$) and represented by the solid line on each bar in figure 5.14D. This represents another departure from the results obtained in PC12 cells, where correlation between syntaxin1a and CTXB appeared to be below random levels. In contrast, the results presented in figure 5.14 imply that localisation of a proportion of syntaxin1a may depend on CTXB but this interaction is not disrupted by MβCD.

**Figure 5.13. Localisation of syntaxin1a and CTXB in untreated and cholesterol depleted N2a cells**

N2a cells were incubated in the presence or absence of 10 mM MβCD for 30 minutes, followed by 5 minutes incubation with FITC-CTXB, fixation and immunostaining using anti-syntaxin1a (HPC-1) antibody. Images from the base, mid-section and top of a representative **A**, untreated cell and **B**, MβCD treated cell, are presented. CTXB is green, syntaxin1a is red. Scale bars = 3 μm.

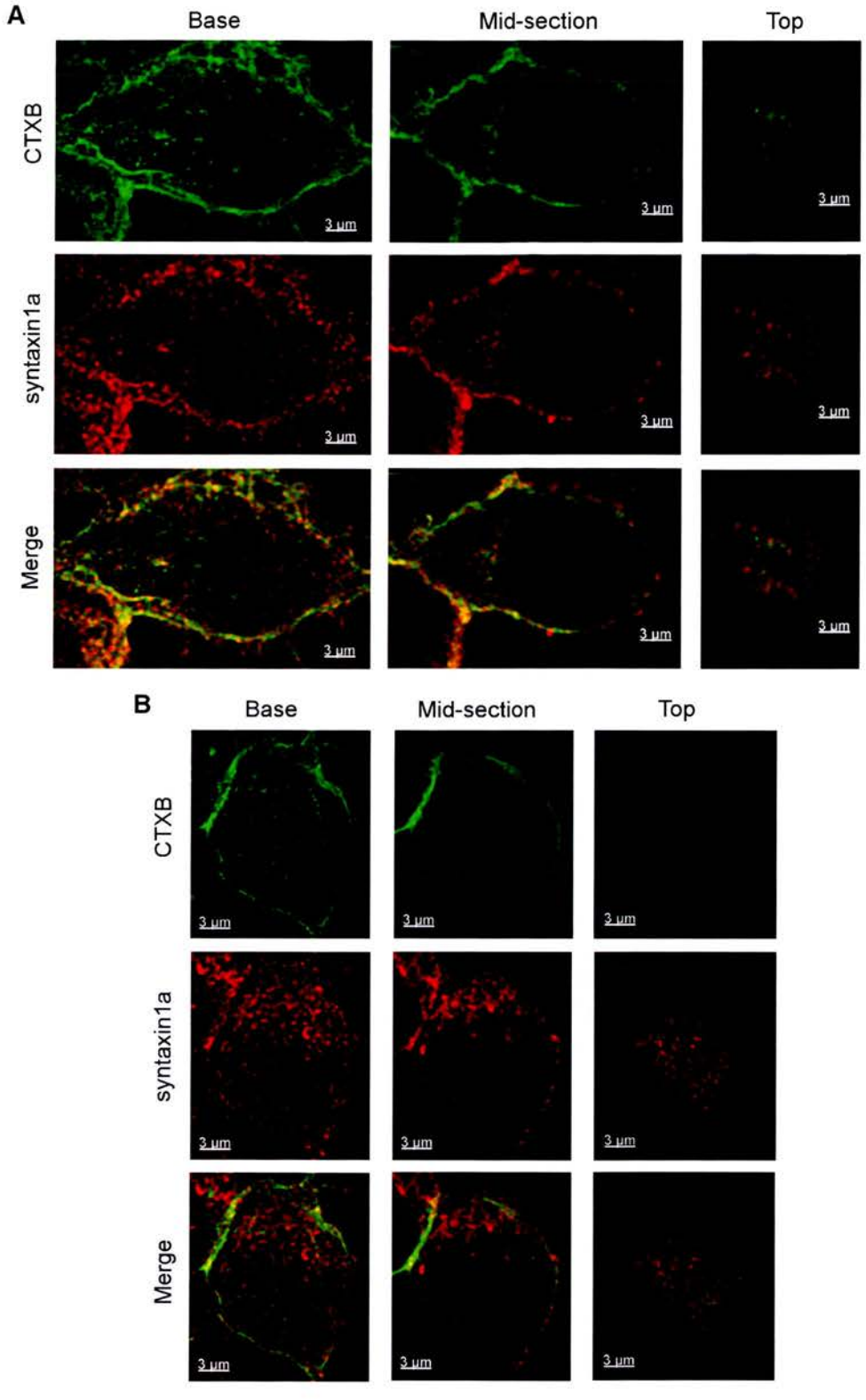


**Figure 5.13. Localisation of syntaxin1a and CTXB in untreated and cholesterol depleted N2a cells**

**Figure 5.14. The coincidence of syntaxin1a with CTXB is not altered by cholesterol depletion in N2a cells**

N2a cells were incubated in the presence or absence of 10 mM MβCD for 30 minutes, followed by 5 minutes incubation with FITC-CTXB (green), fixation and immunostaining using anti-syntaxin1a (HPC-1) antibody (red). **A** Images from the base of representative cells. The right hand panels are scatter plots of the red intensity plotted against the green intensity for each voxel in the image. **B** Colocalisation masks for the merged images in A, generated by automatic thresholding. **C** The mean percentage colocalisation of CTXB with syntaxin1a and syntaxin1a with CTXB. **D** Mean correlation ($R^2$ x 100) of the green channel with the red channel. The mean random correlation calculated by Costes' randomisation algorithm (solid line) + SEM (dashed line) are shown on the bars. Error bars correspond to SEM (n = 16). Scale bars = 2 μm.

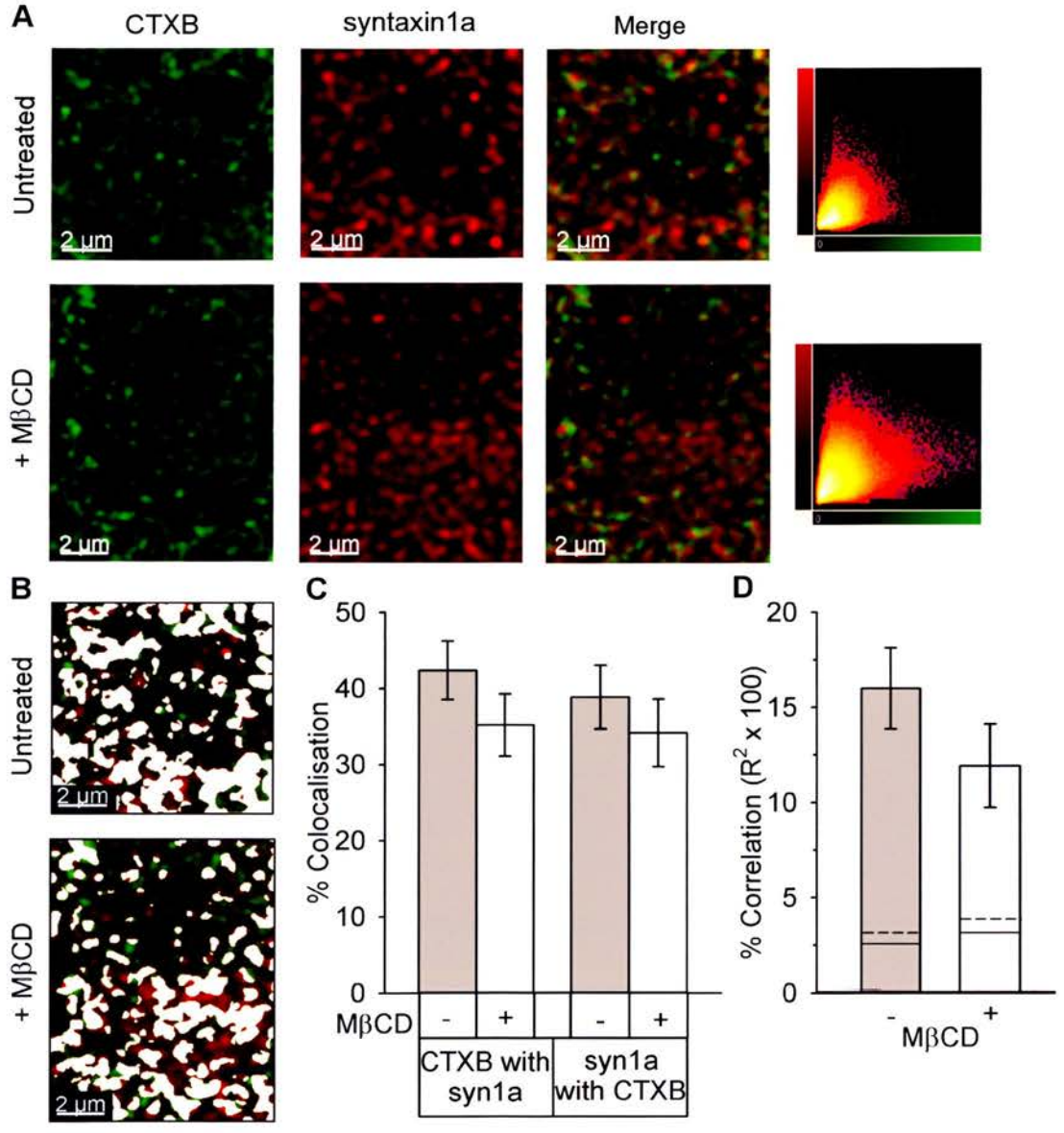


**Figure 5.14. The coincidence of syntaxin1a with CTXB is not altered by cholesterol depletion in N2a cells**

### 5.4.4. The coincidence of SNAP-25 with raft marker CTXB on the N2a plasma membrane is reduced by cholesterol depletion

The localisation of SNAP-25 relative to CTXB in N2a cells was explored following the same procedures as for 14-3-3 and syntaxin1a. Figure 5.15 shows two representative cells that were either left untreated or incubated with MβCD, prior to fixation and immunostaining. The mid-sections through both cells show the localisation of SNAP-25 to the plasma membrane but both images also illustrate that a proportion of SNAP-25 localises to internal cellular structures. SNAP-25, like syntaxin1a, presents a punctate plasma membrane distribution, which appears unchanged by cholesterol depletion. The partial dispersal of CTXB clusters in response to MβCD is evident in these images. From the merged images in figure 5.15A there seems to be some overlap between the green (CTXB) and red (SNAP-25) puncta, though much separate green and red staining is also visible. Less overlapping staining is apparent in the MβCD treated cell in figure 5.15B. However, these are only two examples; to determine whether this reduced overlap was a real and general property induced by MβCD, colocalisation and correlation ($R^2$ x 100) were quantified in a set of 20 similar images.

Enlarged images of the plasma membrane at the base of two more example cells are presented in figure 5.16A. The merged image from the untreated cell again implies a moderate degree of overlap between CTXB and SNAP-25. In contrast, the red and green puncta appear largely separate in the merged image from the MβCD treated cell. Following automatic thresholding of the images in figure 5.16A, much less of the red and green staining registers as colocalised in the MβCD treated cell compared with the untreated cell, as shown by the white masks in figure 5.16B. This result was reflected in the mean results for the whole set of images (figure 5.16C); the colocalisation of CTXB with SNAP-25 and SNAP-25 with CTXB were both significantly reduced by cholesterol depletion (Student's T-test, $p < 0.001$). The ~ 55 % colocalisation observed in untreated cells was similar to the level of colocalisation observed between these two proteins in PC12 cells. However, the decrease in colocalisation of CTXB and SNAP-25 with each other, to only ~ 25 %, suggests that

**Figure 5.15. Overlap between SNAP-25 and CTXB puncta appears to be reduced by cholesterol depletion in N2a cells**

N2a cells were incubated in the presence or absence of 10 mM MβCD for 30 minutes, followed by 5 minutes incubation with FITC-CTXB, fixation and immunostaining using anti-SNAP-25 (SMI81) antibody. Images from the base, mid-section and top of representative **A**, untreated cell and **B**, MβCD treated cell, are presented. CTXB is green, SNAP-25 is red. Scale bars = 3 μm.

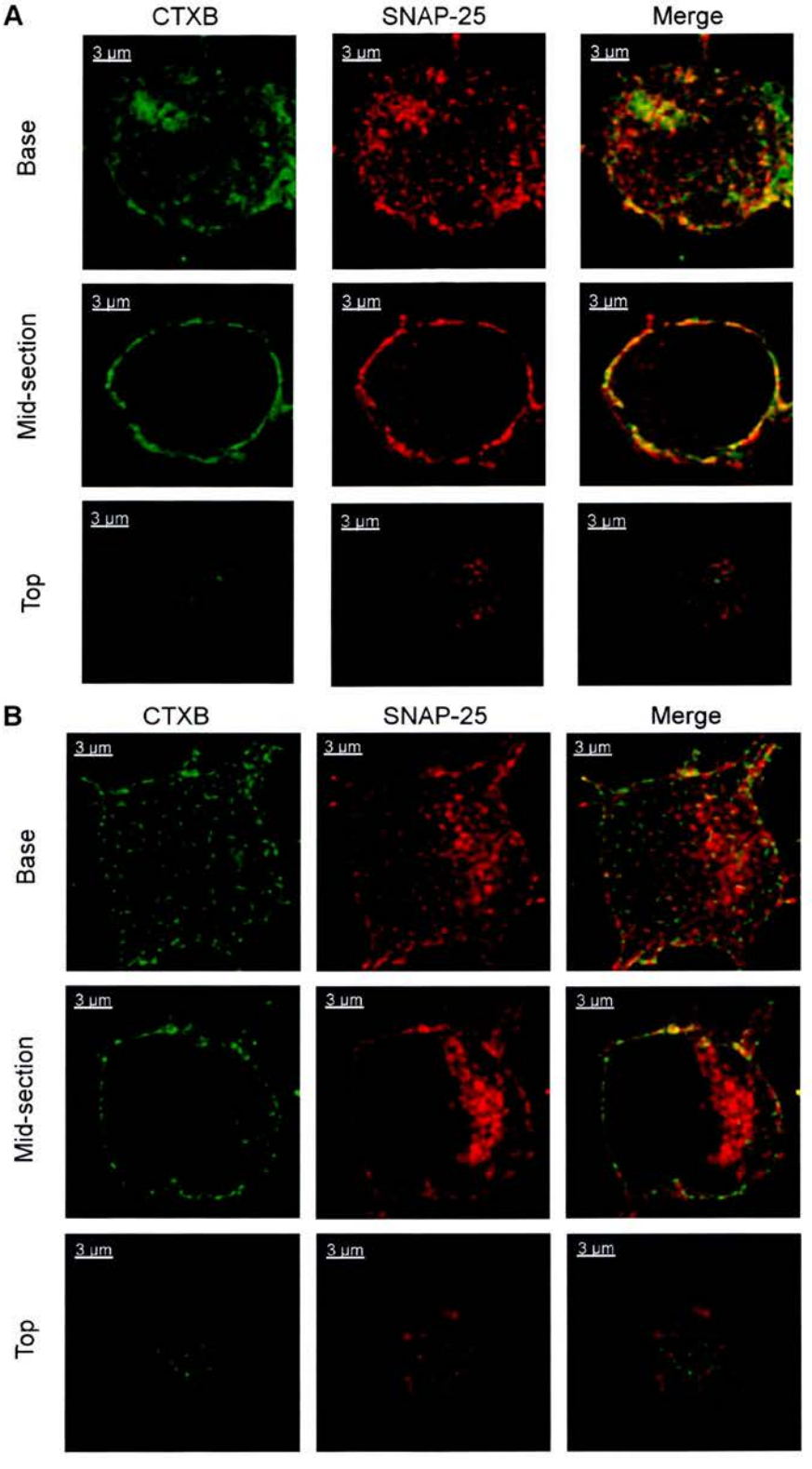


**Figure 5.15. Overlap between SNAP-25 and CTXB puncta appears to be reduced by cholesterol depletion in N2a cells**

in N2a cells cholesterol depletion causes partial segregation of these proteins from each other.

In the scatter plot (figure 5.16A) for the MβCD treated image the points are widely spread implying a low level of dependence of red intensity on green intensity. However, in the untreated scatter plot the points are more concentrated towards the diagonal implying greater correlation. Intensity dependent correlation analysis indeed demonstrated a significant decrease in the dependent localisation of SNAP-25 with CTXB (Student-s T-test, $p < 0.001$), as illustrated by figure 5.13D. $R^2 \times 100$ decreased from a mean of $20 \pm 2$ % (SEM) to a mean of $8 \pm 1$ % in response to cholesterol depletion. These values were both significantly greater than the mean random correlation (paired T-test, $p < 0.001$), calculated by Costes randomisation test (described in Chapter 2, section 2.4.6.2). This indicates that cholesterol depletion reduced but did not completely abolish dependent localisation of SNAP-25 with CTXB.

**Figure 5.16. The coincidence of SNAP-25 with CTXB is significantly decreased by cholesterol depletion of N2a cells**

N2a cells were incubated in the presence or absence of 10 mM MβCD for 30 minutes, followed by incubation with FITC-CTXB (green), fixation and immunostaining using anti-SNAP-25 (SMI81) antibody (red). **A** Images from the base of representative cells. The right hand panels are scatter plots of the red intensity plotted against the green intensity for each voxel in the image. **B** Colocalisation masks for the merged images in A, generated by automatic thresholding. **C** The mean percentage colocalisation of CTXB with SNAP-25 and SNAP-25 with CTXB. **D** Mean correlation ($R^2$ x 100) of the green channel with the red channel. The mean random correlation calculated by Costes' randomisation algorithm (solid line) + SEM (dashed line) are shown on the bars. Error bars correspond to SEM, *** $p < 0.001$, Student's T-test ($n = 20$). Scale bars = 2 μm.

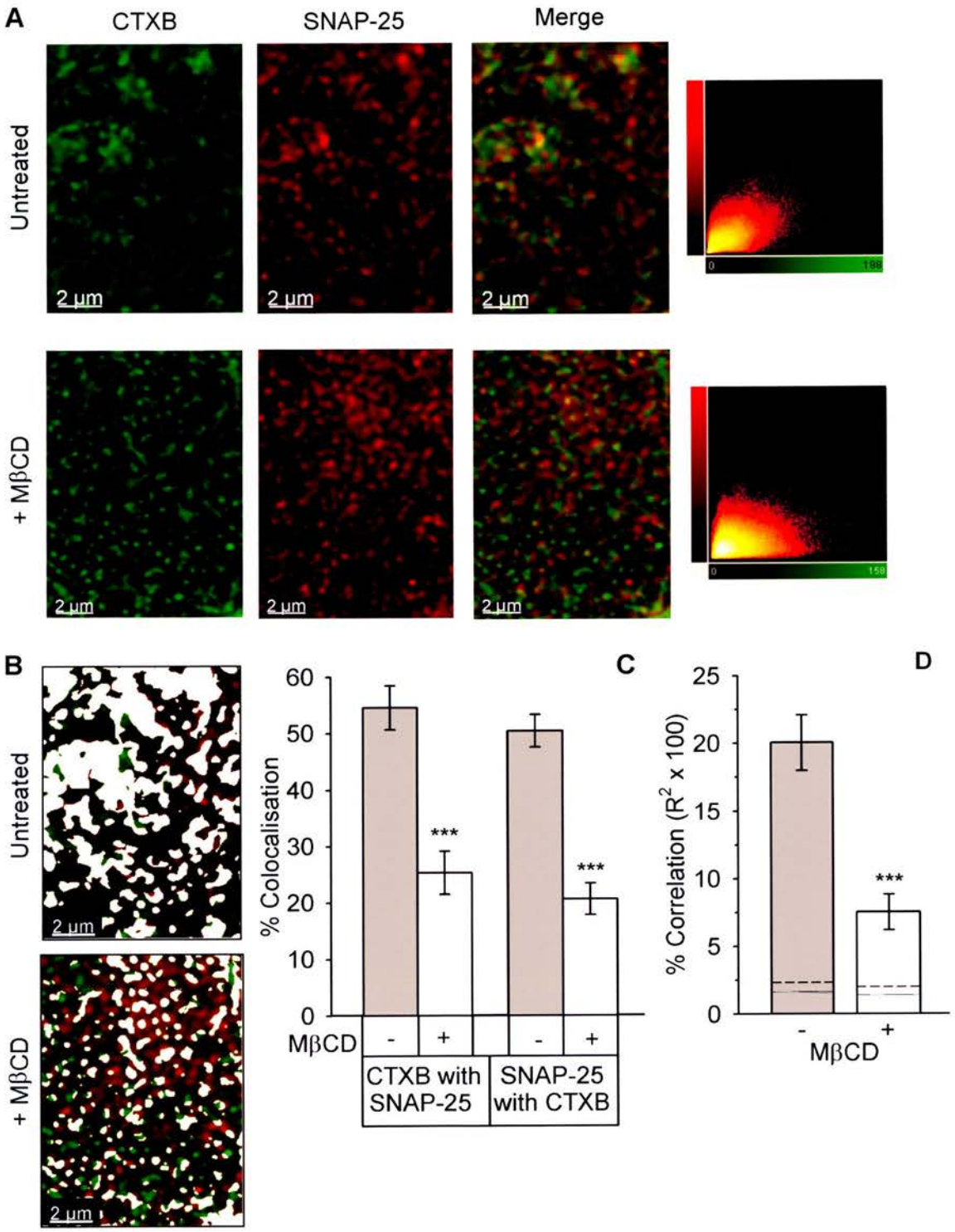


**Figure 5.16. The coincidence of SNAP-25 with CTXB is significantly decreased by cholesterol depletion in N2a cells**

## 5.5. Cholesterol depletion does not alter the size or distribution of SNARE clusters

Cholesterol depletion did not appear to alter the punctate distribution of syntaxin1a or SNAP-25 on the plasma membrane of PC12 or N2a cells, as discussed in sections 5.4.3 and 5.4.4. This observation contrasts with previous reports describing dispersal of the syntaxin1a clusters in response to cholesterol depletion with MβCD (Lang et al., 2001; Ohara-Imaizumi et al., 2004). Therefore syntaxin1a and SNAP-25 staining was analysed in more detail to determine whether cluster size or density were altered by cholesterol depletion. The FWHM cluster size and the cluster density per $\mu m^2$ were calculated (see Chapter 2, section 2.4.6.1). The results of this analysis are presented for PC12 and N2a cells in figures 5.17 and 5.18 respectively. Figures 5.17A and 5.18A show enlarged examples of the plasma membrane at the base of cells immunostained for SNAP-25 or syntaxin1a, following incubation in the presence or absence of MβCD. Little difference is apparent between the staining patterns in the four images for each cell type.

The FWHM cluster size was measured for over 100 clusters from at least 4 separate images and the distribution of cluster sizes for PC12 cells is shown in figure 5.17B. In PC12 cells, a range of cluster FWHM sizes was observed but the peak untreated cluster size (solid line) coincides with the peak MβCD treated cluster size (dashed line) for both SNARE proteins. Statistical analysis confirmed that the mean syntaxin1a cluster size of 661 ± 18 nm (SEM) was not significantly altered by cholesterol depletion, following which the mean size was 632 ± 14 nm. The mean SNAP-25 cluster size in untreated cells (755 ± 17 nm) was also not significantly different from the cluster size in MβCD treated cells (782 ± 16 nm). Interestingly, syntaxin1a clusters were significantly smaller than SNAP-25 clusters (Mann Whitney U test, $p < 0.001$).

For both SNARE proteins, the density of clusters on the PC12 plasma membrane was also unchanged by cholesterol depletion, as shown in figure 5.17C. However, the mean density of syntaxin1a clusters (1.39 ± 0.07 clusters/$\mu m^2$) was significantly

larger than the mean density of SNAP-25 clusters (1.16 ± 0.08 SNAP-25 clusters/$\mu m^2$) in untreated cells (Student's T-test, $p < 0.05$). The mean cluster density remained significantly different between the two SNARE proteins following cholesterol depletion.

The distribution of FWHM cluster sizes in N2a cells is plotted in figure 5.18B. As this plot suggests, there was also no significant difference between the cluster sizes in untreated versus MβCD treated cells for either SNARE protein in this cell type. In addition, the mean FWHM of SNAP-25 clusters (503 ± 8 nm) was not significantly different from the mean FWHM of syntaxin1a clusters (525 ± 10 nm) in untreated or MβCD treated cells. The number of clusters per $\mu m^2$ was also unchanged by MβCD treatment for both SNARE proteins (figure 5.18C). In N2a cells, unlike PC12 cells, both SNARE proteins were detected in similar size clusters.

This analysis of cluster size and density confirms that cholesterol depletion did not disperse or in any way perturb syntaxin1a or SNAP-25 clusters in either cell type.

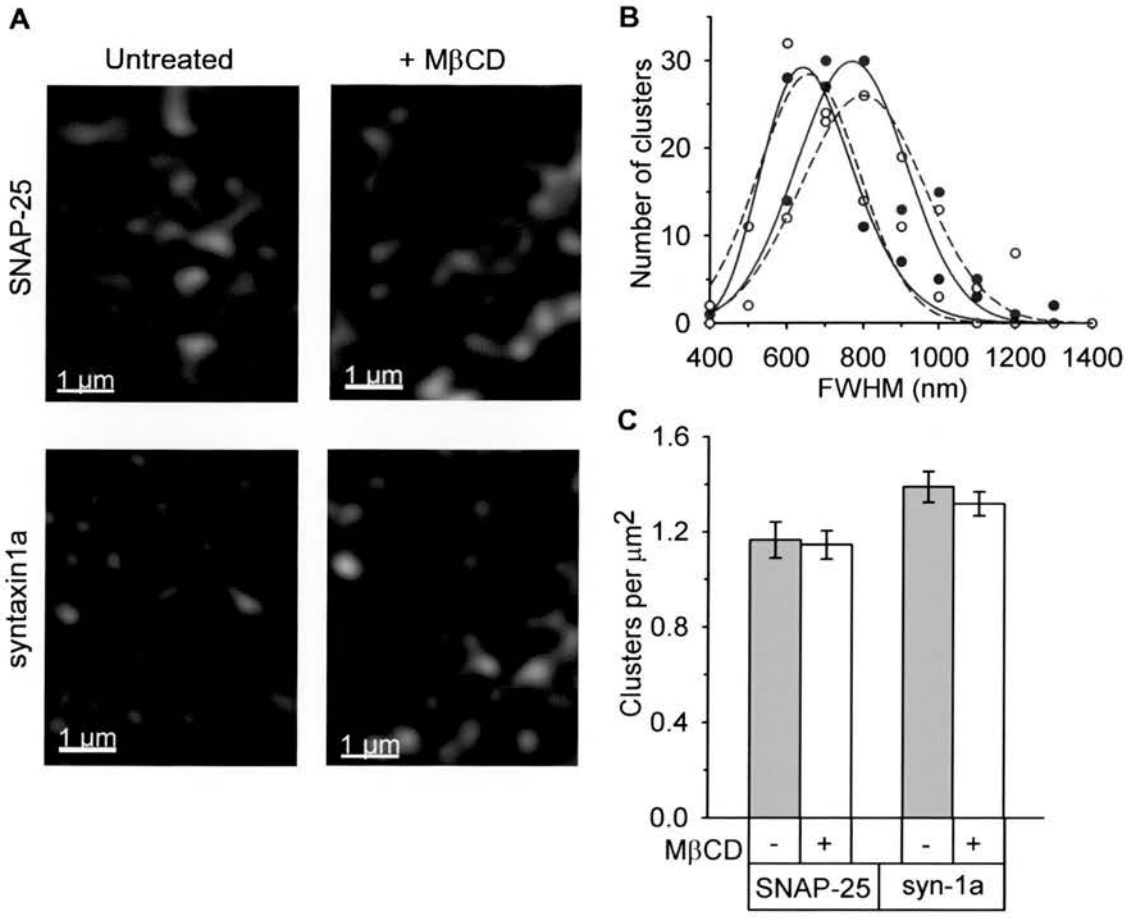


**Figure 5.17. Cholesterol depletion does not alter the size or density of SNAP-25 or syntaxin1a clusters on PC12 cell membranes**

PC12 cells were incubated with or without 20 mM MβCD for 30 minutes, fixed and immunostained for syntaxin1a or SNAP-25. **A** Images from the base of representative cells. **B** Cluster FWHM size was measured as detailed in Chapter 2, section 2.4.6.1, over 100 spots were measured from each set of images. Cluster size is plotted against number of clusters of that size ± 50 nm (solid lines/closed circles = untreated, dashed lines/open circles = MβCD treated, red = SNAP-25, blue = syntaxin1a). **C** Mean cluster density per $\mu m^2$ ± SEM (n = 12).

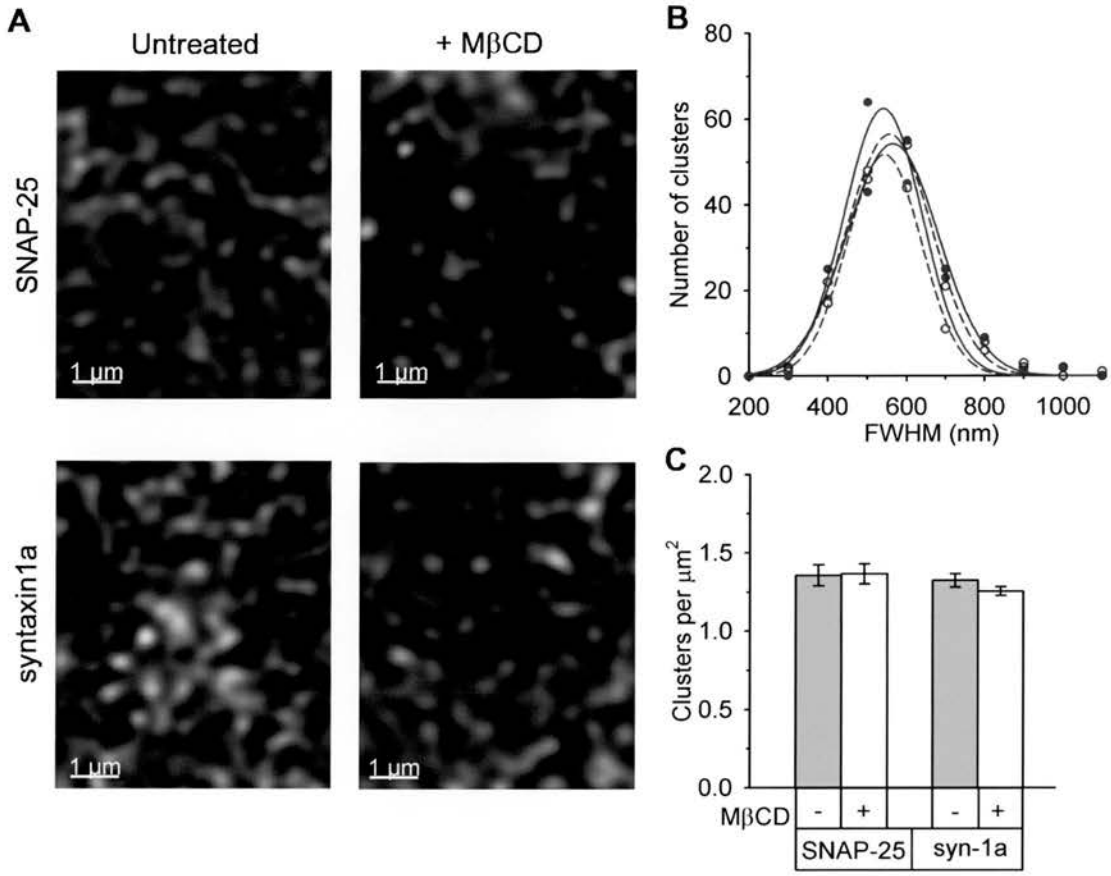


**Figure 5.18. Cholesterol depletion does not alter the size or density of SNAP-25 or syntaxin1a clusters on N2a cell membranes**

N2a cells were incubated with or without 10 mM MβCD for 30 minutes, fixed and immunostained for syntaxin1a or SNAP-25. **A** Images from the base of representative cells. **B** Cluster FWHM size was measured as detailed in Chapter 2, section 2.4.6.1, over 100 spots were measured from each set of images. Cluster size is plotted against number of clusters of that size ± 50 nm (solid lines/closed circles = untreated, dashed lines/open circles = MβCD treated, red = SNAP-25, blue = syntaxin1a. **C** Mean cluster density per $\mu m^2$ ± SEM (n = 12).

## 5.6. Summary and discussion

The main aim of this chapter was to determine whether the localisation of Thy-1, SNAP-25, syntaxin1a and 14-3-3 with lipid raft marker CTXB is cholesterol dependent, which would lend further support to the hypothesis that these proteins localise to cholesterol-rich lipid raft like-domains. The original focus of this study was to test the hypothesis that 14-3-3 associates with lipid rafts. Thy-1 was included as an established lipid raft marker and SNAP-25 and syntaxin1a as examples of inner leaflet DRM proteins. I investigated the relationship between DRM association and coincidence with CTXB for all four proteins, with regard to cholesterol dependence. A further aim was to determine whether the behaviour of these proteins is conserved between the two cell types employed in this study. The following discussion compares the results of DRM isolation and microscopy experiments and analyses differences observed in PC12 and N2a cells.

### 5.6.1. Cholesterol depletion does not reduce the DRM association of all lipid raft markers

There were strong similarities between PC12 and N2a cells concerning the effect of cholesterol depletion on the DRM association of the five proteins of interest. In both cell types no reproducible decrease in the association of CTXB with DRMs was observed. In PC12 cells, the gradient localisation of the GPI-anchored protein Thy-1 was also unaffected by MβCD treatment. Thy-1 was not investigated in N2a cells because it did not reliably associate with DRMs, as discussed in Chapter 4, section 4.1.1. Unlike CTXB and Thy-1, SNAP-25 exhibited a large reduction in DRM association in response to cholesterol depletion in both cell lines, as did 14-3-3. Syntaxin1a was the only protein that showed different results between the two cell lines. In N2a cells an increase in DRM association of this protein was detected in response to cholesterol depletion but in PC12 cells localisation was unchanged. The data agree that MβCD does not remove syntaxin1a from DRMs.

It may be that CTXB and Thy-1 remained associated with DRMs because not enough cholesterol was removed to fully disrupt lipid raft-like domains. If we use the decrease in filipin staining intensity as a measure of cholesterol depleted, then MβCD treatment deceased the cholesterol content of PC12 cells by 31 ± 3 % (n = 12) and that of N2a cells by 21 ± 3 % (n = 12). These values are in line with the results of other studies where similar concentrations of MβCD were used. Lang and co-workers found that incubation of PC12 cells with 15 mM MβCD for 30 minutes depleted ~ 40 % of cellular cholesterol (Lang et al., 2001) and 10 mM MβCD removed ~ 20 % of the cholesterol from synaptosomes (Taverna et al., 2004). Higher concentrations of MβCD (30 – 50 mM) were found to remove > 60 % of cholesterol from synaptosomes (Gil et al., 2005; Taverna et al., 2004). However, increasing the concentration of MβCD above 20 mM had a detrimental effect on cell viability in the live cell studies performed here so higher concentrations were not be employed.

An alternative method for depleting cholesterol involves inhibition of the cholesterol synthesis pathway. Lovastatin (mevinolin) is used to inhibit 3-hydroxy-3-methyl-glutaryl-coenzyme A (HMG-CoA) reductase, with the addition of the compound mevalonate to allow continued synthesis of non-sterol products (Alberts et al., 1980; Kornbrust et al., 1989; MacDonald et al., 1988). This method was investigated, using the protocol described by Keller and Simons (Keller and Simons, 1998), but a number of problems were encountered that discouraged me from employing it in place of MβCD alone. Firstly, incubation with 4 μM lovastatin and 250 μM mevalonate caused apoptosis of N2a cells within 24 hours. The effect on PC12 cells did not appear to be so severe but clearly no comparison between the two cell types would have been possible. In addition, whilst MβCD produced a marked reduction in the DRM association of SNAP-25, very little difference was discernable following incubation of PC12 cells with lovastatin/mevalonate for two days. In agreement with this observation, Keller and Simons detected only a 10 % decrease in the cholesterol content of BHK cells following lovastatin/mevalonate treatment alone. A combination of lovastatin/mevalonate plus 30 minutes incubation with MβCD just prior to DRM isolation was required for a greater decrease in cholesterol content.

Interestingly, the resistance of CTXB and Thy-1 to cholesterol depletion has been observed previously. In three separate studies, a concentration of MβCD that removed ~ 50 % of total cholesterol failed to alter the DRM localisation of CTXB (Ilangumaran and Hoessli, 1998; Panasiewicz et al., 2003; Taverna et al., 2004). It has also been reported that the majority of Thy-1 remains DRM associated following MβCD treatment (Herreros et al., 2001; Ilangumaran and Hoessli, 1998). In contrast, SNAP-25 association with DRMs was reduced by cholesterol depletion in both synaptosomes (Gil et al., 2005; Taverna et al., 2004) and PC12 cells (Chamberlain et al., 2001), in agreement with the results in figure 5.3 and 5.4. However, these studies also observed a reduction in syntaxin1a association, whereas no reduction was detected in the present study.

The different DRM association of CTXB, Thy-1, SNAP-25, syntaxin1a and 14-3-3 in response to cholesterol depletion could be explained in a number of ways. It may reflect their localisation to different raft sub-populations. It has been proposed that lipid rafts are a heterogeneous population of microdomains with respect to protein and lipid composition (Drevot et al., 2002; Madore et al., 1999; Pike, 2004). Distinct sub-populations of DRMs have been isolated either by their slightly different densities (Henke et al., 1996; Nebl et al., 2002) or by immunoaffinity purification (Brugger et al., 2004; Drevot et al., 2002; Madore et al., 1999). Interestingly, thy-1 containing DRMs could be separated from PrP containing DRMs following detergent extraction of rodent brain (Madore et al., 1999) and thy-1 DRMs contained less cholesterol than PrP DRMs (Brugger et al., 2004). Perhaps in PC12 cells thy-1 resides in microdomains that are less susceptible to cholesterol depletion and SNAP-25 and 14-3-3 in more cholesterol-sensitive microdomains. Clearly however, if CTXB is only present in a sub-set of raft-like microdomains then it is not a useful marker.

Alternatively, the different gradient localisation of the five proteins following cholesterol depletion may reflect their different affinities for a more ordered membrane phase. Hao and co-workers observed increased segregation of ordered and fluid domains following cholesterol depletion of CHO cells, as assessed by

microscopy of fluorescently labelled lipid probes (Hao et al., 2001). It has been suggested that an important role of cholesterol might be to prevent the separation of cell membranes into a fluid glycerophospholipid phase and a solid sphingolipid phase (McElhaney, 1982; Ohvo-Rekila et al., 2002). Thus cholesterol depletion may not destroy liquid ordered membrane domains but instead change their composition. CTXB and thy-1 may have a high affinity for this new ordered phase, in contrast to SNAP-25 and 14-3-3 that appear to partition into detergent soluble membrane.

The third possibility to consider is that DRMs are formed during the detergent extraction procedure and their lipid composition does not represent any microdomains present *in vivo*. Munro proposes that TX-100 preferentially extracts the certain lipids in the outer leaflet of the bilayer, whilst fully solubilising the inner leaflet (Munro, 2003). Particular proteins may have an affinity for the unnatural composition of the resulting vesicles and therefore be found in DRMs. Removing membrane cholesterol may differentially alter the affinity of various proteins for these vesicles.

### 5.6.2. CTXB plasma membrane distribution is altered by cholesterol depletion

CTXB was used throughout this study as a marker for lipid raft-like domains. This molecule binds to a glycosphingolipid, GM1 (Critchley et al., 1982; Holmgren, 1973) and has been used extensively as a lipid raft marker (Fra et al., 1994; Harder et al., 1998; Janes et al., 1999; Locke et al., 2005; Magee et al., 2005; Mitchell et al., 2002; Stauffer and Meyer, 1997; Stuermer et al., 2001; Yi et al., 2005). Importantly, model membrane studies have demonstrated the localisation of CTXB-labelled GM1 to the $L_o$ phase (Bacia et al., 2004; Dietrich et al., 2001a; Dietrich et al., 2001b; Kahya et al., 2005; Kahya et al., 2003; Wang and Silvius, 2003).

CTXB distribution on the plasma membrane of PC12 and N2a cells was investigated by confocal microscopy. Table 5.1 summarises the analysis of CTXB staining presented in figures 5.5 and 5.10. MβCD did not induce complete dispersal of CTXB

clusters in either cell type but there were significant changes in particular properties of the clusters. This supports the view that cholesterol depletion perturbs lipid raft-like domains but microdomains of some sort remain, perhaps with altered lipid order as suggested by the work of Hao and co-workers (Hao et al., 2001), discussed in the previous section.

**Table 5.1 Effect of cholesterol depletion on CTXB staining in PC12 and N2a cells**

| | (−) untreated (+) MβCD | FWHM (nm) | Cluster density per μm$^2$ | Total intensity per μm$^2$ (arbitary units) |
|---|---|---|---|---|
| PC12 cells | − | 544 ± 16 | 1.93 ± 0.08 | 5.6 ± 0.6 |
| | + | 585 ± 15 * | 1.77 ± 0.09 | 2.7 ± 0.4 *** |
| N2a cells | − | 527 ± 15 | 1.26 ± 0.06 | 5.7 ± 0.6 |
| | + | 407 ± 8 *** | 1.53 ± 0.09 * | 4.8 ± 0.4 |

Mean values ± SEM. Significantly different from untreated control * $p < 0.05$, *** $p < 0.001$.

Cholesterol depletion had rather different effects on CTXB distribution in the two cell types. In PC12 cells, the main effect of cholesterol depletion was to decrease the total intensity of CTXB staining, whilst leaving clusters intact, implying that the number of GM1 molecules on the plasma membrane is reduced. This suggests that trafficking of GM1 might be affected by cholesterol depletion. In two cell types internalisation of CTXB to the Golgi complex was inhibited by cholesterol depletion (Nichols et al., 2001; Orlandi and Fishman, 1998) and cholesterol depletion also inhibited the trafficking of $L_o$ phase preferring lipid analogues (Hao et al., 2004). However, these studies describe plasma membrane accumulation of the lipids, whereas a loss of GM1 from the membrane is implied by the PC12 cell data.

CTXB clusters in PC12 and N2a cells are of a similar FWHM size in untreated cells, as shown in table 5.1. However, following MβCD treatment there is a slight increase in PC12 cluster size, which contrasts with the large decrease in cluster size in N2a cells. This decrease in cluster size in N2a cells was accompanied by an increase in cluster density, suggesting that cholesterol depletion partially disrupts CTXB clusters in this cell type. This response agrees better with the predicted dispersal of lipid rafts by cholesterol depletion. The membrane distribution of CTXB following cholesterol

depletion has not been extensively investigated. However, a FRET study in COS-7 cells does support clustering of CTXB and reported a decrease in FRET between CTXB molecules in response to cholesterol depletion, suggesting some dispersal of these clusters (Nichols, 2003).

An additional observation regarding CTXB clustering in PC12 cells concerns the original experiments carried out to characterise CTXB staining in live and fixed cells (Figure 4.4, Chapter 4). The FWHM size of CTXB clusters measured in this experiment was on average larger than the cluster size recorded for untreated PC12 cells in figure 5.3. In this chapter MBCD treatment was carried out in serum-free media, as serum contains a high concentration of cholesterol. The untreated control cells were therefore also incubated in serum-free media during the 30 minute treatment period. However, in Chapter 4 cells were incubated in serum containing media until fixation. According to theories concerning the stimulus induced clustering of lipid rafts (Hancock, 2006; Kusumi et al., 2004; Subczynski and Kusumi, 2003), the growth factors in serum might have produced additional clustering of membrane microdomains. It would certainly be interesting to explore this possibility in more detail.

### 5.6.3. Clustered SNARE proteins are not dispersed by cholesterol depletion

Previous studies have suggested that the clustering of syntaxin1a is dependent on cholesterol (Lang et al., 2001; Ohara-Imaizumi et al., 2004). However, in this study, cholesterol deletion had no effect on syntaxin1a cluster size or density on the plasma membrane of PC12 or N2a cells, as demonstrated by figures 5.17 and 5.18 and the results summarised in table 5.2 below. There was also no significant change in the distribution of SNAP-25 in response to MβCD treatment.

**Table 5.2 Size and density of SNARE protein clusters in PC12 and N2a cells**

| | (−) untreated (+) MβCD | PC12 FWHM (nm) | PC12 Cluster density per $\mu m^2$ | N2a FWHM (nm) | N2a Cluster density per $\mu m^2$ |
|---|---|---|---|---|---|
| SNAP-25 | − | 755 ± 17 | 1.16 ± 0.08 | 503 ± 8 | 1.37 ± 0.07 |
| | + | 782 ± 16 | 1.14 ± 0.06 | 514 ± 10 | 1.37 ± 0.06 |
| Syntaxin | − | 661 ± 18 | 1.39 ± 0.07 | 525 ± 9 | 1.32 ± 0.04 |
| | + | 632 ± 14 | 1.32 ± 0.05 | 520 ± 10 | 1.25 ± 0.03 |

Mean values ± SEM.

Lang and co-workers produced the clearest evidence of syntaxin1a cluster dispersal by MβCD (Lang et al., 2001), however these authors used membrane sheets rather than intact cells. A brief ultrasound pulse was used to destroy the upper part of the PC12 cells, leaving only the basal plasma membrane adhering to the coverslip intact (Lang, 2003). Immunostaining for syntaxin1a showed complete dispersal of clusters after 30 minutes incubation with 15 mM MβCD but as membrane sheets were used MβCD had direct access to the inner leaflet of the plasma membrane. The same study also investigated intact PC12 cells, however it is difficult to assess whether complete dispersal of syntaxin1a cluster was achieved as only equatorial sections through cells are presented rather than images of the basal plasma membrane. Ohara-Imaizumi and co-workers also claimed that 10 mM MβCD disperses syntaxin1a clusters in MIN6 insulinoma cells (Ohara-Imaizumi et al., 2004) but the images they present do not show a convincing dispersal; clusters are still visible but the staining intensity appears decreased. Predescu and co-workers also found that clusters of related SNARE proteins, SNAP-23 and syntaxin-4, were not fully dispersed by 15 mM MβCD in intact endothelial cells, though the size of the clusters was increased (Predescu et al., 2005). Thus the effect of cholesterol depletion on SNARE protein clustering is somewhat ambiguous. Furthermore, two recent studies demonstrated that clustering of syntaxin1a and SNAP-25 requires an intact SNARE motif (Rickman et al., 2004; Sieber et al., 2006). Disruption of the SNARE motif dispersed clusters, indicating that localisation to cholesterol-rich microdomains is not sufficient for maintenance of clusters though this could play a secondary role.

Syntaxin1a and SNAP-25 clusters were ~ 500 nm in diameter in N2a cells and ~ 600 – 800 nm in PC12 cells. Other studies have reported cluster sizes of 200 – 300 nm in PC12 and MIN6 cells or ~ 700 nm in chromaffin cells (Lang et al., 2001; Ohara-Imaizumi et al., 2004; Rickman et al., 2004). These studies all determined the FWHM size from immunostained images and corrected for image convolution by measuring the PSF. However, there does not seem to be good agreement between all four studies despite the use of similar protocols.

Whilst syntaxin1a and SNAP-25 clusters were of a similar size and density in N2a cells, in PC12 cells syntaxin1a clusters were significantly smaller than SNAP-25 clusters (see figure 5.17 and table 5.2). This phenomenon was also observed in PC12 cells by Lang and co-workers (Lang et al., 2001). They suggest that not all SNAP-25 is in binary clusters with syntaxin1a and that SNAP-25 may be more diffusely distributed because it is more mobile in the membrane due to its palmitoyl rather than transmembrane mode of anchoring.

The results presented in this study imply that the integrity of syntaxin1a and SNAP-25 clusters does not depend on cholesterol-rich microdomains, however the localisation of these clusters relative to $L_o$ domains could have implications for their function.

### 5.6.4. The cholesterol depletion method

Cholesterol depletion has gained widespread acceptance as a method for confirming that a protein or process depends on lipid rafts. However, some researchers urge caution in interpretation of cholesterol depletion studies (Edidin, 2003; Hancock, 2006; McMullen et al., 2004). A number of studies have reported that MβCD affects cellular processes unrelated to putative lipid rafts. Clathrin dependent endocytosis was inhibited by MβCD mediated cholesterol depletion (Pichler and Riezman, 2004; Rodal et al., 1999; Subtil et al., 1999) and the permeability of the bilayer to small molecules and ions was also reduced (Grunze and Deuticke, 1974; Launikonis and

Stephenson, 2001; Munro, 2003). Recently, MβCD has been suggested to inhibit the lateral diffusion of membrane proteins (Goodwin et al., 2005; Kwik et al., 2003; Shvartsman et al., 2006). Some authors maintain that this inhibition is specific to MβCD as they did not observe the same effect following metabolic inhibition of cholesterol synthesis by lovastatin or compactin (Goodwin et al., 2005; Shvartsman et al., 2006), whilst others report inhibition of protein diffusion in response to either method of cholesterol depletion (Kwik et al., 2003). The decrease in the lateral mobility of proteins is suggested to depend on observed effects on actin cytoskeleton organisation (Kwik et al., 2003). Thus the possibility should be considered that MβCD may have effects additional to disruption of lipid raft-like domains.

It is interesting that cholesterol depletion may perturb the actin cytoskeleton (Grimmer et al., 2002; Kwik et al., 2003) as interactions between this structure and lipid rafts have been reported (Foger et al., 2000; Harder and Simons, 1999; Holowka et al., 2000; Laux et al., 2000; Oliferenko et al., 1999; Rodgers and Zavzavadjian, 2001). The actin cytoskeleton has also been implicated in membrane compartmentalisation by the SPT studies of Kusumi and co-workers (Kusumi et al., 2004; Kusumi and Suzuki, 2005; Subczynski and Kusumi, 2003). They propose that membrane proteins anchored to the cytoskeleton form membrane fences, or corrals, that transiently trap laterally diffusing proteins.

The reduction in the staining intensity of cholesterol binding agent filipin demonstrated that cholesterol is depleted from PC12 and N2a cells by MβCD treatment. However, the studies discussed above suggest that MβCD could have effects additional to cholesterol depletion and may also affect membrane compartmentalisation via the actin cytoskeleton.

### 5.6.5. Cholesterol depletion reduces the coincidence of SNAP-25 with CTXB in N2a cells but other DRM proteins are unaffected

Throughout this chapter two complimentary methods were employed for the analysis of overlap in fluorescent two channel images. Interpretation of the resulting values was discussed in detail in Chapter 2, section 2.4.6.2 and Chapter 4, section 4.4. The colocalisation analysis was consistently in good agreement with Pearson's correlation analysis concerning the relative coincidence of two proteins. This is probably due to the automatic thresholding algorithm employed for colocalisation analysis (described in Chapter 2, section 2.4.6.2), which employs Pearson's coefficient, R to define the thresholds as the intensities below which there is no correlation between the two channels (R = 0). Colocalisation analysis was included as well as Pearson's correlation analysis to aid interpretation of $R^2$ x 100 values and to determine the contribution of each channel or protein to the observed overlap. However, there was no significant difference between the percentage colocalisation of the red with the green and the green with the red channels in any of the images analysed. As discussed in Chapter 4, this may be because all the proteins of interest presented a punctate staining pattern. If the staining patterns were very different, for example a diffuse staining in the red channel and a punctate staining in the green channel, then different percentage contributions to overlap would be more likely.

As very good agreement was observed between the colocalisation and Pearson's correlation analyses I will concentrate on the results of Pearson's correlation analysis for this discussion. A decrease in $R^2$ x 100% can be interpreted as a decrease in the dependent localisation of the two proteins. The results of the correlation analysis carried out in this chapter are summarised in Table 5.3.

**Table 5.3 Summary of coincidence of DRM proteins with CTXB**

| | (−) untreated (+) MβCD | PC12 $R^2$ x 100% | PC12 Paired T-test Randomised vs observed | N2a $R^2$ x 100% | N2a Paired T-test Randomised vs observed |
|---|---|---|---|---|---|
| Thy-1 | − | 25.5 | $p < 0.001$ | - | - |
| | + | 34.9 * | $p < 0.001$ | - | - |
| SNAP-25 | − | 23.2 | $p < 0.001$ | 20.1 | $p < 0.001$ |
| | + | 22.8 | $p < 0.001$ | 7.5 *** | $p < 0.001$ |
| Syntaxin | − | 11.5 | $p = 0.72$ | 16.0 | $p < 0.001$ |
| | + | 12.0 | $p = 0.41$ | 11.9 | $p < 0.001$ |
| 14-3-3 | − | 13.3 | $p = 0.004$ | 5.1 | $p = 0.004$ |
| | + | 12.5 | $p = 0.022$ | 4.2 | $p = 0.021$ |

Mean values. Significantly different from untreated control * $p < 0.05$, *** $p < 0.001$.

N2a and PC12 cells exhibited similarities with respect to the relative levels of coincidence observed in untreated cells (see table 5.3). The coincidence of SNAP-25 with CTXB was significantly higher than the coincidence of syntaxin1a or 14-3-3 with CTXB in both cell types. This implies that SNAP-25 has a higher affinity for CTXB clusters, suggested to represent lipid $L_o$ domains. However the localisation of syntaxin1a differs between the cell lines according to correlation analysis. In PC12 cells, the correlation between syntaxin1a and CTXB is below random levels but in N2a cells correlation is significantly greater than random correlation (see table 5.3), suggesting that syntaxin1a localisation is partially dependent on CTXB localisation.

The observed correlation between 14-3-3 and CTXB in both cell types is very low but is significantly greater than random correlation values calculated from the same set of images. The conclusion that 14-3-3 or syntaxin1a and CTXB show a low level of dependent localisation relies entirely on the randomisation method. The method used throughout this chapter involved splitting the red channel image into tiles of PSF width (~ 300 nm), rearranging these tiles and calculating R with respect to the original green channel (Costes' randomisation method, described in Chapter 2, section 2.4.6.2). Alternatives to this method involve rotating, flipping or shifting one channel and re-calculating R. However, these methods all gave lower mean R random values. Therefore I decided to use Costes' randomisation method to provide the most conservative estimate of true correlation. It is possible though that this

method still underestimates the contribution of random variation to the observed R, in which case localisation of 14-3-3 to CTXB-labelled domains might not be supported. An alternative randomisation method to explore would be to separate and randomise individual puncta. Unfortunately this is not a trivial undertaking; automatic identification of individual puncta of different intensities and sizes was beyond the scope of any software available to me but development of this method would be interesting.

In PC12 cells, none of the four proteins investigated showed any reduction in correlation with CTXB following cholesterol depletion. Though some change in microdomain lipid composition is suggested by the observed decrease in CTXB binding, this alteration does not seem severe enough to affect the preference of SNAP-25 or 14-3-3 for these microdomains. Two alternative conclusions present themselves; either not enough cholesterol was depleted to significantly perturb lipid raft-like domains or the localisation of SNAP-25 and 14-3-3 to these domains is cholesterol independent. Interestingly however, dependent localisation of Thy-1 with CTXB actually increased slightly in response to cholesterol depletion (see Table 5.3). This may represent an increased affinity of Thy-1 for microdomains of altered lipid composition produced by depleting cholesterol. Hao and co-workers reported that cholesterol depletion increases segregation of ordered and fluid domains (Hao et al., 2001), as discussed in section 5.6.1.

Despite the partial dispersal of CTXB clusters induced by cholesterol depletion of N2a cells, neither syntaxin1a nor 14-3-3 exhibited any significant reduction in coincidence with CTXB in N2a cells (see table 5.3). This suggests that the CTXB dependent localisation of these proteins does not rely on cholesterol or that not enough cholesterol was depleted to perturb their localisation. Interestingly, SNAP-25 showed a significant reduction in coincidence with CTXB (see table 5.3). However, interpretation of this result is complicated firstly by the fact that SNAP-25 clusters were not perturbed by MβCD. Secondly, if we scrutinise the merged image of an untreated cell membrane in figure 5.16A it appears that much of the overlap between CTXB and SNAP-25 clusters is partial overlap, rather than spots exactly

superimposed. Considering that the limit of optical resolution is 200 nm, the centre of mass of each spot could be 200 nm apart (as discussed in Chapter 4). Therefore SNAP-25 may be in clusters adjoining rather than within CTXB-labelled $L_o$ domains. However, the cholesterol dependence of this proximity indicates that SNAP-25 clusters have an affinity for CTXB clusters that relies on the presence of cholesterol.

The unaltered coincidence of SNAP-25 with CTXB in PC12 cells conflicts with the decrease observed in N2a cells. However, cholesterol depletion also has very different effects on CTXB distribution in the two cell types; in N2a cells CTXB clusters are partially dispersed, whereas in PC12 cells CTXB cluster size increased slightly (see table 5.1). This implies that cholesterol depletion, with the particular concentrations of MβCD used here, may differently affect cholesterol dependent domains in the two cell types.

The reduced coincidence of SNAP-25 with CTXB in N2a cells agrees with the loss SNAP-25 from N2a DRMs following cholesterol depletion (see figure 5.4). The unaltered coincidence of syntaxin1a and Thy-1 with CTXB also agrees with their conserved DRM localisation following MβCD treatment (figures 5.3 and 5.4). However, the unchanged coincidence of 14-3-3 with CTXB in both cell types and SNAP-25 with CTXB in PC12 cells (see table 5.3) contrasts strongly with the reduction in DRM association of these proteins on cholesterol depletion (figures 5.3 and 5.4). Thus there are clear discrepancies between the association of particular proteins with CTXB enriched DRMs and CTXB-labelled domains in intact cells. These results call into question whether DRMs really represent pre-existing domains in the plasma membrane.

In summary, the findings presented in this chapter do not support cholesterol dependent colocalisation of 14-3-3 with CTXB in either of the cell types investigated. Whilst CTXB clusters were perturbed by cholesterol depletion in both PC12 and N2a cells, the effects of this treatment differed between the two cell types and between the four DRM-associated proteins studied.

# Chapter 6: General discussion

# 6. General discussion

The initial aim of this investigation was to explore the potential association of 14-3-3 with lipid raft-like domains suggested by preliminary DRM isolation experiments in this laboratory. Plasma membrane localisation of 14-3-3 has previously been reported but this aspect of 14-3-3 biology is poorly characterised. The association of 14-3-3 with lipid raft-like domains could influence a number of processes in which both 14-3-3 and lipid rafts have been implicated. The SNARE proteins syntaxin1a and SNAP-25 were originally included in this study as examples of DRM proteins associating with the inner leaflet of the plasma membrane, for comparison with 14-3-3. However, results obtained during the course of this work also provide some insights into the membrane compartmentalisation of syntaxin1a and SNAP-25.

This chapter summarises the findings reported in this thesis concerning both the plasma membrane distribution of 14-3-3 and SNAREs, determined by a combination of DRM isolation and CLSM of CTXB-labelled cells. Whilst cholesterol dependent membrane compartmentalisation of 14-3-3 is not supported, SNAP-25 localisation may be influenced by cholesterol. The results imply that different mechanisms govern the membrane distribution of syntaxin1a and SNAP-25 and the implications of this are discussed. Observations from this study regarding the DRM preparation procedure are also considered with respect to concerns that DRMs may not represent pre-existing membrane domains. The last section describes experiments that might further elucidate the role of cholesterol-dependent membrane compartments in the regulation of SNARE protein distribution at the plasma membrane. Investigation into the membrane compartmentalisation of 14-3-3 in response to growth factor stimulation is also considered.

## 6.1. The spatial distribution of 14-3-3 at the membrane

### 6.1.1. Summary of results

The investigations described in Chapters 3 and 4 demonstrated that a proportion of 14-3-3 associates with DRMs isolated from rat brain extract, PC12 and N2a cells. Cholesterol depletion experiments indicated that the presence of 14-3-3 in DRMs relies on the cholesterol-rich nature of this membrane preparation, which is often taken as evidence of localisation to lipid raft-like domains (Foster et al., 2003; Simons and Toomre, 2000). 14-3-3 isoform specificity was evident in the interaction with DRMs; the highly related 14-3-3 isoforms γ and η showed increased partitioning into DRMs compared with 14-3-3 β, ε and ζ. The competitive inhibitor peptide difopein masks the 14-3-3 amphipathic binding groove and demonstrated that association of 14-3-3 with DRMs is likely to depend on interaction with another DRM associated protein, as predicted from the lack of a membrane anchoring domain in 14-3-3. Taken together these results provide good evidence for the specific localisation of a proportion of 14-3-3 to DRMs.

Concerns regarding whether DRMs represent physiological membrane domains (Edidin, 2001; Heerklotz, 2002; McMullen et al., 2004) led me to investigate the colocalisation of 14-3-3 with a lipid raft marker, CTXB, in intact cells by immunostaining and CLSM. CTXB binds to the glycosphingolipid GM1, which is concentrated in caveolae and DRMs (Badizadegan et al., 2000a; Ilangumaran and Hoessli, 1998; Parton, 1994; Prinetti et al., 2000) and partitions into the $L_o$ phase in model membranes (Bacia et al., 2004; Dietrich et al., 2001a; Dietrich et al., 2001b; Kahya et al., 2005; Kahya et al., 2003; Wang and Silvius, 2003). The coincidence of 14-3-3 with CTXB was compared with that of an established lipid raft marker, the GPI-anchored protein Thy-1. Both CTXB and Thy-1 were located almost exclusively in PC12 cell DRMs but 100 % colocalisation was not observed between these two proteins in intact cells. As 14-3-3 is a cytosolic protein, its association with lipid raft-like domains would be expected to occur at the inner leaflet of the plasma membrane.

The mechanism of coupling of lipid rafts across the bilayer is an unresolved issue (discussed in Chapter 1, section 1.1.4.2); therefore inner leaflet DRM-associating proteins SNAP-25 and syntaxin1a were also investigated by imaging for comparison with Thy-1 and 14-3-3. SNAP-25 coincided with CTXB to a similar extent as Thy-1 in PC12 cells. However, 14-3-3 showed a much lower level of correlation with CTXB in two cell types, though the observed correlation was significantly greater than random correlation as assessed by Costes randomisation test (described in Chapter 2, section 2.4.6.2).

To determine whether the low level coincidence of 14-3-3 with CTXB was dependent on cholesterol, MβCD was employed to deplete cholesterol prior to CTXB-labelling and immunostaining of PC12 and N2a cells. This treatment did not disperse CTXB clusters in PC12 cells as might be expected if CTXB domains rely on cholesterol. Filipin staining demonstrated that membrane cholesterol content was decreased but it could be that not enough cholesterol was removed to disrupt CTXB clusters. Alternatively, Hao and co-workers suggested that cholesterol depletion increases de-mixing of fluid and ordered membrane domains (Hao et al., 2001), as discussed in Chapter 5, section 5.6.1; thus MβCD may not disperse domains but instead change their lipid composition. The slight increase in CTXB cluster size and decrease in CTXB staining intensity support some perturbation of CTXB-labelled domains in PC12 cells. Furthermore, the coincidence of Thy-1 with CTXB was increased following cholesterol depletion, though the coincidences of SNAP-25, syntaxin1a and 14-3-3 with CTXB were unaltered.

In N2a cells, MβCD significantly reduced CTXB cluster size and increased cluster density, implying a partial dispersal of clusters. SNAP-25 demonstrated a decreased coincidence with these modified CTXB clusters but the coincidence of 14-3-3 with CTXB was again unchanged. Imaging of intact cells therefore is not consistent with cholesterol dependent coincidence of 14-3-3 with CTXB clusters, in direct contrast with the observed loss of 14-3-3 from CTXB-rich DRMs following MβCD treatment.

### 6.1.2. Implications for the membrane compartmentalisation of 14-3-3

Lipid raft markers Thy-1 and CTXB were concentrated together in DRMs but the only partial coincidence of Thy-1 with CTXB in intact cells is inconsistent with the stable association of both proteins with the same lipid raft-like domains. Other immunostaining studies have produced mixed results, from a high degree of colocalisation between Thy-1 and CTXB (Harder et al., 1998; Stuermer et al., 2001) to largely independent localisation of these two proteins (Fra et al., 1994; Wilson et al., 2004), though none of these studies quantified the extent of coincidence. The range of colocalisation results obtained may be due in part to cell type specific differences but may also reflect the transient nature of protein association with membrane domains indicated by SPT studies (Dietrich et al., 2002; Kusumi et al., 2004; Sheets et al., 1997; Subczynski and Kusumi, 2003). Imaging of fixed and immunostained cells would produce an averaged picture of the dynamic membrane environment. Thus the partial coincidence of Thy-1 with CTXB may reflect the dynamic partitioning of these molecules into and out of different membrane compartments. The higher coincidence of Thy-1 and SNAP-25 with CTXB, compared with 14-3-3, may therefore represent the relatively greater affinity of Thy-1 and SNAP-25 for the same domains as CTXB. 14-3-3 is likely to spend less time in domains defined by CTXB labelling.

Cholesterol depletion increased the coincidence of Thy-1 with CTXB in PC12 cells and decreased the coincidence of SNAP-25 with CTXB in N2a cells. These results imply that the membrane cholesterol concentration influences the membrane distribution of these two proteins. Gri and co-workers also demonstrated that MβCD alters the co-clustering of lipid raft markers with CTXB in Jurkat T cells (Gri et al., 2004). Clustering of GM1, using CTXB plus anti-CTXB antibody, caused a redistribution of lipid raft markers GPI-GFP and palmitoylated CFP to CTXB clusters and this co-clustering was inhibited by MβCD treatment. Altered membrane compartmentalisation of Thy-1 in response to cholesterol depletion was also detected by SPT; transient confinement of Thy-1 in the plasma membrane of mouse fibroblasts became less frequent following MβCD treatment (Dietrich et al., 2002).

In the present study however, no change in the coincidence of 14-3-3 with CTXB was observed following cholesterol depletion. This was true of both N2a and PC12 cells despite the fact that cholesterol depletion perturbed CTXB clusters in both cells types and altered the coincidence of putative lipid raft proteins Thy-1 and SNAP-25 with CTXB. It is possible that the affinity of 14-3-3 for CTXB labelled domains is not as sensitive to cholesterol as that of Thy-1 or SNAP-25 and possibly not enough cholesterol was removed to perturb 14-3-3 localisation. Alternatively the limited coincidence of 14-3-3 with CTXB may be non-specific; the low level of coincidence in combination with the lack of dependence on cholesterol does not support partitioning of 14-3-3 into cholesterol-dependent lipid raft-like domains. However, the results do not exclude the possibility that some sort of stimulatory signal could alter the membrane domain localisation of 14-3-3.

MβCD reduced the association of 14-3-3 with DRMs isolated from PC12 and N2a cells, whilst CTXB remained DRM associated. This suggested increased segregation of 14-3-3 and CTXB into different membrane domains following cholesterol depletion, which is clearly not reflected by the imaging of intact cells described above. Therefore CTXB-rich DRMs appear not to correspond directly to the CTXB clusters imaged by CLSM. However, even if DRMs do not represent pre-existing membrane domains, the ability of the inhibitor difopein to reduce recovery of 14-3-3 in DRMs suggests that 14-3-3 makes a specific interaction with one or more membrane associated proteins present in DRMs. The observed 14-3-3 isoform specificity of DRM association might then be an important property of 14-3-3's interaction with a membrane protein or proteins. Interestingly, a recent proteomic study of HeLa cell DRMs also detected cholesterol dependent association of 14-3-3, with apparent specificity for the 14-3-3 ζ isoform (Foster et al., 2003). The detection of 14-3-3 isoforms in the synaptic plasma membrane preparation from which LDMs were isolated provides further evidence of a role for 14-3-3 at the plasma membrane, along with two previous reports (Martin et al., 1994; Oksvold et al., 2004).

Taken together the findings presented in this thesis do not support the specific association of 14-3-3 with cholesterol-dependent membrane domains. However, the

results do suggest that localisation of 14-3-3 to other regions of the plasma membrane via interaction with membrane anchored proteins is a subject for investigation.

## 6.2. Observations concerning the classical detergent extraction procedure for the preparation of DRMs

The most established method for the biochemical isolation of lipid raft-like domains involves extraction with the non-ionic detergent TX-100, followed by flotation on a sucrose density gradient. The resulting DRM fraction is thought to contain clustered lipid rafts. This procedure was employed throughout the present study but certain observations indicated that the relationship of DRMs to pre-existing membrane domains is not straightforward.

The membrane protein transferrin receptor (TfR) is frequently used as a 'non-raft' control and is reported to localise only to the soluble protein fractions of the sucrose density gradient (Chamberlain et al., 2001; Roper et al., 2000; Takeda et al., 2003; Taverna et al., 2004). However, results presented in Chapter 3 (section 3.1.2) demonstrated recovery of TfR in the DRM fraction isolated from rat brain extract, in disagreement with reports that TfR is undetectable in DRMs. A proportion of TfR remained associated with DRMs even when the detergent to protein ratio was increased to 10:1 (w/w), though concentration of the DRM fraction was required to detect TfR by immunoblotting. Whilst TfR localises predominantly to the soluble protein fractions these results cast some doubt over the use of TfR as a negative control for DRM association. The recent report that TfR appears in DRMs following stimulation of primary or Jurkat T cells (Batista et al., 2004) provides further evidence that TfR is not totally excluded from DRMs. Despite the high detergent to protein ratio employed in DRM preparations in Chapter 3 it is possible that the association of TfR with DRMs is due to incomplete solubilisation of the bulk plasma membrane. Alternatively, failure to detect TfR in other studies may be due to limited antibody sensitivity or partial solubilisation of lipid raft-like domains. One of the limitations of the DRM isolation procedure is that it is not possible to determine

whether the 'non-raft' bulk membrane phase has been fully solubilised or whether lipid raft-like domains remain completely intact.

In Chapter 4 (section 4.3.1) I attempted to quantify the relative proportions of SNAP-25 and Thy-1 residing in DRMs. However, it became clear that small alterations in the DRM isolation procedure produced large changes in the degree of protein association with DRMs. When PC12 cells were extracted at a detergent to protein ratio of 2:1 (w/w) over 5-fold more SNAP-25 was associated with DRMs than when a detergent to protein ratio of 5:1 was employed. Other studies have also reported that the detergent to protein ratio affects the proportion of particular proteins recovered in DRMs (Chamberlain and Gould, 2002; Ostermeyer et al., 1999). These findings demonstrate that it is important to maintain a constant detergent to protein ratio if any comparison between DRM preparations is intended. Furthermore, the results indicate that quantification of the proportion of a particular protein present in DRMs will not provide a good estimate of the amount of that protein in pre-existing membrane domains.

Recent investigations have led to additional concerns regarding whether DRMs represent pre-existing membrane domains (Edidin, 2003; McMullen et al., 2004; Munro, 2003). It has been suggested that TX-100 may increase formation of $L_o$ domains in the plasma membrane (Hao et al., 2001; Heerklotz, 2002) and other studies imply that some proteins may artificially associate with DRMs during the extraction procedure (Foster et al., 2003; Korzeniowski et al., 2003). These concerns argue that caution should be exercised when interpreting DRM experiments.

In Chapter 5 the recovery of various proteins in DRMs was monitored following cholesterol depletion and compared with the effect of this treatment on intact cells by CLSM. Discrepancies between these two methods of investigating membrane distribution indicate that the CTXB-rich DRMs isolated from N2a and PC12 cells do not correspond directly to CTXB-labelled domains in intact cells. For example, MβCD had no effect on the coincidence of 14-3-3 with CTXB, whilst it did decrease recovery of 14-3-3 in DRMs. Similarly, MβCD reduced SNAP-25 association with

PC12 DRMs but did not alter its coincidence with CTXB in intact PC12 cells. Interestingly though some of the imaging data demonstrated good agreement with the DRM data. In N2a cells the recovery of SNAP-25 in DRMs was reduced by MβCD, whilst the DRM localisation of syntaxin1a was unchanged. Immunostaining of N2a cells demonstrated that MβCD also decreased the coincidence of SNAP-25 but not syntaxin1a with CTXB-labelled domains. The relatively high coincidence of Thy-1 with CTXB compared with 14-3-3 and syntaxin1a agreed broadly with DRM data. If DRMs are completely unrelated to CTXB clusters imaged in intact cells then these similarities are perhaps surprising.

Mayor and Rao suggest that even if DRMs do not represent pre-existing membrane domains they may reveal some relevant biochemical properties of the associated proteins (Mayor and Rao, 2004). The lipid composition of DRMs would be expected to facilitate formation of the $L_o$ phase (Brown and Rose, 1992; Pike, 2003; Pike et al., 2002; Prinetti et al., 2000) and a relationship between detergent insolubility and the Lo phase is supported by model membrane studies. Detergent insolubility correlated with increased formation of the $L_o$ phase in model membranes as cholesterol concentration was increased, as assessed by independent measurements of lipid order (Ahmed et al., 1997; Schroeder et al., 1994; Schroeder et al., 1998; Xu et al., 2001; Xu and London, 2000). Moreover, DRMs isolated from RBL mast cells shared the characteristic lipid lateral mobility and acyl chain ordering of $L_o$ phase model liposomes (Ge et al., 1999). Sceptics of the detergent extraction procedure speculate that DRMs do not represent pre-existing domains and are in fact produced by the extraction conditions (Heerklotz, 2002; Munro, 2003). Even if this is the case, DRMs may represent vesicles with the characteristics of the liquid ordered phase, though their particular composition may not correspond to *in vivo* membrane domains. Thus recovery of a protein in DRMs may still demonstrate an affinity for more ordered lipid phases, although the association may take place during the extraction procedure. This hypothesis, along with the suggested transient nature of membrane compartmentalisation (Hancock, 2006; Kusumi and Suzuki, 2005), could explain why both similarities and discrepancies are often observed between the DRM method and other techniques for investigating $L_o$ domains in intact cells.

## 6.3. Association of SNARE proteins with lipid raft-like domains

Syntaxin1a and SNAP-25 are anchored to the cytosolic face of the plasma membrane bilayer and it has previously been reported that 20-25 % of each partitions into DRMs in PC12 cells (Chamberlain et al., 2001). Syntaxin1a and SNAP-25 are established as residents of DRMs, though a large proportion of both consistently localises to soluble protein fractions (Chamberlain et al., 2001; Chamberlain and Gould, 2002; Foster et al., 2003; Gil et al., 2005; Pombo et al., 2003; Predescu et al., 2005; Salaun et al., 2005a; Taverna et al., 2004). As these proteins are essential regulators of exocytosis their partitioning between different membrane domains could potentially be of functional importance. This concept is supported by results demonstrating that cholesterol depletion reduces exocytosis (Chamberlain et al., 2001; Churchward et al., 2005; Gil et al., 2005; Lang et al., 2001; Ohara-Imaizumi et al., 2004) and the recent report that relative partitioning of SNAP-25 between DRMs and soluble fractions affects the rate of exocytosis in PC12 cells (Salaun et al., 2005b). Findings described in this thesis provide further insights into the partitioning of SNAREs between different plasma membrane domains.

### 6.3.1. Summary of results

Syntaxin1a and SNAP-25 were both detected in DRMs in N2a and PC12 cells, in agreement with previous studies. It appeared that a smaller proportion of total syntaxin1a than total SNAP-25 was DRM-associated. However, the proportion of a particular protein in DRMs was found to be subject to small changes in the DRM isolation procedure and thus may not reflect the physiological situation, as discussed above (see section 6.2). Interestingly though, CLSM demonstrated that the proportion of syntaxin1a coinciding with the lipid raft marker CTXB was significantly lower than the proportion of SNAP-25 coinciding with CTXB in PC12 cells (see Chapter 5, section 5.6.4). However, though a similar trend was observed in N2a cells, the difference in the coincidence of the two SNAREs with CTXB was not significant.

Cholesterol is central to the formation of the $L_o$ phase and therefore lipid raft-like domains. Depletion of cellular cholesterol indicated some difference between the membrane distribution of syntaxin1a and SNAP-25 in N2a cells; this treatment reduced the coincidence of SNAP-25 with CTXB labelled domains but had no significant effect on syntaxin1a distribution (see Chapter 5, figures 5.14 and 5.16 and table 5.3). Interestingly, analysis of DRM association supported this result in N2a cells; whilst SNAP-25 was removed from DRMs by MβCD, syntaxin1a was not (see Chapter 5, figure 5.4). In PC12 cells no significant change in the distribution of the SNAREs was detected by CLSM following cholesterol depletion. However, MβCD also affected the integrity of CTXB-labelled domains differently in the two cell types (discussed in Chapter 5, section 5.6.2); only in N2a cells were CTXB clusters partially disrupted. Thus the CTXB-labelled domains seem to have different properties in the two cell types and membrane compartmentalisation of other proteins may therefore also differ.

An important point to consider is that both SNAP-25 and syntaxin1a puncta often only partially overlap with CTXB clusters. Considering the limit of optical resolution (~ 250 nm), some apparently overlapping SNARE and CTXB puncta may be adjacent rather than the SNAREs being within the same cluster as CTXB (as discussed in Chapter 5, section 5.6.4). However, if we take the dynamic view of membrane compartmentalisation indicated by SPT studies (Dietrich et al., 2002; Kusumi et al., 2004; Sheets et al., 1997; Subczynski and Kusumi, 2003) and currently favoured in lipid raft models (Hancock, 2006; Kusumi and Suzuki, 2005; Mayor and Rao, 2004), then proximity to CTXB clusters may reflect dynamic association. Imaging of fixed cells will produce an averaged view of the membrane environment. Thus the degree of coincidence with CTXB may represent the affinity of each protein for CTXB labelled domains and domain localisation should not necessarily be viewed as stationary or constant.

### 6.3.2. Implications for the spatial distribution of SNARE proteins at the plasma membrane

The results obtained from PC12 and N2a cells display some differences, implying that membrane compartmentalisation of SNARE proteins may be slightly differently regulated in the two cell types. However, the data from N2a and PC12 cells agree that cholesterol depletion does not disrupt syntaxin1a or SNAP-25 clusters.

In PC12 cells, the increased coincidence of SNAP-25 with CTXB compared with syntaxin1a may represent a higher affinity of SNAP-25 compared with syntaxin1a for CTXB-labelled domains. Considering again the dynamic nature of membrane compartmentalisation described by SPT studies, the implication is that some SNAP-25 clusters may be separated from syntaxin1a clusters by an increased preference to transiently partition into particular membrane domains. Consideration of the populations of syntaxin-1 and SNAP-25 on plasma membrane and which of these are detected by the immunostaining procedure are pertinent to interpretation of these results.

In neuronal exocytosis, SNAP-25 and syntaxin1a in the plasma membrane are suggested to form a trans-complex with the SNARE protein synaptobrevin, present in the vesicle membrane. Structural studies suggest that the interaction is formed by four α-helices (one from each SNARE protein and the additional helix from SNAP-25) 'zipping up' from one end to the other, thus forcing the two bilayers into close apposition (Chen and Scheller, 2001; Jahn et al., 2003; Lin and Scheller, 2000; Sutton et al., 1998). A number of studies have suggested that vesicles are already docked at the plasma membrane by formation of the ternary SNARE complex (syntaxin-1a, SNAP-25 plus synaptobrevin) prior to stimulation of exocytosis (An and Almers, 2004; Lonart and Sudhof, 2000; Ungermann et al., 1998; Xu et al., 1999). Syntaxin1a and SNAP-25 may also be stably associated as binary cis-complexes in the plasma membrane (Otto et al., 1997; Xiao et al., 2004); in fact two studies suggest that binary cis-complexes, rather than monomeric SNAP-25 and

syntaxin-1a, are required to promote the interaction with synaptobrevin (Fasshauer and Margittai, 2004; Rickman et al., 2004).

It has been suggested that most of the SNAP-25 and syntaxin1a are present as heterodimers in the plasma membrane of chromaffin cells (Rickman et al., 2004). However, the different coincidence of each SNARE protein with CTXB and the different sizes of SNAP-25 and syntaxin1a clusters (described in Chapters 4 and 5) argue that this is not the case in PC12 cells. Immunoaffinity purifications of SNAP-25 from brain extract and PC12 cells demonstrated that a proportion of both syntaxin1a and SNAP-25 were not bound to each other (Rickman et al., 2005; Xiao et al., 2004). In PC12 cells, other syntaxin isoforms have been shown to bind SNAP-25 (Bajohrs et al., 2005). However, there is also some indication that non-interacting SNAP-25 and syntaxin1a are also present in the plasma membrane, alongside binary or ternary complexes. An and co-workers detected an increase in the formation of binary syntaxin-1a/SNAP-25 complexes in response to increasing the calcium concentration in PC12 cells (An and Almers, 2004). In addition, Xu and co-workers found that an anti-SNAP-25 antibody that blocked complex formation could inhibit the slow, sustained component of exocytosis (Xu et al., 1999). Lang and co-workers go further and suggest that most of the SNAP-25 and syntaxin1a in resting PC12 cells in not in SNARE complexes as judged by the capacity of freshly prepared plasma membrane sheets to bind exogenous SNAREs (Lang et al., 2002). Thus the SNAP-25 and syntaxin1a detected by immunostaining in Chapters 4 and 5 may represent a number of different populations, including monomeric SNAREs, binary cis-complexes and ternary trans-complexes with synaptobrevin.

The antibody employed for SNAP-25 immunostaining (monoclonal SMI81, Sternberger Monoclonals) has been shown to immunopurify all the SNAP-25 from brain extract, indicating that it recognises native SNAP-25 free and in complex with other proteins (Rickman et al., 2005). The anti-syntaxin1a antibody (monoclonal anti-HPC-1, Sigma Aldrich) recognises syntaxin-1a/SNAP-25 heterodimers and free syntaxin1a but not syntaxin1a bound to munc18 (Rickman and Davletov, 2005; Rickman et al., 2004). Munc18 binds syntaxin1a in a closed conformation that

prevents its interaction with other SNAREs (Dulubova et al., 1999; Yang et al., 2000). A proportion of syntaxin1a may be bound to munc18 at plasma membrane but this population will not have been detected by the immunostaining with anti-syntaxin1a in experiments described in this thesis.

Thus the syntaxin1a and SNAP-25 recognised by immunostaining in this thesis may then be in binary or ternary SNARE complexes or non-interacting. If the anti-syntaxin1a antibody recognises all syntaxin-1a/SNAP-25 heterodimers then the higher coincidence of SNAP-25 versus syntaxin1a with CTXB must be due to free SNAP-25. In an attempt to determine whether all syntaxin1a is heterodimerised with SNAP-25, co-immunostaining was attempted with the monoclonal SMI81 and a rabbit anti-syntaxin1a antibody, unfortunately this was unsuccessful. Thus it is unclear whether any of the syntaxin1a on PC12 cell membranes is free or all in SNARE complexes. The apparent propensity of SNAP-25 to partition into different membrane domains could regulate the frequency with which binary and ternary SNARE complexes are formed in PC12 cells.

In N2a cells, the mean correlation of SNAP-25 with CTXB (20 ± 2 % (SEM)) was not significantly different from that of syntaxin1a with CTXB (16 ± 2 %). Thus the partitioning of free SNAP-25 away from syntaxin1a and SNARE complexes implied by the PC12 data does not necessarily occur in N2a cells. However, the coincidences of syntaxin1a and SNAP-25 with CTXB were differently affected by cholesterol depletion; there was a large decrease in the coincidence of SNAP-25 with CTXB (correlation was reduced from 20 ± 2 % (SEM) to 8 ± 1%) whilst coincidence of syntaxin1a with CTXB was not significantly altered. Thus the partitioning of each SNARE protein into CTXB-labelled domains is differently sensitive to membrane cholesterol concentration. This implies that much of the SNAP-25 and syntaxin1a coincident with CTXB is not heterodimerised; otherwise the two proteins would be expected to behave in a similar way.

In contrast with these observations in N2a cells, in PC12 cells cholesterol depletion had no affect on the coincidence of either SNARE protein with CTXB. Decreased

filipin staining demonstrated that cholesterol was depleted from the plasma membrane of both N2a and PC12 cells. However, the partial dispersal of CTXB clusters observed in N2a cells was not replicated in PC12 cells. This suggests that the CTXB-labelled domains in the two cell types have different properties and it could be that not enough cholesterol was depleted from PC12 cells to alter the affinity of SNAP-25 for such clusters. The possibility can not be excluded though that the coincidence of SNAP-25 with CTXB in PC12 cells does not depend on cholesterol. The ability of MβCD to perturb CTXB cluster integrity in N2a cells suggests that CTXB clustering in this cell type is mediated, at least partly, by cholesterol. The observation that this rearrangement of CTXB clusters altered the coincidence of SNAP-25, but not syntaxin-1a, with CTXB implies that the spatial distribution of SNAP-25 clusters is influenced to some extent by membrane cholesterol concentration. These findings support the hypothesis that CTXB clusters represent cholesterol dependent membrane domains for which SNAP-25 clusters have an affinity.

The results from both N2a and PC12 cells indicate that a proportion of free SNAP-25 preferentially partitions away from syntaxin1a and/or SNAP-25/syntaxin1a heterodimers into membrane compartments defined by CTXB-labelling (this hypothesis is illustrated in figure 6.1). CTXB has been demonstrated to segregate into the $L_o$ phase in model membranes and is therefore suggested to label $L_o$ domains (Bacia et al., 2004; Dietrich et al., 2001a; Dietrich et al., 2001b; Kahya et al., 2005; Kahya et al., 2003; Wang and Silvius, 2003). The apparent separation of SNAP-25 in CTXB-labelled domains from syntaxin1a may indicate a negative role for lipid raft-like domains in SNARE complex formation. This would agree with a recent study by Salaun and co-workers that suggested that lipid raft-like domains might negatively regulate exocytosis (Salaun et al., 2005b). Mutations in SNAP-25 that increased its affinity for DRMs decreased the ability of the transfected protein to support exocytosis in Botulinum neurotoxin E (BoNT/E) poisoned PC12 cells. Though concerns exist regarding the relevance of DRMs to pre-existing domains, association with DRMs may represent affinity for more ordered lipid phases (as discussed above,

section 6.2). Thus the localisation of SNAREs and SNAREs complexes outside lipid raft-like domains may be important for exocytosis.

In contrast, Gil and co-workers recently suggested that lipid raft-like domains might be the site of exocytosis (Gil et al., 2006). Potassium depolarisation increased the proportion of syntaxin1a but not munc18 associated with DRMs isolated from rat brain synaptosomes using the detergent Brij 98, leading the authors to suggest that syntaxin1a translocates to DRMs following release from munc18. The results presented in this thesis do not exclude the possibility that stimulation alters the partitioning of SNAREs into lipid raft-like domains. The study by Gil and co-workers does however disagree with that of Salaun and co-workers (Salaun et al., 2005b) but it is unclear exactly how Brij 98 DRMs relate to pre-existing domains and TX-100 DRMs as different lipid and protein compositions have been reported to result from extraction with different detergents (Schuck et al., 2003).

The inhibitory effect of cholesterol depletion on exocytosis (Chamberlain et al., 2001; Churchward et al., 2005; Gil et al., 2005; Lang et al., 2001; Ohara-Imaizumi et al., 2004) is also apparently in disagreement with observations that lipid raft-like domains might negatively regulate exocytosis. However, cholesterol may be involved in aspects of exocytosis other than the controlling the spatial distribution of SNAREs. The presence of cholesterol has been suggested to help provide the correct membrane curvature needed for fusion of two bilayers (Churchward et al., 2005). Treatments that deplete cholesterol have also been suggested to mediate rearrangement of the actin cytoskeleton, as discussed in Chapter 5, section 5.6.4 (Grimmer et al., 2002; Kwik et al., 2003). Such effects on the cytoskeleton might affect the efficiency of exocytosis as disassembly of the submembrane actin cytoskeleton aids vesicle docking (Lin and Scheller, 2000; Toonen et al., 2006; Vitale et al., 1995).

If cholesterol depletion treatment also affects cytoskeleton organisation it is possible that the observed effect of MβCD on CTXB and SNARE proteins in N2a cells may be due to alterations in actin cytoskeleton rather than disruption of putative

cholesterol-rich lipid raft domains. The actin cytoskeleton is also implicated in compartmentalisation of membrane proteins (Kusumi et al., 2004; Subczynski and Kusumi, 2003). Whatever the mechanism involved the results from N2a and PC12 cells indicate that the spatial distribution of SNAP-25 is differently regulated from that of syntaxin-1a. Preferential partitioning of SNAREs between different membrane domains may have functional consequences for the regulation of exocytosis.

### 6.3.3. The organisation of SNARE protein clusters

Plasma membrane SNARE proteins generally present a punctate or clustered appearance on the cell surface (Aoyagi et al., 2005; Lang et al., 2001; Ohara-Imaizumi et al., 2004; Rickman et al., 2004; Sieber et al., 2006) and the contribution of more than one SNARE complex is likely to be necessary for fusion of a vesicle (Hua and Scheller, 2001). There have been reports that syntaxin1a, syntaxin4 and SNAP-23 clusters depend on cholesterol for their integrity (Lang et al., 2001; Ohara-Imaizumi et al., 2004; Predescu et al., 2005). However, findings presented in this thesis do not support this conclusion. Cholesterol depletion had no effect on the size or density of syntaxin1a and SNAP-25 clusters in both PC12 and N2a cells (see Chapter 5, figures 5.17 and 5.18). Other studies also disagree that cholesterol plays a role in maintaining SNARE clusters. There is strong evidence that syntaxin1a forms homo-oligomers and a recent study indicates that no other factors are required for syntaxin1a clustering (Laage et al., 2000; Sieber et al., 2006). In support of this, purified SNAP-25, syntaxin-1 and synaptobrevin formed star-shaped oligomers with 2 – 6 arms per star, as assessed by electron microscopy (Rickman et al., 2005). Each arm was suggested to correspond to a four α-helix SNARE bundle, demonstrating that oligomers of ternary complexes form in the absence of additional factors. Thus much of the clustering of SNAP-25 may be due to the formation of heterodimers with oligomerised syntaxin1a, as suggested by the observation that cleavage of the SNAP-25 with BoNT/E disrupts SNAP-25 clustering in chromaffin cells (Rickman et al., 2004). Most of the evidence points to a mechanism of SNARE clustering that does not rely on cholesterol-rich domains.

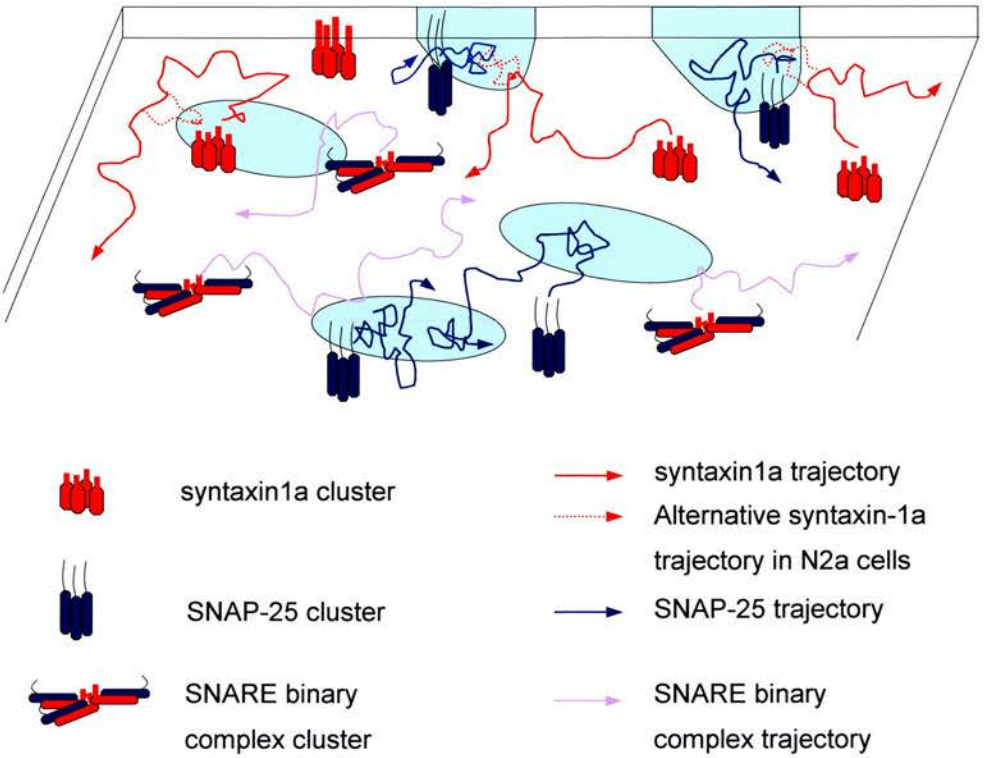


**Figure 6.1. Model for the plasma membrane compartmentalisation of SNAP-25 and syntaxin1a**

Schematic diagram of a model based on the discussion of results in section 6.3.2, showing a section of the plasma membrane bilayer viewed from the cytoplasmic side. Light blue regions represent cholesterol dependent domains labelled by CTXB. The dynamic compartmentalisation of clustered SNARE proteins is illustrated by arrows representing the movement of the indicated clusters through the membrane over a short time period. SNAP-25 clusters (blue) spend more time than syntaxin1a/SNAP-25 heterodimers (red/blue complex, purple arrows) in segregated domains. In PC12 cells syntaxin1a clusters (solid red arrows) are also suggested to spend less time in segregated domains than SNAP-25 but in N2a cells syntaxin1a (dashed red arrows) partitions into domains to a similar degree as SNAP-25. The different preference of the non-interacting SNAREs versus syntaxin1a/SNAP-25 binary complexes for segregated domains produces spatial separation of the clusters that may be involved in the regulation of exocytosis.

The higher coincidence of SNAP-25 than syntaxin1a with CTXB (reported in Chapters 4 and 5) indicates that in PC12 cells all SNAP-25 is not in heterodimers with syntaxin1a, in agreement with other studies described in section 6.4.2. This leads to the question of how SNAP-25 clusters are maintained in the absence of syntaxin1a. SNAP-25 is targeted to the plasma membrane by palmitoylation (Hess et al., 1992; Lane and Liu, 1997; Loranger and Linder, 2002; Veit et al., 1996) and this modification is necessary for the association of SNAP-25 with DRMs (Salaun et al., 2005a). Palmitoylated proteins are often enriched in DRMs so these proteins might be clustered by localisation to lipid raft-like domains (Melkonian et al., 1999). However, this does not seem to be case for SNAP-25 as partial removal of cholesterol (demonstrated by decrease in filipin staining intensity) had no effect on clusters. Interestingly, Gonzalo and co-workers determined that, additional to the putative palmitoylation domain, another motif in SNAP-25 is essential for membrane association (Gonzalo et al., 1999). They suggest that this motif, which is found between the two SNARE motifs, may interact with another membrane protein. This hypothesis presents a possible alternative mechanism for SNAP-25 clustering in the absence of syntaxin1a.

Whilst the findings presented in this thesis do not support a role for cholesterol in maintaining SNARE protein clusters, the altered coincidence of SNAP-25 with CTXB following cholesterol depletion of N2a cells indicates that cholesterol may influence the membrane compartmentalisation of SNAP-25 clusters.

## 6.4. Conclusions

14-3-3 associates with DRMs in a cholesterol dependent and isoform specific manner. This interaction is likely to be mediated by binding to another DRM resident protein. However, CLSM of intact cells did not support the cholesterol dependent localisation of 14-3-3 to membrane domains defined by the lipid raft marker CTXB. Whilst the results are not consistent with 14-3-3 interacting with lipid raft-like domains, they suggest that a role for 14-3-3 at the plasma membrane is still an interesting area for investigation. The discrepancies between DRM and imaging data, along with the difficulties encountered in quantifying protein association with DRMs, lend weight to the argument that DRMs may not represent pre-existing membrane domains. Analysis of CLSM images, rather than DRMs, demonstrated that CTXB clusters were perturbed by cholesterol depletion, supporting the view that CTXB labels cholesterol dependent domains. However, CTXB-labelled domains had different properties in N2a cells compared with PC12 cells, suggesting that the composition of cholesterol dependent domains may be cell type specific. In N2a cells the membrane compartmentalisation of SNAP-25 clusters appears to be partly dependent on cholesterol but in PC12 cells other compartmentalisation mechanisms may be involved. However, in both cell types the spatial distribution of SNAP-25 on the plasma membrane appears to be differently regulated from that of syntaxin1a and this may have implications for the regulation of exocytosis.

## 6.5. Future Work

Findings presented in this study indicate further study of 14-3-3 with respect to steady state cholesterol dependent membrane domains may not be productive. However, plasma membrane localisation of 14-3-3 is supported and the results do not exclude the possibility that growth factor stimulation, for example, may alter the partitioning of 14-3-3 between the plasma membrane and cytosol and/or between different membrane domains. It has been reported that epidermal growth factor (EGF) stimulation induces translocation of 14-3-3 to the plasma membrane (Mineo et al., 1996; Oksvold et al., 2004) and more detailed investigation of this observation might prove interesting. The EGF receptor (EGFR) has recently been reported to associate with low density membrane fractions isolated by a detergent free method, which have a lipid composition consistent with lipid raft-like domains (Pike et al., 2005). Thus it might be interesting to explore the subcellular localisation of 14-3-3 in response to EGF stimulation at the relatively high resolution afforded by CLSM coupled with data deconvolution. To monitor the coincidence of 14-3-3 with markers of ordered lipid domains (perhaps including CTXB, the dye laurdan and saturated lipid probes) it would be useful to both immunostain for endogenous 14-3-3 and express a fluorescently tagged 14-3-3 to permit live cell imaging. Though a role for 14-3-3 has been established in EGF mediated activation of the MAPK pathway via its interaction with c-Raf-1 (as discussed in Chapter 1, section 1.2.3.3), recently direct binding of 14-3-3 to EGFR was suggested from co-immunoprecipitation of the two proteins from stimulated cells (Oksvold et al., 2004). Förster resonance energy transfer (FRET) could usefully be employed to investigate whether 14-3-3 and EGFR interact directly in response to EGF and shed light on the role of 14-3-3 in EGF stimulation.

FRET involves excitation of an acceptor fluorophore by emission from an excited donor fluorophore. Fluorophores must be < 10 nm apart for detectable FRET to occur so FRET reports the very close association of two fluorescently tagged proteins. As well as intensity-based FRET, fluorescence lifetime imaging microscopy (FLIM) can be employed to detect FRET. Because the donor fluorophore is

quenched by FRET its fluorescence lifetime is reduced, thus the populations of non-interacting and interacting molecules can be distinguished by their different lifetimes. When the donor fluorescence lifetime is monitored over a whole image the lifetime in each voxel will reflect the proportion of interacting and non-interacting molecules in that voxel. Fluorescence lifetime maps thus provide information about the subcellular distribution of interacting proteins, making FRET-FLIM is a very useful technique for exploring protein-protein interactions in intact cells.

Further investigation of the partitioning of SNAREs between membrane domains is warranted by the results presented here. It would be interesting to compare the immunostaining studies in this thesis with imaging of live cells expressing fluorescently tagged constructs of SNAP-25 and syntaxin1a, though it is important to keep in mind that overexpression may alter partitioning between membrane domains. In addition to CTXB labelling, it would be useful to explore other markers for lipid order such as saturated lipid probes and the dye laurdan (discussed in Chapter 1, section 1.1.3.1) and also repeat cholesterol depletion experiments using these markers. To further investigate the model presented in figure 6.1, FRET-FLIM between fluorescently tagged SNAP-25 and syntaxin1a could be employed in conjunction with CTXB labelling to determine the distribution of binary SNARE complexes compared with non-interacting SNAP-25 and syntaxin1a, in relation to CTXB domains. It would be particularly interesting to use this procedure following cholesterol depletion or stimulation of exocytosis to provide further information about the membrane compartmentalisation of SNAREs and the question of whether lipid raft-like domains might be the site of exocytosis.

# 7.0 Bibliography


Abrami, L., S. Liu, P. Cosson, S.H. Leppla, and F.G. van der Goot. 2003. Anthrax toxin triggers endocytosis of its receptor via a lipid raft-mediated clathrin-dependent process. *J Cell Biol.* 160:321-8.

Agarwal-Mawal, A., H.Y. Qureshi, P.W. Cafferty, Z. Yuan, D. Han, R. Lin, and H.K. Paudel. 2003. 14-3-3 connects glycogen synthase kinase-3 beta to tau within a brain microtubule-associated tau phosphorylation complex. *J Biol Chem.* 278:12722-8.

Ahmed, S.N., D.A. Brown, and E. London. 1997. On the origin of sphingolipid/cholesterol-rich detergent-insoluble cell membranes: physiological concentrations of cholesterol and sphingolipid induce formation of a detergent-insoluble, liquid-ordered lipid phase in model membranes. *Biochemistry.* 36:10944-53.

Aitken, A. 2006. 14-3-3 proteins: a historic overview. *Semin Cancer Biol.* 16:162-72.

Aitken, A., H. Baxter, T. Dubois, S. Clokie, S. Mackie, K. Mitchell, A. Peden, and E. Zemlickova. 2002. Specificity of 14-3-3 isoform dimer interactions and phosphorylation. *Biochem Soc Trans.* 30:351-60.

Aitken, A., D.B. Collinge, B.P. van Heusden, T. Isobe, P.H. Roseboom, G. Rosenfeld, and J. Soll. 1992. 14-3-3 proteins: a highly conserved, widespread family of eukaryotic proteins. *Trends Biochem Sci.* 17:498-501.

Aitken, A., S. Howell, D. Jones, J. Madrazo, H. Martin, Y. Patel, and K. Robinson. 1995a. Post-translationally modified 14-3-3 isoforms and inhibition of protein kinase C. *Mol Cell Biochem.* 149-150:41-9.

Aitken, A., S. Howell, D. Jones, J. Madrazo, and Y. Patel. 1995b. 14-3-3 alpha and delta are the phosphorylated forms of raf-activating 14-3-3 beta and zeta. In vivo stoichiometric phosphorylation in brain at a Ser-Pro-Glu-Lys MOTIF. *J Biol Chem.* 270:5706-9.

Alberts, A.W., J. Chen, G. Kuron, V. Hunt, J. Huff, C. Hoffman, J. Rothrock, M. Lopez, H. Joshua, E. Harris, A. Patchett, R. Monaghan, S. Currie, E. Stapley, G. Albers-Schonberg, O. Hensens, J. Hirshfield, K. Hoogsteen, J. Liesch, and J. Springer. 1980. Mevinolin: a highly potent competitive inhibitor of hydroxymethylglutaryl-coenzyme A reductase and a cholesterol-lowering agent. *Proc Natl Acad Sci U S A.* 77:3957-61.

Ali, S., J.M. Smaby, H.L. Brockman, and R.E. Brown. 1994. Cholesterol's interfacial interactions with galactosylceramides. *Biochemistry.* 33:2900-6.

Almeida, P.F., A. Pokorny, and A. Hinderliter. 2005. Thermodynamics of membrane domains. *Biochim Biophys Acta.* 1720:1-13.

An, S.J., and W. Almers. 2004. Tracking SNARE complex formation in live endocrine cells. *Science.* 306:1042-6.

Aoyagi, K., T. Sugaya, M. Umeda, S. Yamamoto, S. Terakawa, and M. Takahashi. 2005. The activation of exocytotic sites by the formation of phosphatidylinositol 4,5-bisphosphate microdomains at syntaxin clusters. *J Biol Chem.* 280:17346-52.

Arcaro, A., C. Gregoire, N. Boucheron, S. Stotz, E. Palmer, B. Malissen, and I.F. Luescher. 2000. Essential role of CD8 palmitoylation in CD8 coreceptor function. *J Immunol.* 165:2068-76.

Atger, V.M., M. de la Llera Moya, G.W. Stoudt, W.V. Rodrigueza, M.C. Phillips, and G.H. Rothblat. 1997. Cyclodextrins as catalysts for the removal of cholesterol from macrophage foam cells. *J Clin Invest.* 99:773-80.

Ayllon, V., A. Fleischer, X. Cayla, A. Garcia, and A. Rebollo. 2002. Segregation of Bad from lipid rafts is implicated in the induction of apoptosis. *J Immunol.* 168:3387-93.

Bachmann, M., J.L. Huber, G.S. Athwal, K. Wu, R.J. Ferl, and S.C. Huber. 1996. 14-3-3 proteins associate with the regulatory phosphorylation site of spinach leaf nitrate reductase in an isoform-specific manner and reduce dephosphorylation of Ser-543 by endogenous protein phosphatases. *FEBS Lett.* 398:26-30.

Bacia, K., C.G. Schuette, N. Kahya, R. Jahn, and P. Schwille. 2004. SNAREs prefer liquid-disordered over "raft" (liquid-ordered) domains when reconstituted into giant unilamellar vesicles. *J Biol Chem.* 279:37951-5.

Badizadegan, K., B.L. Dickinson, H.E. Wheeler, R.S. Blumberg, R.K. Holmes, and W.I. Lencer. 2000a. Heterogeneity of detergent-insoluble membranes from human intestine containing caveolin-1 and ganglioside G(M1). *Am J Physiol Gastrointest Liver Physiol.* 278:G895-904.

Badizadegan, K., A.A. Wolf, C. Rodighiero, M. Jobling, T.R. Hirst, R.K. Holmes, and W.I. Lencer. 2000b. Floating cholera toxin into epithelial cells: functional association with caveolae-like detergent-insoluble membrane microdomains. *Int J Med Microbiol.* 290:403-8.

Bajohrs, M., F. Darios, S.Y. Peak-Chew, and B. Davletov. 2005. Promiscuous interaction of SNAP-25 with all plasma membrane syntaxins in a neuroendocrine cell. *Biochem J.* 392:283-9.

Barenholz, Y., J. Suurkuusk, D. Mountcastle, T.E. Thompson, and R.L. Biltonen. 1976. A calorimetric study of the thermotropic behavior of aqueous dispersions of natural and synthetic sphingomyelins. *Biochemistry.* 15:2441-7.

Baron, G.S., K. Wehrly, D.W. Dorward, B. Chesebro, and B. Caughey. 2002. Conversion of raft associated prion protein to the protease-resistant state requires insertion of PrP-res (PrP(Sc)) into contiguous membranes. *Embo J.* 21:1031-40.

Barton, P.G., and F.D. Gunstone. 1975. Hydrocarbon chain packing and molecular motion in phospholipid bilayers formed from unsaturated lecithins. Synthesis and properties of sixteen positional isomers of 1,2-dioctadecenoyl-sn-glycero-3-phosphorylcholine. *J Biol Chem.* 250:4470-6.

Batista, A., J. Millan, M. Mittelbrunn, F. Sanchez-Madrid, and M.A. Alonso. 2004. Recruitment of transferrin receptor to immunological synapse in response to TCR engagement. *J Immunol.* 172:6709-14.

Baumgart, T., S.T. Hess, and W.W. Webb. 2003. Imaging coexisting fluid domains in biomembrane models coupling curvature and line tension. *Nature.* 425:821-4.

Beaudry, P., P. Cohen, J.P. Brandel, N. Delasnerie-Laupretre, S. Richard, J.M. Launay, and J.L. Laplanche. 1999. 14-3-3 protein, neuron-specific enolase, and S-100 protein in cerebrospinal fluid of patients with Creutzfeldt-Jakob disease. *Dement Geriatr Cogn Disord.* 10:40-6.

Beguin, P., R.N. Mahalakshmi, K. Nagashima, D.H. Cher, A. Takahashi, Y. Yamada, Y. Seino, and W. Hunziker. 2005. 14-3-3 and calmodulin control subcellular distribution of Kir/Gem and its regulation of cell shape and calcium channel activity. *J Cell Sci.* 118:1923-34.

Benting, J.H., A.G. Rietveld, and K. Simons. 1999. N-Glycans mediate the apical sorting of a GPI-anchored, raft-associated protein in Madin-Darby canine kidney cells. *J Cell Biol.* 146:313-20.

Benzinger, A., G.M. Popowicz, J.K. Joy, S. Majumdar, T.A. Holak, and H. Hermeking. 2005. The crystal structure of the non-liganded 14-3-3sigma protein: insights into determinants of isoform specific ligand binding and dimerization. *Cell Res.* 15:219-27.

Berg, D., C. Holzmann, and O. Riess. 2003. 14-3-3 proteins in the nervous system. *Nat Rev Neurosci.* 4:752-62.

Bickel, P.E. 2002. Lipid rafts and insulin signaling. *Am J Physiol Endocrinol Metab.* 282:E1-E10.

Bickel, P.E., P.E. Scherer, J.E. Schnitzer, P. Oh, M.P. Lisanti, and H.F. Lodish. 1997. Flotillin and epidermal surface antigen define a new family of caveolae-associated integral membrane proteins. *J Biol Chem.* 272:13793-802.

Binder, W.H., V. Barragan, and F.M. Menger. 2003. Domains and rafts in lipid membranes. *Angew Chem Int Ed Engl.* 42:5802-27.

Blanchette-Mackie, E.J., N.K. Dwyer, L.M. Amende, H.S. Kruth, J.D. Butler, J. Sokol, M.E. Comly, M.T. Vanier, J.T. August, R.O. Brady, and et al. 1988. Type-C Niemann-Pick disease: low density lipoprotein uptake is associated with premature cholesterol accumulation in the Golgi complex and excessive cholesterol storage in lysosomes. *Proc Natl Acad Sci U S A.* 85:8022-6.

Blonder, J., M.L. Hale, D.A. Lucas, C.F. Schaefer, L.R. Yu, T.P. Conrads, H.J. Issaq, B.G. Stiles, and T.D. Veenstra. 2004. Proteomic analysis of detergent-resistant membrane rafts. *Electrophoresis.* 25:1307-18.

Boston, P.F., P. Jackson, and R.J. Thompson. 1982. Human 14-3-3 protein: radioimmunoassay, tissue distribution, and cerebrospinal fluid levels in patients with neurological disorders. *J Neurochem.* 38:1475-82.

Bradford, M.M. 1976. A rapid and sensitive method for the quantitation of microgram quantities of protein utilizing the principle of protein-dye binding. *Anal Biochem.* 72:248-54.

Braselmann, S., and F. McCormick. 1995. Bcr and Raf form a complex in vivo via 14-3-3 proteins. *Embo J.* 14:4839-48.

Brown, D.A., and E. London. 1997. Structure of detergent-resistant membrane domains: does phase separation occur in biological membranes? *Biochem Biophys Res Commun.* 240:1-7.

Brown, D.A., and E. London. 1998. Structure and origin of ordered lipid domains in biological membranes. *J Membr Biol.* 164:103-14.

Brown, D.A., and E. London. 2000. Structure and function of sphingolipid- and cholesterol-rich membrane rafts. *J Biol Chem.* 275:17221-4.

Brown, D.A., and J.K. Rose. 1992. Sorting of GPI-anchored proteins to glycolipid-enriched membrane subdomains during transport to the apical cell surface. *Cell.* 68:533-44.

Brugger, B., C. Graham, I. Leibrecht, E. Mombelli, A. Jen, F. Wieland, and R. Morris. 2004. The membrane domains occupied by glycosylphosphatidylinositol-anchored prion protein and Thy-1 differ in lipid composition. *J Biol Chem.* 279:7530-6.

Brunet, A., A. Bonni, M.J. Zigmond, M.Z. Lin, P. Juo, L.S. Hu, M.J. Anderson, K.C. Arden, J. Blenis, and M.E. Greenberg. 1999. Akt promotes cell survival by phosphorylating and inhibiting a Forkhead transcription factor. *Cell.* 96:857-68.

Brunet, A., F. Kanai, J. Stehn, J. Xu, D. Sarbassova, J.V. Frangioni, S.N. Dalal, J.A. DeCaprio, M.E. Greenberg, and M.B. Yaffe. 2002. 14-3-3 transits to the nucleus and participates in dynamic nucleocytoplasmic transport. *J Cell Biol.* 156:817-28.

Bruses, J.L., N. Chauvet, and U. Rutishauser. 2001. Membrane lipid rafts are necessary for the maintenance of the (alpha)7 nicotinic acetylcholine receptor in somatic spines of ciliary neurons. *J Neurosci.* 21:504-12.

Bunnell, S.C., D.I. Hong, J.R. Kardon, T. Yamazaki, C.J. McGlade, V.A. Barr, and L.E. Samelson. 2002. T cell receptor ligation induces the formation of dynamically regulated signaling assemblies. *J Cell Biol.* 158:1263-75.

Burack, W.R., K.H. Lee, A.D. Holdorf, M.L. Dustin, and A.S. Shaw. 2002. Cutting edge: quantitative imaging of raft accumulation in the immunological synapse. *J Immunol.* 169:2837-41.

Carreno, F.R., C.N. Goni, L.M. Castro, and E.S. Ferro. 2005. 14-3-3 epsilon modulates the stimulated secretion of endopeptidase 24.15. *J Neurochem.* 93:10-25.

Cavet, M.E., S. Lehoux, and B.C. Berk. 2003. 14-3-3beta is a p90 ribosomal S6 kinase (RSK) isoform 1-binding protein that negatively regulates RSK kinase activity. *J Biol Chem.* 278:18376-83.

Celis, J.E., B. Gesser, H.H. Rasmussen, P. Madsen, H. Leffers, K. Dejgaard, B. Honore, E. Olsen, G. Ratz, J.B. Lauridsen, and et al. 1990. Comprehensive two-dimensional gel protein databases offer a global approach to the analysis of human cells: the transformed amnion cells (AMA) master database and its link to genome DNA sequence data. *Electrophoresis.* 11:989-1071.

Chamberlain, L.H. 2004. Detergents as tools for the purification and classification of lipid rafts. *FEBS Lett.* 559:1-5.

Chamberlain, L.H., R.D. Burgoyne, and G.W. Gould. 2001. SNARE proteins are highly enriched in lipid rafts in PC12 cells: implications for the spatial control of exocytosis. *Proc Natl Acad Sci U S A.* 98:5619-24.

Chamberlain, L.H., and G.W. Gould. 2002. The vesicle- and target-SNARE proteins that mediate Glut4 vesicle fusion are localized in detergent-insoluble lipid rafts present on distinct intracellular membranes. *J Biol Chem.* 277:49750-4.

Chamberlain, L.H., D. Roth, A. Morgan, and R.D. Burgoyne. 1995. Distinct effects of alpha-SNAP, 14-3-3 proteins, and calmodulin on priming and triggering of regulated exocytosis. *J Cell Biol.* 130:1063-70.

Chan, T.A., H. Hermeking, C. Lengauer, K.W. Kinzler, and B. Vogelstein. 1999. 14-3-3Sigma is required to prevent mitotic catastrophe after DNA damage. *Nature.* 401:616-20.

Chatterjee, S., and S. Mayor. 2001. The GPI-anchor and protein sorting. *Cell Mol Life Sci.* 58:1969-87.

Chaudhri, M., M. Scarabel, and A. Aitken. 2003. Mammalian and yeast 14-3-3 isoforms form distinct patterns of dimers in vivo. *Biochem Biophys Res Commun.* 300:679-85.

Chen, H.K., P. Fernandez-Funez, S.F. Acevedo, Y.C. Lam, M.D. Kaytor, M.H. Fernandez, A. Aitken, E.M. Skoulakis, H.T. Orr, J. Botas, and H.Y. Zoghbi. 2003a. Interaction of Akt-phosphorylated ataxin-1 with 14-3-3 mediates neurodegeneration in spinocerebellar ataxia type 1. *Cell.* 113:457-68.

Chen, M.S., C.E. Ryan, and H. Piwnica-Worms. 2003b. Chk1 kinase negatively regulates mitotic function of Cdc25A phosphatase through 14-3-3 binding. *Mol Cell Biol.* 23:7488-97.

Chen, Y.A., and R.H. Scheller. 2001. SNARE-mediated membrane fusion. *Nat Rev Mol Cell Biol.* 2:98-106.

Chini, B., and M. Parenti. 2004. G-protein coupled receptors in lipid rafts and caveolae: how, when and why do they go there? *J Mol Endocrinol.* 32:325-38.

Chintagari, N.R., N. Jin, P. Wang, T.A. Narasaraju, J. Chen, and L. Liu. 2006. Effect of cholesterol depletion on exocytosis of alveolar type II cells. *Am J Respir Cell Mol Biol.* 34:677-87.

Chow, C.W., and R.J. Davis. 2000. Integration of calcium and cyclic AMP signaling pathways by 14-3-3. *Mol Cell Biol.* 20:702-12.

Churchward, M.A., T. Rogasevskaia, J. Hofgen, J. Bau, and J.R. Coorssen. 2005. Cholesterol facilitates the native mechanism of Ca2+-triggered membrane fusion. *J Cell Sci.* 118:4833-48.

Cinek, T., and V. Horejsi. 1992. The nature of large noncovalent complexes containing glycosyl-phosphatidylinositol-anchored membrane glycoproteins and protein tyrosine kinases. *J Immunol.* 149:2262-70.

Clark, G.J., J.K. Drugan, K.L. Rossman, J.W. Carpenter, K. Rogers-Graham, H. Fu, C.J. Der, and S.L. Campbell. 1997. 14-3-3 zeta negatively regulates raf-1 activity by interactions with the Raf-1 cysteine-rich domain. *J Biol Chem.* 272:20990-3.

Clokie, S.J., K.Y. Cheung, S. Mackie, R. Marquez, A.H. Peden, and A. Aitken. 2005. BCR kinase phosphorylates 14-3-3 Tau on residue 233. *Febs J.* 272:3767-76.

Coblitz, B., S. Shikano, M. Wu, S.B. Gabelli, L.M. Cockrell, M. Spieker, Y. Hanyu, H. Fu, L.M. Amzel, and M. Li. 2005. C-terminal recognition by 14-3-3 proteins for surface expression of membrane receptors. *J Biol Chem.* 280:36263-72.

Costes, S.V., D. Daelemans, E.H. Cho, Z. Dobbin, G. Pavlakis, and S. Lockett. 2004. Automatic and quantitative measurement of protein-protein colocalization in live cells. *Biophys J.* 86:3993-4003.

Craparo, A., R. Freund, and T.A. Gustafson. 1997. 14-3-3 (epsilon) interacts with the insulin-like growth factor I receptor and insulin receptor substrate I in a phosphoserine-dependent manner. *J Biol Chem.* 272:11663-9.

Critchley, D.R., C.H. Streuli, S. Kellie, S. Ansell, and B. Patel. 1982. Characterization of the cholera toxin receptor on Balb/c 3T3 cells as a ganglioside similar to, or identical with, ganglioside GM1. No evidence for galactoproteins with receptor activity. *Biochem J.* 204:209-19.

Czech, M.P. 2000. Lipid rafts and insulin action. *Nature.* 407:147-8.

Dalal, S.N., M.B. Yaffe, and J.A. DeCaprio. 2004. 14-3-3 family members act coordinately to regulate mitotic progression. *Cell Cycle*. 3:672-7.

Datta, S.R., A. Katsov, L. Hu, A. Petros, S.W. Fesik, M.B. Yaffe, and M.E. Greenberg. 2000. 14-3-3 proteins and survival kinases cooperate to inactivate BAD by BH3 domain phosphorylation. *Mol Cell*. 6:41-51.

Davare, M.A., T. Saneyoshi, E.S. Guire, S.C. Nygaard, and T.R. Soderling. 2004. Inhibition of calcium/calmodulin-dependent protein kinase kinase by protein 14-3-3. *J Biol Chem*. 279:52191-9.

Davies, M.A., H.F. Schuster, J.W. Brauner, and R. Mendelsohn. 1990. Effects of cholesterol on conformational disorder in dipalmitoylphosphatidylcholine bilayers. A quantitative IR study of the depth dependence. *Biochemistry*. 29:4368-73.

Davy, A., C. Feuerstein, and S.M. Robbins. 2000. Signaling within a caveolae-like membrane microdomain in human neuroblastoma cells in response to fibroblast growth factor. *J Neurochem*. 74:676-83.

de Almeida, R.F., A. Fedorov, and M. Prieto. 2003. Sphingomyelin/phosphatidylcholine/cholesterol phase diagram: boundaries and composition of lipid rafts. *Biophys J*. 85:2406-16.

de Almeida, R.F., L.M. Loura, A. Fedorov, and M. Prieto. 2005. Lipid rafts have different sizes depending on membrane composition: a time-resolved fluorescence resonance energy transfer study. *J Mol Biol*. 346:1109-20.

De Caprio, J., J. Yun, and N.B. Javitt. 1992. Bile acid and sterol solubilization in 2-hydroxypropyl-beta-cyclodextrin. *J Lipid Res*. 33:441-3.

Demandolx, D., and J. Davoust. 1997. Multicolour analysis and local image correlation in confocal microscopy. *Journal of microscopy*. 185:21-36.

Demel, R.A., and B. De Kruyff. 1976. The function of sterols in membranes. *Biochim Biophys Acta*. 457:109-32.

Demel, R.A., J.W. Jansen, P.W. van Dijck, and L.L. van Deenen. 1977. The preferential interaction of cholesterol with different classes of phospholipids. *Biochim Biophys Acta*. 465:1-10.

Devaux, P.F. 1991. Static and dynamic lipid asymmetry in cell membranes. *Biochemistry*. 30:1163-73.

Devaux, P.F., and R. Morris. 2004. Transmembrane asymmetry and lateral domains in biological membranes. *Traffic*. 5:241-6.

Dhillon, A.S., S. Meikle, Z. Yazici, M. Eulitz, and W. Kolch. 2002. Regulation of Raf-1 activation and signalling by dephosphorylation. *Embo J*. 21:64-71.

Di Guglielmo, G.M., C. Le Roy, A.F. Goodfellow, and J.L. Wrana. 2003. Distinct endocytic pathways regulate TGF-beta receptor signalling and turnover. *Nat Cell Biol*. 5:410-21.

Dietrich, C., L.A. Bagatolli, Z.N. Volovyk, N.L. Thompson, M. Levi, K. Jacobson, and E. Gratton. 2001a. Lipid rafts reconstituted in model membranes. *Biophys J*. 80:1417-28.

Dietrich, C., Z.N. Volovyk, M. Levi, N.L. Thompson, and K. Jacobson. 2001b. Partitioning of Thy-1, GM1, and cross-linked phospholipid analogs into lipid rafts reconstituted in supported model membrane monolayers. *Proc Natl Acad Sci U S A*. 98:10642-7.

Dietrich, C., B. Yang, T. Fujiwara, A. Kusumi, and K. Jacobson. 2002. Relationship of lipid rafts to transient confinement zones detected by single particle tracking. *Biophys J.* 82:274-84.

Diviani, D., L. Abuin, S. Cotecchia, and L. Pansier. 2004. Anchoring of both PKA and 14-3-3 inhibits the Rho-GEF activity of the AKAP-Lbc signaling complex. *Embo J.* 23:2811-20.

Dougherty, M.K., and D.K. Morrison. 2004. Unlocking the code of 14-3-3. *J Cell Sci.* 117:1875-84.

Douglass, A.D., and R.D. Vale. 2005. Single-molecule microscopy reveals plasma membrane microdomains created by protein-protein networks that exclude or trap signaling molecules in T cells. *Cell.* 121:937-50.

Draberova, L., and P. Draber. 1993. Thy-1 glycoprotein and src-like protein-tyrosine kinase p53/p56lyn are associated in large detergent-resistant complexes in rat basophilic leukemia cells. *Proc Natl Acad Sci U S A.* 90:3611-5.

Drevot, P., C. Langlet, X.J. Guo, A.M. Bernard, O. Colard, J.P. Chauvin, R. Lasserre, and H.T. He. 2002. TCR signal initiation machinery is pre-assembled and activated in a subset of membrane rafts. *Embo J.* 21:1899-908.

Dubois, T., C. Rommel, S. Howell, U. Steinhussen, Y. Soneji, N. Morrice, K. Moelling, and A. Aitken. 1997. 14-3-3 is phosphorylated by casein kinase I on residue 233. Phosphorylation at this site in vivo regulates Raf/14-3-3 interaction. *J Biol Chem.* 272:28882-8.

Dulubova, I., S. Sugita, S. Hill, M. Hosaka, I. Fernandez, T.C. Sudhof, and J. Rizo. 1999. A conformational switch in syntaxin during exocytosis: role of munc18. *Embo J.* 18:4372-82.

Dumaz, N., and R. Marais. 2003. Protein kinase A blocks Raf-1 activity by stimulating 14-3-3 binding and blocking Raf-1 interaction with Ras. *J Biol Chem.* 278:29819-23.

Edidin, M. 2001. Shrinking patches and slippery rafts: scales of domains in the plasma membrane. *Trends Cell Biol.* 11:492-6.

Edidin, M. 2003. The state of lipid rafts: from model membranes to cells. *Annu Rev Biophys Biomol Struct.* 32:257-83.

Efendiev, R., Z. Chen, R.T. Krmar, S. Uhles, A.I. Katz, C.H. Pedemonte, and A.M. Bertorello. 2005. The 14-3-3 protein translates the NA+,K+-ATPase {alpha}1-subunit phosphorylation signal into binding and activation of phosphoinositide 3-kinase during endocytosis. *J Biol Chem.* 280:16272-7.

Elkins, J.M., G.A. Schoch, X. Yang, M. Sundstrom, C. Arrowsmith, A. Edwards, and D.A. Doyle. 2005. 14-3-3 PROTEIN BETA (HUMAN) IN COMPLEX WITH EXOENZYME S PEPTIDE (2C23). Retrieved on 10 Sept 2006 from www.rcsb.org/pdb/cgi/explore.cgi?pdbId=2C23.

Engelman, D.M., and J.E. Rothman. 1972. The planar organization of lecithin-cholesterol bilayers. *J Biol Chem.* 247:3694-7.

Fallon, L., F. Moreau, B.G. Croft, N. Labib, W.J. Gu, and E.A. Fon. 2002. Parkin and CASK/LIN-2 associate via a PDZ-mediated interaction and are co-localized in lipid rafts and postsynaptic densities in brain. *J Biol Chem.* 277:486-91.

Fantl, W.J., A.J. Muslin, A. Kikuchi, J.A. Martin, A.M. MacNicol, R.W. Gross, and L.T. Williams. 1994. Activation of Raf-1 by 14-3-3 proteins. *Nature.* 371:612-4.

Fasshauer, D., and M. Margittai. 2004. A transient N-terminal interaction of SNAP-25 and syntaxin nucleates SNARE assembly. *J Biol Chem.* 279:7613-21.

Feigenson, G.W., and J.T. Buboltz. 2001. Ternary phase diagram of dipalmitoyl-PC/dilauroyl-PC/cholesterol: nanoscopic domain formation driven by cholesterol. *Biophys J.* 80:2775-88.

Fiedler, K., T. Kobayashi, T.V. Kurzchalia, and K. Simons. 1993. Glycosphingolipid-enriched, detergent-insoluble complexes in protein sorting in epithelial cells. *Biochemistry.* 32:6365-73.

Field, K.A., D. Holowka, and B. Baird. 1995. Fc epsilon RI-mediated recruitment of p53/56lyn to detergent-resistant membrane domains accompanies cellular signaling. *Proc Natl Acad Sci U S A.* 92:9201-5.

Field, K.A., D. Holowka, and B. Baird. 1997. Compartmentalized activation of the high affinity immunoglobulin E receptor within membrane domains. *J Biol Chem.* 272:4276-80.

Fishman, P.H., and P.A. Orlandi. 2003. Cholera toxin internalization and intoxication. *J Cell Sci.* 116:431-2; author reply 432-3.

Foger, N., R. Marhaba, and M. Zoller. 2000. CD44 supports T cell proliferation and apoptosis by apposition of protein kinases. *Eur J Immunol.* 30:2888-99.

Foster, L.J., C.L. De Hoog, and M. Mann. 2003. Unbiased quantitative proteomics of lipid rafts reveals high specificity for signaling factors. *Proc Natl Acad Sci U S A.* 100:5813-8.

Fra, A.M., M. Masserini, P. Palestini, S. Sonnino, and K. Simons. 1995. A photo-reactive derivative of ganglioside GM1 specifically cross-links VIP21-caveolin on the cell surface. *FEBS Lett.* 375:11-4.

Fra, A.M., E. Williamson, K. Simons, and R.G. Parton. 1994. Detergent-insoluble glycolipid microdomains in lymphocytes in the absence of caveolae. *J Biol Chem.* 269:30745-8.

Freed, E., M. Symons, S.G. Macdonald, F. McCormick, and R. Ruggieri. 1994. Binding of 14-3-3 proteins to the protein kinase Raf and effects on its activation. *Science.* 265:1713-6.

Friedrichson, T., and T.V. Kurzchalia. 1998. Microdomains of GPI-anchored proteins in living cells revealed by crosslinking. *Nature.* 394:802-5.

Fu, H., R.R. Subramanian, and S.C. Masters. 2000. 14-3-3 proteins: structure, function, and regulation. *Annu Rev Pharmacol Toxicol.* 40:617-47.

Fu, H., K. Xia, D.C. Pallas, C. Cui, K. Conroy, R.P. Narsimhan, H. Mamon, R.J. Collier, and T.M. Roberts. 1994. Interaction of the protein kinase Raf-1 with 14-3-3 proteins. *Science.* 266:126-9.

Fujinaga, Y., A.A. Wolf, C. Rodighiero, H. Wheeler, B. Tsai, L. Allen, M.G. Jobling, T. Rapoport, R.K. Holmes, and W.I. Lencer. 2003. Gangliosides that associate with lipid rafts mediate transport of cholera and related toxins from the plasma membrane to endoplasmic reticulm. *Mol Biol Cell.* 14:4783-93.

Fujita, N., S. Sato, and T. Tsuruo. 2003. Phosphorylation of p27Kip1 at threonine 198 by p90 ribosomal protein S6 kinases promotes its binding to 14-3-3 and cytoplasmic localization. *J Biol Chem.* 278:49254-60.

Fujiwara, T., K. Ritchie, H. Murakoshi, K. Jacobson, and A. Kusumi. 2002. Phospholipids undergo hop diffusion in compartmentalized cell membrane. *J Cell Biol.* 157:1071-81.

Furukawa, Y., N. Ikuta, S. Omata, T. Yamauchi, T. Isobe, and T. Ichimura. 1993. Demonstration of the phosphorylation-dependent interaction of tryptophan hydroxylase with the 14-3-3 protein. *Biochem Biophys Res Commun.* 194:144-9.

Ganguly, S., J.L. Weller, A. Ho, P. Chemineau, B. Malpaux, and D.C. Klein. 2005. Melatonin synthesis: 14-3-3-dependent activation and inhibition of arylalkylamine N-acetyltransferase mediated by phosphoserine-205. *Proc Natl Acad Sci U S A.* 102:1222-7.

Garcia, A., X. Cayla, A. Fleischer, J. Guergnon, F. Alvarez-Franco Canas, M.P. Rebollo, F. Roncal, and A. Rebollo. 2003. Rafts: a simple way to control apoptosis by subcellular redistribution. *Biochimie.* 85:727-31.

Gardino, A.K., S.J. Smerdon, and M.B. Yaffe. 2006. Structural determinants of 14-3-3 binding specificities and regulation of subcellular localization of 14-3-3-ligand complexes: A comparison of the X-ray crystal structures of all human 14-3-3 isoforms. *Semin Cancer Biol.* 16:173-82.

Gaus, K., E. Chklovskaia, B. Fazekas de St Groth, W. Jessup, and T. Harder. 2005. Condensation of the plasma membrane at the site of T lymphocyte activation. *J Cell Biol.* 171:121-31.

Gaus, K., E. Gratton, E.P. Kable, A.S. Jones, I. Gelissen, L. Kritharides, and W. Jessup. 2003. Visualizing lipid structure and raft domains in living cells with two-photon microscopy. *Proc Natl Acad Sci U S A.* 100:15554-9.

Gaus, K., S. Le Lay, N. Balasubramanian, and M.A. Schwartz. 2006. Integrin-mediated adhesion regulates membrane order. *J Cell Biol.* 174:725-34.

Ge, M., K.A. Field, R. Aneja, D. Holowka, B. Baird, and J.H. Freed. 1999. Electron spin resonance characterization of liquid ordered phase of detergent-resistant membranes from RBL-2H3 cells. *Biophys J.* 77:925-33.

Gil, C., R. Cubi, J. Blasi, and J. Aguilera. 2006. Synaptic proteins associate with a sub-set of lipid rafts when isolated from nerve endings at physiological temperature. *Biochem Biophys Res Commun.*

Gil, C., A. Soler-Jover, J. Blasi, and J. Aguilera. 2005. Synaptic proteins and SNARE complexes are localized in lipid rafts from rat brain synaptosomes. *Biochem Biophys Res Commun.* 329:117-24.

Giurisato, E., D.P. McIntosh, M. Tassi, A. Gamberucci, and A. Benedetti. 2003. T cell receptor can be recruited to a subset of plasma membrane rafts, independently of cell signaling and attendantly to raft clustering. *J Biol Chem.* 278:6771-8.

Glebov, O.O., and B.J. Nichols. 2004a. Distribution of lipid raft markers in live cells. *Biochem Soc Trans.* 32:673-5.

Glebov, O.O., and B.J. Nichols. 2004b. Lipid raft proteins have a random distribution during localized activation of the T-cell receptor. *Nat Cell Biol.* 6:238-43.

Godde, N.J., G.M. D'Abaco, L. Paradiso, and U. Novak. 2006. Efficient ADAM22 surface expression is mediated by phosphorylation-dependent interaction with 14-3-3 protein family members. *J Cell Sci.*

Gonzalo, S., W.K. Greentree, and M.E. Linder. 1999. SNAP-25 is targeted to the plasma membrane through a novel membrane-binding domain. *J Biol Chem.* 274:21313-8.

Goodwin, J.S., K.R. Drake, C.L. Remmert, and A.K. Kenworthy. 2005. Ras diffusion is sensitive to plasma membrane viscosity. *Biophys J.* 89:1398-410.

Gorodinsky, A., and D.A. Harris. 1995. Glycolipid-anchored proteins in neuroblastoma cells form detergent-resistant complexes without caveolin. *J Cell Biol.* 129:619-27.

Green, A.J. 2002. Cerebrospinal fluid brain-derived proteins in the diagnosis of Alzheimer's disease and Creutzfeldt-Jakob disease. *Neuropathol Appl Neurobiol.* 28:427-40.

Greene, L.A., and A.S. Tischler. 1976. Establishment of a noradrenergic clonal line of rat adrenal pheochromocytoma cells which respond to nerve growth factor. *Proc Natl Acad Sci U S A.* 73:2424-8.

Gri, G., B. Molon, S. Manes, T. Pozzan, and A. Viola. 2004. The inner side of T cell lipid rafts. *Immunol Lett.* 94:247-52.

Grimmer, S., B. van Deurs, and K. Sandvig. 2002. Membrane ruffling and macropinocytosis in A431 cells require cholesterol. *J Cell Sci.* 115:2953-62.

Grunze, M., and B. Deuticke. 1974. Changes of membrane permeability due to extensive cholesterol depletion in mammalian erythrocytes. *Biochim Biophys Acta.* 356:125-30.

Guo, W., V. Kurze, T. Huber, N.H. Afdhal, K. Beyer, and J.A. Hamilton. 2002. A solid-state NMR study of phospholipid-cholesterol interactions: sphingomyelin-cholesterol binary systems. *Biophys J.* 83:1465-78.

Hamaguchi, A., E. Suzuki, K. Murayama, T. Fujimura, T. Hikita, K. Iwabuchi, K. Handa, D.A. Withers, S.C. Masters, H. Fu, and S. Hakomori. 2003. Sphingosine-dependent protein kinase-1, directed to 14-3-3, is identified as the kinase domain of protein kinase C delta. *J Biol Chem.* 278:41557-65.

Hancock, J.F. 2006. Lipid rafts: contentious only from simplistic standpoints. *Nat Rev Mol Cell Biol.* 7:456-62.

Hao, M., S. Mukherjee, and F.R. Maxfield. 2001. Cholesterol depletion induces large scale domain segregation in living cell membranes. *Proc Natl Acad Sci U S A.* 98:13072-7.

Hao, M., S. Mukherjee, Y. Sun, and F.R. Maxfield. 2004. Effects of cholesterol depletion and increased lipid unsaturation on the properties of endocytic membranes. *J Biol Chem.* 279:14171-8.

Harder, T. 2004. Lipid raft domains and protein networks in T-cell receptor signal transduction. *Curr Opin Immunol.* 16:353-9.

Harder, T., and M. Kuhn. 2000. Selective accumulation of raft-associated membrane protein LAT in T cell receptor signaling assemblies. *J Cell Biol.* 151:199-208.

Harder, T., P. Scheiffele, P. Verkade, and K. Simons. 1998. Lipid domain structure of the plasma membrane revealed by patching of membrane components. *J Cell Biol.* 141:929-42.

Harder, T., and K. Simons. 1999. Clusters of glycolipid and glycosylphosphatidylinositol-anchored proteins in lymphoid cells: accumulation of actin regulated by local tyrosine phosphorylation. *Eur J Immunol.* 29:556-62.

Harrington, M.G., C.R. Merril, D.M. Asher, and D.C. Gajdusek. 1986. Abnormal proteins in the cerebrospinal fluid of patients with Creutzfeldt-Jakob disease. *N Engl J Med.* 315:279-83.

He, H.T., A. Lellouch, and D. Marguet. 2005. Lipid rafts and the initiation of T cell receptor signaling. *Semin Immunol.* 17:23-33.

Heerklotz, H. 2002. Triton promotes domain formation in lipid raft mixtures. *Biophys J.* 83:2693-701.

Hekman, M., S. Wiese, R. Metz, S. Albert, J. Troppmair, J. Nickel, M. Sendtner, and U.R. Rapp. 2004. Dynamic changes in C-Raf phosphorylation and 14-3-3 protein binding in response to growth factor stimulation: differential roles of 14-3-3 protein binding sites. *J Biol Chem.* 279:14074-86.

Henke, R.C., K.A. Hancox, and P.L. Jeffrey. 1996. Characterization of two distinct populations of detergent resistant membrane complexes isolated from chick brain tissues. *J Neurosci Res.* 45:617-30.

Henley, J.R., E.W. Krueger, B.J. Oswald, and M.A. McNiven. 1998. Dynamin-mediated internalization of caveolae. *J Cell Biol.* 141:85-99.

Henriksson, M.L., M.S. Francis, A. Peden, M. Aili, K. Stefansson, R. Palmer, A. Aitken, and B. Hallberg. 2002. A nonphosphorylated 14-3-3 binding motif on exoenzyme S that is functional in vivo. *Eur J Biochem.* 269:4921-9.

Hermeking, H. 2003. The 14-3-3 cancer connection. *Nat Rev Cancer.* 3:931-43.

Hermeking, H., and A. Benzinger. 2006. 14-3-3 proteins in cell cycle regulation. *Semin Cancer Biol.* 16:183-92.

Hermeking, H., C. Lengauer, K. Polyak, T.C. He, L. Zhang, S. Thiagalingam, K.W. Kinzler, and B. Vogelstein. 1997. 14-3-3 sigma is a p53-regulated inhibitor of G2/M progression. *Mol Cell.* 1:3-11.

Herreros, J., T. Ng, and G. Schiavo. 2001. Lipid rafts act as specialized domains for tetanus toxin binding and internalization into neurons. *Mol Biol Cell.* 12:2947-60.

Hess, D.T., T.M. Slater, M.C. Wilson, and J.H. Skene. 1992. The 25 kDa synaptosomal-associated protein SNAP-25 is the major methionine-rich polypeptide in rapid axonal transport and a major substrate for palmitoylation in adult CNS. *J Neurosci.* 12:4634-41.

Hoessli, D., and E. Rungger-Brandle. 1985. Association of specific cell-surface glycoproteins with a triton X-100-resistant complex of plasma membrane proteins isolated from T-lymphoma cells (P1798). *Exp Cell Res.* 156:239-50.

Holmes, T.J., S. Bhattacharyya, J.A. Cooper, D. Hanzel, V. Krishnamurthi, W. Lin, B. Roysam, D.H. Szarowski, and J.N. Turner. 1995. Light microscopic images reconstructed by maximum likelihood deconvolution. *In* Handbook of Biological Confocal Microscopy. J.B. Pawley, editor. Plenum Press, New York. 389-400.

Holmgren, J. 1973. Comparison of the tissue receptors for Vibrio cholerae and Escherichia coli enterotoxins by means of gangliosides and natural cholera toxoid. *Infect Immun.* 8:851-9.

Holopainen, J.M., A.J. Metso, J.P. Mattila, A. Jutila, and P.K. Kinnunen. 2004. Evidence for the lack of a specific interaction between cholesterol and sphingomyelin. *Biophys J.* 86:1510-20.

Holowka, D., E.D. Sheets, and B. Baird. 2000. Interactions between Fc(epsilon)RI and lipid raft components are regulated by the actin cytoskeleton. *J Cell Sci.* 113 ( Pt 6):1009-19.

Homans, S.W., M.A. Ferguson, R.A. Dwek, T.W. Rademacher, R. Anand, and A.F. Williams. 1988. Complete structure of the glycosyl phosphatidylinositol membrane anchor of rat brain Thy-1 glycoprotein. *Nature*. 333:269-72.

Hong-wei, S., and H. McConnell. 1975. Phase separations in phospholipd membranes. *Biochemistry*. 14:847-54.

Horejsi, V. 2005. Lipid rafts and their roles in T-cell activation. *Microbes Infect*. 7:310-6.

Hsich, G., K. Kenney, C.J. Gibbs, K.H. Lee, and M.G. Harrington. 1996. The 14-3-3 brain protein in cerebrospinal fluid as a marker for transmissible spongiform encephalopathies. *N Engl J Med*. 335:924-30.

Hua, Y., and R.H. Scheller. 2001. Three SNARE complexes cooperate to mediate membrane fusion. *Proc Natl Acad Sci U S A*. 98:8065-70.

Huang, J., and G.W. Feigenson. 1999. A microscopic interaction model of maximum solubility of cholesterol in lipid bilayers. *Biophys J*. 76:2142-57.

Ichimura, T., T. Isobe, T. Okuyama, N. Takahashi, K. Araki, R. Kuwano, and Y. Takahashi. 1988. Molecular cloning of cDNA coding for brain-specific 14-3-3 protein, a protein kinase-dependent activator of tyrosine and tryptophan hydroxylases. *Proc Natl Acad Sci U S A*. 85:7084-8.

Ichimura, T., T. Isobe, T. Okuyama, T. Yamauchi, and H. Fujisawa. 1987. Brain 14-3-3 protein is an activator protein that activates tryptophan 5-monooxygenase and tyrosine 3-monooxygenase in the presence of Ca2+,calmodulin-dependent protein kinase II. *FEBS Lett*. 219:79-82.

Ikonen, E. 2001. Roles of lipid rafts in membrane transport. *Curr Opin Cell Biol*. 13:470-7.

Ilangumaran, S., and D.C. Hoessli. 1998. Effects of cholesterol depletion by cyclodextrin on the sphingolipid microdomains of the plasma membrane. *Biochem J*. 335 ( Pt 2):433-40.

Ipsen, J.H., G. Karlstrom, O.G. Mouritsen, H. Wennerstrom, and M.J. Zuckermann. 1987. Phase equilibria in the phosphatidylcholine-cholesterol system. *Biochim Biophys Acta*. 905:162-72.

Ipsen, J.H., O.G. Mouritsen, and M.J. Zuckermann. 1989. Theory of thermal anomalies in the specific heat of lipid bilayers containing cholesterol. *Biophys J*. 56:661-7.

Irles, C., A. Symons, F. Michel, T.R. Bakker, P.A. van der Merwe, and O. Acuto. 2003. CD45 ectodomain controls interaction with GEMs and Lck activity for optimal TCR signaling. *Nat Immunol*. 4:189-97.

Izaki, T., S. Kamakura, M. Kohjima, and H. Sumimoto. 2005. Phosphorylation-dependent binding of 14-3-3 to Par3beta, a human Par3-related cell polarity protein. *Biochem Biophys Res Commun*. 329:211-8.

Jacobson, K., and C. Dietrich. 1999. Looking at lipid rafts? *Trends Cell Biol*. 9:87-91.

Jacobson, K., E.D. Sheets, and R. Simson. 1995. Revisiting the fluid mosaic model of membranes. *Science*. 268:1441-2.

Jahn, R., T. Lang, and T.C. Sudhof. 2003. Membrane fusion. *Cell*. 112:519-33.

Janes, P.W., S.C. Ley, and A.I. Magee. 1999. Aggregation of lipid rafts accompanies signaling via the T cell antigen receptor. *J Cell Biol*. 147:447-61.

Jaumot, M., and J.F. Hancock. 2001. Protein phosphatases 1 and 2A promote Raf-1 activation by regulating 14-3-3 interactions. *Oncogene*. 20:3949-58.

Jaumot, M., J. Yan, J. Clyde-Smith, J. Sluimer, and J.F. Hancock. 2002. The linker domain of the Ha-Ras hypervariable region regulates interactions with exchange factors, Raf-1 and phosphoinositide 3-kinase. *J Biol Chem.* 277:272-8.

Jeanclos, E.M., L. Lin, M.W. Treuil, J. Rao, M.A. DeCoster, and R. Anand. 2001. The chaperone protein 14-3-3eta interacts with the nicotinic acetylcholine receptor alpha 4 subunit. Evidence for a dynamic role in subunit stabilization. *J Biol Chem.* 276:28281-90.

Jiang, K., E. Pereira, M. Maxfield, B. Russell, D.M. Goudelock, and Y. Sanchez. 2003. Regulation of Chk1 includes chromatin association and 14-3-3 binding following phosphorylation on Ser-345. *J Biol Chem.* 278:25207-17.

Jin, J., F.D. Smith, C. Stark, C.D. Wells, J.P. Fawcett, S. Kulkarni, P. Metalnikov, P. O'Donnell, P. Taylor, L. Taylor, A. Zougman, J.R. Woodgett, L.K. Langeberg, J.D. Scott, and T. Pawson. 2004. Proteomic, functional, and domain-based analysis of in vivo 14-3-3 binding proteins involved in cytoskeletal regulation and cellular organization. *Curr Biol.* 14:1436-50.

Jones, D.H., S. Ley, and A. Aitken. 1995a. Isoforms of 14-3-3 protein can form homo- and heterodimers in vivo and in vitro: implications for function as adapter proteins. *FEBS Lett.* 368:55-8.

Jones, D.H., H. Martin, J. Madrazo, K.A. Robinson, P. Nielsen, P.H. Roseboom, Y. Patel, S.A. Howell, and A. Aitken. 1995b. Expression and structural analysis of 14-3-3 proteins. *J Mol Biol.* 245:375-84.

Kabouridis, P.S., J. Janzen, A.L. Magee, and S.C. Ley. 2000. Cholesterol depletion disrupts lipid rafts and modulates the activity of multiple signaling pathways in T lymphocytes. *Eur J Immunol.* 30:954-63.

Kabouridis, P.S., A.I. Magee, and S.C. Ley. 1997. S-acylation of LCK protein tyrosine kinase is essential for its signalling function in T lymphocytes. *Embo J.* 16:4983-98.

Kahya, N., D.A. Brown, and P. Schwille. 2005. Raft partitioning and dynamic behavior of human placental alkaline phosphatase in giant unilamellar vesicles. *Biochemistry.* 44:7479-89.

Kahya, N., D. Scherfeld, K. Bacia, B. Poolman, and P. Schwille. 2003. Probing lipid mobility of raft-exhibiting model membranes by fluorescence correlation spectroscopy. *J Biol Chem.* 278:28109-15.

Kawamoto, Y., I. Akiguchi, S. Nakamura, Y. Honjyo, H. Shibasaki, and H. Budka. 2002. 14-3-3 proteins in Lewy bodies in Parkinson disease and diffuse Lewy body disease brains. *J Neuropathol Exp Neurol.* 61:245-53.

Keller, P., and K. Simons. 1998. Cholesterol is required for surface transport of influenza virus hemagglutinin. *J Cell Biol.* 140:1357-67.

Kenney, K., C. Brechtel, H. Takahashi, K. Kurohara, P. Anderson, and C.J. Gibbs, Jr. 2000. An enzyme-linked immunosorbent assay to quantify 14-3-3 proteins in the cerebrospinal fluid of suspected Creutzfeldt-Jakob disease patients. *Ann Neurol.* 48:395-8.

Kenworthy, A.K., and M. Edidin. 1998. Distribution of a glycosylphosphatidylinositol-anchored protein at the apical surface of MDCK cells examined at a resolution of <100 A using imaging fluorescence resonance energy transfer. *J Cell Biol.* 142:69-84.

Kenworthy, A.K., N. Petranova, and M. Edidin. 2000. High-resolution FRET microscopy of cholera toxin B-subunit and GPI-anchored proteins in cell plasma membranes. *Mol Biol Cell.* 11:1645-55.

Kilsdonk, E.P., P.G. Yancey, G.W. Stoudt, F.W. Bangerter, W.J. Johnson, M.C. Phillips, and G.H. Rothblat. 1995. Cellular cholesterol efflux mediated by cyclodextrins. *J Biol Chem.* 270:17250-6.

King, J., and U.K. Laemmli. 1971. Polypeptides of the tail fibres of bacteriophage T4. *J Mol Biol.* 62:465-77.

Kokubo, H., J.B. Helms, Y. Ohno-Iwashita, Y. Shimada, Y. Horikoshi, and H. Yamaguchi. 2003. Ultrastructural localization of flotillin-1 to cholesterol-rich membrane microdomains, rafts, in rat brain tissue. *Brain Res.* 965:83-90.

Kornbrust, D.J., J.S. MacDonald, C.P. Peter, D.M. Duchai, R.J. Stubbs, J.I. Germershausen, and A.W. Alberts. 1989. Toxicity of the HMG-coenzyme A reductase inhibitor, lovastatin, to rabbits. *J Pharmacol Exp Ther.* 248:498-505.

Korth, C., K. Kaneko, and S.B. Prusiner. 2000. Expression of unglycosylated mutated prion protein facilitates PrP(Sc) formation in neuroblastoma cells infected with different prion strains. *J Gen Virol.* 81:2555-63.

Korzeniowski, M., K. Kwiatkowska, and A. Sobota. 2003. Insights into the association of FcgammaRII and TCR with detergent-resistant membrane domains: isolation of the domains in detergent-free density gradients facilitates membrane fragment reconstitution. *Biochemistry.* 42:5358-67.

Kosaki, A., K. Yamada, J. Suga, A. Otaka, and H. Kuzuya. 1998. 14-3-3beta protein associates with insulin receptor substrate 1 and decreases insulin-stimulated phosphatidylinositol 3'-kinase activity in 3T3L1 adipocytes. *J Biol Chem.* 273:940-4.

Koynova, R., and M. Caffrey. 1995. Phases and phase transitions of the sphingolipids. *Biochim Biophys Acta.* 1255:213-36.

Kumagai, A., and W.G. Dunphy. 1999. Binding of 14-3-3 proteins and nuclear export control the intracellular localization of the mitotic inducer Cdc25. *Genes Dev.* 13:1067-72.

Kumagai, A., P.S. Yakowec, and W.G. Dunphy. 1998. 14-3-3 proteins act as negative regulators of the mitotic inducer Cdc25 in Xenopus egg extracts. *Mol Biol Cell.* 9:345-54.

Kusumi, A., I. Koyama-Honda, and K. Suzuki. 2004. Molecular dynamics and interactions for creation of stimulation-induced stabilized rafts from small unstable steady-state rafts. *Traffic.* 5:213-30.

Kusumi, A., and K. Suzuki. 2005. Toward understanding the dynamics of membrane-raft-based molecular interactions. *Biochim Biophys Acta.* 1746:234-51.

Kwik, J., S. Boyle, D. Fooksman, L. Margolis, M.P. Sheetz, and M. Edidin. 2003. Membrane cholesterol, lateral mobility, and the phosphatidylinositol 4,5-bisphosphate-dependent organization of cell actin. *Proc Natl Acad Sci U S A.* 100:13964-9.

Laage, R., J. Rohde, B. Brosig, and D. Langosch. 2000. A conserved membrane-spanning amino acid motif drives homomeric and supports heteromeric assembly of presynaptic SNARE proteins. *J Biol Chem.* 275:17481-7.

Lachmanovich, E., D.E. Shvartsman, Y. Malka, C. Botvin, Y.I. Henis, and A.M. Weiss. 2003. Co-localization analysis of complex formation among membrane proteins by computerized fluorescence microscopy: application to immunofluorescence co-patching studies. *J Microsc.* 212:122-31.

Lademann, U., T. Kallunki, and M. Jaattela. 2001. A20 zinc finger protein inhibits TNF-induced apoptosis and stress response early in the signaling cascades and independently of binding to TRAF2 or 14-3-3 proteins. *Cell Death Differ.* 8:265-72.

Lagerholm, B.C., G.E. Weinreb, K. Jacobson, and N.L. Thompson. 2005. Detecting microdomains in intact cell membranes. *Annu Rev Phys Chem.* 56:309-36.

Lalle, M., A.M. Salzano, M. Crescenzi, and E. Pozio. 2006. The Giardia duodenalis 14-3-3 protein is post-translationally modified by phosphorylation and polyglycylation of the C-terminal tail. *J Biol Chem.* 281:5137-48.

Lamaze, C., A. Dujeancourt, T. Baba, C.G. Lo, A. Benmerah, and A. Dautry-Varsat. 2001. Interleukin 2 receptors and detergent-resistant membrane domains define a clathrin-independent endocytic pathway. *Mol Cell.* 7:661-71.

Lane, S.R., and Y. Liu. 1997. Characterization of the palmitoylation domain of SNAP-25. *J Neurochem.* 69:1864-9.

Lang, T. 2003. Imaging SNAREs at work in 'unroofed' cells--approaches that may be of general interest for functional studies on membrane proteins. *Biochem Soc Trans.* 31:861-4.

Lang, T., D. Bruns, D. Wenzel, D. Riedel, P. Holroyd, C. Thiele, and R. Jahn. 2001. SNAREs are concentrated in cholesterol-dependent clusters that define docking and fusion sites for exocytosis. *Embo J.* 20:2202-13.

Lang, T., M. Margittai, H. Holzler, and R. Jahn. 2002. SNAREs in native plasma membranes are active and readily form core complexes with endogenous and exogenous SNAREs. *J Cell Biol.* 158:751-60.

Lange, Y., J.S. D'Alessandro, and D.M. Small. 1979. The affinity of cholesterol for phosphatidylcholine and sphingomyelin. *Biochim Biophys Acta.* 556:388-98.

Laronga, C., H.Y. Yang, C. Neal, and M.H. Lee. 2000. Association of the cyclin-dependent kinases and 14-3-3 sigma negatively regulates cell cycle progression. *J Biol Chem.* 275:23106-12.

Launikonis, B.S., and D.G. Stephenson. 2001. Effects of membrane cholesterol manipulation on excitation-contraction coupling in skeletal muscle of the toad. *J Physiol.* 534:71-85.

Laux, T., K. Fukami, M. Thelen, T. Golub, D. Frey, and P. Caroni. 2000. GAP43, MARCKS, and CAP23 modulate PI(4,5)P(2) at plasmalemmal rafts, and regulate cell cortex actin dynamics through a common mechanism. *J Cell Biol.* 149:1455-72.

Layfield, R., J. Fergusson, A. Aitken, J. Lowe, M. Landon, and R.J. Mayer. 1996. Neurofibrillary tangles of Alzheimer's disease brains contain 14-3-3 proteins. *Neurosci Lett.* 209:57-60.

Le, P.U., and I.R. Nabi. 2003. Distinct caveolae-mediated endocytic pathways target the Golgi apparatus and the endoplasmic reticulum. *J Cell Sci.* 116:1059-71.

Ledesma, M.D., J.S. Da Silva, A. Schevchenko, M. Wilm, and C.G. Dotti. 2003. Proteomic characterisation of neuronal sphingolipid-cholesterol microdomains: role in plasminogen activation. *Brain Res.* 987:107-16.

Ledesma, M.D., K. Simons, and C.G. Dotti. 1998. Neuronal polarity: essential role of protein-lipid complexes in axonal sorting. *Proc Natl Acad Sci U S A.* 95:3966-71.

Lee, J., A. Kumagai, and W.G. Dunphy. 2001. Positive regulation of Wee1 by Chk1 and 14-3-3 proteins. *Mol Biol Cell.* 12:551-63.

Leffers, H., P. Madsen, H.H. Rasmussen, B. Honore, A.H. Andersen, E. Walbum, J. Vandekerckhove, and J.E. Celis. 1993. Molecular cloning and expression of the transformation sensitive epithelial marker stratifin. A member of a protein family that has been involved in the protein kinase C signalling pathway. *J Mol Biol.* 231:982-98.

Lehoux, S., J. Abe, J.A. Florian, and B.C. Berk. 2001. 14-3-3 Binding to Na+/H+ exchanger isoform-1 is associated with serum-dependent activation of Na+/H+ exchange. *J Biol Chem.* 276:15794-800.

Lemstra, A.W., M.T. van Meegen, J.P. Vreyling, P.H. Meijerink, G.H. Jansen, S. Bulk, F. Baas, and W.A. van Gool. 2000. 14-3-3 testing in diagnosing Creutzfeldt-Jakob disease: a prospective study in 112 patients. *Neurology.* 55:514-6.

Lencer, W.I., C. Constable, S. Moe, M.G. Jobling, H.M. Webb, S. Ruston, J.L. Madara, T.R. Hirst, and R.K. Holmes. 1995. Targeting of cholera toxin and Escherichia coli heat labile toxin in polarized epithelia: role of COOH-terminal KDEL. *J Cell Biol.* 131:951-62.

Leventhal, A.R., W. Chen, A.R. Tall, and I. Tabas. 2001. Acid sphingomyelinase-deficient macrophages have defective cholesterol trafficking and efflux. *J Biol Chem.* 276:44976-83.

Leventis, R., and J.R. Silvius. 2001. Use of cyclodextrins to monitor transbilayer movement and differential lipid affinities of cholesterol. *Biophys J.* 81:2257-67.

Li, Q., A. Lau, T.J. Morris, L. Guo, C.B. Fordyce, and E.F. Stanley. 2004. A syntaxin 1, Galpha(o), and N-type calcium channel complex at a presynaptic nerve terminal: analysis by quantitative immunocolocalization. *J Neurosci.* 24:4070-81.

Li, S., P. Janosch, M. Tanji, G.C. Rosenfeld, J.C. Waymire, H. Mischak, W. Kolch, and J.M. Sedivy. 1995. Regulation of Raf-1 kinase activity by the 14-3-3 family of proteins. *Embo J.* 14:685-96.

Light, Y., H. Paterson, and R. Marais. 2002. 14-3-3 antagonizes Ras-mediated Raf-1 recruitment to the plasma membrane to maintain signaling fidelity. *Mol Cell Biol.* 22:4984-96.

Lin, R.C., and R.H. Scheller. 2000. Mechanisms of synaptic vesicle exocytosis. *Annu Rev Cell Dev Biol.* 16:19-49.

Lipardi, C., L. Nitsch, and C. Zurzolo. 2000. Detergent-insoluble GPI-anchored proteins are apically sorted in fischer rat thyroid cells, but interference with cholesterol or sphingolipids differentially affects detergent insolubility and apical sorting. *Mol Biol Cell.* 11:531-42.

Lisanti, M.P., M. Sargiacomo, L. Graeve, A.R. Saltiel, and E. Rodriguez-Boulan. 1988. Polarized apical distribution of glycosyl-phosphatidylinositol-anchored proteins in a renal epithelial cell line. *Proc Natl Acad Sci U S A.* 85:9557-61.

Lisanti, M.P., P.E. Scherer, Z. Tang, and M. Sargiacomo. 1994. Caveolae, caveolin and caveolin-rich membrane domains: a signalling hypothesis. *Trends Cell Biol.* 4:231-5.

Liu, D., J. Bienkowska, C. Petosa, R.J. Collier, H. Fu, and R. Liddington. 1995. Crystal structure of the zeta isoform of the 14-3-3 protein. *Nature.* 376:191-4.

Liu, P., Y. Ying, Y.G. Ko, and R.G. Anderson. 1996. Localization of platelet-derived growth factor-stimulated phosphorylation cascade to caveolae. *J Biol Chem.* 271:10299-303.

Liu, Q., S. Guntuku, X.S. Cui, S. Matsuoka, D. Cortez, K. Tamai, G. Luo, S. Carattini-Rivera, F. DeMayo, A. Bradley, L.A. Donehower, and S.J. Elledge. 2000. Chk1 is an essential kinase that is regulated by Atr and required for the G(2)/M DNA damage checkpoint. *Genes Dev.* 14:1448-59.

Liu, Y.C., Y. Liu, C. Elly, H. Yoshida, S. Lipkowitz, and A. Altman. 1997. Serine phosphorylation of Cbl induced by phorbol ester enhances its association with 14-3-3 proteins in T cells via a novel serine-rich 14-3-3-binding motif. *J Biol Chem.* 272:9979-85.

Locke, D., J. Liu, and A.L. Harris. 2005. Lipid rafts prepared by different methods contain different connexin channels, but gap junctions are not lipid rafts. *Biochemistry.* 44:13027-42.

Lommerse, P.H., G.A. Blab, L. Cognet, G.S. Harms, B.E. Snaar-Jagalska, H.P. Spaink, and T. Schmidt. 2004a. Single-molecule imaging of the H-ras membrane-anchor reveals domains in the cytoplasmic leaflet of the cell membrane. *Biophys J.* 86:609-16.

Lommerse, P.H., H.P. Spaink, and T. Schmidt. 2004b. In vivo plasma membrane organization: results of biophysical approaches. *Biochim Biophys Acta.* 1664:119-31.

Lonart, G., and T.C. Sudhof. 2000. Assembly of SNARE core complexes prior to neurotransmitter release sets the readily releasable pool of synaptic vesicles. *J Biol Chem.* 275:27703-7.

London, E., and D.A. Brown. 2000. Insolubility of lipids in triton X-100: physical origin and relationship to sphingolipid/cholesterol membrane domains (rafts). *Biochim Biophys Acta.* 1508:182-95.

Lopez-Girona, A., B. Furnari, O. Mondesert, and P. Russell. 1999. Nuclear localization of Cdc25 is regulated by DNA damage and a 14-3-3 protein. *Nature.* 397:172-5.

Loranger, S.S., and M.E. Linder. 2002. SNAP-25 traffics to the plasma membrane by a syntaxin-independent mechanism. *J Biol Chem.* 277:34303-9.

Low, M.G. 1989. The glycosyl-phosphatidylinositol anchor of membrane proteins. *Biochim Biophys Acta.* 988:427-54.

Low, S.H., A. Vasanji, J. Nanduri, M. He, N. Sharma, M. Koo, J. Drazba, and T. Weimbs. 2006. Syntaxins 3 and 4 are concentrated in separate clusters on the plasma membrane before the establishment of cell polarity. *Mol Biol Cell.* 17:977-89.

Luria, A., V. Vegelyte-Avery, B. Stith, N.M. Tsvetkova, W.F. Wolkers, J.H. Crowe, F. Tablin, and R. Nuccitelli. 2002. Detergent-free domain isolated from Xenopus egg plasma membrane with properties similar to those of detergent-resistant membranes. *Biochemistry.* 41:13189-97.

Ma, Y., S. Pitson, T. Hercus, J. Murphy, A. Lopez, and J. Woodcock. 2005. Sphingosine activates protein kinase A type II by a novel cAMP-independent mechanism. *J Biol Chem*. 280:26011-7.

Macdonald, J.L., and L.J. Pike. 2005. A simplified method for the preparation of detergent-free lipid rafts. *J Lipid Res*. 46:1061-7.

MacDonald, J.S., R.J. Gerson, D.J. Kornbrust, M.W. Kloss, S. Prahalada, P.H. Berry, A.W. Alberts, and D.L. Bokelman. 1988. Preclinical evaluation of lovastatin. *Am J Cardiol*. 62:16J-27J.

Madore, N., K.L. Smith, C.H. Graham, A. Jen, K. Brady, S. Hall, and R. Morris. 1999. Functionally different GPI proteins are organized in different domains on the neuronal surface. *Embo J*. 18:6917-26.

Magee, A.I., J. Adler, and I. Parmryd. 2005. Cold-induced coalescence of T-cell plasma membrane microdomains activates signalling pathways. *J Cell Sci*. 118:3141-51.

Manders, E.M., J. Stap, G.J. Brakenhoff, R. van Driel, and J.A. Aten. 1992. Dynamics of three-dimensional replication patterns during the S-phase, analysed by double labelling of DNA and confocal microscopy. *J Cell Sci*. 103 ( Pt 3):857-62.

Manders, E.M., F.J. Verbeek, and J.A. Aten. 1993. Measurement of co-localization of objects in dual-colour confocal images. *Journal of microscopy*. 169:375-382.

Marella, M., S. Lehmann, J. Grassi, and J. Chabry. 2002. Filipin prevents pathological prion protein accumulation by reducing endocytosis and inducing cellular PrP release. *J Biol Chem*. 277:25457-64.

Martens, J.R., R. Navarro-Polanco, E.A. Coppock, A. Nishiyama, L. Parshley, T.D. Grobaski, and M.M. Tamkun. 2000. Differential targeting of Shaker-like potassium channels to lipid rafts. *J Biol Chem*. 275:7443-6.

Martens, J.R., K. O'Connell, and M. Tamkun. 2004. Targeting of ion channels to membrane microdomains: localization of KV channels to lipid rafts. *Trends Pharmacol Sci*. 25:16-21.

Martin, H., Y. Patel, D. Jones, S. Howell, K. Robinson, and A. Aitken. 1993. Antibodies against the major brain isoforms of 14-3-3 protein. An antibody specific for the N-acetylated amino-terminus of a protein. *FEBS Lett*. 331:296-303.

Martin, H., J. Rostas, Y. Patel, and A. Aitken. 1994. Subcellular localisation of 14-3-3 isoforms in rat brain using specific antibodies. *J Neurochem*. 63:2259-65.

Masters, S.C., and H. Fu. 2001. 14-3-3 proteins mediate an essential anti-apoptotic signal. *J Biol Chem*. 276:45193-200.

Masters, S.C., K.J. Pederson, L. Zhang, J.T. Barbieri, and H. Fu. 1999. Interaction of 14-3-3 with a nonphosphorylated protein ligand, exoenzyme S of Pseudomonas aeruginosa. *Biochemistry*. 38:5216-21.

Masters, S.C., R.R. Subramanian, A. Truong, H. Yang, K. Fujii, H. Zhang, and H. Fu. 2002. Survival-promoting functions of 14-3-3 proteins. *Biochem Soc Trans*. 30:360-5.

Masters, S.C., H. Yang, S.R. Datta, M.E. Greenberg, and H. Fu. 2001. 14-3-3 inhibits Bad-induced cell death through interaction with serine-136. *Mol Pharmacol*. 60:1325-31.

Mayor, S., and F.R. Maxfield. 1995. Insolubility and redistribution of GPI-anchored proteins at the cell surface after detergent treatment. *Mol Biol Cell*. 6:929-44.

Mayor, S., and M. Rao. 2004. Rafts: scale-dependent, active lipid organization at the cell surface. *Traffic*. 5:231-40.

Mayor, S., K.G. Rothberg, and F.R. Maxfield. 1994. Sequestration of GPI-anchored proteins in caveolae triggered by cross-linking. *Science*. 264:1948-51.

McConnell, H.M., and A. Radhakrishnan. 2003. Condensed complexes of cholesterol and phospholipids. *Biochim Biophys Acta*. 1610:159-73.

McElhaney, R.N. 1982. The use of differential scanning calorimetry and differential thermal analysis in studies of model and biological membranes. *Chem Phys Lipids*. 30:229-59.

McMullen, T.P., R.N. Lewis, and R.N. McElhaney. 1993. Differential scanning calorimetric study of the effect of cholesterol on the thermotropic phase behavior of a homologous series of linear saturated phosphatidylcholines. *Biochemistry*. 32:516-22.

McMullen, T.P., and R.N. McElhaney. 1995. New aspects of the interaction of cholesterol with dipalmitoylphosphatidylcholine bilayers as revealed by high-sensitivity differential scanning calorimetry. *Biochim Biophys Acta*. 1234:90-8.

McMullen, T.W.P., R.N.A.H. Lewis, and R.N. McElhaney. 2004. Cholesterol-phospholipid interactions, the liquid-ordered phase and lipid rafts in model and biological membranes. *Current Opinion in Colloid and Interface Science*. 8:459-468.

McPherson, R.A., A. Harding, S. Roy, A. Lane, and J.F. Hancock. 1999. Interactions of c-Raf-1 with phosphatidylserine and 14-3-3. *Oncogene*. 18:3862-9.

Megidish, T., J. Cooper, L. Zhang, H. Fu, and S. Hakomori. 1998. A novel sphingosine-dependent protein kinase (SDK1) specifically phosphorylates certain isoforms of 14-3-3 protein. *J Biol Chem*. 273:21834-45.

Melkonian, K.A., A.G. Ostermeyer, J.Z. Chen, M.G. Roth, and D.A. Brown. 1999. Role of lipid modifications in targeting proteins to detergent-resistant membrane rafts. Many raft proteins are acylated, while few are prenylated. *J Biol Chem*. 274:3910-7.

Merritt, E.A., P. Kuhn, S. Sarfaty, J.L. Erbe, R.K. Holmes, and W.G. Hol. 1998. The 1.25 A resolution refinement of the cholera toxin B-pentamer: evidence of peptide backbone strain at the receptor-binding site. *J Mol Biol*. 282:1043-59.

Michaud, N.R., J.R. Fabian, K.D. Mathes, and D.K. Morrison. 1995. 14-3-3 is not essential for Raf-1 function: identification of Raf-1 proteins that are biologically activated in a 14-3-3- and Ras-independent manner. *Mol Cell Biol*. 15:3390-7.

Michelsen, K., H. Yuan, and B. Schwappach. 2005. Hide and run. Arginine-based endoplasmic-reticulum-sorting motifs in the assembly of heteromultimeric membrane proteins. *EMBO Rep*. 6:717-22.

Mineo, C., G.L. James, E.J. Smart, and R.G. Anderson. 1996. Localization of epidermal growth factor-stimulated Ras/Raf-1 interaction to caveolae membrane. *J Biol Chem*. 271:11930-5.

Minshall, R.D., C. Tiruppathi, S.M. Vogel, W.D. Niles, A. Gilchrist, H.E. Hamm, and A.B. Malik. 2000. Endothelial cell-surface gp60 activates vesicle formation and trafficking via G(i)-coupled Src kinase signaling pathway. *J Cell Biol.* 150:1057-70.

Mirre, C., L. Monlauzeur, M. Garcia, M.H. Delgrossi, and A. Le Bivic. 1996. Detergent-resistant membrane microdomains from Caco-2 cells do not contain caveolin. *Am J Physiol.* 271:C887-94.

Mitchell, J.S., O. Kanca, and B.W. McIntyre. 2002. Lipid microdomain clustering induces a redistribution of antigen recognition and adhesion molecules on human T lymphocytes. *J Immunol.* 168:2737-44.

Miura, Y., K. Hanada, and T.L. Jones. 2001. G(s) signaling is intact after disruption of lipid rafts. *Biochemistry.* 40:15418-23.

Montesano, R., J. Roth, A. Robert, and L. Orci. 1982. Non-coated membrane invaginations are involved in binding and internalization of cholera and tetanus toxins. *Nature.* 296:651-3.

Montixi, C., C. Langlet, A.M. Bernard, J. Thimonier, C. Dubois, M.A. Wurbel, J.P. Chauvin, M. Pierres, and H.T. He. 1998. Engagement of T cell receptor triggers its recruitment to low-density detergent-insoluble membrane domains. *Embo J.* 17:5334-48.

Moore, B.W., Perez, V. J. 1967. Specific acidic proteins of the nervous system. *In* In: Physiological and biochemical aspects of nervous integration. F.D. Carlson, editor. Prentice Hall, Englewood Cliffs, N. J. . 343-359.

Morgan, A., and R.D. Burgoyne. 1992a. Exo1 and Exo2 proteins stimulate calcium-dependent exocytosis in permeabilized adrenal chromaffin cells. *Nature.* 355:833-6.

Morgan, A., and R.D. Burgoyne. 1992b. Interaction between protein kinase C and Exo1 (14-3-3 protein) and its relevance to exocytosis in permeabilized adrenal chromaffin cells. *Biochem J.* 286 ( Pt 3):807-11.

Morris, R. 1985. Thy-1 in developing nervous tissue. *Dev Neurosci.* 7:133-60.

Morrison, D. 1994. 14-3-3: modulators of signaling proteins? *Science.* 266:56-7.

Morrow, I.C., S. Rea, S. Martin, I.A. Prior, R. Prohaska, J.F. Hancock, D.E. James, and R.G. Parton. 2002. Flotillin-1/reggie-2 traffics to surface raft domains via a novel golgi-independent pathway. Identification of a novel membrane targeting domain and a role for palmitoylation. *J Biol Chem.* 277:48834-41.

Munro, S. 2003. Lipid rafts: elusive or illusive? *Cell.* 115:377-88.

Murata, M., J. Peranen, R. Schreiner, F. Wieland, T.V. Kurzchalia, and K. Simons. 1995. VIP21/caveolin is a cholesterol-binding protein. *Proc Natl Acad Sci U S A.* 92:10339-43.

Muslin, A.J., J.W. Tanner, P.M. Allen, and A.S. Shaw. 1996. Interaction of 14-3-3 with signaling proteins is mediated by the recognition of phosphoserine. *Cell.* 84:889-97.

Muslin, A.J., and H. Xing. 2000. 14-3-3 proteins: regulation of subcellular localization by molecular interference. *Cell Signal.* 12:703-9.

Nabi, I.R., and P.U. Le. 2003. Caveolae/raft-dependent endocytosis. *J Cell Biol.* 161:673-7.

Nakagawa, Y., K. Inoue, and S. Nojima. 1979. Transfer of cholesterol between liposomal membranes. *Biochim Biophys Acta.* 553:307-19.

Naslavsky, N., R. Stein, A. Yanai, G. Friedlander, and A. Taraboulos. 1997. Characterization of detergent-insoluble complexes containing the cellular prion protein and its scrapie isoform. *J Biol Chem.* 272:6324-31.

Nebl, T., K.N. Pestonjamasp, J.D. Leszyk, J.L. Crowley, S.W. Oh, and E.J. Luna. 2002. Proteomic analysis of a detergent-resistant membrane skeleton from neutrophil plasma membranes. *J Biol Chem.* 277:43399-409.

Neufeld, E.B., M. Wastney, S. Patel, S. Suresh, A.M. Cooney, N.K. Dwyer, C.F. Roff, K. Ohno, J.A. Morris, E.D. Carstea, J.P. Incardona, J.F. Strauss, 3rd, M.T. Vanier, M.C. Patterson, R.O. Brady, P.G. Pentchev, and E.J. Blanchette-Mackie. 1999. The Niemann-Pick C1 protein resides in a vesicular compartment linked to retrograde transport of multiple lysosomal cargo. *J Biol Chem.* 274:9627-35.

Neumann-Giesen, C., B. Falkenbach, P. Beicht, S. Claasen, G. Luers, C.A. Stuermer, V. Herzog, and R. Tikkanen. 2004. Membrane and raft association of reggie-1/flotillin-2: role of myristoylation, palmitoylation and oligomerization and induction of filopodia by overexpression. *Biochem J.* 378:509-18.

Nichols, B. 2003a. Caveosomes and endocytosis of lipid rafts. *J Cell Sci.* 116:4707-14.

Nichols, B.J. 2003b. GM1-containing lipid rafts are depleted within clathrin-coated pits. *Curr Biol.* 13:686-90.

Nichols, B.J., A.K. Kenworthy, R.S. Polishchuk, R. Lodge, T.H. Roberts, K. Hirschberg, R.D. Phair, and J. Lippincott-Schwartz. 2001. Rapid cycling of lipid raft markers between the cell surface and Golgi complex. *J Cell Biol.* 153:529-41.

Nielsen, P.J. 1991. Primary structure of a human protein kinase regulator protein. *Biochim Biophys Acta.* 1088:425-8.

Niu, S.L., and B.J. Litman. 2002. Determination of membrane cholesterol partition coefficient using a lipid vesicle-cyclodextrin binary system: effect of phospholipid acyl chain unsaturation and headgroup composition. *Biophys J.* 83:3408-15.

Niv, H., O. Gutman, Y. Kloog, and Y.I. Henis. 2002. Activated K-Ras and H-Ras display different interactions with saturable nonraft sites at the surface of live cells. *J Cell Biol.* 157:865-72.

Nomura, M., S. Shimizu, T. Sugiyama, M. Narita, T. Ito, H. Matsuda, and Y. Tsujimoto. 2003. 14-3-3 Interacts directly with and negatively regulates pro-apoptotic Bax. *J Biol Chem.* 278:2058-65.

Nufer, O., and H.P. Hauri. 2003. ER export: call 14-3-3. *Curr Biol.* 13:R391-3.

O'Kelly, I., M.H. Butler, N. Zilberberg, and S.A. Goldstein. 2002. Forward transport. 14-3-3 binding overcomes retention in endoplasmic reticulum by dibasic signals. *Cell.* 111:577-88.

Obsil, T., R. Ghirlando, D.C. Klein, S. Ganguly, and F. Dyda. 2001. Crystal structure of the 14-3-3zeta:serotonin N-acetyltransferase complex. a role for scaffolding in enzyme regulation. *Cell.* 105:257-67.

Ogihara, T., T. Isobe, T. Ichimura, M. Taoka, M. Funaki, H. Sakoda, Y. Onishi, K. Inukai, M. Anai, Y. Fukushima, M. Kikuchi, Y. Yazaki, Y. Oka, and T. Asano. 1997. 14-3-3 protein binds to insulin receptor substrate-1, one of the binding sites of which is in the phosphotyrosine binding domain. *J Biol Chem.* 272:25267-74.

Oh, P., D.P. McIntosh, and J.E. Schnitzer. 1998. Dynamin at the neck of caveolae mediates their budding to form transport vesicles by GTP-driven fission from the plasma membrane of endothelium. *J Cell Biol.* 141:101-14.

Ohara-Imaizumi, M., C. Nishiwaki, T. Kikuta, K. Kumakura, Y. Nakamichi, and S. Nagamatsu. 2004. Site of docking and fusion of insulin secretory granules in live MIN6 beta cells analyzed by TAT-conjugated anti-syntaxin 1 antibody and total internal reflection fluorescence microscopy. *J Biol Chem.* 279:8403-8.

Ohvo-Rekila, H., B. Ramstedt, P. Leppimaki, and J.P. Slotte. 2002. Cholesterol interactions with phospholipids in membranes. *Prog Lipid Res.* 41:66-97.

Oksvold, M.P., H.S. Huitfeldt, and W.Y. Langdon. 2004. Identification of 14-3-3zeta as an EGF receptor interacting protein. *FEBS Lett.* 569:207-10.

Oliferenko, S., K. Paiha, T. Harder, V. Gerke, C. Schwarzler, H. Schwarz, H. Beug, U. Gunthert, and L.A. Huber. 1999. Analysis of CD44-containing lipid rafts: Recruitment of annexin II and stabilization by the actin cytoskeleton. *J Cell Biol.* 146:843-54.

Op den Kamp, J.A.F. 1979. Lipid asymmetry in membranes. *Annual Review of Biochemistry.* 48:47-71.

Orlandi, P.A., and P.H. Fishman. 1998. Filipin-dependent inhibition of cholera toxin: evidence for toxin internalization and activation through caveolae-like domains. *J Cell Biol.* 141:905-15.

Ory, S., M. Zhou, T.P. Conrads, T.D. Veenstra, and D.K. Morrison. 2003. Protein phosphatase 2A positively regulates Ras signaling by dephosphorylating KSR1 and Raf-1 on critical 14-3-3 binding sites. *Curr Biol.* 13:1356-64.

Ostermeyer, A.G., B.T. Beckrich, K.A. Ivarson, K.E. Grove, and D.A. Brown. 1999. Glycosphingolipids are not essential for formation of detergent-resistant membrane rafts in melanoma cells. methyl-beta-cyclodextrin does not affect cell surface transport of a GPI-anchored protein. *J Biol Chem.* 274:34459-66.

Ostrerova, N., L. Petrucelli, M. Farrer, N. Mehta, P. Choi, J. Hardy, and B. Wolozin. 1999. alpha-Synuclein shares physical and functional homology with 14-3-3 proteins. *J Neurosci.* 19:5782-91.

Otto, H., P.I. Hanson, and R. Jahn. 1997. Assembly and disassembly of a ternary complex of synaptobrevin, syntaxin, and SNAP-25 in the membrane of synaptic vesicles. *Proc Natl Acad Sci U S A.* 94:6197-201.

Panasiewicz, M., H. Domek, G. Hoser, M. Kawalec, and T. Pacuszka. 2003. Structure of the ceramide moiety of GM1 ganglioside determines its occurrence in different detergent-resistant membrane domains in HL-60 cells. *Biochemistry.* 42:6608-19.

Parasassi, T., G. De Stasio, A. d'Ubaldo, and E. Gratton. 1990. Phase fluctuation in phospholipid membranes revealed by Laurdan fluorescence. *Biophys J.* 57:1179-86.

Parasassi, T., G. De Stasio, G. Ravagnan, R.M. Rusch, and E. Gratton. 1991. Quantitation of lipid phases in phospholipid vesicles by the generalized polarization of Laurdan fluorescence. *Biophys J.* 60:179-89.

Parasassi, T., E. Gratton, H. Zajicek, M. Levi, and W. Yu. 1999. Detecting membrane lipid microdomains by two-photon fluorescence microscopy. *IEEE Eng Med Biol Mag.* 18:92-9.

Parasassi, T., E.K. Krasnowska, L.A. Bagatolli, and E. Gratton. 1998. Laurdan and Prodan as polarity-sensitive fluorescent membrane probes. *Journal of Fluorescence*. 8:365-373.

Paratcha, G., F. Ledda, L. Baars, M. Coulpier, V. Besset, J. Anders, R. Scott, and C.F. Ibanez. 2001. Released GFRalpha1 potentiates downstream signaling, neuronal survival, and differentiation via a novel mechanism of recruitment of c-Ret to lipid rafts. *Neuron*. 29:171-84.

Parkin, E.T., A.J. Turner, and N.M. Hooper. 1999. Amyloid precursor protein, although partially detergent-insoluble in mouse cerebral cortex, behaves as an atypical lipid raft protein. *Biochem J.* 344 Pt 1:23-30.

Parmryd, I., J. Adler, R. Patel, and A.I. Magee. 2003. Imaging metabolism of phosphatidylinositol 4,5-bisphosphate in T-cell GM1-enriched domains containing Ras proteins. *Exp Cell Res*. 285:27-38.

Parton, R.G. 1994. Ultrastructural localization of gangliosides; GM1 is concentrated in caveolae. *J Histochem Cytochem*. 42:155-66.

Parton, R.G. 2003. Caveolae--from ultrastructure to molecular mechanisms. *Nat Rev Mol Cell Biol*. 4:162-7.

Parton, R.G., and J.F. Hancock. 2004. Lipid rafts and plasma membrane microorganization: insights from Ras. *Trends Cell Biol*. 14:141-7.

Parton, R.G., B. Joggerst, and K. Simons. 1994. Regulated internalization of caveolae. *J Cell Biol*. 127:1199-215.

Parton, R.G., and A.A. Richards. 2003. Lipid rafts and caveolae as portals for endocytosis: new insights and common mechanisms. *Traffic*. 4:724-38.

Patel, Y., H. Martin, S. Howell, D. Jones, K. Robinson, and A. Aitken. 1994. Purification of 14-3-3 protein and analysis of isoforms in chicken brain. *Biochim Biophys Acta*. 1222:405-9.

Peluso, J.J., and A. Pappalardo. 2004. Progesterone regulates granulosa cell viability through a protein kinase G-dependent mechanism that may involve 14-3-3sigma. *Biol Reprod*. 71:1870-8.

Peng, C.Y., P.R. Graves, R.S. Thoma, Z. Wu, A.S. Shaw, and H. Piwnica-Worms. 1997. Mitotic and G2 checkpoint control: regulation of 14-3-3 protein binding by phosphorylation of Cdc25C on serine-216. *Science*. 277:1501-5.

Petosa, C., S.C. Masters, L.A. Bankston, J. Pohl, B. Wang, H. Fu, and R.C. Liddington. 1998. 14-3-3zeta binds a phosphorylated Raf peptide and an unphosphorylated peptide via its conserved amphipathic groove. *J Biol Chem*. 273:16305-10.

Pichler, H., and H. Riezman. 2004. Where sterols are required for endocytosis. *Biochim Biophys Acta*. 1666:51-61.

Pike, L.J. 2003. Lipid rafts: bringing order to chaos. *J Lipid Res*. 44:655-67.

Pike, L.J. 2004. Lipid rafts: heterogeneity on the high seas. *Biochem J*. 378:281-92.

Pike, L.J., X. Han, K.N. Chung, and R.W. Gross. 2002. Lipid rafts are enriched in arachidonic acid and plasmenylethanolamine and their composition is independent of caveolin-1 expression: a quantitative electrospray ionization/mass spectrometric analysis. *Biochemistry*. 41:2075-88.

Pike, L.J., X. Han, and R.W. Gross. 2005. Epidermal growth factor receptors are localized to lipid rafts that contain a balance of inner and outer leaflet lipids: a shotgun lipidomics study. *J Biol Chem*. 280:26796-804.

Plowman, S.J., C. Muncke, R.G. Parton, and J.F. Hancock. 2005. H-ras, K-ras, and inner plasma membrane raft proteins operate in nanoclusters with differential dependence on the actin cytoskeleton. *Proc Natl Acad Sci U S A.* 102:15500-5.

Pombo, I., J. Rivera, and U. Blank. 2003. Munc18-2/syntaxin3 complexes are spatially separated from syntaxin3-containing SNARE complexes. *FEBS Lett.* 550:144-8.

Powell, D.W., M.J. Rane, Q. Chen, S. Singh, and K.R. McLeish. 2002. Identification of 14-3-3zeta as a protein kinase B/Akt substrate. *J Biol Chem.* 277:21639-42.

Pozuelo Rubio, M., K.M. Geraghty, B.H. Wong, N.T. Wood, D.G. Campbell, N. Morrice, and C. Mackintosh. 2004. 14-3-3-affinity purification of over 200 human phosphoproteins reveals new links to regulation of cellular metabolism, proliferation and trafficking. *Biochem J.* 379:395-408.

Pralle, A., P. Keller, E.L. Florin, K. Simons, and J.K. Horber. 2000. Sphingolipid-cholesterol rafts diffuse as small entities in the plasma membrane of mammalian cells. *J Cell Biol.* 148:997-1008.

Prasad, G.L., E.M. Valverius, E. McDuffie, and H.L. Cooper. 1992. Complementary DNA cloning of a novel epithelial cell marker protein, HME1, that may be down-regulated in neoplastic mammary cells. *Cell Growth Differ.* 3:507-13.

Predescu, S.A., D.N. Predescu, K. Shimizu, I.K. Klein, and A.B. Malik. 2005. Cholesterol-dependent syntaxin-4 and SNAP-23 clustering regulates caveolar fusion with the endothelial plasma membrane. *J Biol Chem.* 280:37130-8.

Prinetti, A., V. Chigorno, G. Tettamanti, and S. Sonnino. 2000. Sphingolipid-enriched membrane domains from rat cerebellar granule cells differentiated in culture. A compositional study. *J Biol Chem.* 275:11658-65.

Prior, I.A., A. Harding, J. Yan, J. Sluimer, R.G. Parton, and J.F. Hancock. 2001. GTP-dependent segregation of H-ras from lipid rafts is required for biological activity. *Nat Cell Biol.* 3:368-75.

Prior, I.A., C. Muncke, R.G. Parton, and J.F. Hancock. 2003. Direct visualization of Ras proteins in spatially distinct cell surface microdomains. *J Cell Biol.* 160:165-70.

Puri, V., R. Watanabe, R.D. Singh, M. Dominguez, J.C. Brown, C.L. Wheatley, D.L. Marks, and R.E. Pagano. 2001. Clathrin-dependent and -independent internalization of plasma membrane sphingolipids initiates two Golgi targeting pathways. *J Cell Biol.* 154:535-47.

Pyenta, P.S., D. Holowka, and B. Baird. 2001. Cross-correlation analysis of inner-leaflet-anchored green fluorescent protein co-redistributed with IgE receptors and outer leaflet lipid raft components. *Biophys J.* 80:2120-32.

Rajan, S., R. Preisig-Muller, E. Wischmeyer, R. Nehring, P.J. Hanley, V. Renigunta, B. Musset, G. Schlichthorl, C. Derst, A. Karschin, and J. Daut. 2002. Interaction with 14-3-3 proteins promotes functional expression of the potassium channels TASK-1 and TASK-3. *J Physiol.* 545:13-26.

Rajendran, L., and K. Simons. 2005. Lipid rafts and membrane dynamics. *J Cell Sci.* 118:1099-102.

Rege, T.A., and J.S. Hagood. 2006. Thy-1 as a regulator of cell-cell and cell-matrix interactions in axon regeneration, apoptosis, adhesion, migration, cancer, and fibrosis. *Faseb J.* 20:1045-54.

Remacle-Bonnet, M., F. Garrouste, G. Baillat, F. Andre, J. Marvaldi, and G. Pommier. 2005. Membrane rafts segregate pro- from anti-apoptotic insulin-like growth factor-I receptor signaling in colon carcinoma cells stimulated by members of the tumor necrosis factor superfamily. *Am J Pathol.* 167:761-73.

Rickman, C., and B. Davletov. 2005. Arachidonic acid allows SNARE complex formation in the presence of Munc18. *Chem Biol.* 12:545-53.

Rickman, C., K. Hu, J. Carroll, and B. Davletov. 2005. Self-assembly of SNARE fusion proteins into star-shaped oligomers. *Biochem J.* 388:75-9.

Rickman, C., F.A. Meunier, T. Binz, and B. Davletov. 2004. High affinity interaction of syntaxin and SNAP-25 on the plasma membrane is abolished by botulinum toxin E. *J Biol Chem.* 279:644-51.

Rietveld, A., and K. Simons. 1998. The differential miscibility of lipids as the basis for the formation of functional membrane rafts. *Biochim Biophys Acta.* 1376:467-79.

Rittinger, K., J. Budman, J. Xu, S. Volinia, L.C. Cantley, S.J. Smerdon, S.J. Gamblin, and M.B. Yaffe. 1999. Structural analysis of 14-3-3 phosphopeptide complexes identifies a dual role for the nuclear export signal of 14-3-3 in ligand binding. *Mol Cell.* 4:153-66.

Robbins, S.M., N.A. Quintrell, and J.M. Bishop. 1995. Myristoylation and differential palmitoylation of the HCK protein-tyrosine kinases govern their attachment to membranes and association with caveolae. *Mol Cell Biol.* 15:3507-15.

Rodal, S.K., G. Skretting, O. Garred, F. Vilhardt, B. van Deurs, and K. Sandvig. 1999. Extraction of cholesterol with methyl-beta-cyclodextrin perturbs formation of clathrin-coated endocytic vesicles. *Mol Biol Cell.* 10:961-74.

Rodgers, W., B. Crise, and J.K. Rose. 1994. Signals determining protein tyrosine kinase and glycosyl-phosphatidylinositol-anchored protein targeting to a glycolipid-enriched membrane fraction. *Mol Cell Biol.* 14:5384-91.

Rodgers, W., and J. Zavzavadjian. 2001. Glycolipid-enriched membrane domains are assembled into membrane patches by associating with the actin cytoskeleton. *Exp Cell Res.* 267:173-83.

Rommel, C., G. Radziwill, J. Lovric, J. Noeldeke, T. Heinicke, D. Jones, A. Aitken, and K. Moelling. 1996. Activated Ras displaces 14-3-3 protein from the amino terminus of c-Raf-1. *Oncogene.* 12:609-19.

Roper, K., D. Corbeil, and W.B. Huttner. 2000. Retention of prominin in microvilli reveals distinct cholesterol-based lipid micro-domains in the apical plasma membrane. *Nat Cell Biol.* 2:582-92.

Rosenquist, M. 2003. 14-3-3 proteins in apoptosis. *Braz J Med Biol Res.* 36:403-8.

Rosenquist, M., P. Sehnke, R.J. Ferl, M. Sommarin, and C. Larsson. 2000. Evolution of the 14-3-3 protein family: does the large number of isoforms in multicellular organisms reflect functional specificity? *J Mol Evol.* 51:446-58.

Rotblat, B., I.A. Prior, C. Muncke, R.G. Parton, Y. Kloog, Y.I. Henis, and J.F. Hancock. 2004. Three separable domains regulate GTP-dependent association of H-ras with the plasma membrane. *Mol Cell Biol.* 24:6799-810.

Roth, D., J. Birkenfeld, and H. Betz. 1999. Dominant-negative alleles of 14-3-3 proteins cause defects in actin organization and vesicle targeting in the yeast Saccharomyces cerevisiae. *FEBS Lett.* 460:411-6.

Roth, D., and R.D. Burgoyne. 1995. Stimulation of catecholamine secretion from adrenal chromaffin cells by 14-3-3 proteins is due to reorganisation of the cortical actin network. *FEBS Lett.* 374:77-81.

Roth, D., A. Morgan, H. Martin, D. Jones, G.J. Martens, A. Aitken, and R.D. Burgoyne. 1994. Characterization of 14-3-3 proteins in adrenal chromaffin cells and demonstration of isoform-specific phospholipid binding. *Biochem J.* 301 ( Pt 1):305-10.

Rothblum-Oviatt, C.J., C.E. Ryan, and H. Piwnica-Worms. 2001. 14-3-3 binding regulates catalytic activity of human Wee1 kinase. *Cell Growth Differ.* 12:581-9.

Rothman, J.E., and D.M. Engelman. 1972. Molecular mechanism for the interaction of phospholipid with cholesterol. *Nat New Biol.* 237:42-4.

Roy, S., R. Luetterforst, A. Harding, A. Apolloni, M. Etheridge, E. Stang, B. Rolls, J.F. Hancock, and R.G. Parton. 1999. Dominant-negative caveolin inhibits H-Ras function by disrupting cholesterol-rich plasma membrane domains. *Nat Cell Biol.* 1:98-105.

Roy, S., R.A. McPherson, A. Apolloni, J. Yan, A. Lane, J. Clyde-Smith, and J.F. Hancock. 1998. 14-3-3 facilitates Ras-dependent Raf-1 activation in vitro and in vivo. *Mol Cell Biol.* 18:3947-55.

Rudd, P.M., M.R. Wormald, D.R. Wing, S.B. Prusiner, and R.A. Dwek. 2001. Prion glycoprotein: structure, dynamics, and roles for the sugars. *Biochemistry.* 40:3759-66.

Russell, S., and J. Oliaro. 2006. Compartmentalization in T-cell signalling: membrane microdomains and polarity orchestrate signalling and morphology. *Immunol Cell Biol.* 84:107-13.

Saarma, M. 2001. GDNF recruits the signaling crew into lipid rafts. *Trends Neurosci.* 24:427-9.

Sabharanjak, S., P. Sharma, R.G. Parton, and S. Mayor. 2002. GPI-anchored proteins are delivered to recycling endosomes via a distinct cdc42-regulated, clathrin-independent pinocytic pathway. *Dev Cell.* 2:411-23.

Salaun, C., G.W. Gould, and L.H. Chamberlain. 2005a. The SNARE proteins SNAP-25 and SNAP-23 display different affinities for lipid rafts in PC12 cells. Regulation by distinct cysteine-rich domains. *J Biol Chem.* 280:1236-40.

Salaun, C., G.W. Gould, and L.H. Chamberlain. 2005b. Lipid raft association of SNARE proteins regulates exocytosis in PC12 cells. *J Biol Chem.* 280:19449-53.

Salaun, C., D.J. James, and L.H. Chamberlain. 2004a. Lipid rafts and the regulation of exocytosis. *Traffic.* 5:255-64.

Salaun, C., D.J. James, J. Greaves, and L.H. Chamberlain. 2004b. Plasma membrane targeting of exocytic SNARE proteins. *Biochim Biophys Acta.* 1693:81-9.

Sankaram, M.B., and T.E. Thompson. 1990a. Interaction of cholesterol with various glycerophospholipids and sphingomyelin. *Biochemistry.* 29:10670-5.

Sankaram, M.B., and T.E. Thompson. 1990b. Modulation of phospholipid acyl chain order by cholesterol. A solid-state 2H nuclear magnetic resonance study. *Biochemistry.* 29:10676-84.

Sankaram, M.B., and T.E. Thompson. 1991. Cholesterol-induced fluid-phase immiscibility in membranes. *Proc Natl Acad Sci U S A.* 88:8686-90.

Sargiacomo, M., M. Sudol, Z. Tang, and M.P. Lisanti. 1993. Signal transducing molecules and glycosyl-phosphatidylinositol-linked proteins form a caveolin-rich insoluble complex in MDCK cells. *J Cell Biol.* 122:789-807.

Saslowsky, D.E., J.C. Lawrence, R.M. Henderson, and J.M. Edwardson. 2003. Syntaxin is efficiently excluded from sphingomyelin-enriched domains in supported lipid bilayers containing cholesterol. *J Membr Biol.* 194:153-64.

Schagger, H., and G. von Jagow. 1987. Tricine-sodium dodecyl sulfate-polyacrylamide gel electrophoresis for the separation of proteins in the range from 1 to 100 kDa. *Anal Biochem.* 166:368-79.

Schroeder, R., E. London, and D. Brown. 1994. Interactions between saturated acyl chains confer detergent resistance on lipids and glycosylphosphatidylinositol (GPI)-anchored proteins: GPI-anchored proteins in liposomes and cells show similar behavior. *Proc Natl Acad Sci U S A.* 91:12130-4.

Schroeder, R.J., S.N. Ahmed, Y. Zhu, E. London, and D.A. Brown. 1998. Cholesterol and sphingolipid enhance the Triton X-100 insolubility of glycosylphosphatidylinositol-anchored proteins by promoting the formation of detergent-insoluble ordered membrane domains. *J Biol Chem.* 273:1150-7.

Schuck, S., M. Honsho, K. Ekroos, A. Shevchenko, and K. Simons. 2003. Resistance of cell membranes to different detergents. *Proc Natl Acad Sci U S A.* 100:5795-800.

Schuck, S., and K. Simons. 2004. Polarized sorting in epithelial cells: raft clustering and the biogenesis of the apical membrane. *J Cell Sci.* 117:5955-64.

Schutz, G.J., G. Kada, V.P. Pastushenko, and H. Schindler. 2000. Properties of lipid microdomains in a muscle cell membrane visualized by single molecule microscopy. *Embo J.* 19:892-901.

Scientific Volume Imaging. 2006a. The Nyquist Rate. SVI wiki, SVI, Hilversum, The Netherlands. Retrieved on 28 Aug 2006 from http://support.svi.nl/wiki/NyquistRate.

Scientific Volume Imaging. 2006b. Pearsons Interpretation. SVI wiki, SVI, Hilversum, The Netherlands. Retrieved on 28 Aug 2006 from http://support.svi.nl/wiki/PearsonsInterpretation.

Seimiya, H., H. Sawada, Y. Muramatsu, M. Shimizu, K. Ohko, K. Yamane, and T. Tsuruo. 2000. Involvement of 14-3-3 proteins in nuclear localization of telomerase. *Embo J.* 19:2652-61.

Sekimoto, T., M. Fukumoto, and Y. Yoneda. 2004. 14-3-3 suppresses the nuclear localization of threonine 157-phosphorylated p27(Kip1). *Embo J.* 23:1934-42.

Sharma, P., R. Varma, R.C. Sarasij, Ira, K. Gousset, G. Krishnamoorthy, M. Rao, and S. Mayor. 2004. Nanoscale organization of multiple GPI-anchored proteins in living cell membranes. *Cell.* 116:577-89.

Shaw, P.J. 1995. Comparison of wide-field/deconvolution and confocal microscopy for 3D imaging. *In* Handbook of Biological Confocal Microscopy. J.B. Pawley, editor. Plenum Press, New York. 373-385.

Sheets, E.D., G.M. Lee, R. Simson, and K. Jacobson. 1997. Transient confinement of a glycosylphosphatidylinositol-anchored protein in the plasma membrane. *Biochemistry.* 36:12449-58.

Shenoy-Scaria, A.M., D.J. Dietzen, J. Kwong, D.C. Link, and D.M. Lublin. 1994. Cysteine3 of Src family protein tyrosine kinase determines palmitoylation and localization in caveolae. *J Cell Biol.* 126:353-63.

Shimshick, E.J., and H.M. McConnell. 1973a. Lateral phase separation in phospholipid membranes. *Biochemistry.* 12:2351-60.

Shimshick, E.J., and H.M. McConnell. 1973b. Lateral phase separations in binary mixtures of cholesterol and phospholipids. *Biochem Biophys Res Commun.* 53:446-51.

Shogomori, H., and D.A. Brown. 2003. Use of detergents to study membrane rafts: the good, the bad, and the ugly. *Biol Chem.* 384:1259-63.

Shogomori, H., and A.H. Futerman. 2001a. Cholera toxin is found in detergent-insoluble rafts/domains at the cell surface of hippocampal neurons but is internalized via a raft-independent mechanism. *J Biol Chem.* 276:9182-8.

Shogomori, H., and A.H. Futerman. 2001b. Cholesterol depletion by methyl-beta-cyclodextrin blocks cholera toxin transport from endosomes to the Golgi apparatus in hippocampal neurons. *J Neurochem.* 78:991-9.

Shvartsman, D.E., O. Gutman, A. Tietz, and Y.I. Henis. 2006. Cyclodextrins but not Compactin Inhibit the Lateral Diffusion of Membrane Proteins Independent of Cholesterol. *Traffic.* 7:917-26.

Shvartsman, D.E., M. Kotler, R.D. Tall, M.G. Roth, and Y.I. Henis. 2003. Differently anchored influenza hemagglutinin mutants display distinct interaction dynamics with mutual rafts. *J Cell Biol.* 163:879-88.

Sieber, J.J., K.I. Willig, R. Heintzmann, S.W. Hell, and T. Lang. 2006. The SNARE motif is essential for the formation of syntaxin clusters in the plasma membrane. *Biophys J.* 90:2843-51.

Silvius, J.R. 2003a. Role of cholesterol in lipid raft formation: lessons from lipid model systems. *Biochim Biophys Acta.* 1610:174-83.

Silvius, J.R. 2003b. Fluorescence energy transfer reveals microdomain formation at physiological temperatures in lipid mixtures modeling the outer leaflet of the plasma membrane. *Biophys J.* 85:1034-45.

Silvius, J.R., D. del Giudice, and M. Lafleur. 1996. Cholesterol at different bilayer concentrations can promote or antagonize lateral segregation of phospholipids of differing acyl chain length. *Biochemistry.* 35:15198-208.

Simons, K., and R. Ehehalt. 2002. Cholesterol, lipid rafts, and disease. *J Clin Invest.* 110:597-603.

Simons, K., and E. Ikonen. 1997. Functional rafts in cell membranes. *Nature.* 387:569-72.

Simons, K., and D. Toomre. 2000. Lipid rafts and signal transduction. *Nat Rev Mol Cell Biol.* 1:31-9.

Simons, K., and G. van Meer. 1988. Lipid sorting in epithelial cells. *Biochemistry.* 27:6197-202.

Simons, K., and W.L. Vaz. 2004. Model systems, lipid rafts, and cell membranes. *Annu Rev Biophys Biomol Struct.* 33:269-95.

Simson, R., E.D. Sheets, and K. Jacobson. 1995. Detection of temporary lateral confinement of membrane proteins using single-particle tracking analysis. *Biophys J.* 69:989-93.

Singer, S.J., and G.L. Nicolson. 1972. The fluid mosaic model of the structure of cell membranes. *Science.* 175:720-31.

Smaby, J.M., H.L. Brockman, and R.E. Brown. 1994. Cholesterol's interfacial interactions with sphingomyelins and phosphatidylcholines: hydrocarbon chain structure determines the magnitude of condensation. *Biochemistry.* 33:9135-42.

Smaby, J.M., M.M. Momsen, H.L. Brockman, and R.E. Brown. 1997. Phosphatidylcholine acyl unsaturation modulates the decrease in interfacial elasticity induced by cholesterol. *Biophys J.* 73:1492-505.

Smart, E.J., Y.S. Ying, C. Mineo, and R.G. Anderson. 1995. A detergent-free method for purifying caveolae membrane from tissue culture cells. *Proc Natl Acad Sci U S A.* 92:10104-8.

Song, K.S., S. Li, T. Okamoto, L.A. Quilliam, M. Sargiacomo, and M.P. Lisanti. 1996. Co-purification and direct interaction of Ras with caveolin, an integral membrane protein of caveolae microdomains. Detergent-free purification of caveolae microdomains. *J Biol Chem.* 271:9690-7.

Spence, S.L., B.R. Dey, C. Terry, P. Albert, P. Nissley, and R.W. Furlanetto. 2003. Interaction of 14-3-3 proteins with the insulin-like growth factor I receptor (IGFIR): evidence for a role of 14-3-3 proteins in IGFIR signaling. *Biochem Biophys Res Commun.* 312:1060-6.

Sprenger, R.R., D. Speijer, J.W. Back, C.G. De Koster, H. Pannekoek, and A.J. Horrevoets. 2004. Comparative proteomics of human endothelial cell caveolae and rafts using two-dimensional gel electrophoresis and mass spectrometry. *Electrophoresis.* 25:156-72.

Stauffer, T.P., and T. Meyer. 1997. Compartmentalized IgE receptor-mediated signal transduction in living cells. *J Cell Biol.* 139:1447-54.

Steinacker, P., P. Schwarz, K. Reim, P. Brechlin, O. Jahn, H. Kratzin, A. Aitken, J. Wiltfang, A. Aguzzi, E. Bahn, H.C. Baxter, N. Brose, and M. Otto. 2005. Unchanged survival rates of 14-3-3gamma knockout mice after inoculation with pathological prion protein. *Mol Cell Biol.* 25:1339-46.

Strochlic, L., A. Cartaud, A. Mejat, R. Grailhe, L. Schaeffer, J.P. Changeux, and J. Cartaud. 2004. 14-3-3 gamma associates with muscle specific kinase and regulates synaptic gene transcription at vertebrate neuromuscular synapse. *Proc Natl Acad Sci U S A.* 101:18189-94.

Stryer, L. 1978. Fluorescence energy transfer as a spectroscopic ruler. *Annu Rev Biochem.* 47:819-46.

Stuermer, C.A., D.M. Lang, F. Kirsch, M. Wiechers, S.O. Deininger, and H. Plattner. 2001. Glycosylphosphatidyl inositol-anchored proteins and fyn kinase assemble in noncaveolar plasma membrane microdomains defined by reggie-1 and -2. *Mol Biol Cell.* 12:3031-45.

Subczynski, W.K., and A. Kusumi. 2003. Dynamics of raft molecules in the cell and artificial membranes: approaches by pulse EPR spin labeling and single molecule optical microscopy. *Biochim Biophys Acta.* 1610:231-43.

Subtil, A., I. Gaidarov, K. Kobylarz, M.A. Lampson, J.H. Keen, and T.E. McGraw. 1999. Acute cholesterol depletion inhibits clathrin-coated pit budding. *Proc Natl Acad Sci U S A.* 96:6775-80.

Suginta, W., N. Karoulias, A. Aitken, and R.H. Ashley. 2001. Chloride intracellular channel protein CLIC4 (p64H1) binds directly to brain dynamin I in a complex containing actin, tubulin and 14-3-3 isoforms. *Biochem J.* 359:55-64.

Sunayama, J., F. Tsuruta, N. Masuyama, and Y. Gotoh. 2005. JNK antagonizes Akt-mediated survival signals by phosphorylating 14-3-3. *J Cell Biol.* 170:295-304.

Sutton, R.B., D. Fasshauer, R. Jahn, and A.T. Brunger. 1998. Crystal structure of a SNARE complex involved in synaptic exocytosis at 2.4 A resolution. *Nature.* 395:347-53.

Takeda, M., G.P. Leser, C.J. Russell, and R.A. Lamb. 2003. Influenza virus hemagglutinin concentrates in lipid raft microdomains for efficient viral fusion. *Proc Natl Acad Sci U S A.* 100:14610-7.

Tang, S.J., T.C. Suen, R.R. McInnes, and M. Buchwald. 1998. Association of the TLX-2 homeodomain and 14-3-3eta signaling proteins. *J Biol Chem.* 273:25356-63.

Tansey, M.G., R.H. Baloh, J. Milbrandt, and E.M. Johnson, Jr. 2000. GFRalpha-mediated localization of RET to lipid rafts is required for effective downstream signaling, differentiation, and neuronal survival. *Neuron.* 25:611-23.

Taraboulos, A., M. Scott, A. Semenov, D. Avrahami, L. Laszlo, and S.B. Prusiner. 1995. Cholesterol depletion and modification of COOH-terminal targeting sequence of the prion protein inhibit formation of the scrapie isoform. *J Cell Biol.* 129:121-32.

Tavano, R., G. Gri, B. Molon, B. Marinari, C.E. Rudd, L. Tuosto, and A. Viola. 2004. CD28 and lipid rafts coordinate recruitment of Lck to the immunological synapse of human T lymphocytes. *J Immunol.* 173:5392-7.

Taverna, E., E. Saba, J. Rowe, M. Francolini, F. Clementi, and P. Rosa. 2004. Role of lipid microdomains in P/Q-type calcium channel (Cav2.1) clustering and function in presynaptic membranes. *J Biol Chem.* 279:5127-34.

Taylor, C.M., T. Coetzee, and S.E. Pfeiffer. 2002. Detergent-insoluble glycosphingolipid/cholesterol microdomains of the myelin membrane. *J Neurochem.* 81:993-1004.

Thorson, J.A., L.W. Yu, A.L. Hsu, N.Y. Shih, P.R. Graves, J.W. Tanner, P.M. Allen, H. Piwnica-Worms, and A.S. Shaw. 1998. 14-3-3 proteins are required for maintenance of Raf-1 phosphorylation and kinase activity. *Mol Cell Biol.* 18:5229-38.

Tiruppathi, C., W. Song, M. Bergenfeldt, P. Sass, and A.B. Malik. 1997. Gp60 activation mediates albumin transcytosis in endothelial cells by tyrosine kinase-dependent pathway. *J Biol Chem.* 272:25968-75.

Toker, A., L.A. Sellers, B. Amess, Y. Patel, A. Harris, and A. Aitken. 1992. Multiple isoforms of a protein kinase C inhibitor (KCIP-1/14-3-3) from sheep brain. Amino acid sequence of phosphorylated forms. *Eur J Biochem.* 206:453-61.

Toonen, R.F., O. Kochubey, H. de Wit, A. Gulyas-Kovacs, B. Konijnenburg, J.B. Sorensen, J. Klingauf, and M. Verhage. 2006. Dissecting docking and tethering of secretory vesicles at the target membrane. *Embo J.* 25:3725-37.

Tsuruta, F., J. Sunayama, Y. Mori, S. Hattori, S. Shimizu, Y. Tsujimoto, K. Yoshioka, N. Masuyama, and Y. Gotoh. 2004. JNK promotes Bax translocation to mitochondria through phosphorylation of 14-3-3 proteins. *Embo J.* 23:1889-99.

Tzivion, G., Z. Luo, and J. Avruch. 1998. A dimeric 14-3-3 protein is an essential cofactor for Raf kinase activity. *Nature.* 394:88-92.

Ubl, A., D. Berg, C. Holzmann, R. Kruger, K. Berger, T. Arzberger, A. Bornemann, and O. Riess. 2002. 14-3-3 protein is a component of Lewy bodies in Parkinson's disease-mutation analysis and association studies of 14-3-3 eta. *Brain Res Mol Brain Res.* 108:33-9.

Ungermann, C., K. Sato, and W. Wickner. 1998. Defining the functions of trans-SNARE pairs. *Nature.* 396:543-8.

Van Der Hoeven, P.C., J.C. Van Der Wal, P. Ruurs, M.C. Van Dijk, and J. Van Blitterswijk. 2000. 14-3-3 isotypes facilitate coupling of protein kinase C-zeta to Raf-1: negative regulation by 14-3-3 phosphorylation. *Biochem J.* 345 Pt 2:297-306.

van Dijck, P.W. 1979. Negatively charged phospholipids and their position in the cholesterol affinity sequence. *Biochim Biophys Acta.* 555:89-101.

Van Dijck, P.W., B. De Kruijff, L.L. Van Deenen, J. De Gier, and R.A. Demel. 1976. The preference of cholesterol for phosphatidylcholine in mixed phosphatidylcholine-phosphatidylethanolamine bilayers. *Biochim Biophys Acta.* 455:576-87.

van Meer, G. 1989. Lipid traffic in animal cells. *Annu Rev Cell Biol.* 5:247-75.

van Meer, G., and K. Simons. 1982. Viruses budding from either the apical or the basolateral plasma membrane domain of MDCK cells have unique phospholipid compositions. *Embo J.* 1:847-52.

van Meer, G., and K. Simons. 1986. The function of tight junctions in maintaining differences in lipid composition between the apical and the basolateral cell surface domains of MDCK cells. *Embo J.* 5:1455-64.

van Meer, G., and K. Simons. 1988. Lipid polarity and sorting in epithelial cells. *J Cell Biochem.* 36:51-8.

van Meer, G., E.H. Stelzer, R.W. Wijnaendts-van-Resandt, and K. Simons. 1987. Sorting of sphingolipids in epithelial (Madin-Darby canine kidney) cells. *J Cell Biol.* 105:1623-35.

Varma, R., and S. Mayor. 1998. GPI-anchored proteins are organized in submicron domains at the cell surface. *Nature.* 394:798-801.

Veatch, S.L., and S.L. Keller. 2003. Separation of liquid phases in giant vesicles of ternary mixtures of phospholipids and cholesterol. *Biophys J.* 85:3074-83.

Veatch, S.L., and S.L. Keller. 2005. Seeing spots: complex phase behavior in simple membranes. *Biochim Biophys Acta.* 1746:172-85.

Veatch, S.L., I.V. Polozov, K. Gawrisch, and S.L. Keller. 2004. Liquid domains in vesicles investigated by NMR and fluorescence microscopy. *Biophys J.* 86:2910-22.

Veit, M., T.H. Sollner, and J.E. Rothman. 1996. Multiple palmitoylation of synaptotagmin and the t-SNARE SNAP-25. *FEBS Lett.* 385:119-23.

Venkatesan, S., J.J. Rose, R. Lodge, P.M. Murphy, and J.F. Foley. 2003. Distinct mechanisms of agonist-induced endocytosis for human chemokine receptors CCR5 and CXCR4. *Mol Biol Cell.* 14:3305-24.

Vercoutter-Edouart, A.S., J. Lemoine, X. Le Bourhis, H. Louis, B. Boilly, V. Nurcombe, F. Revillion, J.P. Peyrat, and H. Hondermarck. 2001. Proteomic analysis reveals that 14-3-3sigma is down-regulated in human breast cancer cells. *Cancer Res.* 61:76-80.

Vey, M., S. Pilkuhn, H. Wille, R. Nixon, S.J. DeArmond, E.J. Smart, R.G. Anderson, A. Taraboulos, and S.B. Prusiner. 1996. Subcellular colocalization of the cellular and scrapie prion proteins in caveolae-like membranous domains. *Proc Natl Acad Sci U S A*. 93:14945-9.

Vial, C., and R.J. Evans. 2005. Disruption of lipid rafts inhibits P2X1 receptor mediated currents and arterial vasoconstriction. *J Biol Chem.*

Vincenz, C., and V.M. Dixit. 1996. 14-3-3 proteins associate with A20 in an isoform-specific manner and function both as chaperone and adapter molecules. *J Biol Chem.* 271:20029-34.

Viola, A., S. Schroeder, Y. Sakakibara, and A. Lanzavecchia. 1999. T lymphocyte costimulation mediated by reorganization of membrane microdomains. *Science*. 283:680-2.

Vist, M.R., and J.H. Davis. 1990. Phase equilibria of cholesterol/dipalmitoylphosphatidylcholine mixtures: 2H nuclear magnetic resonance and differential scanning calorimetry. *Biochemistry*. 29:451-64.

Vitale, M.L., E.P. Seward, and J.M. Trifaro. 1995. Chromaffin cell cortical actin network dynamics control the size of the release-ready vesicle pool and the initial rate of exocytosis. *Neuron*. 14:353-63.

Vitetta, E.S., E.A. Boyse, and J.W. Uhr. 1973. Isolation and characterization of a molecular complex containing Thy-1 antigen from the surface of murine thymocytes and T cells. *Eur J Immunol*. 3:446-53.

von Haller, P.D., S. Donohoe, D.R. Goodlett, R. Aebersold, and J.D. Watts. 2001. Mass spectrometric characterization of proteins extracted from Jurkat T cell detergent-resistant membrane domains. *Proteomics*. 1:1010-21.

Wandinger-Ness, A., M.K. Bennett, C. Antony, and K. Simons. 1990. Distinct transport vesicles mediate the delivery of plasma membrane proteins to the apical and basolateral domains of MDCK cells. *J Cell Biol*. 111:987-1000.

Wang, B., H. Yang, Y.C. Liu, T. Jelinek, L. Zhang, E. Ruoslahti, and H. Fu. 1999. Isolation of high-affinity peptide antagonists of 14-3-3 proteins by phage display. *Biochemistry*. 38:12499-504.

Wang, H., L. Zhang, R. Liddington, and H. Fu. 1998. Mutations in the hydrophobic surface of an amphipathic groove of 14-3-3zeta disrupt its interaction with Raf-1 kinase. *J Biol Chem*. 273:16297-304.

Wang, T.Y., R. Leventis, and J.R. Silvius. 2000a. Fluorescence-based evaluation of the partitioning of lipids and lipidated peptides into liquid-ordered lipid microdomains: a model for molecular partitioning into "lipid rafts". *Biophys J*. 79:919-33.

Wang, T.Y., and J.R. Silvius. 2001. Cholesterol does not induce segregation of liquid-ordered domains in bilayers modeling the inner leaflet of the plasma membrane. *Biophys J*. 81:2762-73.

Wang, T.Y., and J.R. Silvius. 2003. Sphingolipid partitioning into ordered domains in cholesterol-free and cholesterol-containing lipid bilayers. *Biophys J*. 84:367-78.

Wang, W., and D.C. Shakes. 1996. Molecular evolution of the 14-3-3 protein family. *J Mol Evol*. 43:384-98.

Wang, Y., C. Jacobs, K.E. Hook, H. Duan, R.N. Booher, and Y. Sun. 2000b. Binding of 14-3-3beta to the carboxyl terminus of Wee1 increases Wee1 stability, kinase activity, and G2-M cell population. *Cell Growth Differ*. 11:211-9.

Waterman, M.J., E.S. Stavridi, J.L. Waterman, and T.D. Halazonetis. 1998. ATM-dependent activation of p53 involves dephosphorylation and association with 14-3-3 proteins. *Nat Genet.* 19:175-8.

Wattenberg, B.W., and D.F. Silbert. 1983. Sterol partitioning among intracellular membranes. Testing a model for cellular sterol distribution. *J Biol Chem.* 258:2284-9.

Webb, R.H., and K.C. Dorey. 1995. The Pixilated Image. *In* Handbook of Biological Confocal Microscopy. J.B. Pawley, editor. Plenum Press, New York. 55-66.

Wilker, E., and M.B. Yaffe. 2004. 14-3-3 Proteins--a focus on cancer and human disease. *J Mol Cell Cardiol.* 37:633-42.

Wilker, E.W., R.A. Grant, S.C. Artim, and M.B. Yaffe. 2005. A structural basis for 14-3-3sigma functional specificity. *J Biol Chem.* 280:18891-8.

Wilson, B.S., S.L. Steinberg, K. Liederman, J.R. Pfeiffer, Z. Surviladze, J. Zhang, L.E. Samelson, L.H. Yang, P.G. Kotula, and J.M. Oliver. 2004. Markers for detergent-resistant lipid rafts occupy distinct and dynamic domains in native membranes. *Mol Biol Cell.* 15:2580-92.

Wiltfang, J., M. Otto, H.C. Baxter, M. Bodemer, P. Steinacker, E. Bahn, I. Zerr, J. Kornhuber, H.A. Kretzschmar, S. Poser, E. Ruther, and A. Aitken. 1999. Isoform pattern of 14-3-3 proteins in the cerebrospinal fluid of patients with Creutzfeldt-Jakob disease. *J Neurochem.* 73:2485-90.

Wolf, A.A., M.G. Jobling, S. Wimer-Mackin, M. Ferguson-Maltzman, J.L. Madara, R.K. Holmes, and W.I. Lencer. 1998. Ganglioside structure dictates signal transduction by cholera toxin and association with caveolae-like membrane domains in polarized epithelia. *J Cell Biol.* 141:917-27.

Woodcock, J.M., J. Murphy, F.C. Stomski, M.C. Berndt, and A.F. Lopez. 2003. The dimeric versus monomeric status of 14-3-3zeta is controlled by phosphorylation of Ser58 at the dimer interface. *J Biol Chem.* 278:36323-7.

Wu, C., S. Butz, Y. Ying, and R.G. Anderson. 1997. Tyrosine kinase receptors concentrated in caveolae-like domains from neuronal plasma membrane. *J Biol Chem.* 272:3554-9.

Wurtele, M., C. Jelich-Ottmann, A. Wittinghofer, and C. Oecking. 2003. Structural view of a fungal toxin acting on a 14-3-3 regulatory complex. *Embo J.* 22:987-94.

Xavier, R., T. Brennan, Q. Li, C. McCormack, and B. Seed. 1998. Membrane compartmentation is required for efficient T cell activation. *Immunity.* 8:723-32.

Xia, F., X. Gao, E. Kwan, P.P. Lam, L. Chan, K. Sy, L. Sheu, M.B. Wheeler, H.Y. Gaisano, and R.G. Tsushima. 2004. Disruption of pancreatic beta-cell lipid rafts modifies Kv2.1 channel gating and insulin exocytosis. *J Biol Chem.* 279:24685-91.

Xiang, X., M. Yuan, Y. Song, N. Ruderman, R. Wen, and Z. Luo. 2002. 14-3-3 facilitates insulin-stimulated intracellular trafficking of insulin receptor substrate 1. *Mol Endocrinol.* 16:552-62.

Xiao, B., S.J. Smerdon, D.H. Jones, G.G. Dodson, Y. Soneji, A. Aitken, and S.J. Gamblin. 1995. Structure of a 14-3-3 protein and implications for coordination of multiple signalling pathways. *Nature.* 376:188-91.

Xiao, J., Z. Xia, A. Pradhan, Q. Zhou, and Y. Liu. 2004. An immunohistochemical method that distinguishes free from complexed SNAP-25. *J Neurosci Res.* 75:143-51.

Xu, T., B. Rammner, M. Margittai, A.R. Artalejo, E. Neher, and R. Jahn. 1999. Inhibition of SNARE complex assembly differentially affects kinetic components of exocytosis. *Cell.* 99:713-22.

Xu, X., R. Bittman, G. Duportail, D. Heissler, C. Vilcheze, and E. London. 2001. Effect of the structure of natural sterols and sphingolipids on the formation of ordered sphingolipid/sterol domains (rafts). Comparison of cholesterol to plant, fungal, and disease-associated sterols and comparison of sphingomyelin, cerebrosides, and ceramide. *J Biol Chem.* 276:33540-6.

Xu, X., and E. London. 2000. The effect of sterol structure on membrane lipid domains reveals how cholesterol can induce lipid domain formation. *Biochemistry.* 39:843-9.

Yaffe, M.B. 2002. How do 14-3-3 proteins work?-- Gatekeeper phosphorylation and the molecular anvil hypothesis. *FEBS Lett.* 513:53-7.

Yaffe, M.B., K. Rittinger, S. Volinia, P.R. Caron, A. Aitken, H. Leffers, S.J. Gamblin, S.J. Smerdon, and L.C. Cantley. 1997. The structural basis for 14-3-3:phosphopeptide binding specificity. *Cell.* 91:961-71.

Yamauchi, T., H. Nakata, and H. Fujisawa. 1981. A new activator protein that activates tryptophan 5-monooxygenase and tyrosine 3-monooxygenase in the presence of Ca2+-, calmodulin-dependent protein kinase. Purification and characterization. *J Biol Chem.* 256:5404-9.

Yancey, P.G., W.V. Rodrigueza, E.P. Kilsdonk, G.W. Stoudt, W.J. Johnson, M.C. Phillips, and G.H. Rothblat. 1996. Cellular cholesterol efflux mediated by cyclodextrins. Demonstration Of kinetic pools and mechanism of efflux. *J Biol Chem.* 271:16026-34.

Yang, B., M. Steegmaier, L.C. Gonzalez, Jr., and R.H. Scheller. 2000. nSec1 binds a closed conformation of syntaxin1A. *J Cell Biol.* 148:247-52.

Yang, H., S.C. Masters, H. Wang, and H. Fu. 2001. The proapoptotic protein Bad binds the amphipathic groove of 14-3-3zeta. *Biochim Biophys Acta.* 1547:313-9.

Yang, J., K. Winkler, M. Yoshida, and S. Kornbluth. 1999. Maintenance of G2 arrest in the Xenopus oocyte: a role for 14-3-3-mediated inhibition of Cdc25 nuclear import. *Embo J.* 18:2174-83.

Yi, J.S., J.Y. Lee, S.G. Chi, J.H. Kim, S.G. Park, S. Kim, and Y.G. Ko. 2005. Aminoacyl-tRNA synthetase-interacting multi-functional protein, p43, is imported to endothelial cells via lipid rafts. *J Cell Biochem.*

Yip-Schneider, M.T., W. Miao, A. Lin, D.S. Barnard, G. Tzivion, and M.S. Marshall. 2000. Regulation of the Raf-1 kinase domain by phosphorylation and 14-3-3 association. *Biochem J.* 351:151-9.

Yoshida, K., T. Yamaguchi, T. Natsume, D. Kufe, and Y. Miki. 2005. JNK phosphorylation of 14-3-3 proteins regulates nuclear targeting of c-Abl in the apoptotic response to DNA damage. *Nat Cell Biol.* 7:278-85.

Yuan, H., K. Michelsen, and B. Schwappach. 2003. 14-3-3 dimers probe the assembly status of multimeric membrane proteins. *Curr Biol.* 13:638-46.

Zacharias, D.A., J.D. Violin, A.C. Newton, and R.Y. Tsien. 2002. Partitioning of lipid-modified monomeric GFPs into membrane microdomains of live cells. *Science*. 296:913-6.

Zajchowski, L.D., and S.M. Robbins. 2002. Lipid rafts and little caves. Compartmentalized signalling in membrane microdomains. *Eur J Biochem*. 269:737-52.

Zeng, Y., K.C. Forbes, Z. Wu, S. Moreno, H. Piwnica-Worms, and T. Enoch. 1998. Replication checkpoint requires phosphorylation of the phosphatase Cdc25 by Cds1 or Chk1. *Nature*. 395:507-10.

Zeng, Y., and H. Piwnica-Worms. 1999. DNA damage and replication checkpoints in fission yeast require nuclear exclusion of the Cdc25 phosphatase via 14-3-3 binding. *Mol Cell Biol*. 19:7410-9.

Zerr, I., M. Bodemer, O. Gefeller, M. Otto, S. Poser, J. Wiltfang, O. Windl, H.A. Kretzschmar, and T. Weber. 1998. Detection of 14-3-3 protein in the cerebrospinal fluid supports the diagnosis of Creutzfeldt-Jakob disease. *Ann Neurol*. 43:32-40.

Zeyda, M., and T.M. Stulnig. 2006. Lipid Rafts & Co.: an integrated model of membrane organization in T cell activation. *Prog Lipid Res*. 45:187-202.

Zha, J., H. Harada, E. Yang, J. Jockel, and S.J. Korsmeyer. 1996. Serine phosphorylation of death agonist BAD in response to survival factor results in binding to 14-3-3 not BCL-X(L). *Cell*. 87:619-28.

Zhang, L., J. Chen, and H. Fu. 1999. Suppression of apoptosis signal-regulating kinase 1-induced cell death by 14-3-3 proteins. *Proc Natl Acad Sci U S A*. 96:8511-5.

Zhang, L., H. Wang, D. Liu, R. Liddington, and H. Fu. 1997. Raf-1 kinase and exoenzyme S interact with 14-3-3zeta through a common site involving lysine 49. *J Biol Chem*. 272:13717-24.

Zhang, W., R.P. Trible, and L.E. Samelson. 1998. LAT palmitoylation: its essential role in membrane microdomain targeting and tyrosine phosphorylation during T cell activation. *Immunity*. 9:239-46.

Zhou, B.B., and S.J. Elledge. 2000. The DNA damage response: putting checkpoints in perspective. *Nature*. 408:433-9.

Zhu, P., Y. Sang, H. Xu, J. Zhao, R. Xu, Y. Sun, T. Xu, X. Wang, L. Chen, H. Feng, C. Li, and S. Zhao. 2005. ADAM22 plays an important role in cell adhesion and spreading with the assistance of 14-3-3. *Biochem Biophys Res Commun*. 331:938-46.

Zhu, P., Y. Sun, R. Xu, Y. Sang, J. Zhao, G. Liu, L. Cai, C. Li, and S. Zhao. 2003. The interaction between ADAM 22 and 14-3-3zeta: regulation of cell adhesion and spreading. *Biochem Biophys Res Commun*. 301:991-9.